

TECH LIBRARY KAFB, NM
0000822

SCIENCE & ENGINEERING SYMPOSIUM PROCEEDINGS 16-19 OCTOBER



THEME: "Advanced Technologies - Key to Capabilities at Affordable Costs"

DISTRIBUTION STATEMENT A
Approved for Public Release
Distribution Unlimited

VOL. V. MATERIAL

**CO-SPONSORED BY
NAVAL MATERIAL COMMAND
AIR FORCE SYSTEMS COMMAND**



- Avionics
- Propulsion
- Flight Dynamics
- Basic Research

- Material
- Armament
- Human Resources

~~General~~
TL
505
.S45
1978
v.5

Reproduced From
Best Available Copy

19991214 078

TECH LIBRARY KAFB, NM



0000822

PROCEEDINGS
OF THE
1978 SCIENCE AND ENGINEERING SYMPOSIUM

16 - 19 OCTOBER 1978

NAVAL AMPHIBIOUS BASE
CORONADO, CALIFORNIA

VOLUME V

APPROVED FOR PUBLIC RELEASE,
DISTRIBUTION UNLIMITED

U.S. Air Force
Air Force Weapons Laboratory
Technical Library

SYMPOSIUM OFFICIALS

CO-SPONSORS

NAVAL MATERIAL
COMMAND

AIR FORCE SYSTEMS
COMMAND

HOSTS

NAVAL OCEAN SYSTEMS
CENTER
WEST COAST COORDINATOR

NAVAL AMPHIBIOUS BASE
FACILITIES

CO-CHAIRMEN

WILLIAM KOVEN
Associate Technical Director
Naval Air Research and
Technology
Naval Air Systems Command

DR. BERNARD KULP
Chief Scientist
Director of Science and
Technology
Air Force Systems Command

DEPUTY CO-CHAIRMEN

JAMES MULQUIN
Advanced Systems Technology
Planning
Naval Air Research and
Technology
Naval Air Systems Command

MAJOR LARRY FEHRENBACHER
Assistant to Chief Scientist
Director of Science and
Technology
Air Force Systems Command

U.S. Air Force
Air Force Weapons Laboratory
Technical Library

TL
505
.545
1978
v.5

PREFACE

The initial co-sponsored Air Force Systems Command/Naval Material Command Science and Engineering Symposium was held at the Naval Amphibious Base, Coronado on 16 - 19 October 1978. The theme of the 1978 Symposium was "Advanced Technologies - Key to Capabilities at Affordable Cost."

The objectives of this first joint Navy/Air Force Science and Engineering Symposium were to:

- . Provide a forum for military and civilian laboratory scientific and technical researchers to demonstrate the spectrum and nature of 1978 achievements by their services in the areas of
 - . Armament
 - . Avionics
 - . Basic Research
 - . Flight Dynamics
 - . Human Resources
 - . Materials
 - . Propulsion
- . Recognize outstanding technical achievement in each of these areas and select the outstanding technical paper within the Navy and the Air Force for 1978
- . Assist in placing the future Air Research and Development of both services in correct perspective and to promote the exchange of ideas between the Navy and Air Force Laboratories
- . Stress the need for imagination, vision and overall excellence within the technology community, assuring that the air systems of the future will not only be effective but affordable.

Based upon the success of the initial joint symposium (which was heretofore an Air Force event), future symposia are planned with joint Navy/Air Force participation.

TABLE OF CONTENTS

VOLUME I

AVIONICS

R. S. VAUGHN, NADC

COL R. LOPINA, AFAL

CO-CHAIRMEN

The Airborne Electronic Terrain Map System (AETMS) Capt F. Barney, USAF and Dr. L. Tamburino, AFAL	1
The Assessment of GaAs Passivation and Its Applications Dr. F. Schuermeyer, J. Blassingame, AFAL and Dr. H. Hartnagel, Univ. of New Castle-Upon-Thames, England	17
Identification of Impurity Complexes in Gallium Arsenide Device Material by High Resolution Magneto-Photoluminescence G. McCoy, Maj R. Almasy, USAF, D. Reynolds and C. Litton, AFAL	50
Microcircuit Analysis Techniques Using Field-Effect Liquid Crystals D. J. Burns, RADC	69
Surface Acoustic Wave Frequency Synthesizer for JTIDS P. H. Carr, A. J. Budreau and A. J. Slovodnik, RADC	85
Enhanced Measurement Capability Using a Background Suppression Scheme G. A. Vanasse and E. R. Huppi, AFGL	110
Spectrum Estimation and Adaptive Controller for Long-Range Complex Scattering Targets R. F. Ogrodnik, RADC	122
Spatial and Temporal Coding of GaAs Lasers for a Laser Line Scan Sensor Capt R. S. Shinkle, USAF, ASD	149

VOLUME II

PROPULSION

AERO-PROPULSION

A. A. MARTINO, NAPC

COL G. STRAND, AFAPL

CO-CHAIRMEN

ROCKET PROPULSION

B. W. HAYES, NWC

COL W. F. MORRIS, AFRPL

CO-CHAIRMEN

Airbreathing Propulsion Functional Area Review Col G. E. Strand, USAF, AFAPL	164
Rocket Propulsion Overview Col W. F. Morris, USAF, AFRPL	196
Role of Turbine Engine Technology on Life Cycle Cost R. F. Panella and R. G. McNally, AFAPL	212
VORBIX Augmentation - An Improved Performance Afterburner for Turbo Fan Engines W. W. Wagner, NAPC	247
A Retirement for Cause Study of an Engine Turbine Disk R. Hill, AFAPL, R. Reimann, AFML and L. Ogg, ASD	265
Payoffs of Variable Cycle Engines for Supersonic VSTOL Aircraft R. T. Lazarick and P. F. Piscopo, NAPC	296
The Coanda/Refraction Concept for Gasturbine Engine Exhaust Noise Suppression During Ground Testing D. Croce, NAEC	322
Expendable Design Concept Lt D. C. Hall, USAF, AFAPL and H. F. Due, Teledyne CAE	349
The Supersonic Expendable Turbine Engine Development Program T. E. Elsasser, NAPC	363
Unique Approach for Reducing Two Phase Flow Losses in Solid Rocket Motors Lt D. C. Ferguson, USAF, AFRPL	383
Missile System Propulsion Cook-Off R. F. Vetter, NWC	414
A Powerful New Tool for Solid Rocket Motor Design W. S. Wolosz, AFRPL	428
Quantification of the Thermal Environment for Air-Launched Weapons H. C. Schafer, NWC	453

A Study of Rocket-Propelled Stand-Off Missiles 470
Lt L. K. Slimak, USAF, AFRPL

Prediction of Rocket Motor Exhaust Plume Effects on Missile Effectiveness 496
A. C. Victor, NWC

VOLUME III

FLIGHT DYNAMICS

C. A. DeCRESCENTE, NADC COL G. CUDAHY, USAF, AFFDL
CO-CHAIRMEN

Air Force Flight Dynamics Functional Area Review 521
Col G. F. Cudahy, USAF, AFFDL

A Functional Area Review (FAR) of Navy Flight Dynamics 592
C. A. DeCrescente, NADC

Aircraft Aft-Fuselage Sonic Damping 615
G. Pigman, E. Roeser and M. Devine, NADC

Active Control Applications to Wing/Store Flutter Suppression 626
L. J. Hutsell, T. E. Noll and D. E. Cooley, AFFDL

Maximum Performance Escape System (MPES) 657
J. J. Tyburski, NADC and W. J. Stone, NWC

Status of Circulation Control Rotor and X-Wing VTOL Advanced Development Program 673
T. M. Cancy, D. G. Kirkpatrick and R. M. Williams, DTNSRDC

AFFTC Parameter Identification Experience 697
Lt D. P. Maunder, USAF, AFFTC

Developments in Flight Dynamics Technology for Navy V/STOL Aircraft 719
J. W. Clark, Jr., and C. Henderson, NADC

Cost Effective Thrust Drag Accounting 750
R. B. Sorrells, III, AEDC

Drag Prediction for Wing-Body-Nacelle Configurations 766
T. C. Tai, DTNSRDC

Numerical Solution of the Supersonic and Hypersonic Viscous Flow Around Thin Delta Wings 793
Maj G. S. Bluford, USAF and Dr. W. L. Hankey, AFFDL

Optimization of Airframe Structures: A Review and Some
Recommendations 828
V. B. Venkayya, AFFDL

Use of Full Mission Simulation for Aircraft Systems Evaluation 870
K. A. Adams, AFFDL

VOLUME IV

BASIC RESEARCH

DR. E. H. WEINBERG, NAL

DR. L. KRAVITZ, AFOSR

CO-CHAIRMEN

The Electronic and Electro-Optic Future of III-V Semiconductor
Compounds 885
H. L. Lessoff, NRL and J. K. Kennedy, RADC

Collective Ion Acceleration and Intense Electron Beam Propagation
Within an Evacuated Dielectric Tube 912
Capt R. L. Gullickson, USAF, AFOSR, R. K. Parker and J. A.
Pasour, NRL

High Spatial Resolution Optical Observations Through the
Earth's Atmosphere 939
Capt S. P. Worden, USAF, AFGL

High Burnout Schottky Barrier Mixer Diodes for X-Band and
Millimeter Frequencies 954
A. Christou, NRL

New Energetic Plasticizers: Synthesis, Characterization and
Potential Applications 968
Lt R. A. Hildreth, USAF, Lt S. L. Clift, USAF and Lt J. P.
Smith, FJSRL

Improved Corrosion and Mechanical Behavior of Alloys by Means
of Ion Implantation 981
J. K. Hirvonen and J. Butler, NRL

Symmetric Body Vortex Wake Characteristics in Supersonic Flow 1000
Dr. W. L. Oberkampf, Univ of Texas at Austin and Dr. D. C.
Daniel, AFATL

Materials Effects in High Reflectance Coatings 1033
H. E. Bennett, NWC

Improved Substrate Materials for Surface Acoustic Wave (SAW) Devices Capt R. M. O'Connell, USAF, RADC	1058
A Simple Prediction Method for Viscous Drag and Heating Rates T. F. Zien, NSWC	1075
Assessing the Impact of Air Force Operations on the Stratosphere Composition C. C. Gallagher and Capt R. V. Pieri, USAF, AFGL	1110
On the Modelling of Turbulence Near a Solid Wall K. Y. Chien, NSWC	1131
Atmospheric Electric Hazards to Aircraft L. H. Ruhnke, NRL	1146
Efficient Operation of a 100 Watt Transverse Flow Oxygen-Iodine Chemical Laser Maj W. E. McDermott, USAF, Capt N. R. Pchelkin, USAF, Dr. J. Bernard and Maj R. R. Bousek, USAF, AFWL	1161

VOLUME V

MATERIALS

F. S. WILLIAMS, NADC	COL P. O. BOUCHARD, USAF, AFML	
CO-CHAIRMEN		
Advanced Materials Technologies - The Key to New Capabilities at Affordable Costs Col P. O. Bouchard, USAF, AFML	1173	
Ceramics in Rolling Element Bearings C. F. Bersch, NAVAIR	1182	
Group Technology Key to Manufacturing Process Integration Capt D. Shunk, USAF, AFML	1198	
An Attempt to Predict the Effect of Moisture on Carbon Fiber Composites J. M. Augl, NSWC	1213	
Evaluation of Spectrometric Oil Analysis Techniques for Jet Engine Condition Monitoring Lt T. J. Thomson, USAF and K. J. Eisentraut, AFML	1252	

Characterization of Structural Polymers, Using Nuclear Magnetic Resonance Techniques W. B. Moniz, C. F. Poranski, Jr., A. N. Garroway and H. A. Resing, NRL	1287
On the Variation of Fatigue Crack Opening Load with Measurement Location D. E. Macha, D. M. Corbly, J. W. Jones, AFML	1308
Environmentally Induced Catastrophic Damage Phenomena and Control Dr. J. L. DeLuccia, NADC	1335
Improved High Temperature Capability of Titanium Alloys by Ion Implantation/Plating S. Fujishiro, AFML and E. Eylon, Univ of Cincinnati	1366
Measurement of the Physical Properties and Recombination Process in Bulk Silicon Materials Lt T. C. Chandler, USAF, AFML	1384
Deuterated Synthetic Hydrocarbon Lubricant A. A. Corte, NADC	1396
The Cordell Plot: Key to a Better Understanding of the Behavior of Fiber-Reinforced Composites T. M. Cordell, AFML	1410

VOLUME VI

ARMAMENT

DR. J. MAYERSAK, AFATL	R. M. HILLYER, NWC	
CO-CHAIRMEN		
Armament Technology - Functional Overview Dr. J. R. Mayersak, AFATL	1434	
The Digital Integrating Subsystem-Modularity, Flexibility and Standardization of Hardware and Software D. L. Gardner, AFATL	1449	
Bank-To-Turn (BTT) Technology R. M. McGehee, AFATL	1490	
Advances in Microwave Striplines with Applications J. A. Mosko, NWC	1507	

Considerations for the Design of Microwave Solid-State Transmitters M. Afendykiew, Jon Bumgardner and Darry Kinman, NWC	1543
Strapdown Seeker Guidance for Air-to-Surface Tactical Weapons Capt T. R. Callen, USAF, AFATL	1590
Optimizing the Performance of Antennas Mounted on Complex Airframes Dr. C. L. Yu, NWC	1614

VOLUME VII

HUMAN RESOURCES

H. J. CLARK, AFHRL	DR. J. HARVEY, NTEC	
CO-CHAIRMEN		
Human Resources Research and Development H. J. Clark, AFHRL		1640
Human Resources in Naval Aviation Dr. J. Harvey, NTEC		1649
LCCIM: A Model for Analyzing the Impact of Design on Weapon System Support Requirements and LCC H. A. Baran, AFHRL, A. J. Czuchry and J. C. Gocłowski, Dynamics Research Corp		1683
Pacts: Use of Individualized Automated Training Technology Dr. R. Breaux, NTEC		1703
Increasing the Affordability of I-Level Maintenance Training Through Simulation G. G. Miller, D. R. Baum and D. I. Downing, AFHRL		1711
Psychomotor/Perceptual Measures for the Selection of Pilot Trainees D. R. Hunter, AFHRL		1741
Modern Maintenance Training Technology and Our National Defense Posture Dr. W. J. King and Dr. P. E. Van Hemel, NTEC		1758
Prediction of System Performance and Cost Effectiveness Using Human Operator Modelling LCDR N. E. Lane, USN, W. Leyland, NADC and H. I. Strieb (Analytics)		1781

An Inflight Physiological Data Acquisition and Analysis System Capt J. T. Merrifield, USAF, T. P. Waddell, D. G. Powell, USAF/SAM and E. B. Croson, PMTC	1804
Synthetic Selection of Naval Aviators: A Novel Approach D. E. Norman, D. Wightman, NTEC and CDR L. Waldeisen, NAMRL	1821
Modeling: The Air Force Manpower and Personnel System for Policy Analysis Capt S. B. Polk, USAF, AFHRL	1831
Evoked Brain Potentials as Predictors of Performance: The Hemispheric Assymetry as Related to Pilot and Radar Intercept Officer Performance Dr. B. Rimland and Dr. G. W. Lewis, NPRDC	1841
Launch Opportunity for Air-to-Ground Visually Delivered Weapons R. A. Erickson and C. J. Burge, NWC	1863

VOLUME VIII

AVIONICS, PROPULSION, AND FLIGHT DYNAMICS (CLASSIFIED)

Functional Area Review of Avionics Col R. F. Lopina, USAF, AFAL	1
The MADAIR System J. A. Titus, NCSC	27
Electronically Agile Array for Long-Range Airborne Surveillance Radar Dr. J. K. Smith, NADC	89
Automatic Ship Classification System W. G. Hueber and Dr. L. A. Wilson, NWC	118
Reduction of False Alarm Rates in Aircraft Attack Warning Systems H. L. Jaeger, NWC	144
Impact of Focal Plane Array Technology on Airborne Forward Looking Infrared Sensors M. Hess and S. Campana, NADC	179
Advanced Sonobuoy Technology - ERAPS (Expendable Reliable Acoustic Path Sonobuoy) J. J. Stephenosky, NADC	200
NAVSTAR Global Positioning System Field Test Results Aboard Air Force and Navy Test Vehicles LCDR J. A. Strada, USN, SAMSO	220
An Overview of Soviet Propulsion Capabilities W. A. Zwart, FTD	240
Reduced Observables - An Approach for Providing More Effective and Affordable Combat Weapon Systems D. E. Fraga, AFFDL	273
Soviet Method of Calculating the Aerodynamic Characteristics of Wings Flying in Ground Effect Lt C. R. Gallaway, USAF, FTD	330

VOLUME IX

MATERIALS, ARMAMENT, AND HUMAN RESOURCES (CLASSIFIED)

Soviet Materials for Aircraft Engines R. F. Frontani, FTD	362
CCD Camera/Tracker Seeker Technology G. F. Teate, NWC	390
Warhead Designs for Wide Area Antiarmor Cluster Munitions Dr. J. C. Foster and Capt E. M. Cutler, USAF, AFATL	404
Active Moving Target Tracking Seeker Captive Flight Test A. N. DiSalvio, AFATL	427
Inter-Laboratory Air-to-Air Missile Technology - An Innovative Approach T. C. Aden, AFATL	449
Aimable Ordnance for Tactical Anti-Air and Anti-Surface Missiles T. R. Zulkoski and P. H. Amundson, NWC	485
Manned Threat Quantification Capt G. J. Valentino, USAF and Lt R. B. Kaplan, USAF, AMRL	549

ADVANCED MATERIALS TECHNOLOGIES -
THE KEY TO NEW CAPABILITIES AT AFFORDABLE COSTS

The Air Force Materials Laboratory is the Air Force organization charged with planning and executing the USAF exploratory and selected advanced development and research programs for materials. It provides technical and management assistance in system studies, analyses, development planning activities, system acquisition, test, evaluation, modification and operation of aerospace systems, and related equipment. It manages and directs the manufacturing methods program.

The Laboratory maintains an aggressive program leading to reduction of system acquisition and life cycle costs and new weapon system options. This is done through a selective in-house and contract program encompassing a range of materials and processes. This requires a wide spectrum of technical effort, exploiting innovations, revolutionary and evolutionary concepts.

To further this work the Laboratory is guided by goals which:

1. Establish major integrated AFML programs in Research, Exploratory and Advanced Development, and Manufacturing Technology directed at reduction in acquisition and ownership costs in the systems acquisition phase, with systems payoff within five years.
2. Provide leadership in Materials Technology for reduction in Systems O&S costs with emphasis on near term payoff.
3. Provide timely solutions to Systems materials problems and actively propose materials options for systems in operation, systems in development, and conceptual systems.
4. Establish a pacing technology base effort in selected areas of Materials Science and Technology.
5. Select high priority materials technical areas and carry them through the critical technical validation necessary for the earliest transition to systems development acquisition and O&M programs.
6. Assure existence of AFML programs to advance materials technology for increased performance in selected areas of desired military capability.
7. Develop approaches to enable the Air Force to meet high priority needs in consonance with industry commercial markets and emerging, transitionable foreign capabilities.
8. Emphasize efforts responsive to Air Force needs which in addition are responsive to and/or yield by-products which converge with major national goals and priorities.

These goals are subject to continuous scrutiny to ensure currency with Air Force needs and requirements.

The AFML is a full spectrum Laboratory. Its program includes innovative and creative in-house and contractual programs. It exploits technological opportunities of the basic sciences for the development of materials and manufacturing technology required for the gamut of space, strategic and tactical, aeronautical and electronic systems and subsystems. Its program is developed with primary emphasis on the needs and interests of aerospace missions and systems.

The AFML program uses the expertise of the national materials and processing industries as well as the capabilities of the manufacturing and aerospace industries. Therefore, the Laboratory is organized to implement metallic, electromagnetic, and nonmetallic materials development, accomplish advanced development demonstrations and manufacturing methods efforts, and provide materials engineering consultation and solutions of problems in applications of materials in systems development and acquisition.

ORGANIZATION

The Laboratory has been organized to respond to the full breadth and depth of the Air Force materials needs. The organization is set up to implement materials development, such as metallic nonmetallic and electromagnetic materials, manage manufacturing methods development, and provide materials engineering consultation and solution of problems in applications of materials in system development and acquisition. The organizational chart for the Laboratory shows five divisions which are identifiable with the above functions. A sixth division provides support services to the Laboratory as a whole. The management and operating process involved the total capability of the organization to ensure effective response to Air Force needs.

To meet AF customer needs, the AFML has a collocated engineer activity where AFML engineers work with user organizations in transitioning materials technology to systems use and providing on-site technical expertise and evaluation. AFML engineers have been collocated at ESD, ASD, SAMSO and ADTC. As of 1 October 1978, 417 personnel were assigned to the Laboratory. (365 civilians, 57 military). This highly professional force possesses 88MS degrees and 66 PhD's.

FUNDS

<u>PROGRAM ELEMENT (NO/TITLE)</u>		<u>ACTUAL</u>	<u>EST</u>	<u>EST</u>	<u>EST</u>
		<u>FY 78</u>	<u>FY 79</u>	<u>FY 80</u>	<u>FY 81</u>
61101F	ILIR	760	800	800	800
61102F	Research	4255	4682	5215	5215
62102F	Materials	30400	31700	34200	34700
63211F	Laser Hardened Materials	5670	4750	3350	3350
78011F	Manufacturing Methods	41300	27100	56200	63200
Other Sources		10264	6455	6989	3984
		<u>92649</u>	<u>75487</u>	<u>106754</u>	<u>111249</u>

The recent increase in the Laboratory Independent Research fund (up from \$500K in FY76 and \$660K in FY77) is a welcome and healthy trend. These funds are a major source for exploiting high risk or innovative materials concepts. Past ILIR efforts that have led to new Laboratory thrusts (ordered polymers, rapid solidification rate powder alloys polymeric bead coatings, nuclear transmutation doped silicon, etc.) attest to the value of this fund in replenishing the materials technology base. The major dip in the FY79 Manufacturing Methods budget, which results from a DOD cut of about \$25M in the 3010 account, will be partly offset by the work load of AFML management of Approximately \$25M of F-16 FY79 modernization funds. Most of the F-16 money by necessity will apply to manufacturing programs specific to the F-16, so the loss of generic MM programs resulting from the DOD cut will, only be partly recouped. The downward trend in the Laser Hardened Materials program reflects cuts in the overall 63211F budget in FY79 and beyond. The major impact in the LHM program will be delays in the development and demonstration of laser hardening for aircraft, cruise missiles, and infrared missiles. Reimbursements are expected to jump from \$2.8M in FY78 to \$3.5M in FY79. Most of the increase will be from other AF Laboratories and Product Divisions, as the various Memoranda of Agreement signed in CY78 become fully effective.

RELATIONSHIP OF THE LABORATORY PROGRAMS TO OTHER EFFORTS

The organization and program of the Laboratory has evolved over a period of years in response to the diverse and unique materials needs of the Air Force. Its discipline oriented elements provide emphasis in the research and exploratory development areas with well integrated in-house and contract programs. The materials support, advanced development and manufacturing technology elements reflect the needs and interest of materials applications and demonstrations in system development, test, evaluation and production. These system oriented activities also provide technical consultation and assistance and participation in system materials engineering through on-site system program office activity. Significant efforts on materials development are also performed by the other Services, DARPA, NASA, DOE, and Industrial Independent Research and Development Programs. This Laboratory maintains a concerted drive for coordination and cooperation of these efforts through definitive joint planning and program assessments as well as an awareness of foreign technology developments.

PROGRAM MAJOR THRUSTS

The AFML research and development program is divided into 6 technology planning objectives, each containing specific major thrusts. These are presented in the following paragraphs.

AFML TPO NUMBER 1, THERMAL PROTECTION MATERIALS

The efforts in this area, utilizing some \$2.4 million of FY79 resources provides materials and processes for thermal protection of systems and componentry subject to severe thermal and erosive environments. Major applications are in strategic ballistic and maneuverable reentry vehicles and high mach number (hypersonic) aircraft. The effects of erosion due to ice, snow, rain, and dust particles on reentry body accuracy and survivability in addition to the severe thermal environment require that this TPO emphasize

materials and technology to improved performance and survivability of ballistic and maneuvering reentry vehicles.

Within this TPO there are five major thrusts. Work on Shape Stable Nosetips is concerned with erosion resistant carbon-carbon composites and alternate carbon-carbon composites. In Lightweight Heatshields emphasis is on the development of a low cost carbon fabric as a replacement for rayon-based carbon materials which will likely not be available in the future. Modeling and Guidance efforts are devoted to quantifying the effect of composite microstructure on materials ablation, erosion and thermo-structural performance. The thrust on Advanced Materials Concepts identifies and demonstrates the basic materials for future system needs. Carbon-Carbon Processing Science efforts are focused on establishing effects and criteria for the influence of process variables on composite microstructure and properties.

Efforts under this TPO primarily impact the Strategic Offense area, specifically reentry vehicles. Close liaison is maintained with the ABRES and Advanced ICBM programs at SAMSO. Efforts impact improved performance needs, survivability, and accuracy, the latter through ensuring predictable and uniform ablation behavior and shape retention.

AFML TPO NUMBER 2, AEROSPACE STRUCTURAL MATERIALS

The general objective in this area, utilizing some \$25 million FY79 resources is to provide reliable materials and processes with optimum combinations of properties from cryogenic temperatures to 1200°F for use in aerospace structural applications. Major applications are in subsonic and supersonic aircraft, missiles, and spacecraft. The objective encompasses the development of alloys having high toughness/density ratios, new or improved low cost organic matrix composites having improved durability and high strength/density and stiffness/density ratios. improved processing and joining techniques for metals and composites, processing science, and nondestructive measurement, evaluation, and inspection techniques essential to a high degree of quality assurance and structural integrity. It includes the development of behavioral methods of analysis and their experimental validation under anticipated service loads and environments, as well as the determination of appropriate design data necessary to predict performance levels and capabilities with high confidence.

In this TPO there are eighteen major thrusts in the areas of metals, nonmetals and nondestructive evaluation. In the metals area, the thrust in Improved Performance and Structural Integrity provides approaches to safety, durability, and life management requirements that can be implemented with no increase in costs. Acquisition Cost Reduction programs are aimed at reducing the acquisition cost of metallic airframes by 20-30% without incurring a weight penalty or increasing maintenance costs. Cost of Ownership Reduction has the goals of a 15-20 reduction in the maintenance costs of airframes. Metal and Alloys, and Joining and Processing cover the technology base for the metals area, and address the technology for low cost titanium, high performance alloys, metal matrix composites, fatigue and fracture, chemical/environmental effects, analytical process modeling, enhanced materials utilization, processing efficiency, improved service life of metal, improved durability, and predictable, reliable structural behavior.

In the nonmetals area, the Advanced Composite Materials Development thrust is concerned with developing low cost, moisture resistant materials with 350-600°F capability and low cost processability. The Advanced Fabrication

thrust, which has the goal of reduced fabrication costs for composite components, includes work on low cost tooling and manufacturing, and stresses the design/manufacturing interface to reduce acquisition cost. The goal of the Production Confidence thrust for composites is to develop integrated and economical methods and assembly procedures for quantity production of composite structures, and to develop a broad industrial production base. In Advanced Composite Materials Durability there is work on developing design/manufacturing alternatives to aluminum honeycomb sandwich, establishing chemical composition and processing specifications with 100% acceptance by industry, developing capability to predict composite laminate static and fatigue strength, and establishing defect accept/reject criteria to reduce repair and rejection rates. Adhesive Bonding, Non-metallic Composites and Polymers for Structural Materials provide the nonmetal technology base thrusts with efforts in improved processability, durability, and performance of adhesives and composites, failure mechanisms and durability roles in mechanics of composites, new resin polymer systems and self reinforcing polymers and new high temperature seals.

The area of nondestructive evaluation includes thrusts covering both metals and nonmetals. NDE of Fastened Joints covers nondestructive evaluation methods for detecting outerlayer and interior layer cracks and determining hole quality in composite materials. Field NDE Reliability Improvements is concerned with efforts on ultrasonic methods, liquid penetrants and sensitivity/capability definition. The Composites In-Service Inspection Methods thrust develops near term field capability to detect service induced flaws of 1/4 square inch and to develop a broad base structural NDE capability for water degradation, FOD, etc. NDE of Complex Shapes covers computer-aided methods for low cost, high quality inspection of complex, near-net-shape engine and airframe components. NDE Technology provides the technology base in quantitative flaw characterization, NDE of advanced materials, and quantitative NDE for surface flaws.

A principal thrust in this TPO is that of Computer Aided Manufacturing. It focuses on the disciplined application of integrated computer aided manufacturing systems to the major functions of manufacturing, with the overall goal of increased productivity and flexibility in the manufacturing and production of defense-related material. Major areas of emphasis include manufacturing architecture, fabrication, data base/data automation, design manufacturing interaction, planning and group technology, manufacturing control and external interfaces, assembly, simulation modeling and operations research, materials handling and storage, and test inspection and evaluation.

This TPO deals with the development of structural materials and related processes, methodologies and capabilities that contribute to increased structural systems performance levels and durabilities, greater integrity reliability and survivability, and to lower acquisition and O&M costs. This TPO primarily supports the areas of strategic offense, strategic defense tactical warfare and airlift. While major efforts are devoted to aircraft structures, there are applications to space and missile needs. A major driving function of the total TPO is cost reduction, with broad AFIC implications.

AFML TPO NUMBER 3, AEROSPACE PROPULSION MATERIALS

The general objective in this area represents a \$9 million FY79 investment. It provides improved materials and processes for application to current and future aircraft and rocket engine propulsion systems. Emphasis is in the areas of disks, turbine blades and vanes, fan and compressor blading, coatings, gas path seals, materials processing and joining, non-destructive inspection methods for aircraft turbine engines, and solid rocket nozzles and exit cones. Materials of interest for these components are titanium alloys, metallic and nonmetallic matrix composites, superalloys, dispersion strengthened alloys, directionally solidified alloys and eutectics, titanium aluminides, ceramics, and carbon/carbon composites.

The major efforts are concerned with reducing the high acquisition and ownership costs, increasing durability, and providing increased performance.

Within this TPO there are eight major thrusts. Life Cycle Management addresses weld repair for superalloys, surface treatment and refurbishment of turbine engine parts, component life prediction, rejuvenation of high value engine components, critical rotating component integrity, titanium combustion prevention, jet engine damping, and corrosion prediction. The thrust on Rocket Propulsion is centered on nozzle and exit cone materials while that on Small Engines stresses processing of ceramic turbine components, unique turbine rotating component concepts, and low cost composite parts. Developments in Performance/Durability will emphasize materials for advanced turbine disks, directionally solidified eutectics, titanium rotating components, hot section core combustors and vanes, titanium aluminides for static components, noncombustible engine alloys, engine seal systems for high pressure compressors and turbines, and advanced composite components. Work on Low Acquisition Cost-Metals is concerned with efforts to reduce cost of titanium and superalloy cases and frames, metal removal, titanium disks, turbine airfoils, superalloy disks and fan/compressor blading. In Low Acquisition Cost-Nonmetals there are developments in composite low cost fan blades and engine static structure. The technology base portion of this TPO includes thrusts on Ceramics, centered on identifying novel processing approaches to improve reproducibility and High Temperature Alloys, which includes efforts on developing ductility in titanium aluminides, improving fatigue resistance of turbine coatings, identifying causes of low transverse ductility, directionally solidified eutectics, and new powder metallurgy alloys.

Efforts under this TPO impact propulsion systems for most AF systems and options. The more critical options which this TPO provides include materials for high performance, lightweight propulsion systems for ICBM's, materials for turbojet and composite ramjets for high mach number with long range cruise capabilities, materials for solid propellant rocket motors and integral rocket/ramjet combustors for air-to-air missiles, materials for transonic and supersonic engines, and highly survivable, repetitive use, unmanned systems. This programs also provides materials and manufacturing methods to reduce the acquisition costs of these engines. Engine O&M costs are supported in this area through work on lower cost and more durable turbine vane and blade materials which will decrease the frequency of overhaul and reduce blade replacement cost.

AFML TPO NUMBER 4, FLUIDS, LUBRICANT, AND ELASTOMERIC MATERIALS

The efforts in this area, involving some FY79 \$4.3 million are aimed at materials and supporting technology for lubricants, energy transfer fluids, fluid containment and sealing. In the area of lubrication, materials are developed for liquid, semisolid, and solid lubricants for aircraft, spacecraft, and cruise missiles along with an understanding and prediction of their performance. Fluids work primarily involves materials for hydraulic fluids and related heat transfer applications. Fluid containment and sealing efforts provide fuel tank sealants, fluid system seals, and expulsion diaphragms. The various areas encompass the complete scope of activity from synthetic chemistry to the engineering aspects involved in application to systems.

Within this TPO there are ten thrusts. Hydraulic Fluids involve efforts on high temperature, nonflammable hydraulic fluids. Programs in Fluid System Seals are concerned with seal systems for use with non-flammable fluids, cryogenic cooler seals, and expulsion diaphragms for SAMSO systems. In the thrust on Integral Fuel Tank Sealants, emphasis is on O&S cost reduction, life prediction, and exploratory development. A new thrust, Fluids, Lubricants, and Elastomers for Cruise Missiles, is focused on development of high temperature fluids and seals for ASALM with ten year storage capability and on corrosion inhibiting lubricants for the ALCM F107 engine. Another new thrust, Solid Lubrication for Rolling Element Bearings, covers development of solid lubrication systems for rolling element bearings used in cruise missiles, oscillating bearings, and satellite and missile gyros.

Instrument Lubrication addresses requirements for lubrication of miniature ball bearings. The objective of Accelerated Life Prediction is to predict the performance of lubricants for space bearings. The thrust on Lubrication Systems Analysis explores oil analysis techniques and engine wear diagnostics. The Turbine Oil Additives thrust is concerned with OSHA approved additives for MIL-L-7808 and with synthetic base fluids to replace petroleum based fluids and lubricants.

Efforts under this TPO impact all aspects of AF operational systems, including aircraft, spacecraft, missiles, and ground equipment. Specific requirements include applications in strategic offense, strategic defense, tactical warfare, airlift, command, control and communications, reconnaissance and surveillance, and mission support. The lubricants, fluids and elastomeric materials are all high cost operational and support items. From a performance point of view they play significant roles in space systems and communications capability, while major step function improvements in cost savings can be shown for ballistic missile systems and aircraft.

AFML TPO NUMBER 5, PROTECTIVE COATINGS AND MATERIALS

This TPO represents \$9 million of FY79 effort to provide materials and concepts to enhance the survivability of aircrew and vital components of Air Force systems in natural and induced hostile environments. Although related to materials needs discussed in other TPO's, materials considered here have as a primary concern a protective function that is essential to the survival of the crew, structure, avionics, and other critical subsystems of the military systems. Materials efforts covered by this TPO are in the areas of laser hardened materials, protective coatings and materials, and munitions.

Within this TPO there are three major thrusts. Work on Laser Hardened Materials is concerned with satellite components, aircraft hardening, sensor missile hardening, and with response and evaluation of laser hardened materials. In Protective Coatings and Materials the work includes extended life satellite materials, O&S reduction for coatings, and coatings for camouflage and all weather operations. For Munitions the goals are low cost manufacturing methods for projectiles, cases, and propellants and materials for advanced air to air weaponry.

This TPO supports a wide range of Air Force requirements. Among the more critical are the extension of the lifetimes of U.S. satellite systems, protection of strategic bomber and satellite systems against laser weapons, and reduction of O&M cost of operational aircraft. The space stable materials and conductive coatings being developed under this TPO have already had a significant impact on satellite life and provide confidence that the ultimate goal of 7 - 10 year satellite service life can be reached. Providing laser hardness without compromising systems performance dictates the use of passive countermeasures to the greatest extent possible, and this forms the driving function of the AFML laser hardened materials program. Improving the durability, stripability, applicability, and disposability of ordinary aircraft paint and primer coatings will have a large impact on the costs of maintaining the flying AF. The munitions area has a great impact on cost reduction by developing manufacturing method improvements for greater efficiency and lower cost.

AFML TPO NUMBER 6, ELECTROMAGNETIC WINDOWS AND ELECTRONICS

The overall objective in this area is to provide materials and manufacturing processes for optical, electromagnetic, and electronic subsystems. The investment in this area for FY79 is \$12.7 million. Emphasis is in the area of materials and processes for detectors, infrared windows, radomes and antenna windows, high energy laser components, packaging and interconnections, data processing and memories, data presentation, windshields and canopies, microwave devices and energy sources. These materials are required for application to a broad range of electromagnetic and electronic devices, components, and subsystems critical to system operation and survival in natural and induced hostile environments.

Within this TPO there are ten major thrusts. In the area of Detectors work will concentrate on short, medium, and long wavelength sources for acquisition and tracking of man made objects and on mosaic staring sensor arrays to provide a significant increase in sensitivity, resolution, and real time data handling capacity for surveillance and meteorological satellite systems. In Infrared Windows work will be focused on meeting the needs for IR windows and domes for a variety of tactical target acquisition and seeker systems. Radomes and Antenna Windows includes work on broadband high temperature radomes for high performance antiradiation missiles and millimeter wave radomes for all weather target acquisition. In High Energy Energy Laser Components materials will be developed for both windows and mirrors for high energy airborne and spaceborne lasers. Work on Packaging and Interconnections will stress low cost, improved reliability avionics packages. Windshields and Canopies is concerned with the materials, maintenance, and manufacturing of transparent enclosures for aircraft possessing long life, impact and erosion resistance, and high optical quality. Microwave Devices impacts upon producibility of low cost components for ECM and communications equipment. Data Processing and Memories is concerned with complex circuits

for avionics, C³, and space systems. Programs in Data Presentation address airborne information subsystems and solid state cockpit displays. Energy Sources is concerned with manufacturability of new materials for aerospace power supplies.

The current and anticipated efforts of this TPO are designed to provide materials systems which result in lower LCC, enhanced capabilities, and new capabilities for operational and future systems. Laser and infrared window materials, advanced infrared detector materials, radome and antenna window materials, exploratory development on microelectronic reliability, energy source materials -- all of these are specifically directed to achieving enhanced capabilities for command, control and communication, reconnaissance and tracking, information processing, etc. Underlying all of the current and anticipated efforts are such basic characteristics as efficiency, reliability, life cycle costs, and when appropriate, radiation hardening. These can be presumed to be the major driving forces behind these efforts in addition to consideration of achieving low weight and low volume in the electronic devices and components.

TOMMOROWS MATERIALS

The Air Force materials program provides the critical materials and manufacturing technology required to maintain or extend Air Force system capabilities, considering critically needed performance, and life cycle costs. In the structures area, existing state of the art is being extended to new capabilities:

- in aluminum through powder technology and metal matrix composites.
- in titanium through superplastic forming, powder technology and selective reinforcements.
- in composites to new organic matrix materials and ordered polymers.

For aeropropulsion new capabilities are being developed:

- in titanium through titanium aluminides
- in superalloys through eutectics, ceramics, ceramic composites and high temperature metal matrix composites.

Surveillance and electro optical systems will acquire new capabilities:

- in detectors through mercury cadmium telluride and new doped silicon
- in IR Windows through zinc sulphide and zinc selenide
- in radomes through silicon nitride

The Air Force materials program utilizes the expertise of the national and foreign materials and processing industries, as well as the capabilities of the manufacturing and aerospace industries. It integrates the efforts of government academic and industrial communities. It is through this coordinated effort that the technical opportunities can be focussed toward the missions and weapon systems of the Air Force.

for avionics, C³, and space systems. Programs in Data Presentation address airborne information subsystems and solid state cockpit displays. Energy Sources is concerned with manufacturability of new materials for aerospace power supplies.

The current and anticipated efforts of this TPO are designed to provide materials systems which result in lower LCC, enhanced capabilities, and new capabilities for operational and future systems. Laser and infrared window materials, advanced infrared detector materials, radome and antenna window materials, exploratory development on microelectronic reliability, energy source materials -- all of these are specifically directed to achieving enhanced capabilities for command, control and communication, reconnaissance and tracking, information processing, etc. Underlying all of the current and anticipated efforts are such basic characteristics as efficiency, reliability, life cycle costs, and when appropriate, radiation hardening. These can be presumed to be the major driving forces behind these efforts in addition to consideration of achieving low weight and low volume in the electronic devices and components.

TOMMOROWS MATERIALS

The Air Force materials program provides the critical materials and manufacturing technology required to maintain or extend Air Force system capabilities, considering critically needed performance, and life cycle costs. In the structures area, existing state of the art is being extended to new capabilities:

- in aluminum through powder technology and metal matrix composites.
- in titanium through superplastic forming, powder technology and selective reinforcements.
- in composites to new organic matrix materials and ordered polymers.

For aeropropulsion new capabilities are being developed:

- in titanium through titanium aluminides
- in superalloys through eutectics, ceramics, ceramic composites and high temperature metal matrix composites.

Surveillance and electro optical systems will acquire new capabilities:

- in detectors through mercury cadmium telluride and new doped silicon
- in IR Windows through zinc sulphide and zinc selenide
- in radomes through silicon nitride

The Air Force materials program utilizes the expertise of the national and foreign materials and processing industries, as well as the capabilities of the manufacturing and aerospace industries. It integrates the efforts of government academic and industrial communities. It is through this coordinated effort that the technical opportunities can be focussed toward the missions and weapon systems of the Air Force.

for avionics, C³, and space systems. Programs in Data Presentation address airborne information subsystems and solid state cockpit displays. Energy Sources is concerned with manufacturability of new materials for aerospace power supplies.

The current and anticipated efforts of this TPO are designed to provide materials systems which result in lower LCC, enhanced capabilities, and new capabilities for operational and future systems. Laser and infrared window materials, advanced infrared detector materials, radome and antenna window materials, exploratory development on microelectronic reliability, energy source materials -- all of these are specifically directed to achieving enhanced capabilities for command, control and communication, reconnaissance and tracking, information processing, etc. Underlying all of the current and anticipated efforts are such basic characteristics as efficiency, reliability, life cycle costs, and when appropriate, radiation hardening. These can be presumed to be the major driving forces behind these efforts in addition to consideration of achieving low weight and low volume in the electronic devices and components.

TOMMOROWS MATERIALS

The Air Force materials program provides the critical materials and manufacturing technology required to maintain or extend Air Force system capabilities, considering critically needed performance, and life cycle costs. In the structures area, existing state of the art is being extended to new capabilities:

- in aluminum through powder technology and metal matrix composites.
- in titanium through superplastic forming, powder technology and selective reinforcements.
- in composites to new organic matrix materials and ordered polymers.

For aeropropulsion new capabilities are being developed:

- in titanium through titanium aluminides
- in superalloys through eutectics, ceramics, ceramic composites and high temperature metal matrix composites.

Surveillance and electro optical systems will acquire new capabilities:

- in detectors through mercury cadmium telluride and new doped silicon
- in IR Windows through zinc sulphide and zinc selenide
- in radomes through silicon nitride

The Air Force materials program utilizes the expertise of the national and foreign materials and processing industries, as well as the capabilities of the manufacturing and aerospace industries. It integrates the efforts of government academic and industrial communities. It is through this coordinated effort that the technical opportunities can be focussed toward the missions and weapon systems of the Air Force.

CERAMICS IN ROLLING ELEMENT BEARINGS

BY

Charles F. Bersch

Materials Branch

Naval Air Systems Command
Washington, D. C. 20361

1182

Ceramics in Rolling Element Bearings

Abstract

The feasibility of using hot pressed silicon nitride (HPSN) for rolling elements and for races in ball bearings and roller bearings has been explored. HPSN offers opportunities to alleviate many current bearing problems including DN and fatigue life limitations, lubricant and cooling system deficiencies and extreme environment demands. The history of ceramic bearings and the results of various element tests, bearing tests in rigs and bearing tests in a turbine engine will be reviewed. The advantages and problems associated with the use of HPSN in rolling element bearings will be discussed.

Introduction

Ceramic bearing technology is presently in the Materials Research and Development stage, that is, the feasibility of using hot pressed silicon nitride in rolling element bearings (ball bearings and roller bearings) is being explored. There is a simultaneous attempt to demonstrate that feasibility to the bearing community. Subsequent sections of this paper describe briefly why and how this effort was initiated and where it appears to be going.

The essence of the current effort is a study of how hot pressed silicon nitride performs in the various functions demanded of a bearing material, including studies of when it fails, how it fails and why it fails, in order to provide guidance for optimization. Out of such attention has come the awareness that the quality of the surface is at least as crucial as the quality and uniformity of the material. In over-simplified terms, the surface finish must be smooth to less than 1μ inch AA and there must be no subsurface grinding damage.

Before proceeding, it seems appropriate to amplify on the distinctions between a materials R&D effort and a bearing R&D effort. Earlier investigations^{1,2} of ceramics as materials for rolling element bearings can be described as bearing R&D efforts in that bearing design factors were the variables and the ceramic material and the associated processing were considered as givens, and ceramics worked or they didn't. As it turned out, they didn't. There is a residue of that viewpoint in the current activity in some of the computer evaluation and prediction programs used by the bearing community. These programs, when applied to ceramics, are based on the assumption that ceramics will perform like metals. In the absence of specific knowledge of how ceramics differ, especially in a bearing environment, users of these programs have no choice but to make that assumption. The resultant computer predictions describe a limited future for ceramic bearings. However, as evidence accumulates that good quality, properly machined hot pressed silicon nitride ceramics should not experience fatigue failures and should provide other operational advantages or options, the computer programs will have to be modified to accommodate and predict a new reality.

History

The current ceramic bearing program developed slowly. The first stage was a developing awareness of the vast spectrum

of properties potentially available from ceramics and the belief that within ceramics there must exist a tremendous potential to solve critical Department of Defense materials problems and to provide new performance capabilities for future defense systems.

The decision to concentrate on bearing applications developed out of a synthesis of many factors, such as:

- a. Figures of revolution, by virtue of the absence of corners and edges, afford the best chance of success in structural applications.
- b. Interior applications are safer from impact damage.
- c. Ceramics perform much better in compression than in other loading modes.

Once the ceramic bearings program was conceived and initiated, it quickly became evident that the concept was not new. Zaretsky^{1,2} at NASA Lewis, Sibley and others³ at SKF and Godfrey⁴ had reported earlier efforts which had demonstrated that the concept of using ceramics in rolling element bearings probably had merit, especially if stronger ceramics became available. The advent of hot pressed silicon nitride and high purity, high density aluminas offering new levels of strength and very good uniformity appeared to overcome the earlier deficiencies.

Announcement of the intention to initiate a materials program to explore the feasibility of using ceramics in rolling element bearings exposed an already existing, low level, joint effort by the Norton Co. and Federal Mogul which became the nucleus of the current activity.

Selected Results - General

From the beginning the ceramic bearing program has included both element tests and bearing tests in test rigs. Recently bearing tests in engines have been added. The element tests provide relatively inexpensive qualitative and quantitative information about specific functional capabilities such as rolling contact fatigue resistance, coefficients of friction, wear, elastohydrodynamic lubrication, failure modes, etc. The bearing tests are appreciably more expensive and those conducted on test rigs are generally of an accelerated nature, that

is, the bearings are typically grossly overloaded to provide for failures within a timeframe that is manageable. The advantages of testing actual bearings include:

- a. The fabrication of the bearings demands production of material in appropriate sizes and highlights production requirements and cost drivers.
- b. The fabrication of the bearings demands demonstration of machining capabilities. The need to machine actual bearings has exposed various problems.
- c. Designers and fabricators are confronted by the need to recognize and provide for material differences such as higher modulus, lower density, and, in some cases, lower thermal conductivity.
- d. New concepts are needed to mount ceramic bearings or to attach them to shafts.
- e. Testing of actual bearings provides information unavailable from element tests, both because it simultaneously combines the features of all the element tests and because it includes factors not addressed by element tests. Where element test data contradicts bearing test experience, one must go with the latter.

Selected Results - Element Tests

A quick summary and evaluation of the element tests indicates:

- a. Hot pressed silicon nitride is the only currently credible ceramic candidate for rolling element bearings.
- b. Silicon nitride of adequate quality and with satisfactory surface quality (surface smoothness better than 1 μ AA and no subsurface damage) may never experience fatigue failures.
- c. Silicon nitride and conventional lubricants provide essentially the same lubrication and elastohydrodynamic lubrication characteristics

as do bearing steels with the same lubricants.

- d. The coefficient of friction of unlubricated silicon nitride against itself is about the same as that of lubricated steel on steel. However, there are indications that as the temperature rises, the friction of silicon nitride against itself rises. The prospects for very high temperature unlubricated bearings of silicon nitride are not ruled out but appear limited.
- e. Silicon nitride appears to wear much more rapidly than most ceramics, both against itself and against steel. This may not be a factor in roller bearings which experience only rolling contact, but may be important in ball bearings where both rolling and sliding occur. Current evidence suggests that wear is a function of surface finish and that wear may be eliminated when surface smoothness is measured at less than 1μ inch AA.
- f. Silicon nitride usually fails by spalling, as do bearing steels. In rolling contact fatigue (RCF) tests some failures have been caused by inclusions in the materials. Numerous failures have been attributed to slow crack growth of subsurface machining damage, possibly with an assist from the high Hertzian stresses used in RCF tests. The remaining RCF failures have been associated with Hertzian cracking attributable to loads far in excess of those encountered in real bearings. (In rolling contact fatigue tests there have been no failures at 600,000 psi, few failures at 700,000 and many instances of suspended tests after over 100 million cycles at 800,000 psi. Hertzian stresses in roller bearings may be under 100,000 psi).
- g. Silicon nitride has failed quite rapidly after lubricant shutoff during RCF tests. On the other hand, roller bearings have run as much as 120 hours without damage after lubricant shutoff in the test rig and for several

hours in an engine without damage. It is uncertain whether the very high stress of the RCF test (800,000 psi Hertzian stress) versus the more normal stress in the actual bearings can account for the different behaviors.

Selected Results - Bearing Tests in Rigs

The initial objective was the fabrication, assembly, test and evaluation of a turbine engine main shaft roller bearing. This particular bearing was chosen for two reasons: 1) the rotating velocity of turbine engines is limited by the ability of the outer races of the bearings to cope with the centrifugal forces of the rollers as well as the loads they are intended to carry, and the lower specific gravity of silicon nitride versus bearing steels (2.4 vs 6) promised to ease that problem; and 2) roller bearings experience essentially only rolling contact forces whereas ball bearings also encounter slipping and sliding, which introduces a somewhat uncontrollable unknown. It was thus planned to conduct a simple substitution of ceramic rollers for metal rollers, with no changes in lubrication or any other factor except to redesign the crown on the roller to compensate for the difference in Young's modulus.

Six 55m bore bearings were fabricated, three having silicon nitride rollers and M50 steel races and three having silicon nitride rollers and races. Each bearing had twenty ceramic rollers 0.345 inch in diameter and length. The races had a 2.25 inch bore and 3.74 inch outer diameter. The design operating conditions were for speeds up to 65000 rpm and radial loads up to 400 pounds. The available test rig was limited to 10000 rpm so that high DN capability could not be tested directly. Instead, two bearings of each type were tested under overload conditions to simulate the heavy outer race loading that would be sustained in high speed operation. The bulk of the testing was performed at a speed of 10000 rpm and 2500 pounds load. (Under these conditions, the calculated L_{10} life of a similar, all steel bearing is 120 hours.) The tests were highly successful. Testing of the two steel race bearings was suspended after 221 and 641 hours, respectively, of total test time. Testing of the all ceramic bearings was suspended after 62 and 331 hours. The tests were suspended because the programmed funding had been expended and the test equipment was scheduled for other work. All of the bearings were in excellent condition when the tests were suspended.

Since prediction of bearing performance is based on statistical parameters, the next objective in this program was to make ten bearings and test them to failure, to learn how they fail and to get a feel for the distribution of their lives. The shaft speed was 5400 rpm and the radial load was 5050 pounds (408,000 psi Hertzian stress). Overall the results summarized in Table 1 were encouraging.

- a. The L_{10} life was 45 hours, in comparison with an AFBMA calculated L_{10} life of 21.6 hours for a similar all steel bearing.
- b. Bearings 2, 5 and 6 used the same ceramic rollers in three sets of steel races.
- c. After 365 hours of full load testing, bearing 9 was run at a 2000 lb radial load for an additional 117 hours with the lubricant shutoff without sustaining damage.
- d. Both steel race and ceramic roller failures occurred. All the ceramic roller failures except one could be traced to the combination of high loading, full roller contact and unblended roller corner radii-- an unfortunate combination of circumstances that undoubtedly reduced the L_{10} life.
- e. The one "bad" result, bearing 10, was a massive failure of several rollers, subsequently attributed to an isolated, irregular surface finishing procedure during the preparation of the roller blanks. This failure was useful in two ways. It illustrated what would happen in the event of a massive failure, thereby serving to inhibit unchecked speculation, and it reaffirmed the critical importance of the surface quality of ceramics to their performance in bearings.

There have been several subsequent bearing rig test projects. Most notable are two in which ceramic elements (balls and rollers) were tested side by side with steel elements in a high speed test rig. Test speeds went up to 71500 rpm (2.5 million DN).

General observations and conclusions from a review of

bearing rig test results include:

- a. There appears to be considerable potential for silicon nitride ball bearings and for silicon nitride roller bearings, both with steel races and with ceramic races. But the future of all-ceramic bearings versus ceramic element and steel race bearings has not been sorted out.
- b. Silicon nitride rolling element bearings may be attractive for some applications solely because of the excellent fatigue life of silicon nitride. (It is not yet clear whether some of the benefit may be offset by the higher modulus of the silicon nitride--or whether design techniques can take care of the higher modulus.)
- c. The low specific gravity of silicon nitride in rolling elements proffers higher DN numbers, and it also offers higher fatigue life (quite apart from the excellent prospective fatigue life of ceramic components) by virtue of the lower loading on the outer race and the opportunity to reduce the preload.
- d. Bearings with silicon nitride rolling elements seem to run cooler than steel bearings. So far ball bearings seem to do better than roller bearings. There is no data available for bearings with ceramic races, but conceivably they might run even cooler. This feature might lead to smaller lubrication systems because of reduced coolant requirements.
- e. Silicon nitride rolling element bearings have performed outstandingly in lubricant-starved situations. This is probably related both to the low coefficient of friction and the cooler operation, but considerably more investigation is required before one can try to capitalize on it.
- f. Silicon nitride rolling element bearings run noticeably more quietly than comparable all

steel bearings. The reasons, and any potential benefits, are unclear.

Selected Results - Bearing Tests in Engines

As the ceramic bearings program progressed and modest successes accumulated, interest in testing bearings in actual engines increased. Throwaway engines used to power cruise missiles and non man-rated engines used to power target drones seemed to be candidates both for tests and for early applications of ceramic bearings. They were attractive for tests because the consequences of a bearing failure were not known and their relatively low costs reduced the risk. They were attractive for early applications because they were not man-rated and because it seemed likely that ceramics might satisfy their unusually severe environmental and operational requirements better than metals.

The Teledyne J402 family of engines fitted these criteria excellently. The J402-CA-400 engine is used in the Harpoon missile and the J402-CA-700 engine is used for the VSTT target drone. In both cases the rear bearing is contained essentially within the burner can and does not have recirculating lubrication. The Harpoon bearing is fitted with a grease cup containing 15cc of Krytox grease while the VSTT rear bearing is lubricated by a 60 cc/min fuel flow through the bearing.

Six all-ceramic bearings were made to be tested in the VSTT engine. The intention was to demonstrate the utility of a ceramic bearing in an engine and to explore the possibility of operating the engine without lubrication for the bearings.

Table II summarizes the results obtained with the first five bearings. Test 4 was a complete success, with 48 minutes total time without lubrication. Tests 1 and 2 were qualified successes in that bearing failure followed failure of some other component. Tests 3 and 5 were partial successes; the failure in number 5 has been attributed to poor surface quality on the bearing surface of the inner race. The cause of failure in number 3 is not known at present. It was reassuring to note, in all cases, that bearing failure did not result in freeze-up and subsequent engine damage; rather, in the most extreme cases, the failed component was pulverized and the shaft continued to rotate till shutdown.

This test program is continuing to expand experience with ceramic bearings in engines and to pursue further the prospect

for a successful bearing that would operate without the need for lubricant or coolant after indefinite storage. The design simplicity, cost savings and system reliability are very attractive.

At least two other projects are underway to explore the use of ceramic bearings in engines. The Army is exploring the prospects of ceramic element bearings and maybe all-ceramic bearings in the 10KW Gemini turboalternator.⁵ Recently two ceramic ball-steel race bearings were run at 93500 rpm for over 800 hours.

The Air Force recently initiated a Manufacturing Technology program to produce hybrid (ceramic rolling elements) and all-ceramic bearings for the Williams Research Company F107 (Cruise Missile) engine.⁶ They are interested in a retrofit replacement for the present metal bearings.

Problem Areas

The first requirement for a viable ceramic bearing technology is the availability of a bearing quality material. At present, good quality hot pressed silicon nitride material is available only in pilot-plant quantities, not production scale quantities. Also, it is available only in hot pressed billets that necessitate extensive diamond grinding to be converted to bearing components. (There is some current effort addressing pressing to shape--that is, pressing rough balls and cylinders). Lastly, Norton's NC 132, the material used so far almost exclusively, is not necessarily the optimum bearing material.

The second requirement for a viable ceramic bearing technology is the ability to machine silicon nitride into bearing components with acceptable surface quality (surface finish and subsurface damage) at acceptable cost. Excellent progress was made recently with balls but much remains to be done with rollers and races.

The third requirement for a viable ceramic bearing technology is the ability to measure and control the quality of the material and its surface. Substantial improvements in NDT/I techniques are required, especially to assess the presence and extent of subsurface damage in a flat black material.

In addition to the above, massive amounts of information and data are needed to address many issues such as load-life relationships, material characterization, design modifications

necessitated by differences in modulus, toughness, specific gravity, thermal conductivity, etc.

Attractive Features and Prospective Applications

Sprinkled throughout the foregoing are many attractive features of silicon nitride as a rolling element bearing material such as low specific gravity, outstanding fatigue life, attractive lubrication (and non-lubrication) characteristics, low thermal conductivity, low heat generation and low noise generation. To those can be added electrical nonconductivity, wide thermal stability range and excellent corrosion resistance.

Many or all of the above features offer prospective solutions to high DN requirements, extreme endurance requirements, lubrication problem areas, corrosion prone applications, stray current problem areas, extreme thermal environments, prolonged storage and minimum coolant requirements.

References

1. Zaretsky, E. V. and Anderson, W. J., "Rolling Contact Fatigue Studies with Four Tool Steels and Crystallized Glass Ceramics", J. Basic Engineering, TRANS ASME, Series D, 83, 603 (1961).
2. Parker, R. J., Grisafee, S. G. and Zaretsky, E. V., "Rolling Contact Studies with Four Refractory Materials to 2000°F", ASLE Trans., 8, 208 (1965).
3. Taylor, K. M., Sibley, L. B. and Lawrence, J. C., "Development of a Ceramic Rolling Contact Bearing for High Temperature Use", Wear, 6, 266 (1963).
4. Godfrey, D. J. and Taylor, P. G., "Inorganic Non-Metallic Bearings, with Special Reference to Silicon Nitride", Special Ceramics 4, p. 265 ed. by P. Popper, British Ceramic Research Association 1967.
5. Contract DAAG53-76-C-0228 from U. S. Army Mobility Equipment Research and Development Command, Electromechanical Division, Fort Belvoir, VA 22060 to Solar Group of International Harvester Company, San Diego, CA 92138 with sub-contract to SKF Industries, Inc., King of Prussia, PA 19406.
6. Contract F33615-78-C-5110 from Air Force Systems Command, Aeronautical Systems Division, Wright-Patterson AFB, OH 45433 to SKF Industries, Inc., King of Prussia, PA 19406.

TABLE I

SUMMARY OF RESULTS OF 10 ROLLER BEARINGS RUN IN TEST RIG

<u>Bearing No.</u>	<u>Endurance Test Hrs*</u>	<u>Comments</u>
1	846	Test suspended. Good condition.
2	164	Outer race failure.
3	461	Roller spalls (2) and outer race spall.
4	146	Roller spall and damaged races.
5	83	Inner race failure. Rollers were reclaimed from #2 test bearing.
6	26	Outer race failure. Reclaimed rollers from test #2 & #5 still in good condition.
7	185	Roller spall and damaged races. Assembly contained slightly deviate rollers.
8	222	Roller spall and inner race spall.
9	365	Endurance test suspended after 365 hours. Bearing tested additional 117 hours under lube shutoff conditions**. Final condition good.
10	21	Previously run 117 hours as lubricated companion bearing in lube shutoff test for #9. Failure with severe race and roller damage.

*Endurance test conditions: 5400 rpm. ~ 200°F. Load 5050 lb. (408.5 Ksi Hertz). AFBMA L₁₀ for M50 steel = 21.6 hours.

**Lube shutoff conditions: L₁₀ for Si₃N₄ = 45 hours. 5400 rpm. ~ 210°F. Load 2000 lb.

TABLE II

SUMMARY OF RESULTS OF 5 ROLLER BEARINGS RUN IN VSTT ENGINE

<u>Test No.</u>	<u>Date</u>	<u>Lube Flow</u>	<u>Test Time</u>	<u>Results</u>
1	8-19-77	60cc/MIN.	17 MIN.	Bearing failed @ 34,000 RPM (Retaining ring failure)
2	11-11-77	60cc/MIN.	5.1 HRS.	Visual inspection after 1 HR: Bearing in excellent condition. Continued testing - turbine rotor failed after 4 HRS. of scheduled 5 HR. run.
3	3-9-78	60cc to Zero	2 HRS.	Shaft @ 39,000 RPM - 15 MIN. - Zero lube. Shaft @ 41,200 RPM - 3 MIN. - 10cc lube. Attempted 41,200 RPM with Zero lube; Bearing temp climbed steadily - Test aborted - Outer race failed on rundown.
4	3-31-78	60cc to Zero	1 HR. 41MIN.	Shaft @ 41,200 RPM - 22 MIN. - 10cc lube Bearing temp 627°F Shaft @ 41,200 RPM - 4 MIN. - 0 - 10cc lube Bearing temp 670°F Shaft @ 39,000 RPM - 33 MIN. - Zero lube Bearing temp 573°F Bearing in excellent condition.
5	5-11-78	600cc to Zero	35 MIN.	Shaft @ 39,000 RPM - 3 MIN. - Zero lube Bearing temp climbed steadily Test aborted - Inner race disintegrated Remaining new bearing returned to manufacturer for race surface analysis.

Bibliographical Sketch

Charles F. Bersch was born in Sheboygan, Wisconsin on January 23, 1927. He graduated from St. Norbert College in W. DePere, Wisconsin with a B.S. in Chemistry in 1951. After eight years in the Plastics Section of the National Bureau of Standards, he joined the Materials Branch of the Bureau of Aeronautics, which became, successively, the Bureau of Naval Weapons and the Naval Air Systems Command.

Mr. Bersch has over 25 years experience in research, development and application of nonmetallic materials, especially composites, adhesives and ceramics. At present he is head of the Nonmetallic Materials Section in the Materials Branch, Engineering Division of the Naval Air Systems Command. He is a member of the American Chemical Society and the American Association for the Advancement of Science and a Fellow of the American Ceramic Society.

GROUP TECHNOLOGY
KEY TO MANUFACTURING PROCESS INTEGRATION

BY

Dan L. Shunk, Captain, USAF

Materials Division

Air Force Materials Laboratory
Wright-Patterson AFB, Ohio

1198

GROUP TECHNOLOGY
KEY TO MANUFACTURING PROCESS INTEGRATION

Abstract

In a survey of most critical manufacturing technology needs, aerospace companies listed group technology (GT) as their number one priority. In engineering design and manufacturing planning, properly applied GT has the potential to: reduce new parts inventory by at least 25%, substantially reduce in-process inventory, cut the cost of part programming by 50% and provide the key to generative process planning. With all of this potential, one might expect a concerted rush to apply this simple yet powerful concept; however, even though it has been around for more than 50 years, GT has only begun to be applied in American industry. There have been basically two reasons for this: (1) the absence of a strong accepted theoretic foundation, and (2) the absence of a standardized implementation approach. Recently, within the Air Force Program for Integrated Computer Aided Manufacturing (ICAM) both of these barriers have been overcome. This paper will explore the background and potential of GT and the Air Force approach to maximize its benefits.

Introduction - The USAF ICAM Program

The Integrated Computer Aided Manufacturing (ICAM) program of the Air Force is a long-term project which includes the development of a number of modular sub-systems designed to computer-assist various phases of design, fabrication and distribution processes, and the management hierarchy associated therewith, according to a prioritized master plan. At appropriate times, these modules, which are mutually compatible, will be combined to give a comprehensive control and management package which is capable of continual adjustment as production needs and state-of-the-art change.

In essence, the ICAM program provides "seed money" to advance the frontier of the technology in general. As a large customer with great potential for gain, the Department of Defense is willing to fund what might be termed "risk capital" for extending the technology. Industry is not geared to fund a program as ambitious in scope, primarily because of the long term pay-off. With government funding and industry cooperation the technology can be developed and applied in a totally open manner; industry can acquire and apply the elements freely.

The Basis of ICAM

The ICAM program of the Air Force is visualized as a complex cooperative effort between the Department of Defense and industry. Among its constituent elements are system components (computer hardware; programming software; integration of new and existing systems, such as IPAD), utilitarian components (mechanism of operation; manuals; educational activity), and program implementation components (the development plan).

The concept defining the construction of the ICAM program system is called "manufacturing architecture", that is, the integrated collection of all the phases associated with the making of a product. Among these phases are the following:

- Executive control
- Management control, with its planning and reporting features

- Technical support
- Process control
- Direct manufacturing

There is, of course, continual interplay and communication up and down between these phases as well as interaction between various subphases within a phase. The nature of the subphases is dependent upon the type of manufacturing operation being performed. In Figure 1 are shown three common operations (milling, sheet metal forming, and assembly) and various representative subphases which could be associated therewith, grouped according to the appropriate phase.

The ICAM program, through its manufacturing architecture, identifies the system structure, analyzes the many interactions and functions, and establishes the framework and standards to integrate the functional elements into a unified construction to meet present and future needs. A means of linking is Group Technology (GT).

The View of Group Technology by Others

Industry has come to accept the diagram shown in Figure 2 as very descriptive of the percentages of the life of the average workpiece in batch type production. It is widely accepted that only $1\frac{1}{2}\%$ of the total time has the workpiece in cut. In order to improve productivity, the American manufacturing community must increase this $1\frac{1}{2}\%$ figure. GT has the theoretical ability to do exactly this. GT not only tackles the reduction of time required for positioning loading, and gaging but also reduces the moving and waiting time. This is accomplished by identifying the families of parts that flow through manufacturing and working on the larger lots and the more highly related parts in a more efficient manner.

A survey by CAM-I (Computer Aided Manufacturing - International, Inc.) in April 1975, shown in Table 1, also provides strong evidence of the importance of the priority status of Group Technology applications for batch type manufacturing industries not only in the United States but also in Europe and Japan. The survey clearly points out the consensus high priority for GT and the number one priority given by the aerospace participants.

The ICAM View of Group Technology

As the architecture forms the environment of ICAM, Group Technology forms the basis for linking the features of the environment of ICAM. The concept of Group Technology pervades all of the thinking of ICAM and productive manufacturing. As one views the ICAM roadmap shown in Figure 3, one must remember that this roadmap is for the development and use of Group Technology tools. But the concept of Group Technology extends far beyond the coding and classification methods. GT is truly a philosophy. It requires strict definition of attributes and requirements; it requires the organization of these attributes and requirements into generic strata, and the development of solutions to these strata based upon a common principle.

The architecture of manufacturing is evolving. And in this same context the current ICAM projects on manufacturing control-material management and material flow characteristics are all evolving as well. The Group Technology philosophy is present in each. But also the Group Technology modus operandi is present in each. Manufacturing control deals with the control of the shop that has GT cells as well as common functional cells. It must attain information as parts travel intra- and inter-cell. Material flow characteristics must handle families of parts in an efficient manner.

The amazing insight attained by the concept of Group Technology even pervades such areas as simulation and data base design. By using the GT concepts, "smart" simulations and "smart" data bases are truly realizable. These smart simulations and smart data bases would be capable of identifying a situation and relating that situation to others of the same generic type. What evolves is almost artificial intelligence.

The shop floor processes are the most graphic, tangible display of the GT concept. Part families are introduced and manufacturing cells are formed to manufacture these parts. The shop floor is reorganized.

In summary, ICAM sees the potential of a GT-based manufacturing environment. The efficiencies are philosophically attainable but much work is required to move GT from philosophy to practice. The ICAM seed money hopes to continue this migration. This paper outlines the continuation of the significant push of the Group Technology state-of-the-art started by AFML Project F33615-77-C-5012 by SofTech and Penn State University, called "Task II" because the GT effort was the second task in a three task initial solicitation.

The Previous ICAM Group Technology Project

This previous contract titled "ICAM Task II" resulted in the identified needs and roadblocks seen by industry to GT applications. Table 2 of this section summarizes the prioritized, overall needs of manufacturing control and design engineering. From analysis of Table 2, it can readily be determined that industry views GT as broadly as ICAM. From aiding in part coding, to design retrieval, to process plan development, to forming part families, to machine loading - the GT characterization code (GTCC) scheme developed may be the "glue" that binds all of design and manufacturing.

Task II began by conducting one of the most comprehensive surveys and analyses of the Group Technology state-of-the-art. The survey work was broken into three primary portions:

- 1) survey of needs
- 2) survey of coding parameters
- 3) world survey of coding systems

From this foundation evolved a comparative evaluation of currently available commercial coding systems. Parts were supplied for coding then the code segments were evaluated for their utility. Each coding vendor had something novel and useful about his system. Each met many of the needs identified. But it was the conclusion of the Task II coalition of companies that:

"....no existing commercial system will meet the needs of ICAM."

The Task II team then tackled the problem of the conceptualization of a characterization code that would meet the ICAM needs. What evolved is the concept of "ICODE" which is the recommended scheme by the Task II contractor. ICODE is a modular GTCC that is based upon the concept of a classification network. ICODE presents several new, exciting possibilities. Among these are:

- a. Coding machines and materials, as well as operations and geometries.
- b. Presenting only the right information to the right people at the right time.
- c. Tying the characterization code to the generic architecture of manufacturing.

The ICODE concept also points out the need for establishment of the theoretical foundation of a GTCC. Such concepts as information needs and information presentation are necessary as well as the more theoretical methodology for network description and network manipulation. All of these techniques have proven feasibility but the applications are for other technical disciplines. What must be done is the derivation of the generic aspects of these applications and the transition of these generic aspects into the manufacturing environment.

The ICAM Current Project

As one can perceive from reading this brief background as to the previous GT work and the view of GT use, the anticipated benefits from the Group Technology concept and the functioning GTCC are significant. The ICAM Program has initiated a follow-on project to move the status of "GT Glue" from philosophy to practice. This migration requires three (3) related tasks to be conducted. The first is the continued development of the theoretical foundation for the second and third tasks which characterize the GT applications in manufacturing and develop a GTCC Information Base focused on sheet metal which is capable of testing existing code segments for their usefulness and developing new code segments where the needs arise. Finally an option is allowed which shall take the sheet metal portion of the GTCC and demonstrate its worth, while developing some support software functional requirements.

Conclusion

Thus the philosophy shall evolve into a useful product. A goal for the GTCC is shown on the ICAM GT roadmap, Figure 3. The use of GT in process planning is quite evident. It is this mechanism which shall be developed by the ICAM current project. But GT is not only to be used by process planning. Figure 4 shows how GT through a CC can be used through-out manufacturing. A final remark is necessary prior to the conclusion of this paper. The GTCC will not be directly applicable to all manufacturing situations. Just as Mitrofanov, Opitz and others have suggested, the actual resolution required from the GTCC shall be its flexibility in management philosophy. The secret of the GTCC shall be its flexibility in allowing each manufacturer to tailor the GTCC to his needs and yet continue to conform to the overall structure and be able to communicate at a common, higher level of abstraction with other manufacturing organizations. Manufacturing organizations should not expect to be able to directly install a GTCC without first analyzing the goals of a GTCC for their organization. One consistent theme throughout the previously conducted Task II GT study was that management must understand the commitments required for a GTCC installation as well as the benefits perceived. Another secret to the development of the GTCC shall be the ability of the developer to incorporate existing code segments into the overall philosophy. It would be naive to suggest that manufacturers drop their existing C.C. systems in order to tie in with the ICAM developments. Just the opposite is actually the case. It is the responsibility of ICAM to insure that existing codes are compatible with the GTCC and that the only new developments are in virgin areas where no code segments exist.

MACROVIEW OF CAM

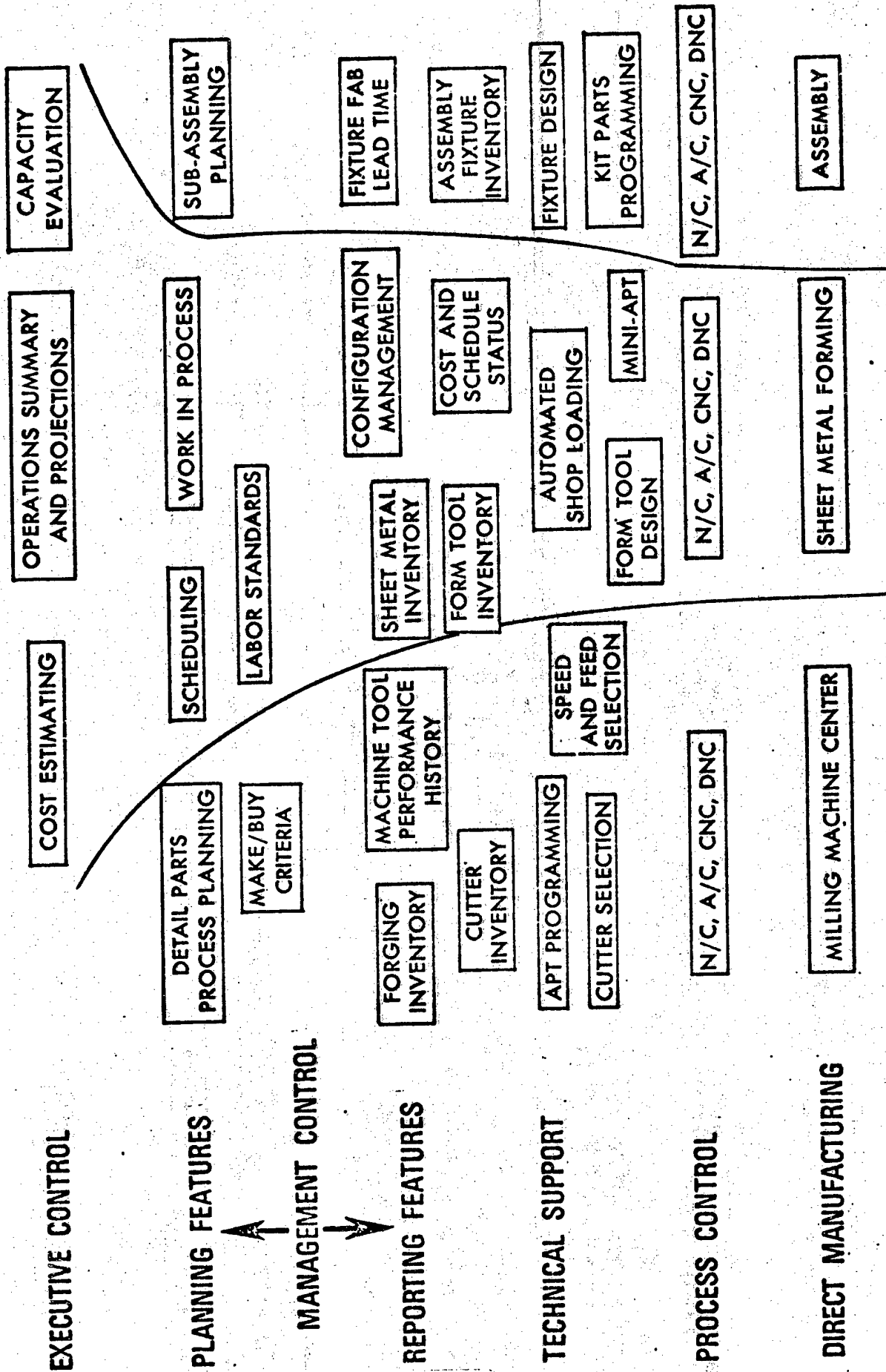
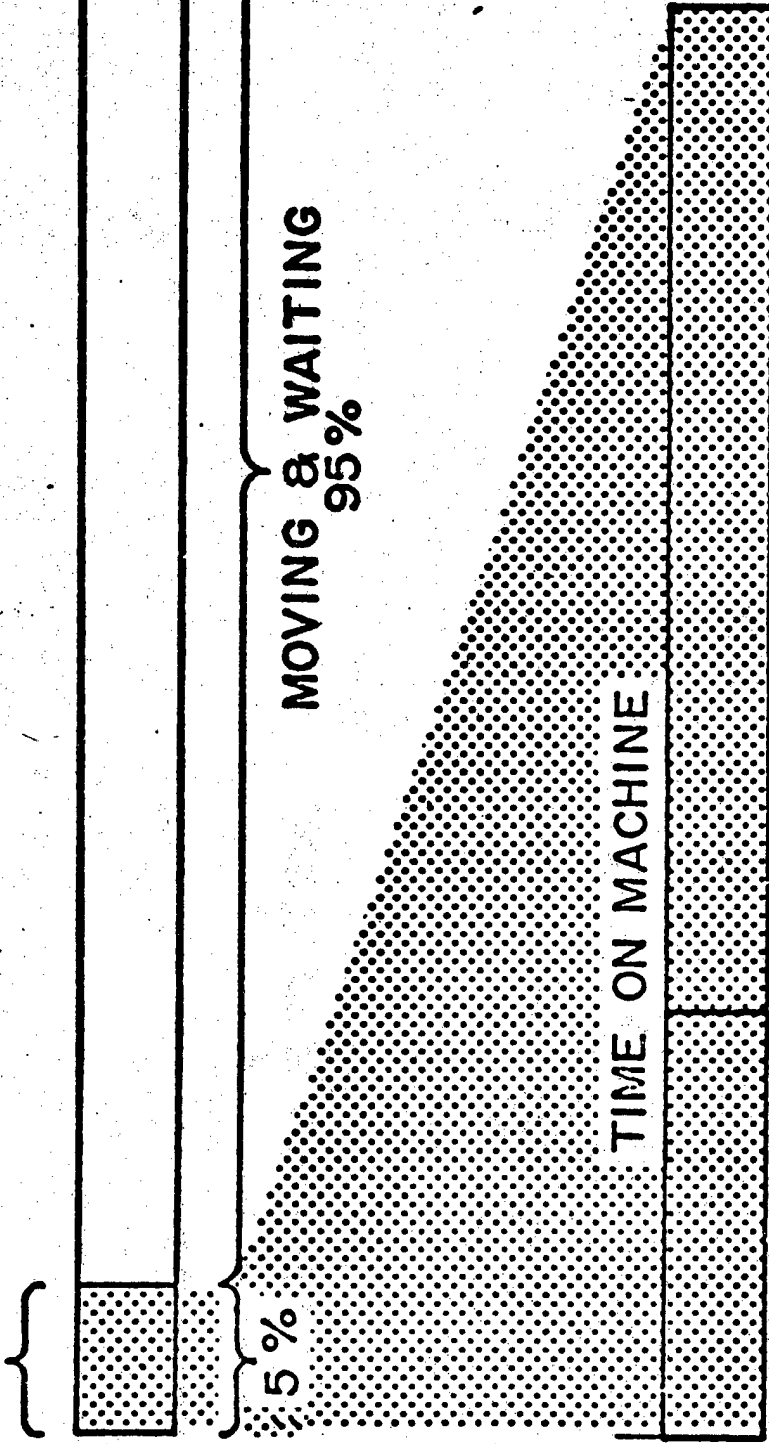


FIGURE 1

TIME IN SHOP

TIME ON MACHINE



MOVING & WAITING
95%

TIME ON MACHINE

INCUT LESS THAN 30% POSITIONING, LOADING, GAGING, IDLE, ETC. 70%

AREA: TIA (CAW)
 THRUST: PLANNING AND GROUP TECHNOLOGY

GOAL: DERIVE A GENERATIVE APPROACH TO FACTORY SYSTEMS PLANNING WHICH RANGES FROM CONSIDERATION OF SHOP FLOOR OPERATIONS TO CEO STRATEGIZING

FY 77 | FY 78 | FY 79 | FY 80 | FY 81 | FY 82 | TOTAL

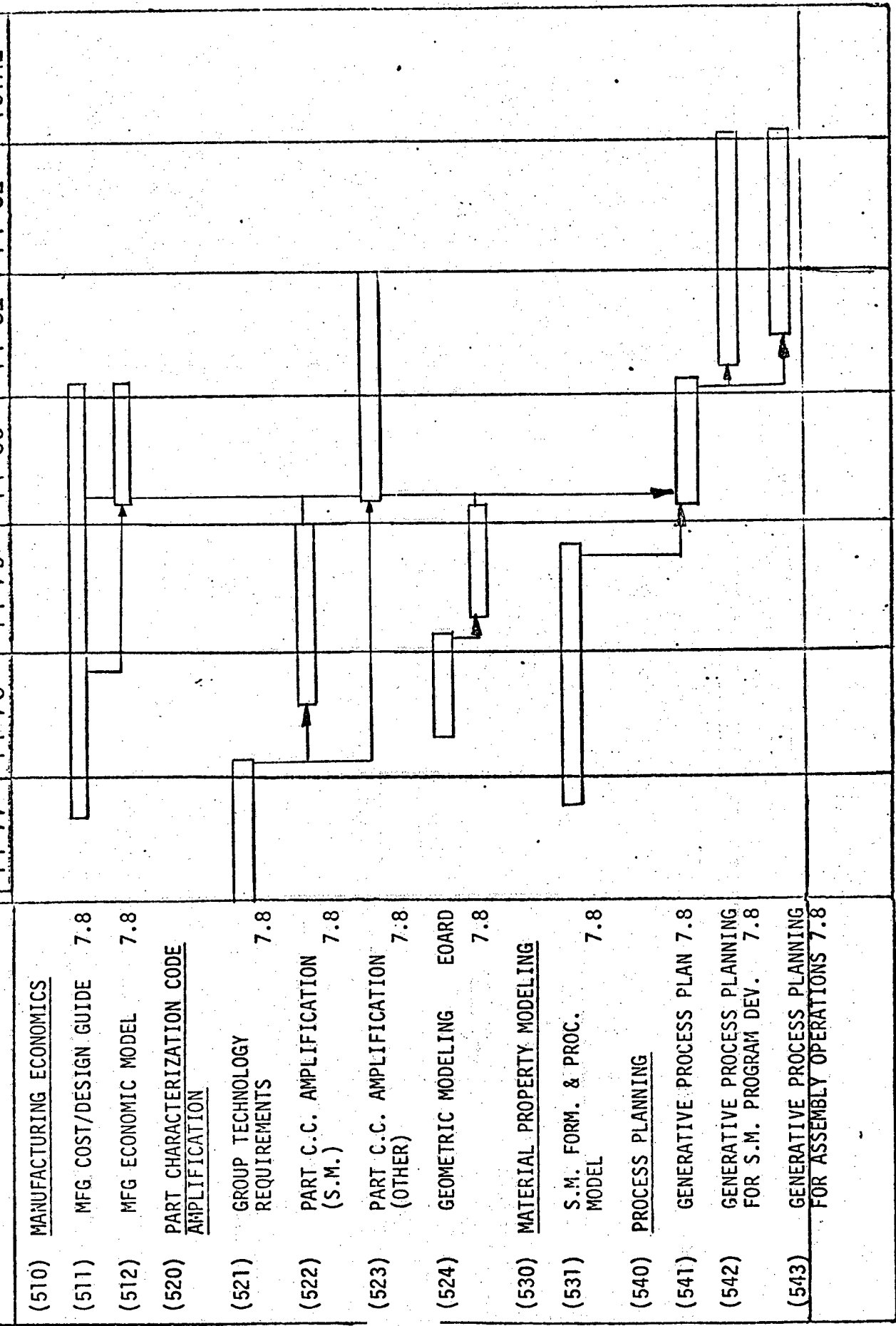


FIGURE 3

G.T. SYSTEM INTERACTIONS

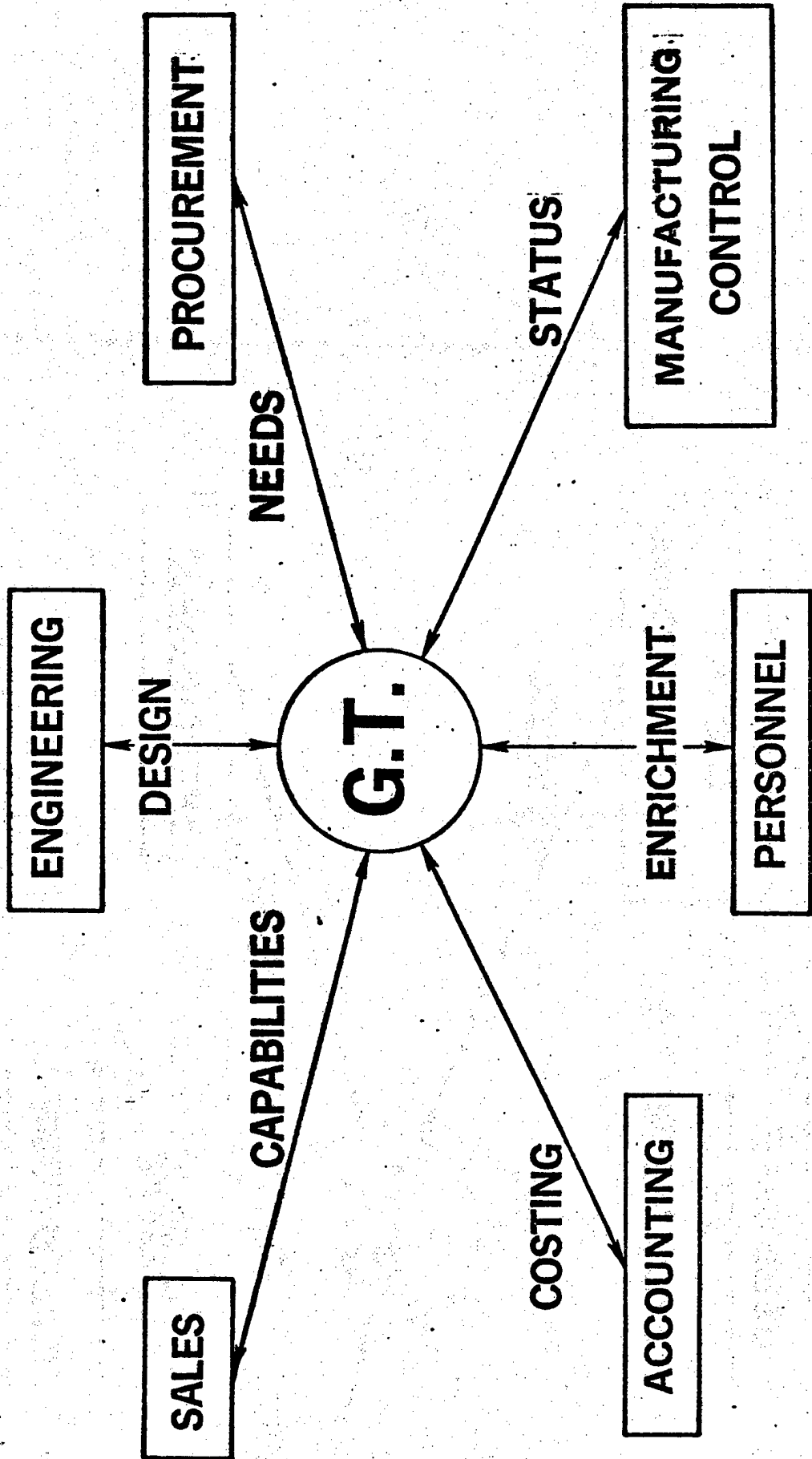


FIGURE 4

TABLE 1

CAM-1 INDUSTRY SURVEY (summary)		PRIORITIES				PRIORITIES			
JAPAN	EUROPE	UNITED STATES	COMBINED	AUTOMOTIVE	ELECTRICAL	AEROSPACE	MACHINE TOOL	RESEARCH	
4	2	1	1	Mfg. Data Base Design	4	1	1	1	6
6	11	9	10	Computerized Mtrl. Handling	9	11	7	6	11
9	11	14	13	Comp. Controlled Transfer Ln.	1	12	12	14	12
3	9	13	12	Comp. Controlled Assy. Line Ops.	8	9	11	10	10
10	7	8	8	In-Process Inspection	10	2	8	11	4
2	8	12	11	Die Sinking	3	8	10	13	9
7	6	2	4	Scheduling	11	3	5	3	7
4	3	10	5	N/C Verification System	11	7	4	7	1
1	7	11	7	Automated Drawing Generation	2	8	9	12	5
3	4	5	3	Interactive Graphics	6	1	3	8	2
5	1	4	2	Group Technology	5	6	1	5	3
11	12	6	9	Adaptive Control (A/C)	7	10	3	9	7
8	5	7	8	Direct Numerical Control (DNC)	13	4	2	4	3
12	10	3	6	Computerized Numerical Control	12	5	6	2	8

TABLE 2

TOP TEN PRIORITIZED OVERALL NEEDS OF A
GROUP TECHNOLOGY CHARACTERIZATION CODE

1. Provide information to form part families.
2. Provide engineering design file retrieval capability
3. Provide data for evaluation of manufacturing capability and economics.
4. Establish part information in standard form.
5. Provide information needed to form part families.
6. Provide methodology for efficient machine loading and operation.
7. Structure and classify manufacturing methods.
8. Provide adaptability to engineering change.
9. Provide for fast retrieval of process plans.
10. Allow establishment of master data base.

BIOGRAPHICAL SKETCH

Captain Dan L. Shunk was born October 18, 1947, in LaPorte, Indiana. He received his BSIE, MSIE, and Ph.D in Industrial Engineering from Purdue University in 1971, 1972 and 1976 respectively. During this time he worked as an Industrial Engineer at Eastmak Kodak, a consultant for Indiana small business and as an Instructor of Production Planning and Control.

Captain Shunk came on active duty in April 1975 at the Air Force Materials Laboratory in the Manufacturing Technology Division. He served on the AFSC Computer-Aided Manufacturing Study and has been affiliated with the Integrated Computer Aided Manufacturing Program since its inception. He is a Senior Member of the American Institute of Industrial Engineers, Charter Member of the Robotics Institute of America. He has published six (6) papers in this and related area; his latest presentation was an invited paper on Group Technology at the International Conference on Production Research in Haifa, Israel.

UNCLASSIFIED

AN ATTEMPT TO PREDICT THE EFFECT OF MOISTURE ON
CARBON FIBER COMPOSITES

BY

Joseph M. Augl

Materials Division

NAVAL SURFACE WEAPONS CENTER
White Oak Laboratory
Dahlgren, Virginia

1213

AN ATTEMPT TO PREDICT THE EFFECT OF MOISTURE ON
CARBON FIBER COMPOSITES

Abstract

The mechanical properties of a carbon fiber composite are functions of temperature, moisture, ply-stacking and angle distribution, and the properties of the individual components (resin and fiber). These properties change on a microscopic as well as on a macroscopic level as the composite is exposed to the environment of its service conditions. Some of the service conditions change the properties in a reversible, some in an irreversible, fashion. An attempt to predict these property changes in carbon fiber composites for a real environment is presented. The main emphasis of the paper is a discussion of reversible mechanical property changes in the light of moisture diffusion, modeling of a real environment micromechanics, modified laminated plate theory and an experimental program to verify these predictions.

While the reversible property changes can be estimated as a function of time, if the environmental conditions (such as climatic environment) and service conditions (such as mission profile) can be sufficiently defined, the predictions of the superimposed irreversible property changes are, at present, of a considerably lower order of certainty. Much more experimental work is required for the understanding of the irreversible property degradation before a sufficiently accurate modeling for prediction of changes in structural integrity can be given with confidence.

Introduction

Fiber reinforced composites will be used more and more as structural materials in advanced military weapons systems such as aircraft and missiles. During the last two decades there have been a number of advances made that allows one to predict the mechanical behaviors of these nonhomogeneous, anisotropic materials. The elastic behavior of a unidirectional lamina and even its strength, its elasto-plastic and its viscoelastic behavior can be reasonably well predicted by micromechanical theories from its constituent properties (resin and fiber). Laminate theory allows us, also, to predict the elastic behavior of multilayer angle-ply laminates. The strength of multilayer angle-ply composites is more a question of definition since there can be various irreversible property degradations without total fracture (e.g., partial cracking of the 90° plies in a $0/90^\circ$ crossplied laminate when loaded in the 0° direction such that the ultimate strain of the 90° plies are exceeded). For practical purposes various design criteria as those described in the Air Force Design Guide are such that the stresses or strain do not exceed values that would lead to intolerable degradation of stiffnesses and to permanent deformations.

Most failure criteria for lamina and laminates are more intuitive, empirical or phenomenological than based on a solid theoretical foundation. Only recently, attempts have been made to predict failure modes and mechanisms under various loading conditions in unidirectional composites by finite difference or finite element methods. It appears that these numerical methods, though not without their shortcomings, will lead to a better understanding of the actual failure mechanisms in composite materials. Notably the finite element method (FEM) is particularly useful because it can be used for modeling various effects (such as multiaxial loading conditions, less than ideal resin-fiber bond strength and debonding, residual thermal stresses, stresses due to thermal excursions, creep under multiaxial loading, and elasto-plastic deformations) on a microscopic scale of the magnitude of less than a fiber diameter and on a macroscopic scale on the order of several ply thicknesses.

Yet the properties of an organic matrix composite will undergo changes partially caused by loading conditions of its intended mission (static, dynamic and thermal) and partially by the environment itself (temperature and humidity). Each of those conditions may lead to reversible and irreversible property changes.

Aside from excessive, mechanical or thermal loading conditions, it appears that moisture will perhaps lead to the most significant property changes in organic matrix composites at least for the matrix dominated lamina properties such as intralamina shear, transverse tensile and both transverse and longitudinal compressive properties. Since moisture will have to penetrate into the composite to affect its properties and since the rate of penetration depends on the temperature and on the moisture concentration these property changes will be gradual, strongly dependent on the thickness of the composite and on the environment it is exposed to. The question is, therefore: will one be able to predict or at least estimate these property changes with time or must one rely on testing combinations of many variables which would quickly discourage the design engineer or should one simply rely on faith and hope for the best?

The purpose of this paper is to present some of the aspects that we feel have to be considered if one intends to predict the changes in composite properties affected by the environment. We do not claim that the approach we have chosen is complete. Thus far we have considered only the "reversible" moisture effects, though, with a considerable effort, irreversible effects also can be treated by FEM. Also, lack of time will not allow us to discuss the subject reasonably detailed for a full appreciation of the rather complex problem area. I shall, therefore, try to sketch the approach we have taken, rather than treat it more rigorously.

Background

Several investigators have presented experimental evidence that the matrix dominated properties of advanced organic matrix composites are degraded by moisture (1-5). This effect increases as the temperature of the composite is raised. (For an example see Figure 1, reference 4). We have also demonstrated that the property deterioration levels out after the absorbed moisture has reached equilibrium with the surrounding humidity (see Figure 2, reference 4) and is therefore, a function of the average relative humidity. This deterioration is reversible for matrixes that are not chemically changed by moisture (as is the case for most amine cured epoxy composites where moisture is thought only to plasticize the resin and thus make it more flexible (see Figure 3, reference 3)). Note that it is not only the glass transition temperature that is lowered but the whole modulus curve is affected far below glass transition temperature and increases as the glass transition temperature is approached.

This is important for the understanding of the deterioration of property in composites. Under reversible property changes it is meant that if the moisture is removed (in vacuum or by heating) the original properties will be regained within the experimental uncertainties. We do not intend to review here all the experimental evidences of moisture effects on fiber reinforced composites but refer only to a number of additional papers dealing with this subject (6-11). The question is: can we quantitatively describe and thus predict these composite property changes in a real environment?

Approach to the Problem

Various investigators have carried out schemes of solving the problem to predict the macroscopic lamina properties from its constituent properties (of matrix and fiber) by analytic or numerical methods (12-16). Finite difference and finite element methods proved to be quite powerful tools in this area of micromechanics (18-21). The Halpin-Tsai equations (see Appendix) that relate the constituent elastic constants ($E_m, \nu_m, G_m, E_{12f}, E_{22f}, \nu_{12f}, G_{12f}$) to the lamina elastic constants ($E_{11}, E_{22}, G_{12}, \nu_{12}$) for any given fiber volume fraction (V_f) are useful for design estimates and rapid computational purposes.

The next step to predict the elastic behavior of multi-layer angle-ply laminates from lamina properties is the subject of laminate theory. Since there are several excellent texts available (22-25) we shall not discuss this subject here but simply state that it is a procedure of summing up the directional elastic properties of all the plies in the composite, to give the overall macroscopic behavior of the laminate.

How can we use these theories for our purpose where we expect that the moisture distribution in a composite will not be uniform at least not until equilibrium will be reached with the environment. There will be a continuous matrix property change throughout each ply and throughout the whole composite thickness.

Let us assume, however, we know this moisture concentration distribution; then we could imagine to build the composite up out of fictitious Δ -layers of finite thicknesses (not necessarily all of the same thickness) though thin enough so that the average Δ -layer properties are not significantly different from its front and back face. Then we

could, using laminate theory, predict the properties of the composite just from the properties of the matrix and fiber, assuming the elastic properties of the matrix and fiber are known as a function of temperature and moisture concentration. These informations are relatively easy to obtain without a great deal of experimentable effort.

That leaves us now with the question of determining the interior moisture distribution. The formalism of solving such problems is analogous to heat conduction and temperature distribution of a body with given boundary conditions. In other words, it is a question of solving the diffusion equation for the laminate with varying boundary conditions since the temperature and the humidity will change over the period of a day and in the average over a month, season and year.

If all this can be done without excessive computational work we would have a reasonable foundation for a prediction of environmental effects.

To summarize, we will have to combine the concepts of moisture diffusion, of micromechanics, of laminate theory and of modeling the environment such that the diffusion equation can be solved. The rest of the paper is intended to sketch some highlights and connected experimental and computational efforts in solving the posed problem. Each of the above mentioned concepts has a sub-set of questions that have to be carefully considered for various problem areas and for a possible reduction and optimization in experimental and computational effort.

Discussion

A. Diffusion

We have discussed in some detail questions concerning moisture diffusion in composite materials elsewhere (26). The internal moisture distribution and overall moisture concentration can be obtained from the solution of the Fick's equation:

$$\frac{\partial c}{\partial t} = D_1 (V_f, T, c) \frac{\partial^2 c}{\partial \xi^2} + D_2 (V_f, T, c) \frac{\partial^2 c}{\partial \eta^2} + D_3 (V_f, T, c) \frac{\partial^2 c}{\partial \zeta^2}$$

Where c = concentration, t = time, and D_1, D_2, D_3 are the principal diffusion coefficients

Using a finite difference approach we have derived a solution that describes the change of the principal diffusion coefficients of the composite as a function of the fiber volume fraction (V_f) (see Figure 4, reference 26). The derived curve is applicable for carbon fiber composites where it was assumed that no moisture transport goes through the carbon fibers. Incidentally, the numerically derived curve is almost identical to a curve by Lord Rayleigh derived for an analog electrical conductivity problem (27). It differs, however, from the solution of Springer, et al. (28) who used a simplified thermal model where the transport of moisture is considered essentially in straight paths parallel to the Z-direction of the composite plate without considering the least resistant flux around the fibers.

For the composite characterization, it is necessary to determine the diffusion coefficient and its concentration and temperature dependence either directly from the composite or from the resin by carrying out sorption and/or desorption measurements at various constant boundary conditions (different moisture vapor concentrations and at least at two different temperatures). It might be advisable to combine these measurements also with permeation experiments at different pressures to ascertain whether or not the moisture transport is governed by diffusion of moisture through the solid or through pores. Figure 5 shows an example of the temperature and moisture concentration dependent diffusion coefficient of Hercules 3501-6 resin (to be used for the F18 fighter aircraft). (These data were obtained from the total sorption and desorption curves carried out with a Cahn electro balance in a closed system at various relative humidities at 30° and 50°C).

It becomes obvious that with a concentration dependent diffusion coefficient a numerical method (finite difference method) is required to solve the diffusion equation.

B. Modeling of the Environment

The environment of an aircraft will change; first: simply due to hourly changes in temperature and humidity which determine the boundary conditions of the exposed composite; second: due to mission profiles (e.g., down time, flight hours, supersonic dashes, etc.). We can, of course, do it the hard way and obtain tapes of weather data with hourly changes in temperature and humidity for a given location and solve for each time step the diffusion equation (which we have actually done). As a consequence, there are daily

sorption and desorption cycles at the immediate surface layer. Considering, that one has to run the calculation over several hundred thousand time steps for most practical composites, the computer time may not be without concern.

This brings up the following questions:

1. Can one use some averaging procedure that will allow the use of monthly or even yearly average temperatures and humidities that can be found in encyclopedias or meteorological maps and thus reduce the computational effort?

2. How does one account for surface heating due to sun radiation?

3. Is it possible to use some average diffusivity instead of the full concentration dependent diffusion coefficient?

4. Is it worthwhile to search for an organic coating that will prevent moisture uptake in composites?

We have discussed these questions in some detail before (29) and will give here only the results.

We have shown that one can easily derive a "kinetic average temperature" (T_{kav}) and a "kinetic average relative humidity" (RH_{kav}) which are different from their arithmetical averages) that would have the same effect as if the composite would be exposed to these constant boundary conditions with the exception of a very thin surface layer. It should be pointed out that this averaging procedure requires the knowledge of the material sorption isotherm as shown in Figure 6 (a by-product of the sorption measurements) and some representative seasonal daily excursions in temperature and humidity. This averaging is, of course, not valid for a very thin layer at the surface of the composite where an instantaneous equilibrium with the actual surrounding relative humidity is assumed.

Figure 7 shows the difference between three hourly and monthly average input data. The agreement is excellent. (It should be mentioned that the apparent three yearly oscillation is due to the fact that we had tapes of weather information only over a three year period which we repeated over and over again.)

Even yearly averaging compares quite well with the hourly or monthly averaging as can be seen in Figure 8. This averaging procedure also gives excellent results as to the internal moisture distribution (see Figure 9) where we compared monthly and yearly averages in a 36-ply composite (only half of the symmetrical distribution is shown). Again one observes slight deviations only on a thin surface layer. One can thus derive simple diagrams such as Figure 10 that indicate the time required to obtain various percentages of the equilibrium concentration of moisture as a function of composite thickness.

If the environment of an aircraft (flight time standing on a runway, etc.) can be specified, the change in the average diffusivity due to radiation heating can be estimated and the rate of moisture uptake can be corrected accordingly (29, 30).

The question, whether or not, one can use an average rather than a concentration dependent diffusion coefficient depends of course on the shape of the diffusion coefficient curve and on the excursion in relative humidities over a daily cycle. There is no simple procedure. However, sample calculations with 3501-6 resin, where the diffusivity between 30% and 80% RH does not change very much, show that the differences in these calculations are small in both distribution and total moisture uptake. Therefore, the use of a judiciously chosen average (=concentration independent) diffusion coefficient for a given temperature seems quite permissible. (A forthcoming TR will discuss this subject in more detail.)

As we have shown previously (29) organic coatings will not prevent moisture permeation into composites, at best they will slow down the process. However, it might be that very special fillers such as impermeable inorganic or metallic platelets could improve the barrier capability of paints. A thin metal coating would obviously be a perfect barrier, as we have shown on nylon plates coated with a 1 mil chemically deposited copper film (31).

C. Micromechanics

There are various analytical, statistical, finite difference and finite element approaches to micromechanics. All have the obvious shortcomings of having to use some simplified, mathematically tractable models. Some of these models use regular fiber arrangements (tetragonal-,

hexagonal-, diamond- arrangement, etc.), they assume ideal interfacial bonding, no voids, perfect alignment of the fibers, no residual stress concentration, the matrix has everywhere the same properties as the bulk resin, the fibers have the same diameter and are flawless and both resin and fiber behave linearly elastic. Though it should be noted that the finite element technique can take into account voids, partial debonding between resin and fiber, elastoplastic deformations, viscoelastic phenomena, residual stresses due to cooling from cure temperature, thermal stresses due to heating or cooling, stresses generated due to moisture sorption, effect of multiaxial and multidirectional stresses. Excellent papers on these subjects have been published by Adams (17), Karlak (18), Branca (32), Herakovich, et al (33), and Ebert, et al (34), among others. However, imperfections are usually taken into account, if at all, one at a time, and, in dimensions within a unit cell (= fiber to fiber distance). Micromechanics appears to give some understanding of the various failure mechanisms, the cause and even the location of the initiation under specific loading conditions. Yet, the macroscopic quantitative results differ frequently more than one would like.

How then should micromechanics be of help to us for predictive purposes?

We believe that this can be done by a normalization to real, uniaxial lamina data (standardized to some uniform moisture concentration, preferably dry lamina). If moisture penetrates into such a composite, it would leave most imperfections unchanged with the possible exception of creation of additional debondings.

Thus the only property change would be due to the matrix. (There is no change in fabrication, curing condition, fiber distribution, alignment, voids, etc.). If we know the matrix changes i.e., the changes in the stress strain curves of the matrix as a function of temperature for various uniform humidity loadings then the changes in each Δ -layer can be predicted and therefore those of the total composite. The elastic stress-strain response of each Δ -layer can then be given by an expression (35, 36):

$$\left[\sigma_j(T, C_{H_2O}, t) \right]_{k\Delta} = \left[\bar{Q}_{ij}(T, C_{H_2O}, t) \right]_{k\Delta} \left[\epsilon_j^0(t) + z\kappa_j(t) - \alpha_j(k\Delta) T(z, t) - \beta_j(k\Delta) M(z, t) \right], (i, j = 1, 2, 6)$$

Where σ_j , \bar{Q}_{ij} , ϵ_j^0 , k_j are the stresses, stiffness components, inplane and bending strains; α_j and β_j are the thermal and hygroscopic expansion coefficients and $T(z,t)$ and $M(z,t)$ are the temperature and moisture concentration distributions at the time t . The subscript $k\Delta$ refers to the k^{th} Δ -layer. Because of the simplicity of the Halpin-Tsai equations we have used them to calculate the Δ -layer properties. (It should be noted that Karlak and Crossman (18) have confirmed the validity of the Halpin-Tsai equations by a large number of finite element calculations where they obtained essentially the same results. Prediction of strength changes and nonlinear effects seem possible but are more involved since there are no simple relations such as the Halpin-Tsai equations that would provide a quick computation of partial fracture of a Δ -layer. This part of our investigation is still in progress. Whatever the required computational effort will be, it is obvious that we need the following resin input data: Young's and shear moduli, ultimate strengths and strains in tensile and compression all as a function of temperature and moisture concentration (as shown for example in Figures 11-14 for Hercules 3501-6), and preferably the total stress strain curves. This is not only important for estimating ply failures, but also for obtaining information of where and under what loading conditions the limit load exceeded on a microscale, thus giving rise to irreversible deformations. Figure 15 shows the stress strain curves of a brittle epoxy resin at different temperatures and Figure 16 shows the effect of moisture on the same resins (at 150°C). A ductile resin on the other hand may behave strongly nonlinear (Figure 17). It is quite obvious that each temperature and moisture loading condition has to be treated accordingly. It is not surprising, therefore, that +45° composites (that are shear critical) show a behavior as indicated in Figure 18. The condition is considerably more complex than in metal-matrix composites. Thus, it appears a great deal more effort on a micromechanical level (FEM) is required before one might hope to derive relations for a simple prediction of failure in a specific Δ -layer of the composite under stress.

D. Laminate Theory

We have said that a composite exposed to the environment will gradually absorb moisture, which, depending on the thickness, may require several decades to reach equilibrium. We also stated that if we know the internal distribution and the resin properties as a function of moisture content we can describe the elastic behavior of the composite

by a relatively simple finite difference process of assuming the composite built up of Δ -layers (which are not to be confused with the natural plies). These Δ -layers are treated, however, as if they were plies forming the laminate, and for each Δ -layer the elastic components of the stiffness matrix are calculated and summed by the usual procedures of laminate theory.

As an example of such a calculation, we have assumed an eight ply (+45)_s 5208/T300 composite exposed to Washington, D.C. conditions. Since the shear-stiffness is matrix dominated we expect to see a strong change. The test temperature was assumed to be 100°C. Figure 19 shows the resulting uptake of moisture with time, the change in the composite shear stiffness (represented by the A_{66} matrix element) and the corresponding change in strain under the same test load (note, this is not creep but instantaneous strain).

Frequently another question was asked:

Is the change of elastic properties dependent only on the total moisture content or also on the way the moisture is distributed? In other words, is there a difference between a uniform and nonuniform moisture distribution with the same overall concentration? Intuitively, one will expect a difference depending on the kind of test. We were interested to see how significant this difference would be. To answer this question we assumed several composites (see Figure 20), symmetric and nonsymmetric, and we assumed various symmetric and nonsymmetric arbitrary and naturally (by diffusion) obtained moisture distributions.

It is not surprising that the effect was strongest in +45° composites, though even there, the difference between a "natural" nonuniform and a uniform moisture content did not exceed 1% during the entire assumed "exposure time" to equilibrium. This is less than the experimental error. Thus, one can state that there is no significant difference for the elastic behavior in composites on the way the moisture is distributed (which does not say that the same holds for failure).

Summary

We believe that it is possible to estimate composite property changes in a real and service environment. We have proposed that at least four concepts have to be simultaneously treated by various numerical methods: diffusion,

modeling of the environment, micromechanics, and laminate theory.

A large effort is still required for predicting laminate failure in composites with nonuniform moisture distribution. Our effort thus far is not complete and at best a step in a promising direction.

Acknowledgement

The author would like to thank Messrs. M. Stander and C. Bersch of the Naval Air Systems Command for their interest and support of this work.

LITERATURE REFERENCES

1. Hertz, J., et al., "Advanced Composite Application for Spacecraft and Missiles," AFML-TR-71-186 Vol II. (General Dynamics-Convair, San Diego, California Mar 1972).
2. Browning, C. E., and J. E. Whitney, "The Effect of Moisture on the Properties of High Performance Structural Resins and Composites," American Chem. Soc., Div. of Org. Coatings and Plastic Chem., 33, No. 2, 1973 pp. 137-148.
3. Augl, J. M., Paper presented at the TTCP-Panel P3 Meeting Melbourne, Australia, 1975, and paper presented at the Air Force Workshop on Durability Characteristics of Resin Matrix Composites, Battelle-Columbus Laboratories, Ohio (1975).
4. Augl, J. M. "The Effect of Moisture on Carbon Fiber Reinforced Composites. II Mechanical Property Changes," NSWC/WOL/TR 76-149 (1977).
5. Browning, C. E., Husman, G. E., and Whitney, J. M., "Moisture Effects in Epoxy Matrix Composites," Composite Materials: Testing and Design ASTM STP 617 (1976), pp. 481.
6. Hofer, K. E., Rao, N., and Larson, D., "Development of Engineering Data on the Mechanical and Physical Properties of Advanced Composite Materials," AFML-TR-72-205 (IIT Research Institute, 1974).
7. Browning, C. E., and Hartness, J. T., "Effect of Moisture on the Properties of High Performance Structural Resins and Composites," Composite Materials: Testing and Design ASTM STP 546 (1974) pp. 284-302.
8. Kaelble, D. H., Dynes, P. J., and Crane, L. W., "Interfacial Mechanisms of Moisture Degradation in Graphite-Epoxy Composites," J. of Adhesion 7, 25 (1977).
9. Kaelble, D. H., and Dynes, P. J., "Surface Energy Analysis of Treated Graphite Fibers," J. Adhesion 6, 239 (1974).
10. Ashbee, K. H. G., and Wyatt, R. C., "Water Damage in Glass Fiber/Resin Composites," Proc. Royal Soc. Series A 312, 553 (1969).

11. Halpin, J. C., and Pagano, N. J., "Consequences of Environmentally Induced Dilation in Solids," AFML-TR-68-395 (1969).
12. Ekvall, J. C., ASME paper 61 AV-56 Aviation Conference, Los Angeles, Mar 1961.
13. Haskin, Z., and Rosen, B. W., "The Elastic Moduli of Fiber Reinforced Materials," J. Appl. Mech. 223 (1969).
14. Rosen, B. W., Don, N. F., and Haskin, Z., "Mechanical Properties of Fiber Composites," NASA CR31 (1969).
15. Tsai, S. W., "Structural Behavior of Composite Materials", NASA CR-71 (1964).
16. Ekvall, AIAA 6th Structural and Material Conf., Palm Springs, Apr 1964, "Failure Mechanisms in Composite Systems."
17. Adams, D. F., and Donner, D. R., "Transverse. Normal Loading of a Unidirectional Composite," J. Comp. Mat. 1, 152 (1967).
18. Karlak, R. F., and Crossman, F. W., LMSC-D457462 (1975). Lockheed Missile and Space Corp., Palo Alto, California.
19. Baker, J. D., and Foye, R. L., "Advanced Design Concepts for Advanced Composite Airframes." North American Rockwell Corp. AFML Contract F33616-68-C-1199 (1969).
20. Lin, T. H., Salina, D., and Ito, Y. M., "Elasto-Plastic Analysis of Unidirectional Composites." J. Comp. Mat. 6, 48 (1972).
21. Adams., F. D., and Miller, A. K., Hygrothermal Microstresses in a Unidirectional Composite Exhibiting Inelastic Material Behavior," J. Comp. Mat. 11, 285 (1977).
22. Lekhnitskii, S. G., "Theory of Elasticity of an Anisotropic Elastic Body," Holden-Day, Inc. (1963).
23. Ashton, J. E., Halpin, J. C., and Petit, P. H., "Primer on Composite Materials." Composite Materials Workshop, Technomic Publ. Co. (1969).

24. Vinson, J. R., and Chou, T. W., "Composite Materials and Their Use in Structures," John Wiley, 1975.
25. Tsai, S. W., "Mechanics of Composite Materials. Part II" AFML-TR-149 (1966)
26. Augl, J. M., and Berger, A. E., "The Effect of Moisture on Carbon Fiber Reinforced Composites. I Diffusion," NSWC/WOL TR 76-7 (1976).
27. Lord Rayleigh, Phil. Mag. 34, 481 (1892).
28. Shen, C. H., and Springer, G. S., "Moisture Absorption and Desorption of Composite Materials," J. Comp. Mat. 10, 2 (1976).
29. Augl, J. M., and Berger, A. E., "The Effect of Moisture on Carbon Fiber Reinforced Composites. III Prediction of Moisture Sorption in a Real Outdoor Environment," NSWC/WOL TR 77-13 (1977).
30. Tompkins, S. S., Analytical Study of Effects of Surface and Environmental Thermal Properties on Moisture in Composites. NASA TMX-3562 (1977).
31. Augl, J. M., "Prediction of Moisture Absorption in the 5"54 HIFRAG Discarding Rotating Band for Various Climatic Environments," NSWC/WOL/TR 76-167 (1976).
32. Branca, T. R., "Creep of a Uniaxial Metal Matrix Composite Subjected to Axial and Normal Lateral Loads," NAVAIRSYSCOM Contract No. N00019-71-C-0323 (1971), Univ. of Illinois T.E.A.M. Report 341.
33. Reniere, G. D., and Herakovich, C. T., "Nonlinear-Analysis of Laminated Fibrous Composites, Doctoral Thesis, Virginia Polytech. Inst. (1976).
34. Ebert, L. J., Griesbach, T. J., and Flynn, P. L., "Finite Element Analysis System for the Mechanical Behavior of Oriented Fiber Composite Materials Under Combined Stresses," AFOSR-TR-75-0042 (1974).
35. Augl, J. M., and Berger, A. E., "The Effect of Moisture on Carbon Fiber Reinforced Composites. IV Prediction of Changes in the Elastic Behavior," NSWC/WOL TR 77-61 (1977).

36. Pipes, B. R., Vinson, J. R., and Chou, T. W., "On the Hygrothermal Response of Laminated Composite Systems," J. Comp. Mat. 10, 126 (1976).

1220
1824
1000
15
15

APPENDIX A

Halpin-Tsai Equations

For design purposes and rapid computational procedures Halpin and Tsai have proposed a set of equations which are simpler than most of the formulas derived from micromechanical analyses, however, are good enough for estimating with reasonable accuracy the ply properties:

$$E_{11} \approx E_f V_f + E_m V_m$$

$$\nu_{12} \approx \nu_f V_f + \nu_m V_m$$

$$\frac{\bar{p}}{p_m} = \frac{(1 + \zeta \eta V_f)}{(1 - \eta V_f)}$$

where

$$\eta = \frac{[(p_f/p_m) - 1]}{[(p_f/p_m) + \zeta]}$$

\bar{p} = composite moduli E_{22} , G_{12} , or G_{23} ;

p_f = corresponding fiber modulus E_{11f} , G_{12f} , ν_{12f} (or ν_{23f});

p_m = corresponding matrix modulus E_m , G_m , ν_m ;

ζ = a measure of reinforcement which depends on the boundary conditions. Approximate values are given by $\zeta_{E_{22}} =$

$2(a/b)$ and by $\log \zeta_{G_{12}} = 3 \log (a/b)$, i.e., for round

fibers $\zeta_{E_{12}} = 2$ and $\zeta_{G_{12}} = 1$

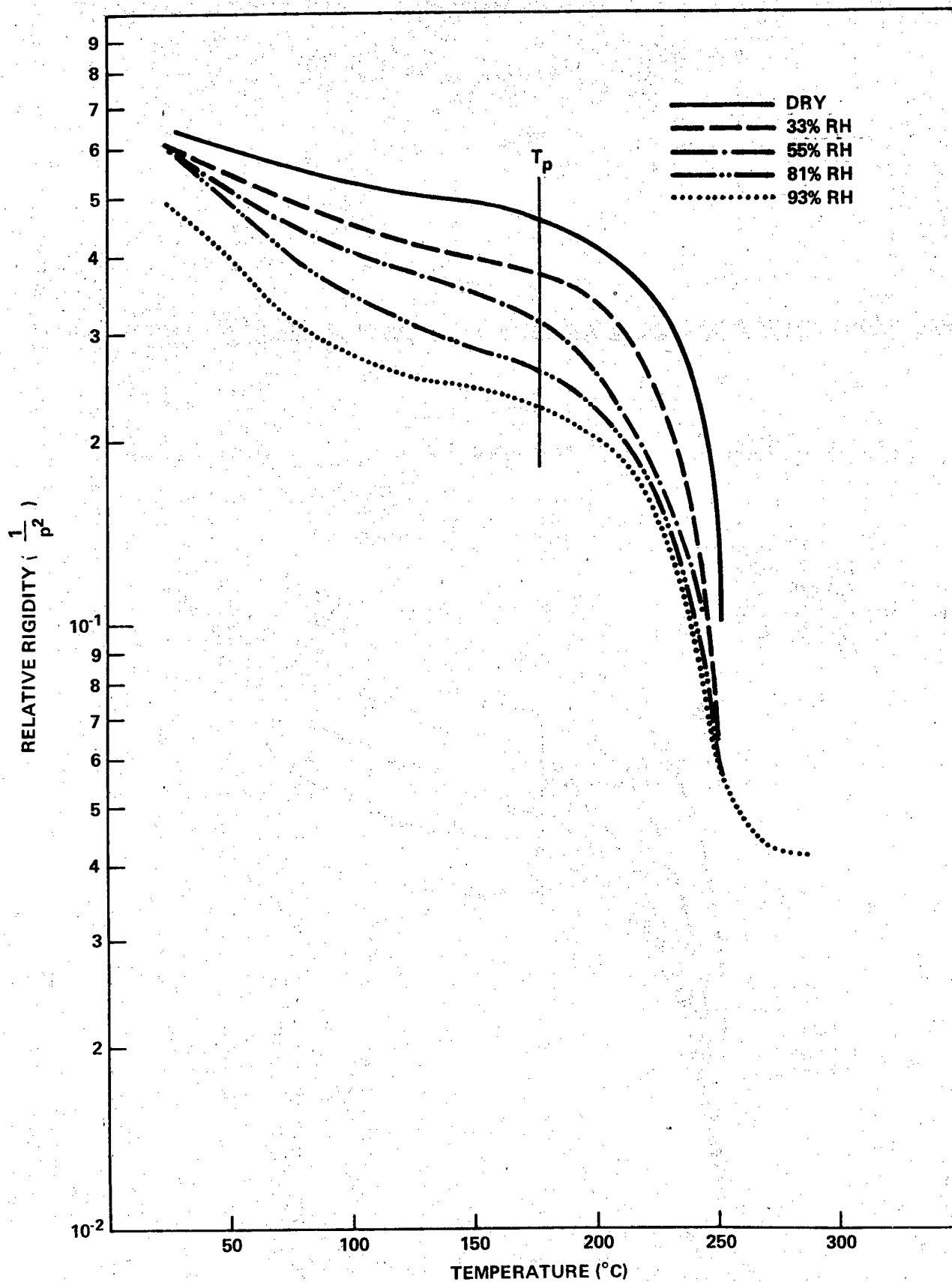


FIG. 1 EFFECT OF VARIOUS RELATIVE HUMIDITIES ON RESIN MODULUS (DETERMINED BY TBA AFTER 10 DAYS' EXPOSURE. RESIN: NARMCO 5208).

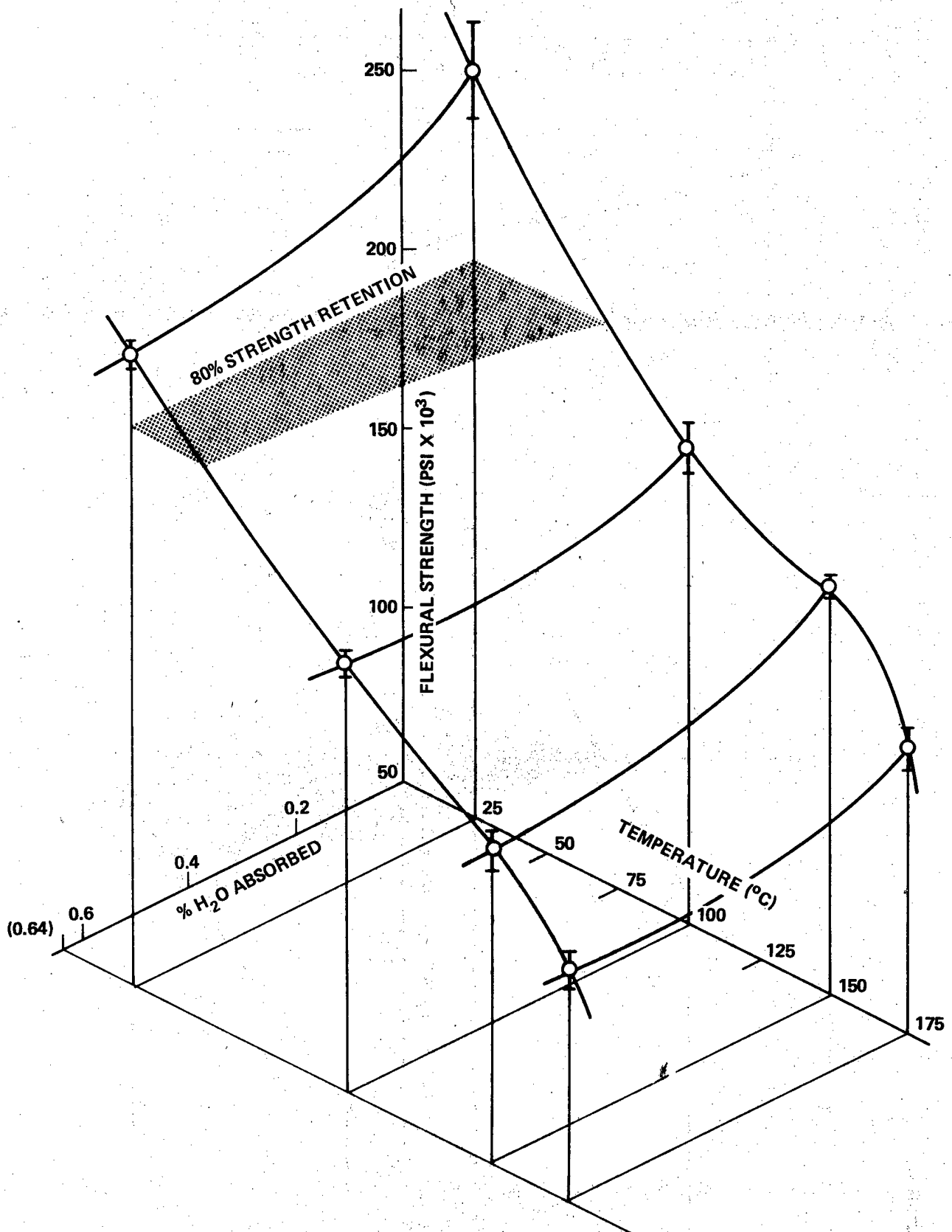


FIG. 2 FLEXURAL STRENGTH OF UNIDIRECTIONAL CARBON FIBER COMPOSITES (NARMCO 5208/T300) AS A FUNCTION OF TEMPERATURE AND PERCENT MOISTURE ABSORBED

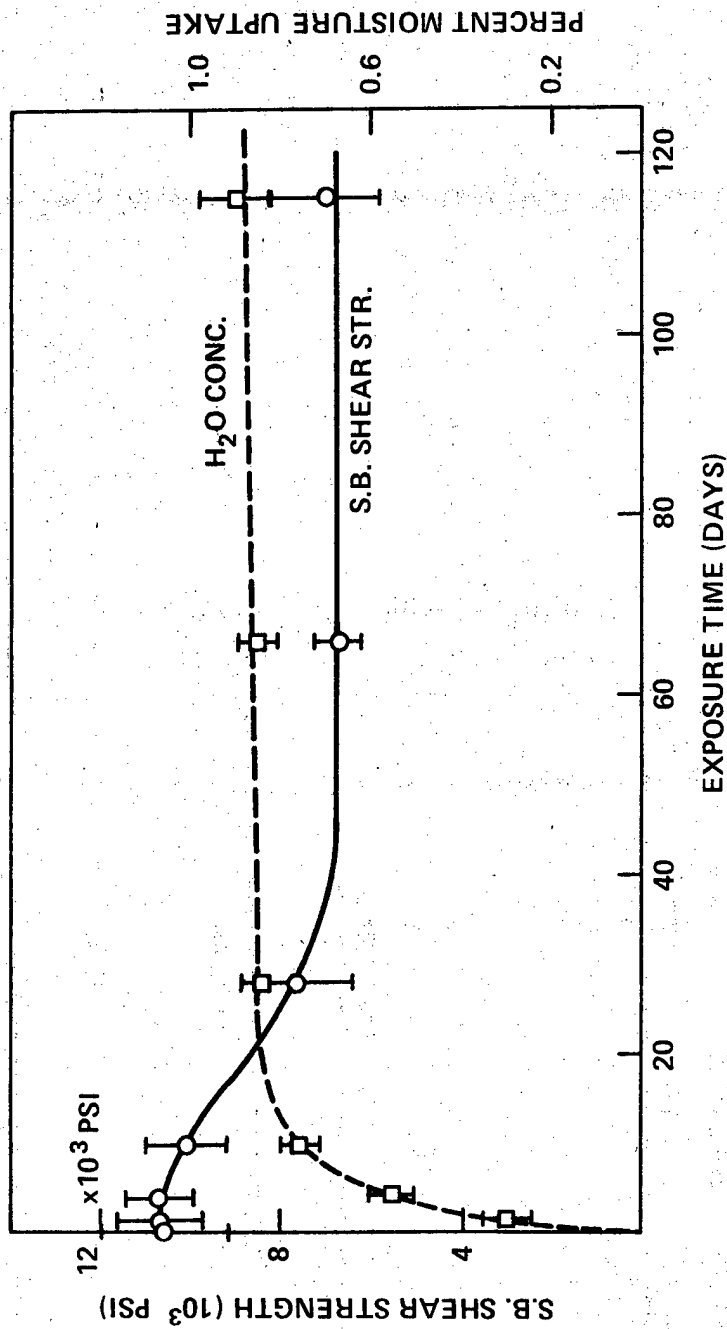


FIG. 3 SHORT BEAM SHEAR STRENGTH OF NARMCO 5208/HMS COMPOSITE, TESTED AT 125° C AFTER EXPOSURE TO 80% RH AT 75° C

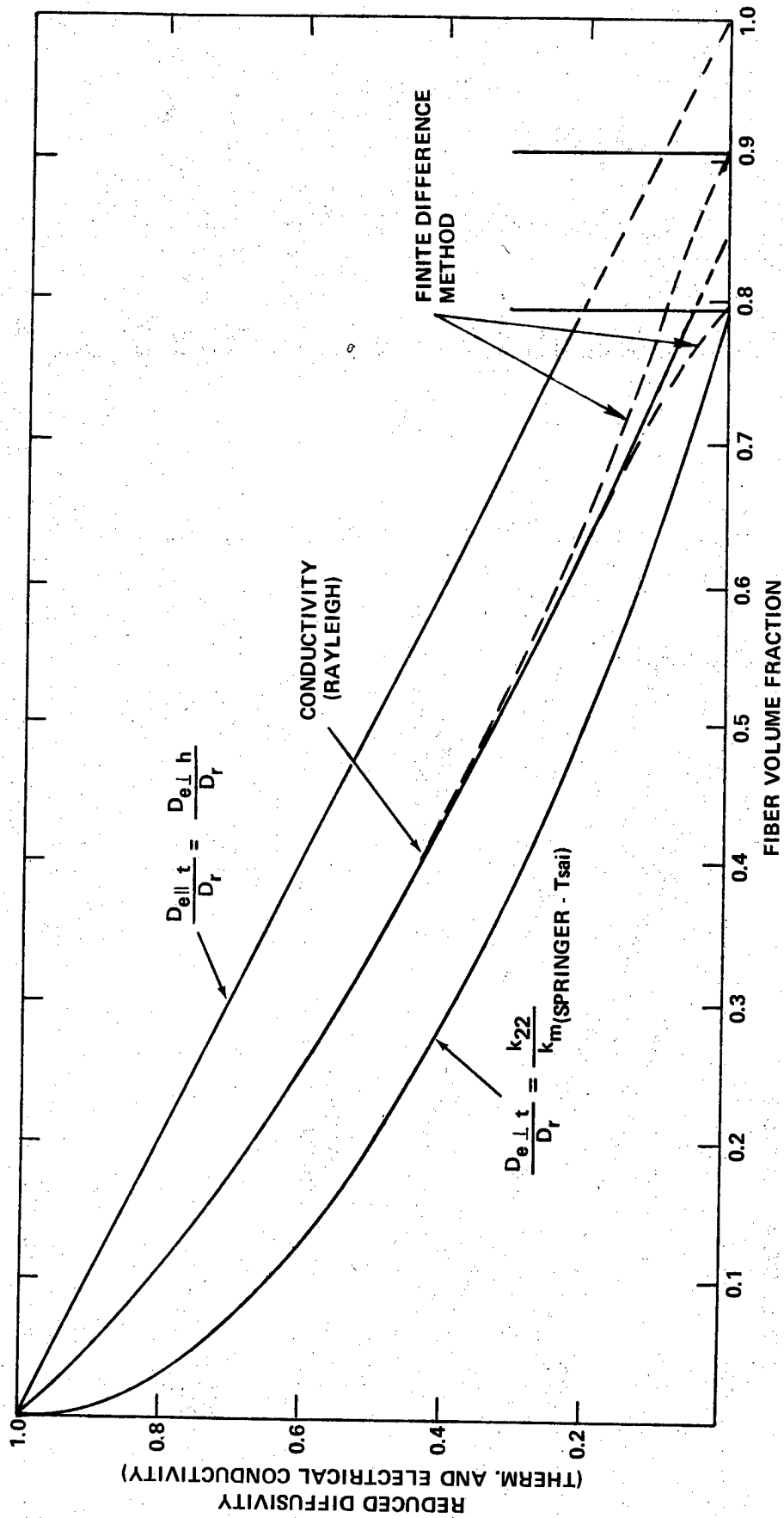


FIG. 4 A COMPARISON OF THE REDUCED DIFFUSIVITY VERTICAL TO THE FIBER DIRECTION WITH THERMAL AND ELECTRICAL ANALOGS.

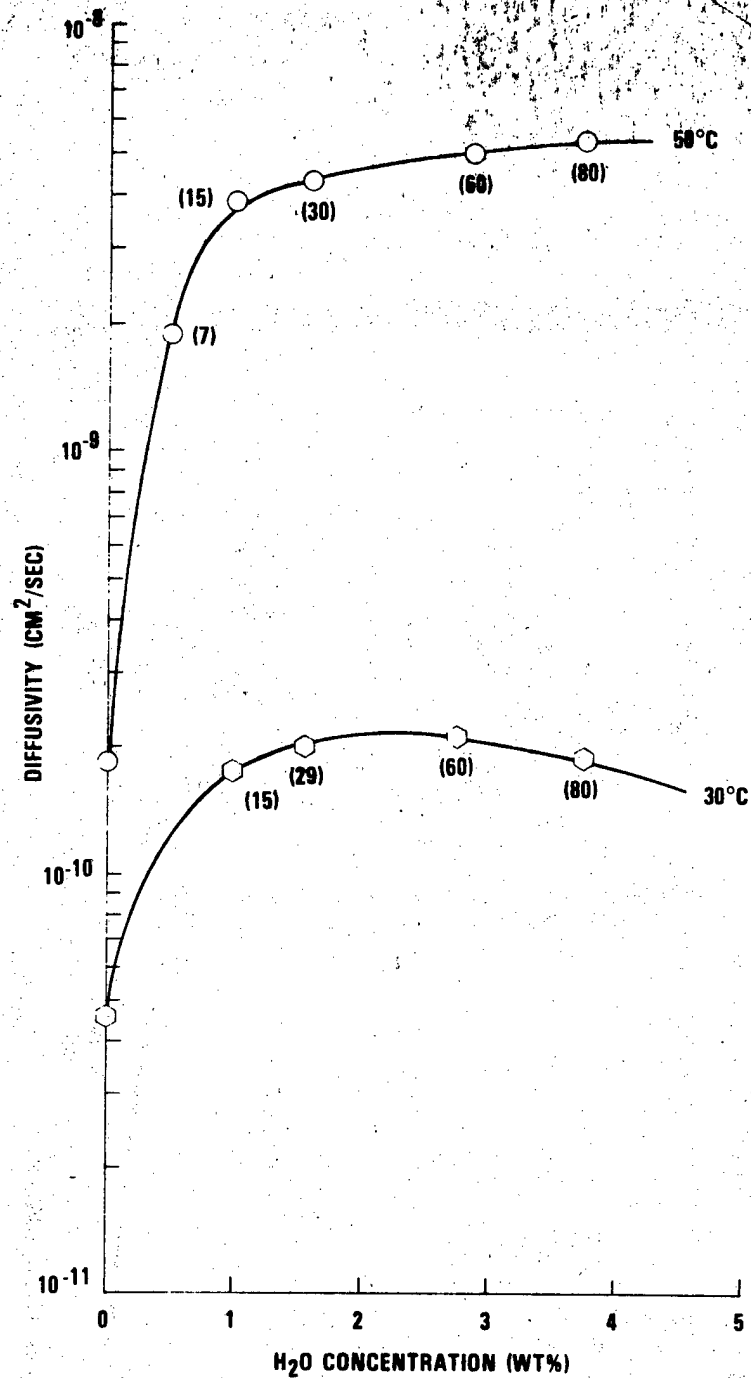


FIG. 5 MOISTURE DIFFUSIVITY $D(C)$ OF HERCULES 3501-6 EPOXY RESIN. (FOR 3501-6/AS COMPOSITES ($V_v = 0.65$) $D(C)$ IS MULTIPLIED BY 0.25) THE NUMBERS IN PARENTHESIS INDICATE THE REL. HUMIDITY AT WHICH $D(C)$ WAS MEASURED. $D(0)$ WAS OBTAINED FROM DESORPTION MEASUREMENTS

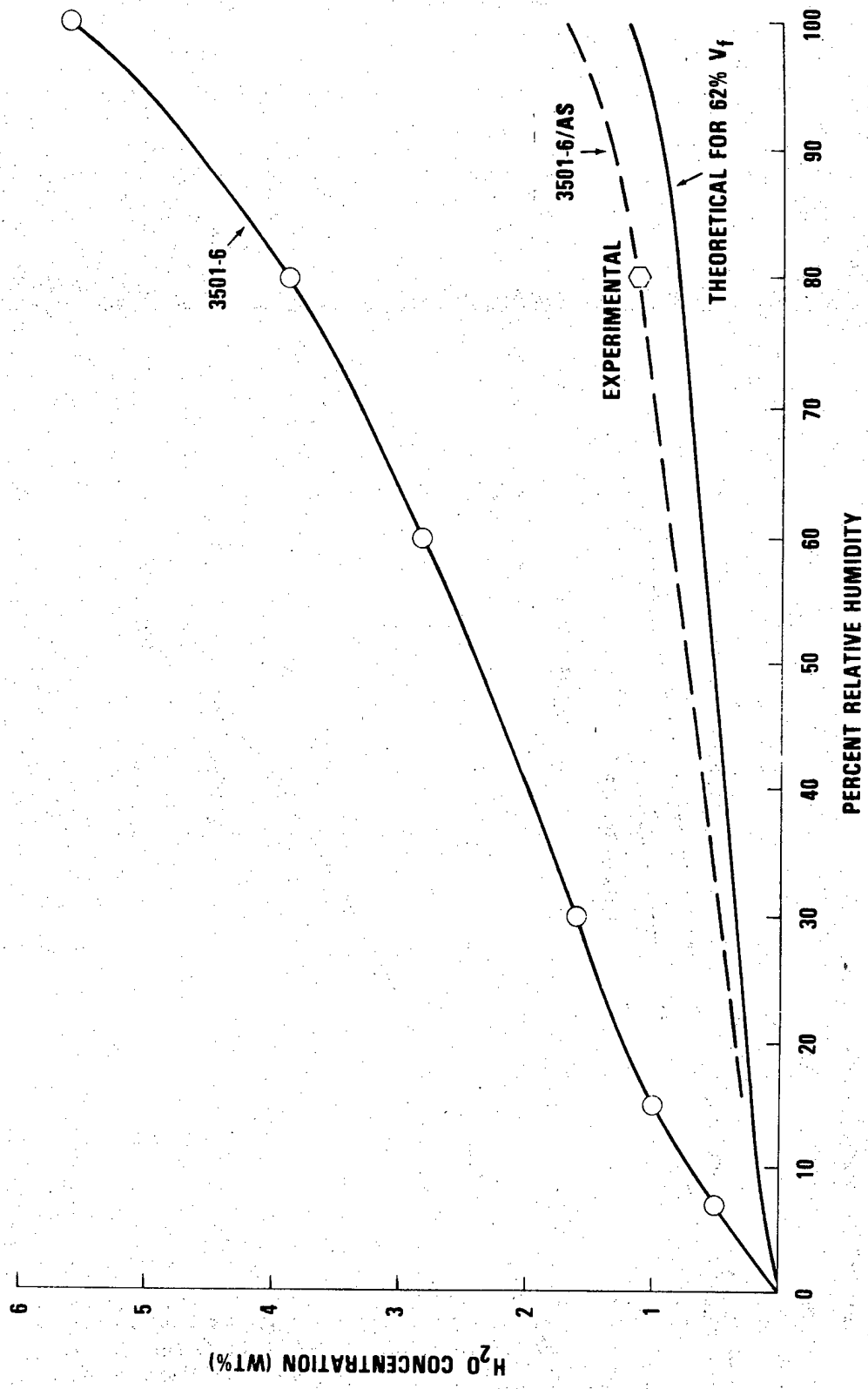


FIG. 6 EQUILIBRIUM CONCENTRATION OF MOISTURE IN HERCULES 3501-6

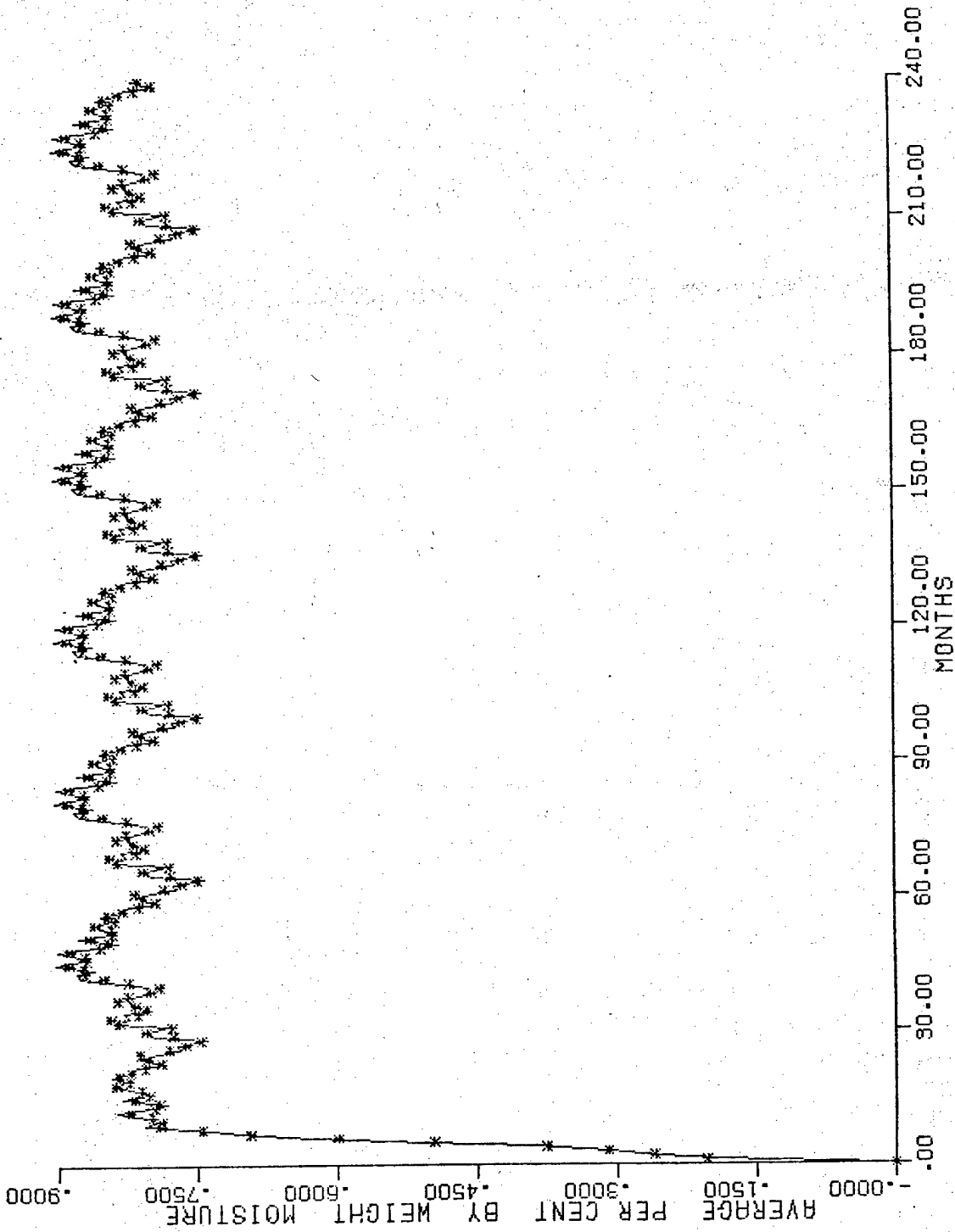


FIG. 7 PERCENT MOISTURE UPTAKE OF A SIX PLY NARMCO 5208/T300 (V_f=.7) CARBON FIBER COMPOSITE CALCULATED FOR WASHINGTON D.C. CLIMATIC CONDITION. (SOLID LINE: 3 HOURLY WEATHER DATA, *: FROM MONTHLY AVERAGES). THE 3-YEARLY CYCLE WAS REPEATED.

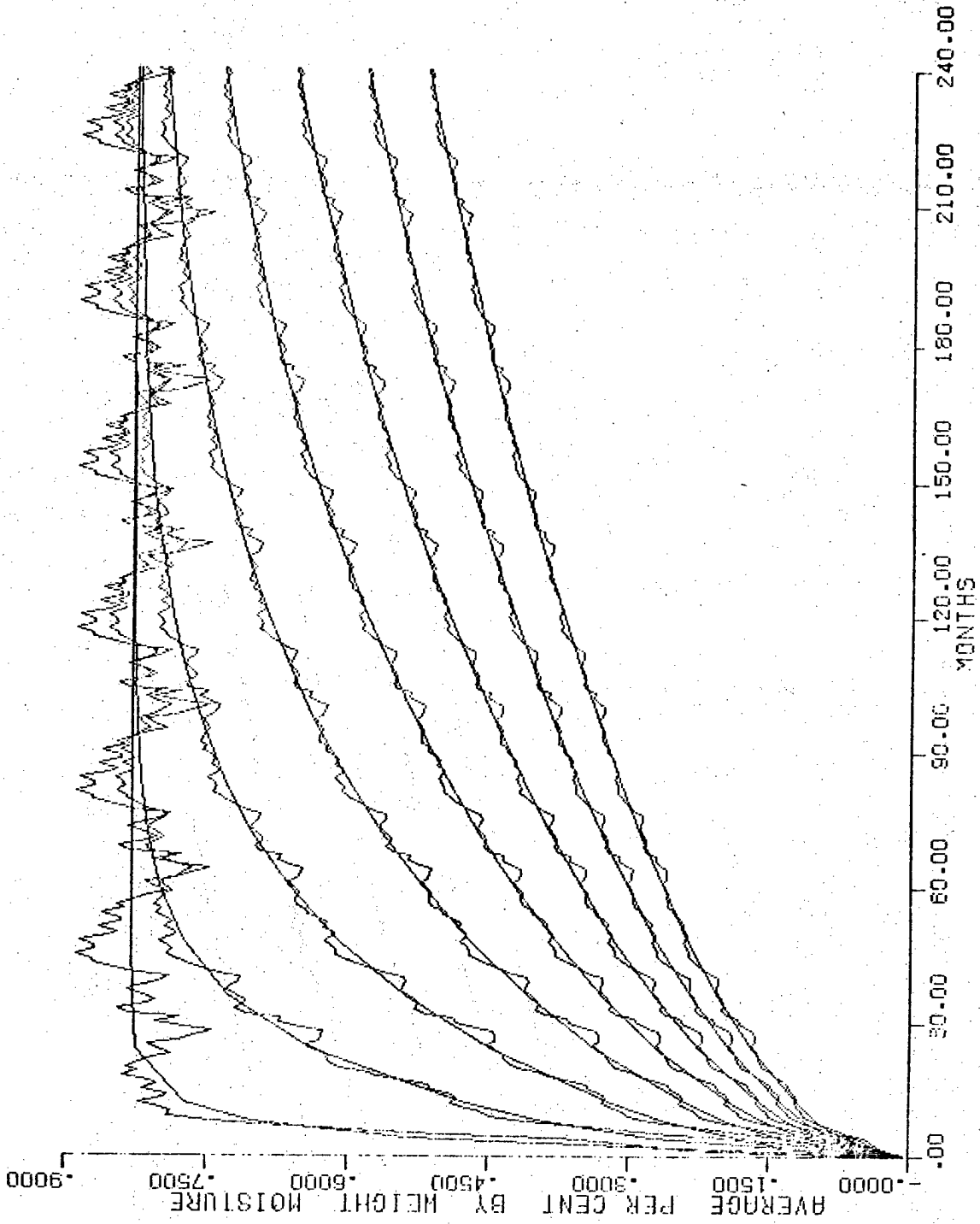


FIG. 8 PERCENT MOISTURE UPTAKE OF 6, 12, 18, 24, 30, 36, 42, AND 48 PLY 5208/T300 CF COMPOSITES (WASHINGTON D.C. CONDITIONS). SMOOTH LINE: FROM 3-YEARLY AVERAGES (T_{kav} , RH_{kav}). FLUCTUATING LINE: FROM MONTHLY AVERAGES.

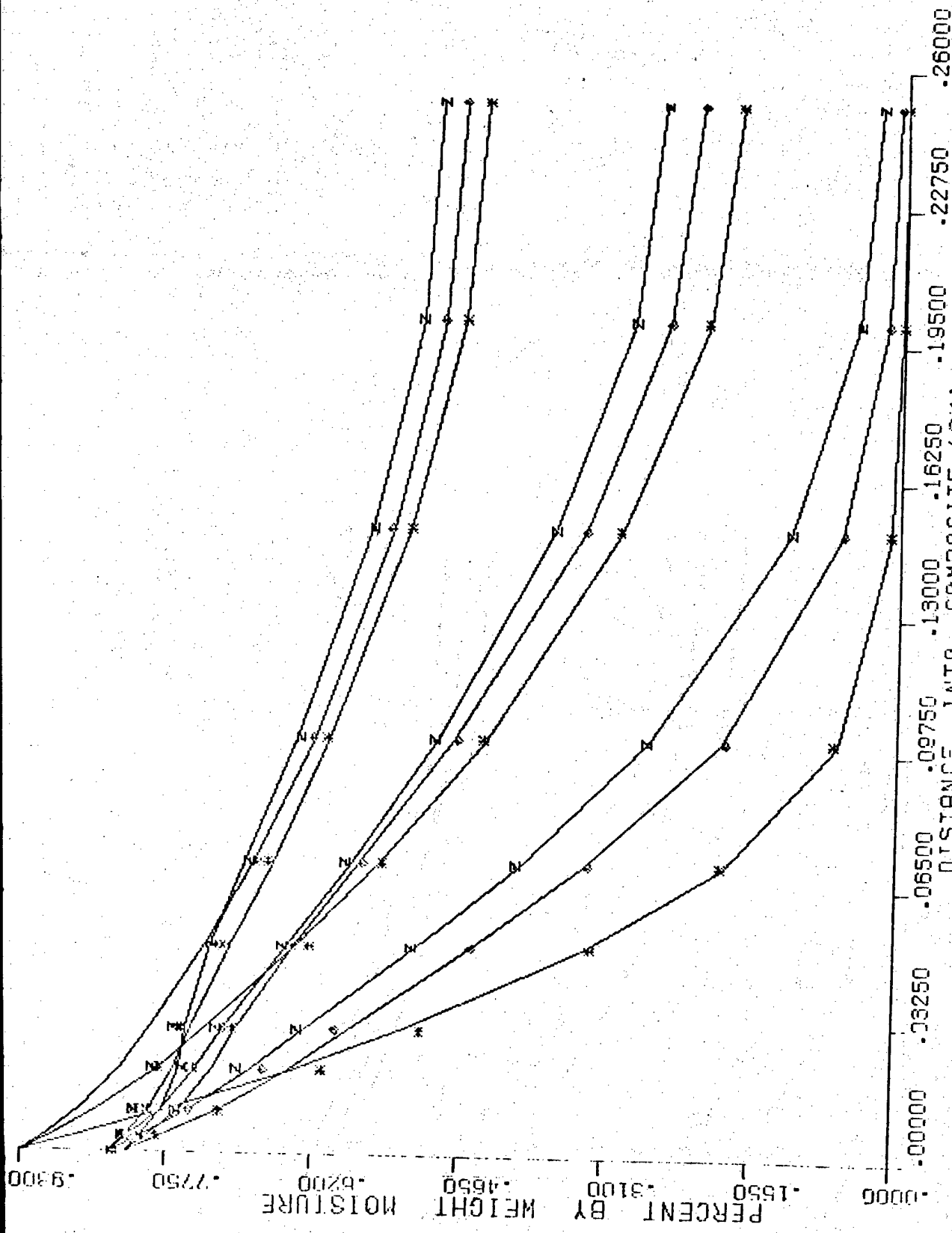


FIG. 9 INTERNAL MOISTURE DISTRIBUTION IN A NARMCO 5208/T300 CF COMPOSITE (36 PLYS) (WASHINGTON, D.C.) AFTER 1, 2, 3, 7, 8, 9, 15, 16, AND 17 YEARS (MONTHLY AVERAGES, POINTS: 3 YEARLY AVERAGES).

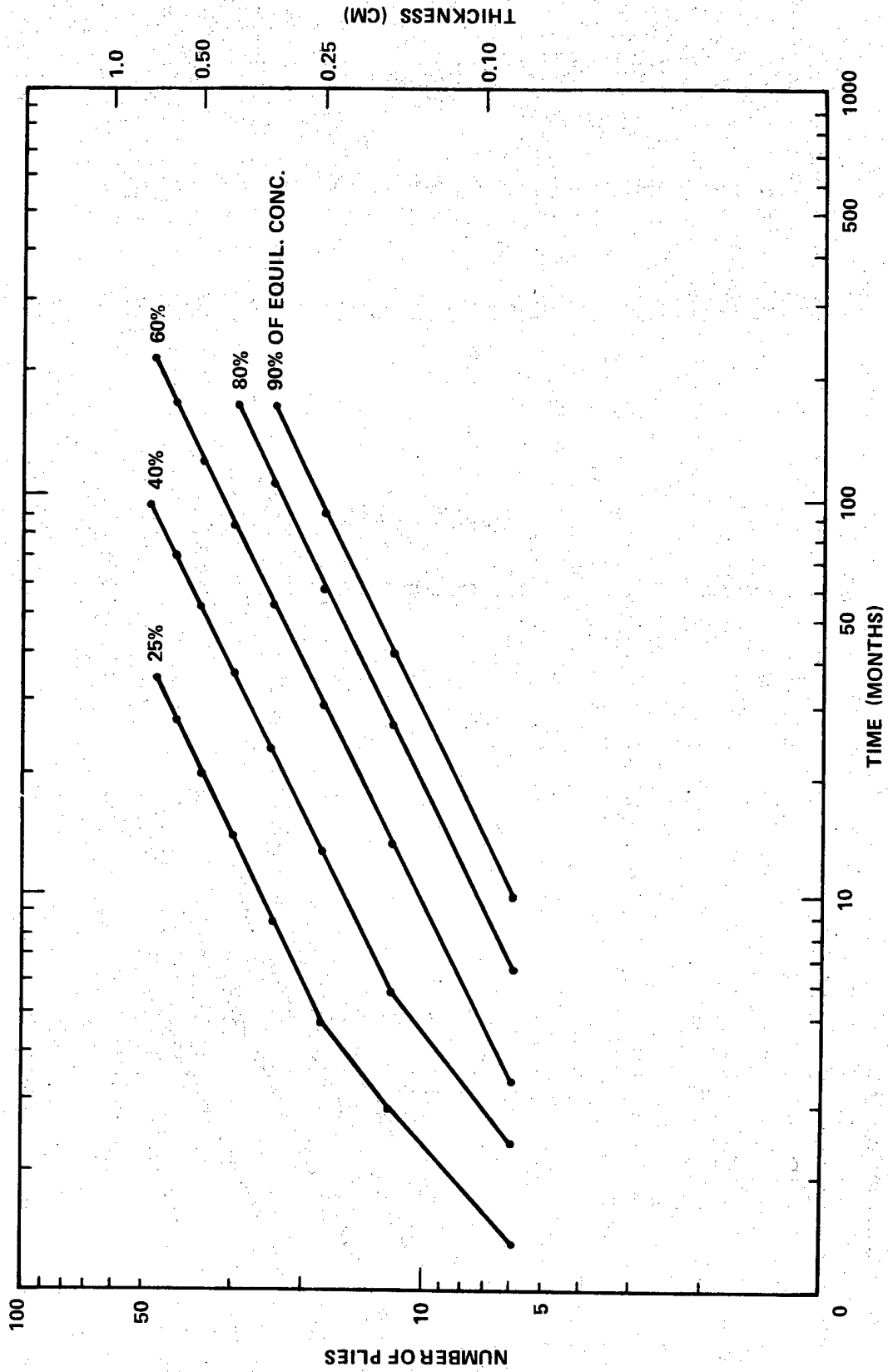


FIG. 10 TIME TO REACH VARIOUS LEVELS OF THE RESPECTIVE EQUILIBRIUM CONCENTRATIONS AS A FUNCTION OF NUMBERS OF PLYS OF NARMCO 5208/T300 ($V_f = .70$) (THE THICKNESS IN CM IS OBTAINED BY MULTIPLYING THE PLY NUMBER WITH .01397)

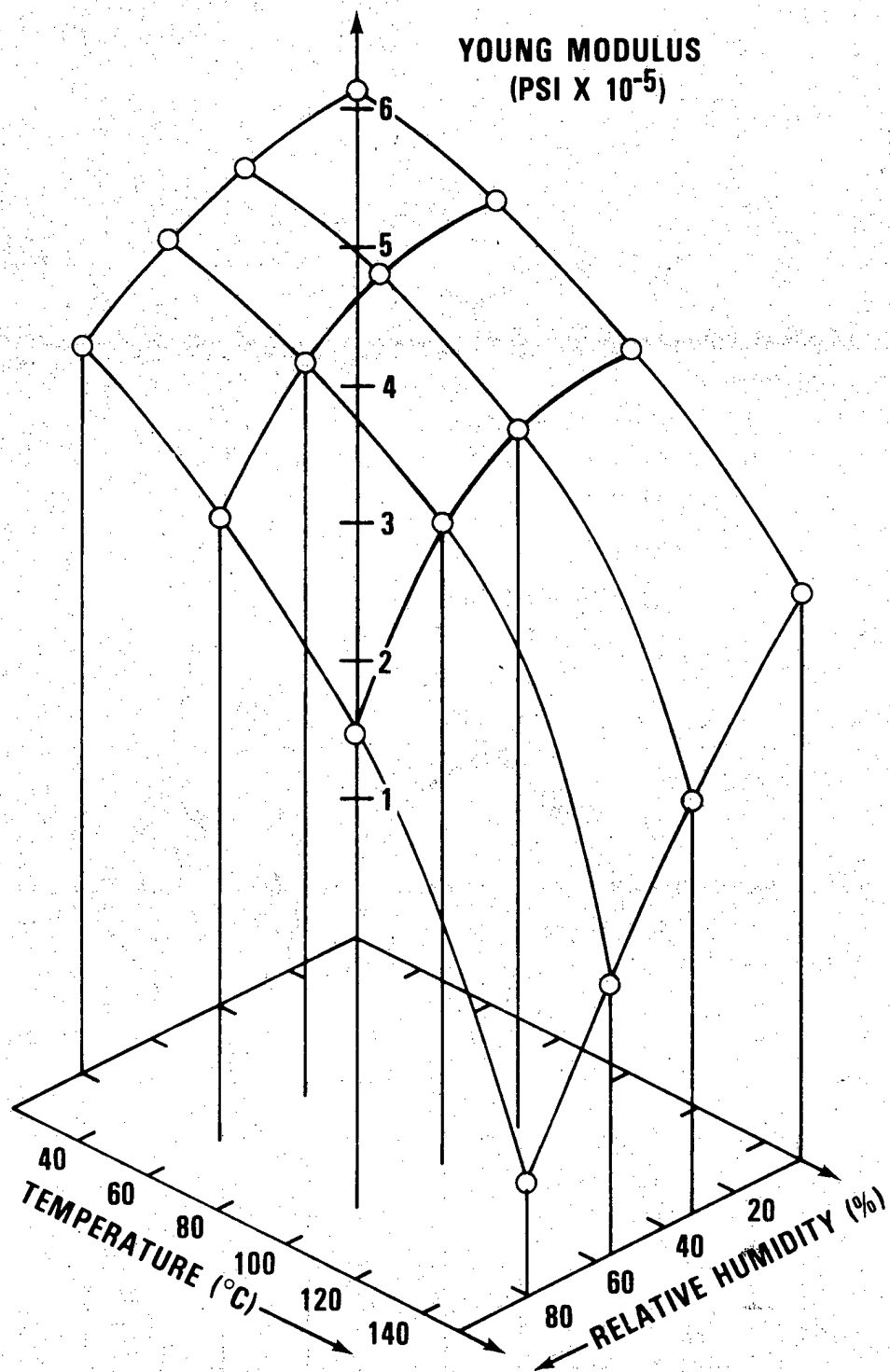


FIG. 11 YOUNGS MODULUS OF HERCULES 3501-6 AS A FUNCTION OF TEMPERATURE AND MOISTURE (CORRESPONDING TO THE EQUILIBRIUM CONCENTRATION OF INDICATED RELATIVE HUMIDITIES)

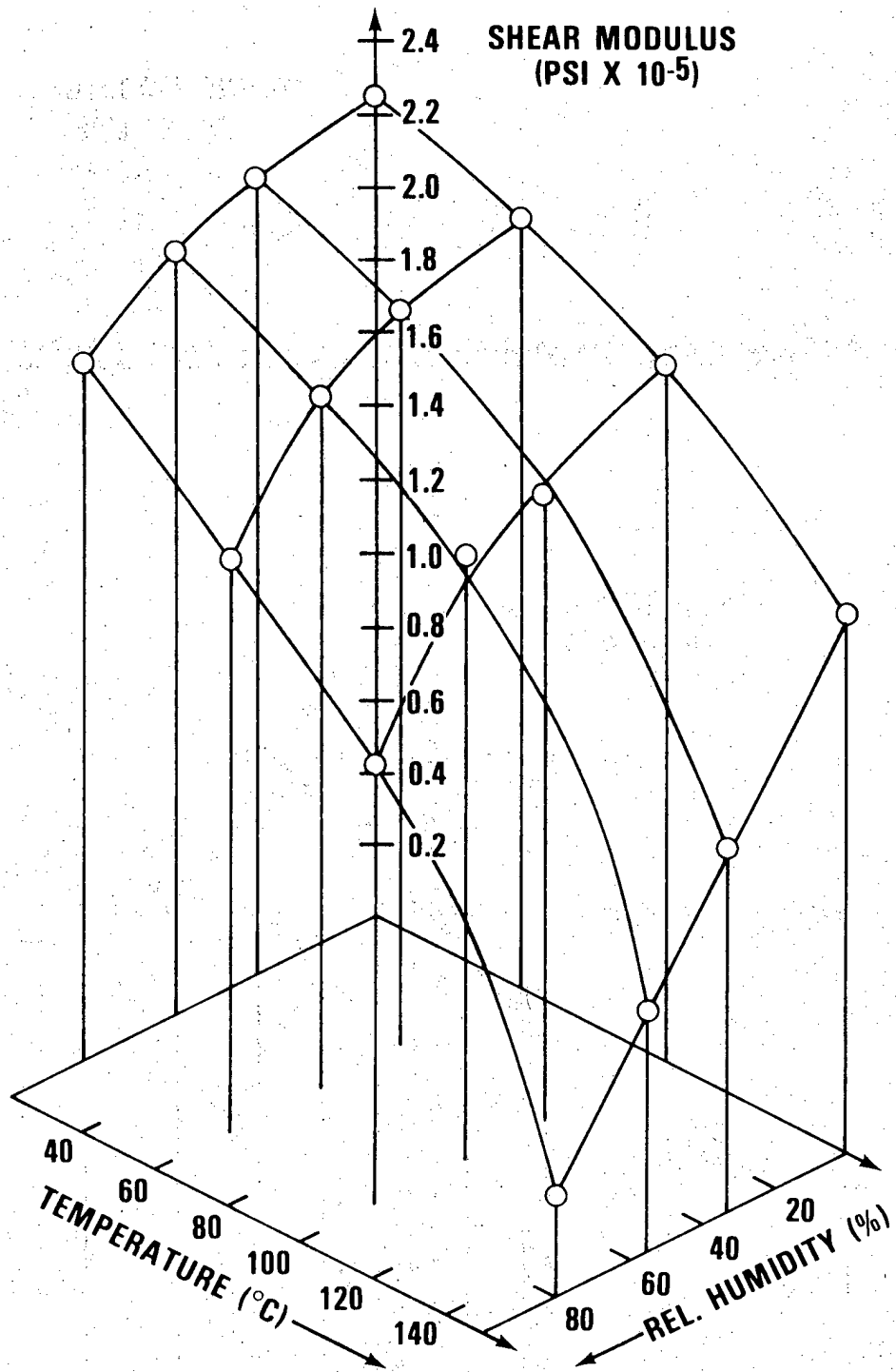


FIG. 12 SHEAR MODULUS OF HERCULES 3501-6 AS A FUNCTION OF TEMPERATURE AND MOISTURE (CORRESPONDING TO THE EQUILIBRIUM CONCENTRATION OF INDICATED RH)

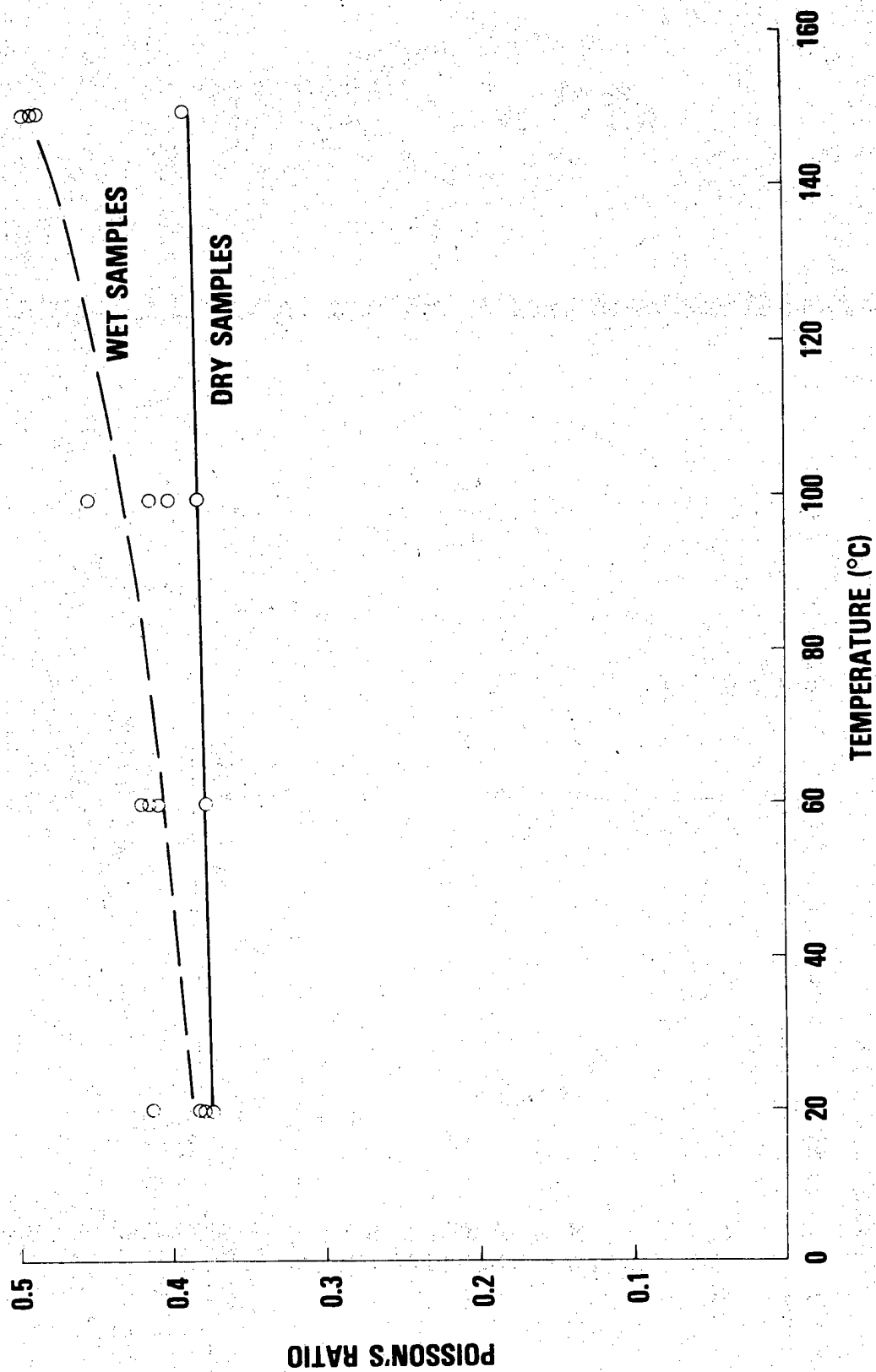


FIG. 13 POISSON'S RATIO OF HERCULES 3501 - 6 AS A FUNCTION OF TEMPERATURE

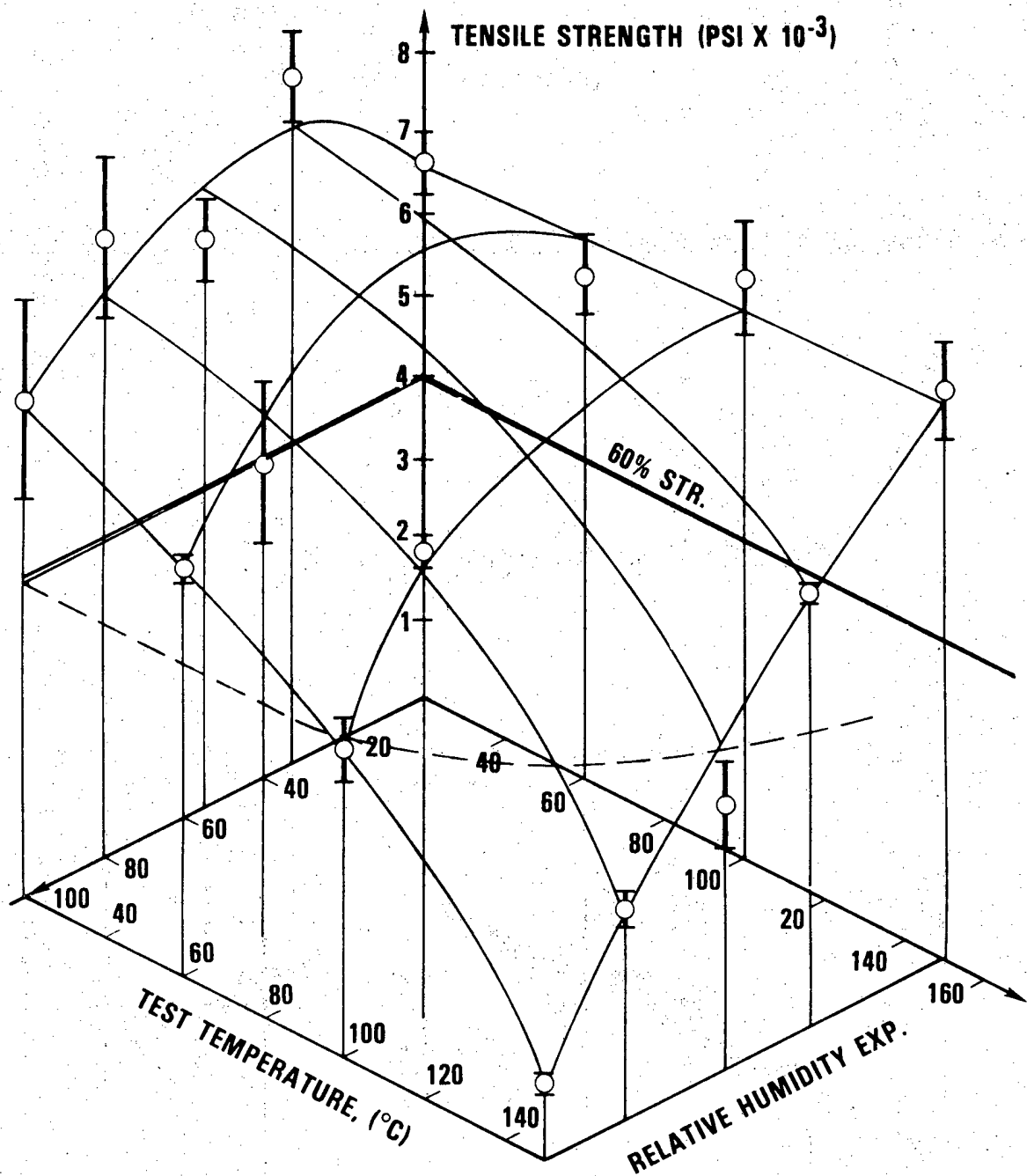


FIG. 14 TENSILE STRENGTH OF HERCULES 3501-6 (EQUILIBRATED AT VARIOUS RELATIVE HUMIDITIES) AS A FUNCTION OF TEMPERATURE

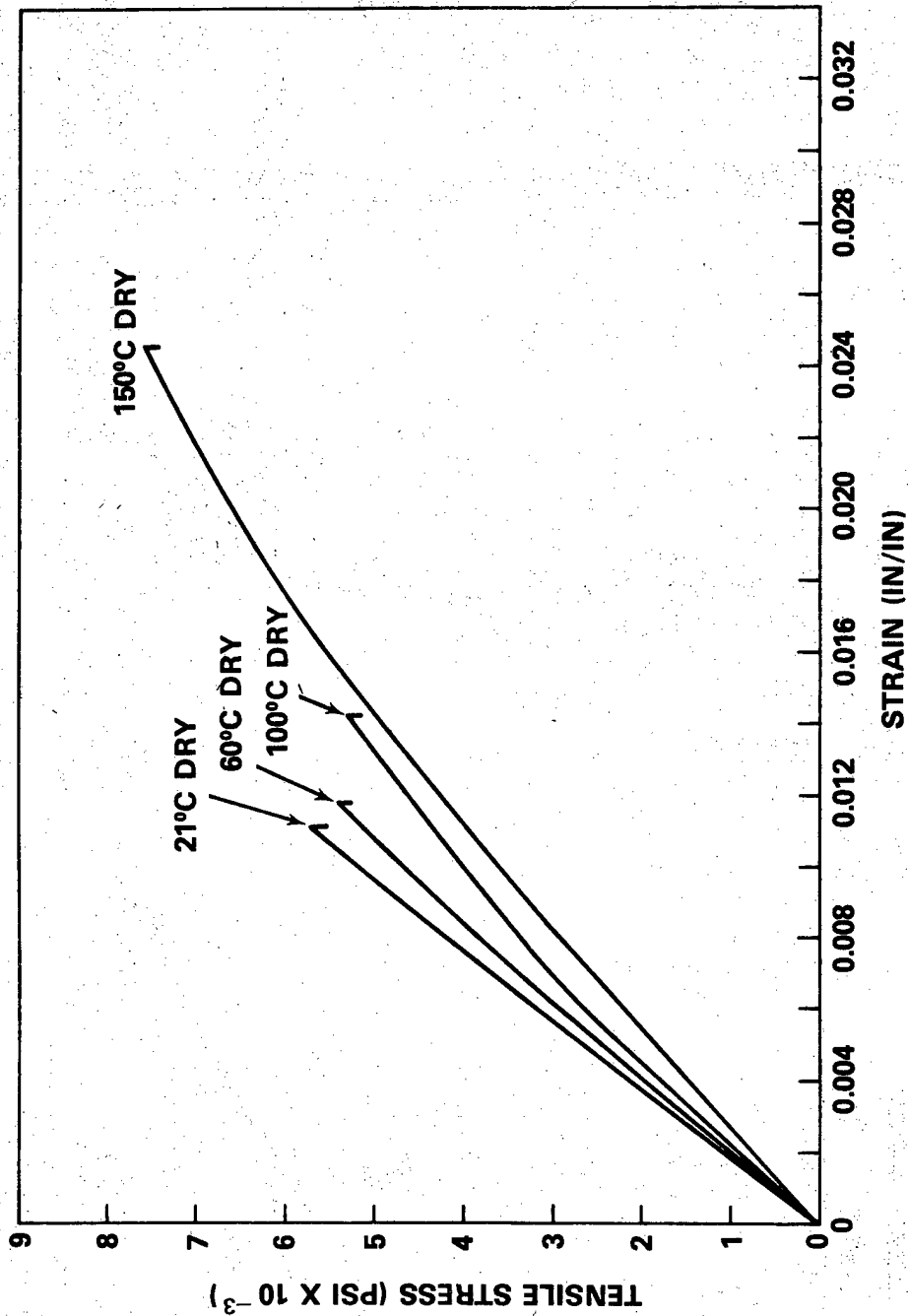


FIG. 15 TYPICAL STRESS-STRAIN CURVE OF A BRITTLE EPOXY RESIN (3501-6, DRY) AS A FUNCTION OF TEMPERATURE

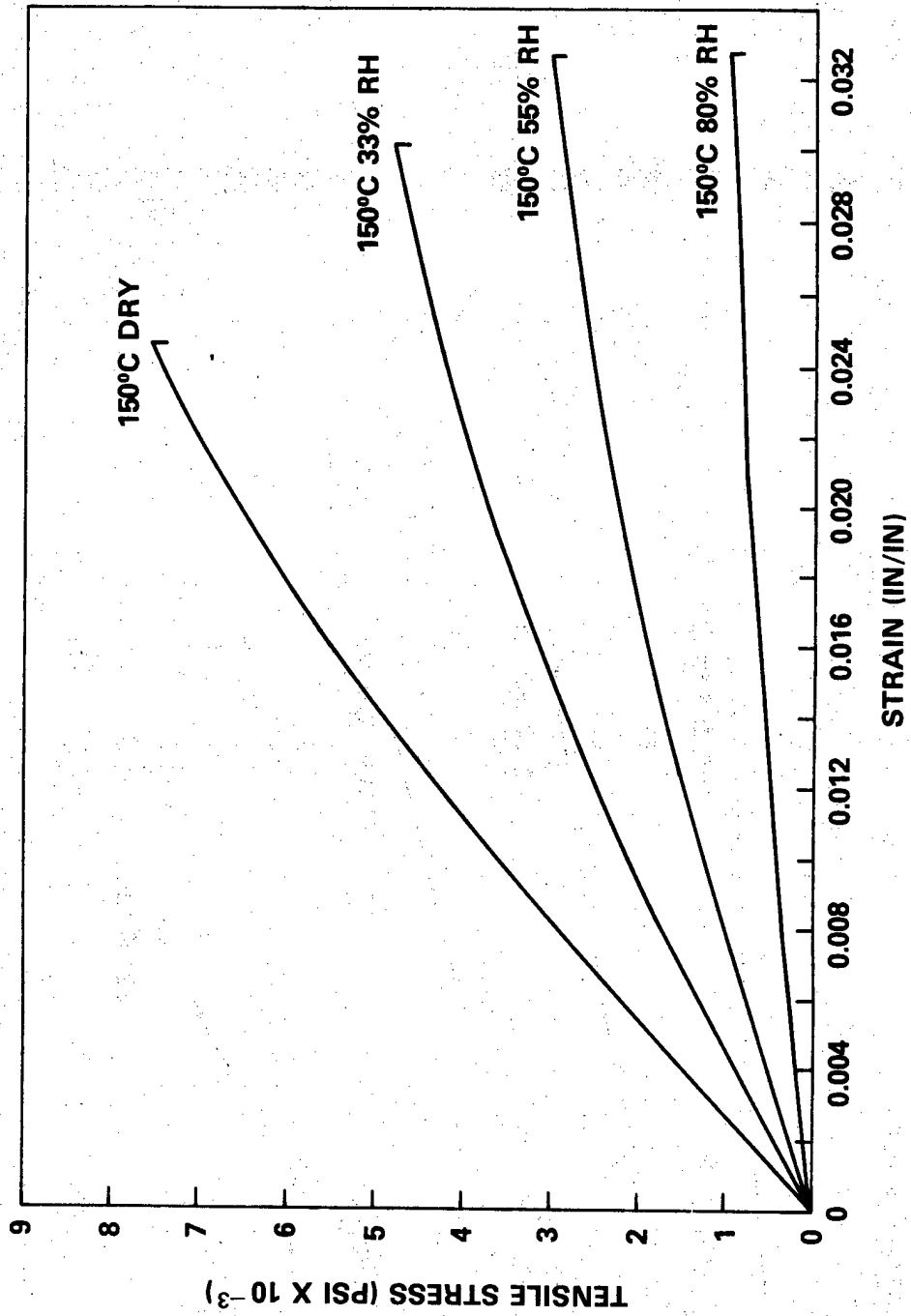


FIG. 16 TYPICAL STRESS-STRAIN CURVE OF A BRITTLE EPOXY RESIN (3501-6, AT 150°C) EQUILIBRATED AT DIFFERENT RELATIVE HUMIDITIES

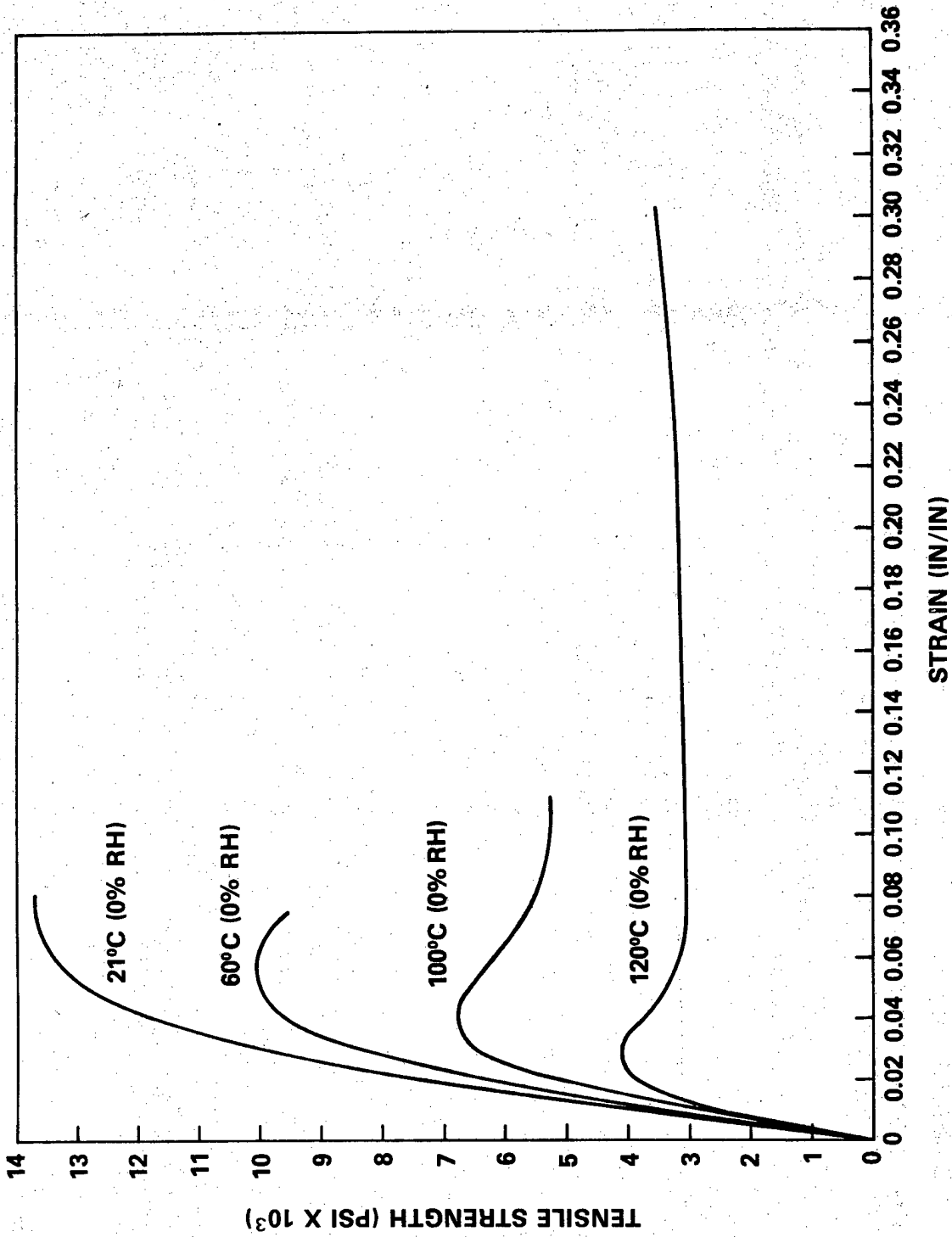


FIG. 17 TYPICAL STRESS-STRAIN CURVES OF A DUCTILE EPOXY RESIN (DGBA-RD2-TONOX DRY) AS A FUNCTION OF TEMPERATURE

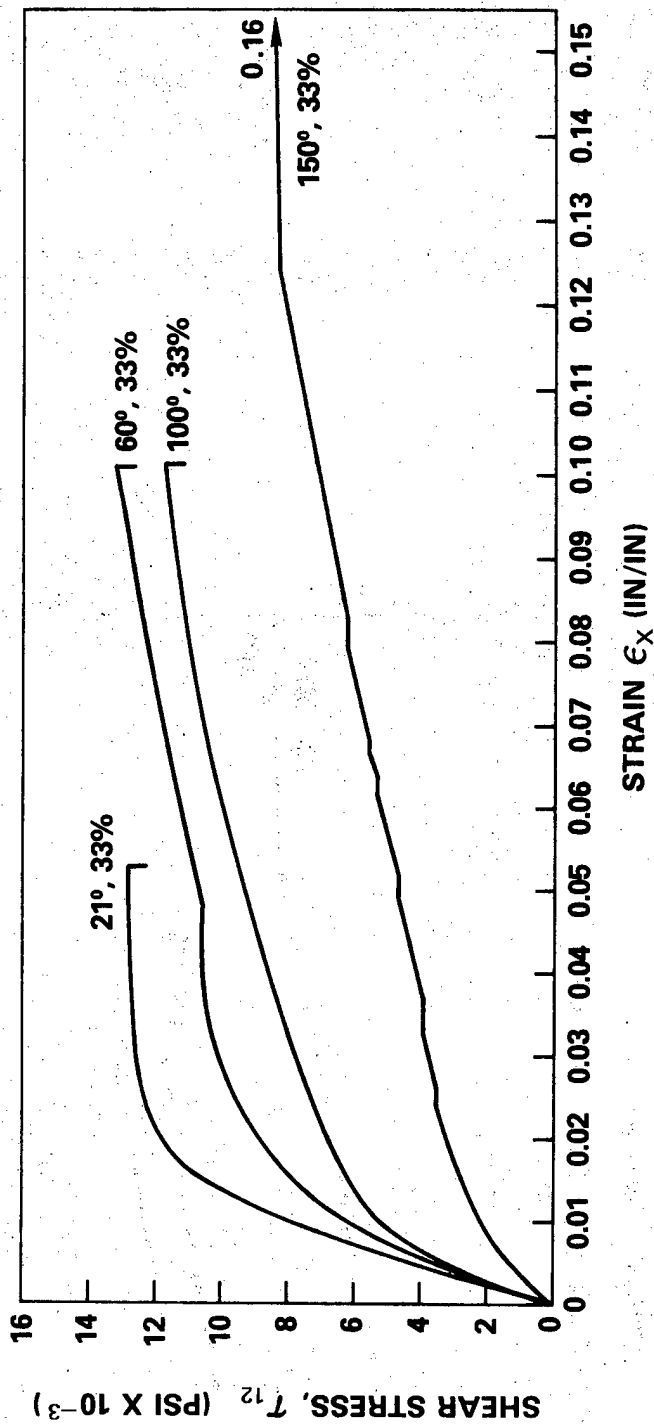


FIG. 18 TYPICAL STRESS-STRAIN CURVES OF $\pm 45^\circ$ CARBON FIBER COMPOSITE SPECIMENS (3501-6/AS) AS A FUNCTION OF TEMPERATURE

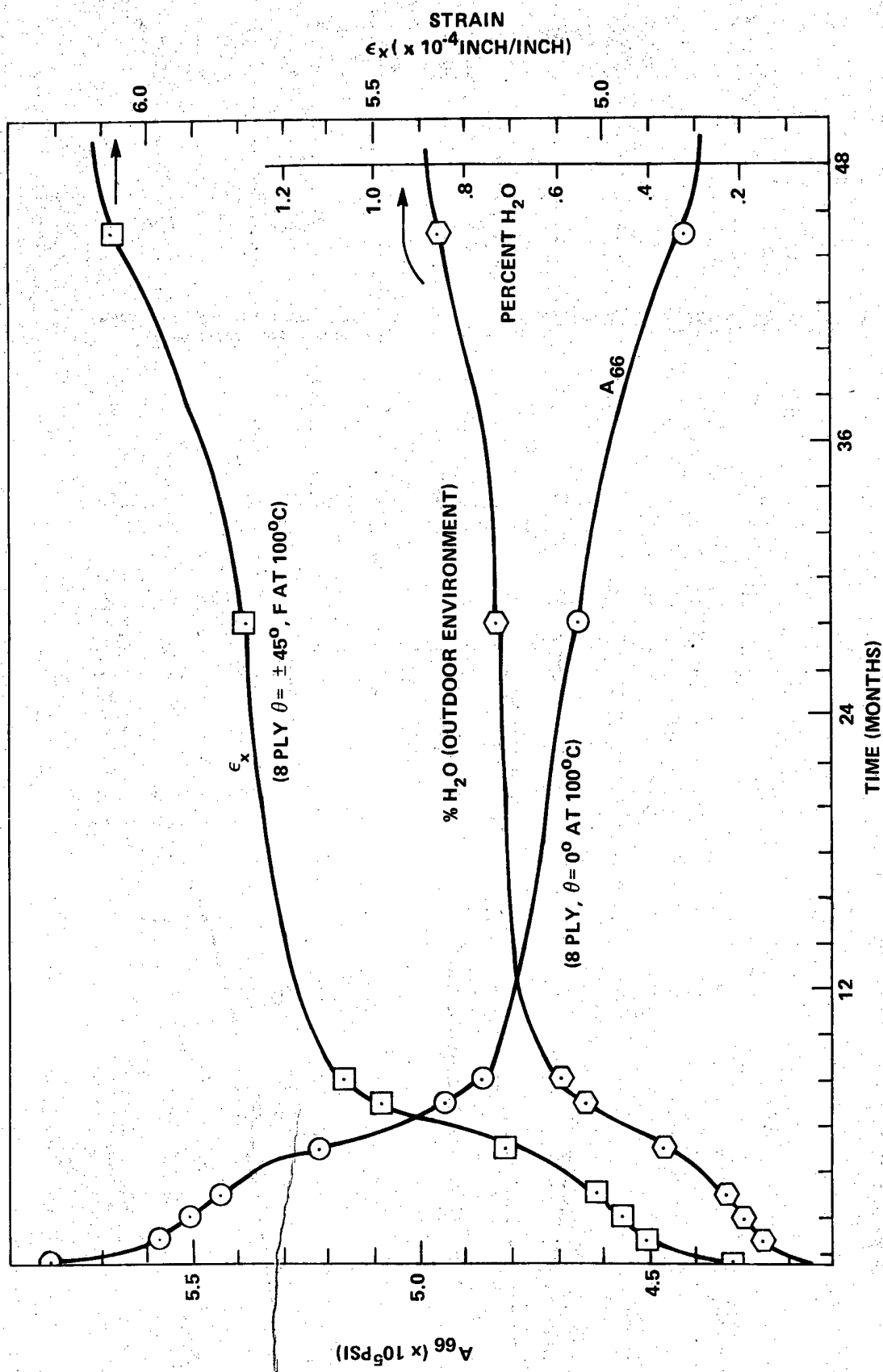


FIG. 19 CHANGE IN SHEAR STIFFNESS, STRAIN AT CONSTANT LOAD (500 LB), AND MOISTURE UPTAKE OF AN 8 PLY LAMINATE 5208/T300 AS A FUNCTION OF TIME (WASHINGTON DC)

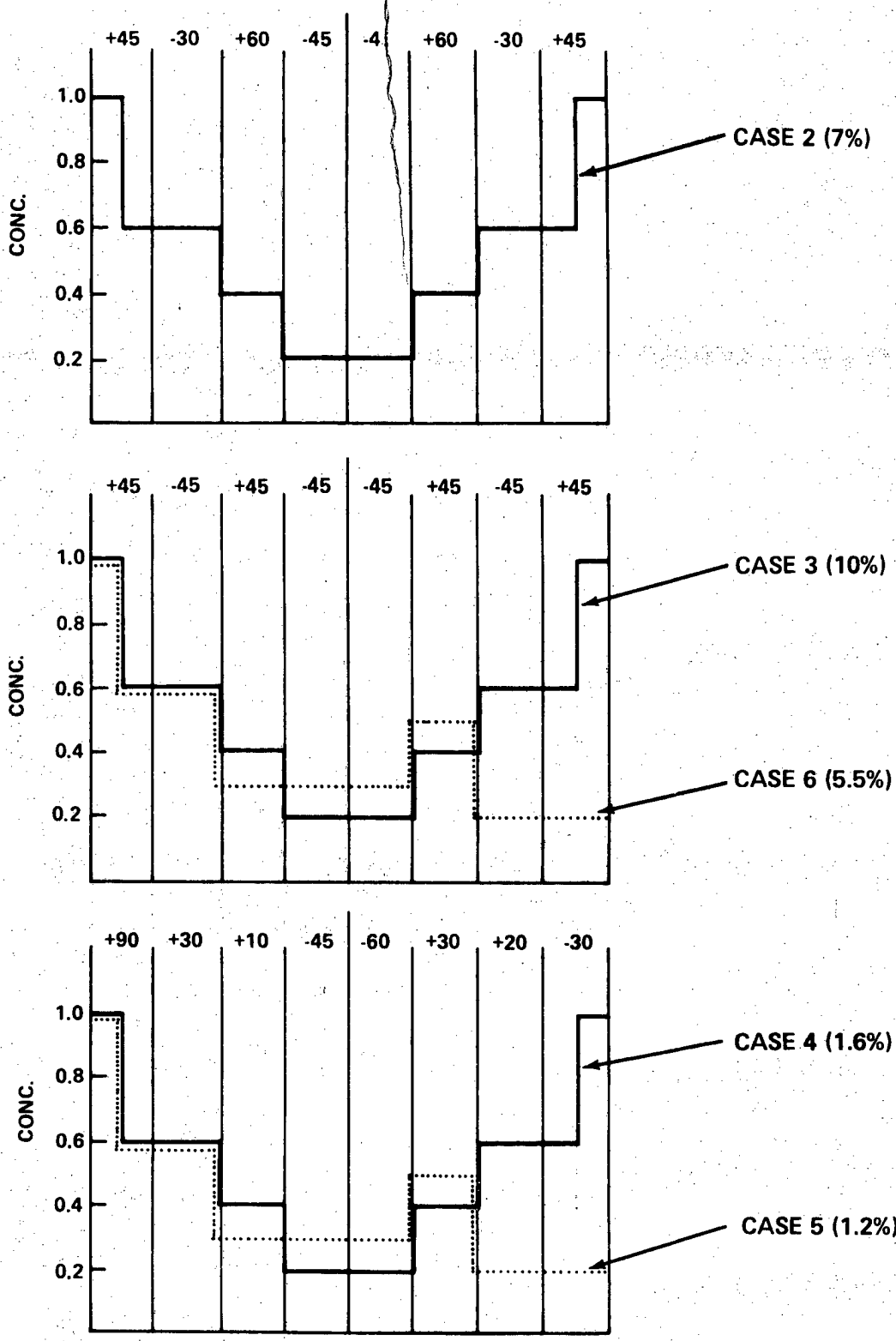


FIG. 20 ARBITRARY MOISTURE DISTRIBUTION IN 8 PLY LAMINATES. (NUMBER IN PARENTHESIS INDICATES PERCENTAGE DIFFERENCE IN ϵ_x FROM UNIFORM MOISTURE DISTRIBUTION)

Biographical Sketch

Dr. Joseph M. Augl graduated from the University of Vienna (Austria) in 1959, with a Ph. D. in chemistry. From 1959-1961, he was a teaching assistant at the University.

From 1961-1963, he was employed as Project Leader by the Research Laboratory of Standard Oil Company of Ohio; from 1963-1968, he was Senior Research Scientist at Melpar, Inc., Falls Church, Virginia; and from 1968 to the present he is with the Naval Surface Weapons Center. He has worked in various fields of organic and polymer chemistry contributing over 80 publications and numerous papers in these areas. At the Naval Surface Weapons Center, he has received two Meritorious Civilian Service Awards. Presently, he investigates various aspects of materials degradation.

EVALUATION OF SPECTROMETRIC OIL ANALYSIS TECHNIQUES FOR
JET ENGINE CONDITION MONITORING

BY

LT. THOMAS THORNTON AND KENT J. EISENTRAUT

Nonmetallic Materials Division

Air Force Materials Laboratory
Wright-Patterson AFB, Ohio 45433

1252

ABSTRACT

The monitoring of wear metals in aircraft engine oils is being done on all Air Force aircraft under the Spectrometric Oil Analysis Program (SOAP). Unusual changes in concentrations of wear metals in the oil usually indicates that abnormal wear is occurring in the oil-wetted system of the engine. The instrumental techniques employed by SOAP are limited by the fact that their ability to analyze wear metal particles is directly related to the size of the wear particles. Preliminary results from an on-going study are presented, in which the analyzability of wear metals versus particle size is being determined for the two techniques presently used by the Air Force, as well as for two plasma atomic emission techniques; inductively coupled plasma and DC argon plasma. The purpose of the study is to evaluate these instrumental techniques in order to determine the capabilities of the two plasma source spectrometers for improved engine condition monitoring.

Introduction

This paper presents preliminary results from a study whose goal is to find an instrumental technique which can be best used for quantitatively analyzing wear metal particles in used oils. Four instrumental techniques are being evaluated in this study, of which two are currently used for oil analysis (atomic absorption and rotating disk atomic emission) and two are new plasma techniques (DC plasma atomic emission and inductively coupled plasma atomic emission).

The results of this study will provide important information, which will result in improved oil analysis procedures which can be used by the Air Force Spectrometric Oil Analysis Program (SOAP) in monitoring gas turbine engine health. Before going into a discussion of the study some background on spectrometric oil analysis is needed.

Spectrometric Oil Analysis Program (SOAP)

Spectrometric oil analysis is a preventive maintenance tool used to determine the type and amount of wear metals in lubricating fluid samples. Engines and gearboxes are the types of equipment most frequently monitored. The presence of unusual concentrations, or changes in concentration of a metal in the oil indicates abnormal wear of the equipment. Once abnormal wear is verified and pinpointed, the equipment may be repaired or removed from service before a failure of the oil-wetted component occurs. This procedure enhances personnel safety and equipment readiness at a minimum cost, and serves as a very important tool in preventive maintenance.

The Air Force SOAP monitors all aircraft engines in the inventory through oil analysis. SOAP has set up guidelines such as in Plate 1 which spell out what concentration and changes in concentration of wear metals are considered normal or abnormal. The two tables give the guidelines for a TF-34 engine for wear metal concentration data obtained from the two instruments currently used by SOAP for oil analysis; the atomic absorption spectrometer (PE-305B) and the rotating-disk atomic spectrometer (A/E35U-3).

There are limitations in the ability of SOAP to monitor engine health. Spectrometric oil analysis is effective in predicting only impending failures which are characterized by an abnormal increase in the wear metal content of the lubricating fluids. Examples of detectable and undetectable failures are shown on Plates 2 and 3. Currently, SOAP detects more than 90% of the cases, where abnormal wear of oil wetted parts is found. The Program is very effective in reducing engine overhaul and maintenance costs.

Objective

The goal of this study is to attempt to determine why some impending failures are not detected by the present SOAP instrumentation. We

primarily wanted to evaluate the capabilities of spectrometers to detect the large particles generated by some wear mechanisms.

Experimental

The study was broken up into three phases. One phase involved preparing metal powder suspensions in oil in order to simulate wear particles of known composition and size, to define the limit of each metal's analyzability relative to particle size. Another phase involved analyzing used oil samples on all four instruments to see how they compare in analyzing actual used oil samples. The last phase involved determining what size metal particles are actually present in used oil samples by using a combination of filtering and microscopy.

Instrumentation

1. Atomic Absorption Spectrometer (PE-305B)

One of the two instruments used by SOAP for oil analysis. With the atomic absorption spectrometer a diluted oil sample is nebulized, and the mist is vaporized in a flame (Plate - 4B). The amount of metal present is determined by the amount of light having a "characteristic" wavelength absorbed by the atomized metal in the flame. This instrument is slowly being phased out of the Program, but will still be used for several more years.

2. Rotating Disk Atomic Emission Spectrometer (Baird-Atomic A/E35U-3)

This is the other instrument used by SOAP for oil analysis. With this instrument a sample of undiluted oil is picked up by the rotating disk and passed through a high voltage spark which vaporizes and excites the metal(s) present, causing the metal atoms to emit light characteristic of each metal. (Plate 4-A) The intensity of the emitted light is directly proportional to the concentration of the metal present in the oil.

3. Inductively Coupled Plasma Atomic Emission Spectrometer (Baird-Atomic FAS-2PL)

This instrument is similar to the A/E35U-3, except the rotating disk source is replaced by an inductively coupled plasma source. The plasma torch (Plate 5) consists of three tubes; the outer tube supplies cooling gas, the next inner tube supplies plasma gas, and the center tube injects the nebulized diluted oil mist into the center of the plasma where it is vaporized. The plasma is sustained by the coil sending in a 27 megahertz radio signal.

4. DC Argon Plasma Atomic Emission Spectrometer (Spectrametrics SMI-III)

The operating principle of this instrument is the same as the other two emission spectrometers, except an echelle grating is employed in the monochromator and a DC plasma is used as the source. The DC plasma (Plate 6)

consists of the system of three electrodes which are bathed in a stream of argon and form an inverted Y-shaped plasma. The nebulized diluted oil mist coming from the center tube is sent into the junction of the plasma column. The sample mist reaches a high enough temperature just below the plasma for the metal to be atomized and emit light.

Plate 7 and 8 describe the experimental procedures used in this study. The acid method described is a procedure which dissolves all the wear metal particles, and by employing it, the total amount of metal can be analyzed quantitatively.

Results

Before discussing analytical results on metal powder analyzabilities, it is important to discuss some of the factors which affect particle analyzability. The basic factors are the source, the temperature the sample attains in the source, type of metal, the sample introduction system, and standards used to calibrate the instrument.

It is expected that metal particles will behave differently in the three different types of sources (flame, argon plasma, and spark) because the environments differ drastically from each other. In order to accomplish a quantitative analysis of metal particles they must be completely vaporized. The source temperature becomes very important for metals with high boiling points. Such metal particles in a cooler source, like a flame, will be very difficult to completely vaporize. Associated with the effect of temperature on vaporizing the metal present is the further problem that only a small region of the source can be focused on the inlet slit of the spectrometer, and calibration is usually accomplished by adjusting the source position for a maximum signal for the organometallic standard. The problem is illustrated in Plate 9 which shows how the organometallic standard and an oil sample behave in an atomic absorption flame. The used oil samples behave differently from the standard. Consequently, positioning of the flame is critical in obtaining meaningful results. Similar situations occur with the argon plasma sources.

Another major factor involved with particle analyzability is the ability of the sample introduction system to deliver a representative sample into the source. If the sample introduction system doesn't deliver the wear particles into the source they will not be analyzed. Such a situation occurs after a sample is nebulized, because in the process of transferring the sample mist to the source, the dense metal particles tend to settle out before getting into the flame or plasma.

Analyzability of Metal Powder Suspensions in Oil

Plates 10-16 present the results obtained for suspended metal powder samples when analyzed by the various instruments. In an attempt to get a handle on analyzability of the particles, samples were analyzed after being

filtered through various pore size filters. The acid method provided an indication of the total amount of metal present in the filtrate.

For the SMI-III analysis the data was obtained with the plasma positioned for the optimization of metal powder emission, except for titanium. For some metal suspension there were not enough small particles present, which passed through the smaller size filter, to provide meaningful data, so some plots are abbreviated. From the results it appears that all instruments in their present configuration are limited in their ability to quantitatively analyze large suspended metal particles. Generally the SMI-III gave the best analysis followed by the A/E35U-3, FAS-2PL and PE305B. It is also apparent that the type of metal being analyzed has an affect on analyzability.

It was anticipated that atomic absorption (AA) would give the poorest analyses since the flame temperature ($\sim 3000^{\circ}\text{K}$) is the lowest of all sources studied. Therefore, large particles will not be quantitatively vaporized. In contrast the plasma sources possess a much higher effective temperature ($6000-10,000^{\circ}\text{K}$). At present the SMI-III is capable of analyzing larger particles than the PE305B or FAS-2PL, but it is not equally effective for all metals, i.e. it does better for iron than copper. The rotating disk A/E35U-3 seems to do a better job in analyzing particles than atomic absorption, but it also is limited in capability to analyze larger metal particles.

Analysis of Used Oil Samples

Through the support of several Air Force SOAP labs several hundred oil samples were obtained. The SOAP labs also provided other information with the oil samples, such as engine type, hours since overhaul on oil change, etc. The samples were then categorized into four groups: "Hits" - where abnormal wear was detected. "High Concentration" - where the concentration of a metal was high, but no abnormal wear seemed to be occurring, "Failure" - where the failure was not detected in time, "Routine" - where the amount of wear metal was low or within normal limits.

The data presented in this section deals solely with the results from the analysis of the high metal concentration samples. The values obtained, for the amount of iron detected by various instruments or methods, were plotted against each other for comparison.

Plates 17 and 18 are plots of the iron concentration in parts per million (ppm) obtained by using the acid method, (which gives the total concentration of iron present), against the results obtained by using the SMI-III and the A/E35U-3. The SMI-III seems to be able to analyze most of the wear metal present in the sample, but it seems to not do as well at higher concentrations (possibly due to the presence of large particles). The A/E35U-3 seems to give artificially higher results, and generally doesn't correlate very well with the results from the acid method. There are no clear reasons why the results from the A/E35U-3 are like this, however it is suspected it may have to do with matrix effects of the oil

(viscosity problems or interferences due to oil composition). When oil samples are run by the SOAP Labs, the A/E35U-3 normally gives artificially higher results than the PE-305B. This is because the standards used are more viscous than the oils being analyzed. However in this study the standards were made up in the same type and viscosity oil as the samples. (Mil. 7808). Consequently it was expected any viscosity effect would be minimized.

Plates 19 and 20 are the plots of the results from the SMI-III versus the FAS-2PL and PE-305B. The results indicate that FAS-2PL correlates well with the SMI-III, which suggests the FAS-2PL is seeing most of the wear metal particles present in these samples. The results obtained by the PE-305B generally agree with the SMI-III results, but apparently the PE-305B is not seeing all the metal particles present in some samples.

Plates 21 and 22 are the plots for the A/E35U-3 versus the PE-305B and the SMI-III. The results obtained from using the PE-305B and the SMI-III generally don't correlate well with the A/E35U-3 results, and again the A/E35U-3 gives higher values for the wear metal concentration. We again suspect that matrix effects due to the oil cause the poor correlation and artificially higher results. We suspect this because the samples run on the SMI-III and PE-305B were diluted so matrix effects due to the oil are minimized.

Characterizing Oil Samples

In an effort to characterize the particle sizes of the metal present in used oil, specimens, randomly selected from the four classes of oil samples, were filtered through various pore size filters and the filtrates were analyzed using the SMI-III. Along with the filtered samples, an unfiltered sample was analyzed by the acid method to determine the total amount of iron present.

Plate 23 contains the results obtained for the samples with lower total concentrations of iron, and Plate 24 contains the results obtained for the samples with higher total concentrations of iron. The vertical lines at the end of some plots indicate the concentrations obtained by the acid method if it was different from that obtained using the SMI-III. Iron was chosen for examination because it was the only metal which was consistently present in detectable concentrations. In a few cases the actual particle sizes of the metal may not be effectively represented by filtering, because some metal particles may form agglomerates, and be caught by larger pore sized filters.

From these results it can be concluded that all samples are not alike, since the particle size distributions don't fit a definite pattern. For most samples having low iron content, most of the mass is found in particles below 5 microns in size. For samples with a high total concentration of iron there usually are metal particles larger than 5 microns present. Not all the metal in some samples is detected by the SMI-III, as can be seen by comparison with the acid values. The fact that the SMI-III, which

analyzes larger iron particles than the PE-305B, is not detecting all the iron present in some samples means that the PE305B would also not detect some of the iron.

Also of interest is the fact discovered through microscopic examination of the filters after filtering the oil samples, that there are considerable amounts of nonmetallic particles present in some used oils.

Conclusions

The research being performed provides an indication of the limitations of various spectrometers to provide a quantitative analysis for metal particulates suspended in oil. All spectrometric techniques examined in this work have been found to be limited in capability to analyze larger metal particles. The plasma and atomic absorption techniques do not detect all the wear metal present in some authentic samples when compared against the results of the particle size independent procedure. The SMI-III with its present sampling system appears to possess a greater capability to analyze larger metal particles than the FAS-2PL. Both plasma spectrometers should be superior to AA when analyzing for wear metals in used oil samples. It is difficult, at this point, to compare the A/E35U-3 against the other instruments studied since it gives values higher than those of the particle independent procedure, which reflects the true metal content.

The oil analysis spectrometers used by the Air Force are probably not detecting all the metal present in some samples. These samples may include the most important samples, i.e. from engines nearing failure. It is felt that the capability of plasma spectrometers to analyze large metal particles can be greatly increased through the incorporation of improved sample introduction systems.

ACKNOWLEDGEMENTS

We would like to acknowledge the University of Dayton research group who work under Air Force Contract No. F33615-76-C-5312 and were responsible for obtaining a considerable amount of the data in this study: Wendell Rhine, Costandy Saba, John Brown, Pat Synder Fair and Charles Tobin.

We would also like to acknowledge CMSgt Robert Muthart, USAF who ran most of the samples on the A/E35U-3 spectrometer.

BIBLIOGRAPHY

1. J.H. Taylor, T.T. Bartels and R. L. Crump, *Analytical Chemistry* 43, 19780 (1971).
2. Joint Oil Analysis Program Laboratory Manual, T.O. 33-1-37, 1 May 1977.
3. John R. Brown, University of Dayton Research Institute, DAYton, Ohio 45469.

GUIDELINES FOR TF-34
AIRCRAFT: (A-10) (S-3)

A/E35U-3

	Fe	Ag	Al	Cr	Cu	Mg	Ni	Ti
Abnormal Trend (PPM Increase in 10 hrs)	4	2	2	2	3		2	3
Normal Range	0-15	0-3	0-3	0-3	0-8		0-3	0-5
Marginal Range	16-18	N/A	N/A	N/A	9-10		N/A	6
High Range	19-22	4	4	4	11-12		4	7-8
Abnormal	23+	5+*	5+	5+	13+		5+	9+

Average Concentration Other Elements:

Pb=4

Si=14

Sn=11

Mo=1

*Disregard high Ag for Navy Engines

Source of Ag: Spline wear on PTO shaft

ATOMIC ABSORPTION

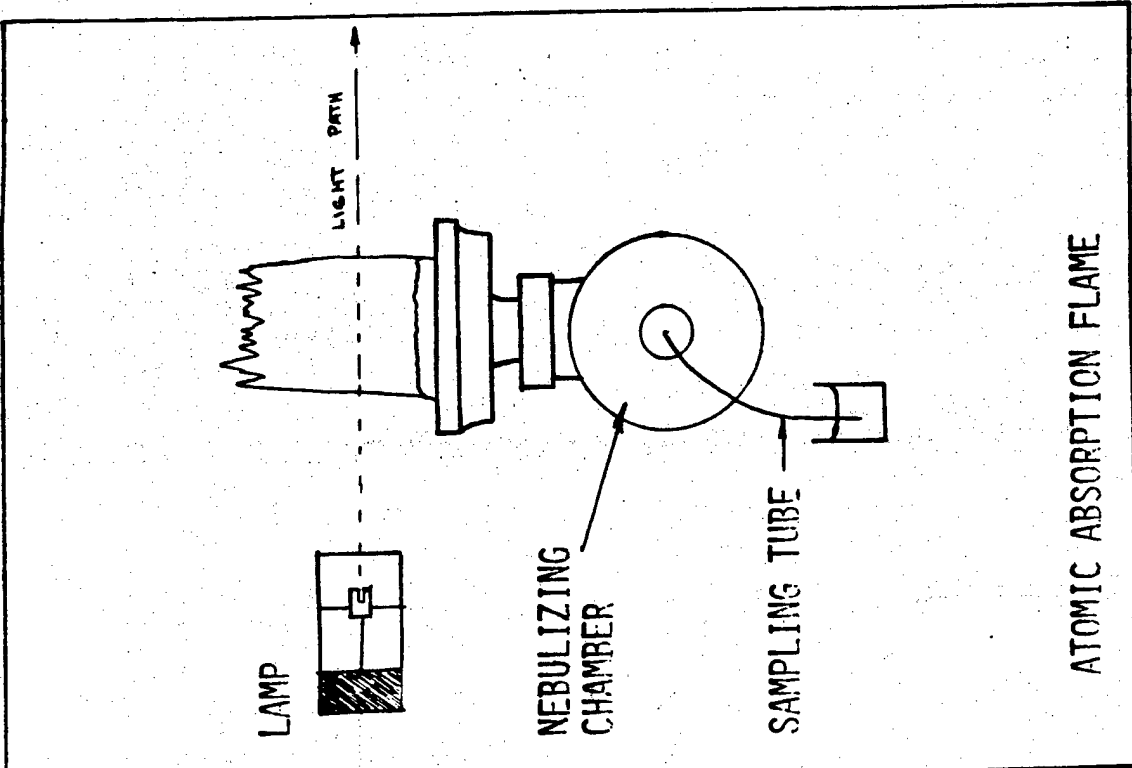
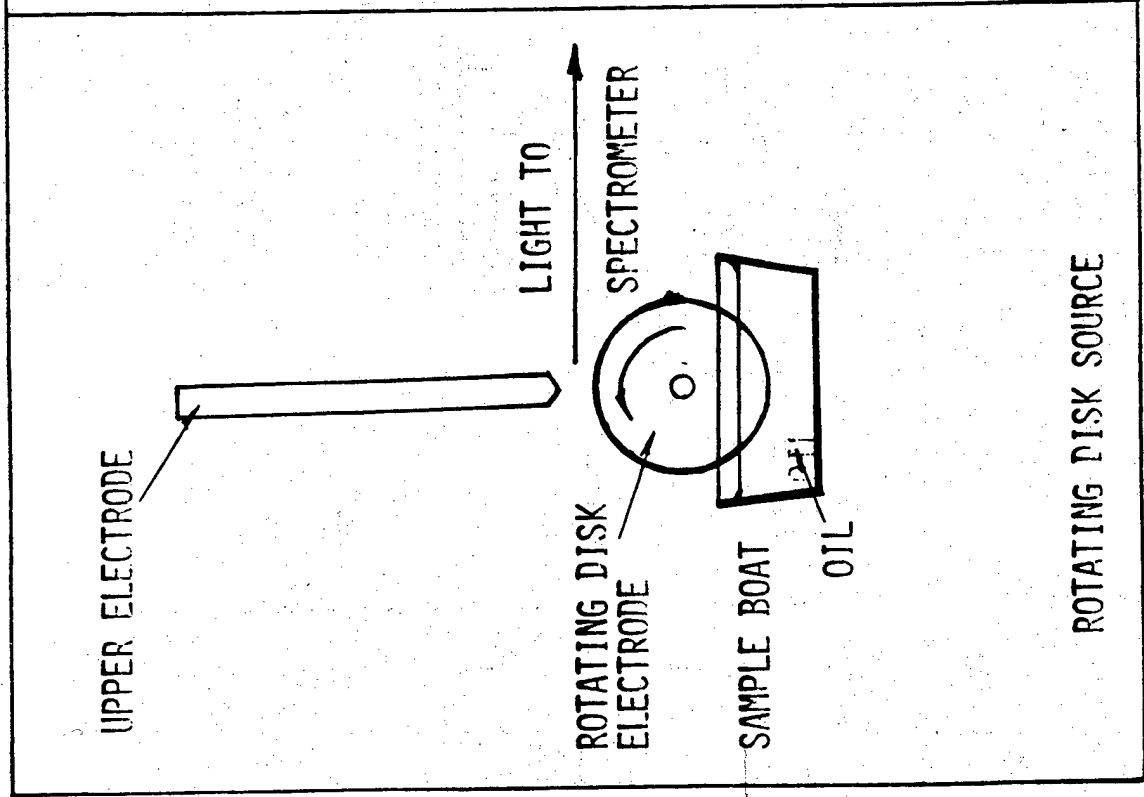
	Fe	Ag	Al	Cr	Cu	Mg	Ni	Ti
Abnormal Trend (PPM Increase in 10 hrs)	2	2	2	2	2			2
Normal Range	0-5	0-3	0-3	0-3	0-3		0-1	0-2
Marginal Range	6	N/A	N/A	N/A	4		N/A	N/A
High Range	7	4	4	4	5		2	3
Abnormal	8+	5+	5+	5+	6+		3+	4+

NORMALLY DETECTABLE FAILURES

1. CYLINDER DAMAGE IN RECIPROCATING ENGINES.
2. WORN, MISALIGNED, OR BROKEN ANTI-FRICTION BEARINGS AND RETAINERS.
3. WORN, MISALIGNED, OR SCORED GEARS.
4. WORN OR SCORED JOURNAL BEARING SURFACES.
5. SLOWLY PROGRESSIVE FAILURES WHICH ADD TO THE WEAR METALS CONTENT OF THE LUBRICATION SYSTEM, EITHER DIRECTLY BY RUBBING BETWEEN MATING SURFACES OR INDIRECTLY BY MISALIGNMENT OR MISMATING SURFACES.

FAILURES WHICH CANNOT BE DETECTED BY SPECTROMETRIC ANALYSIS

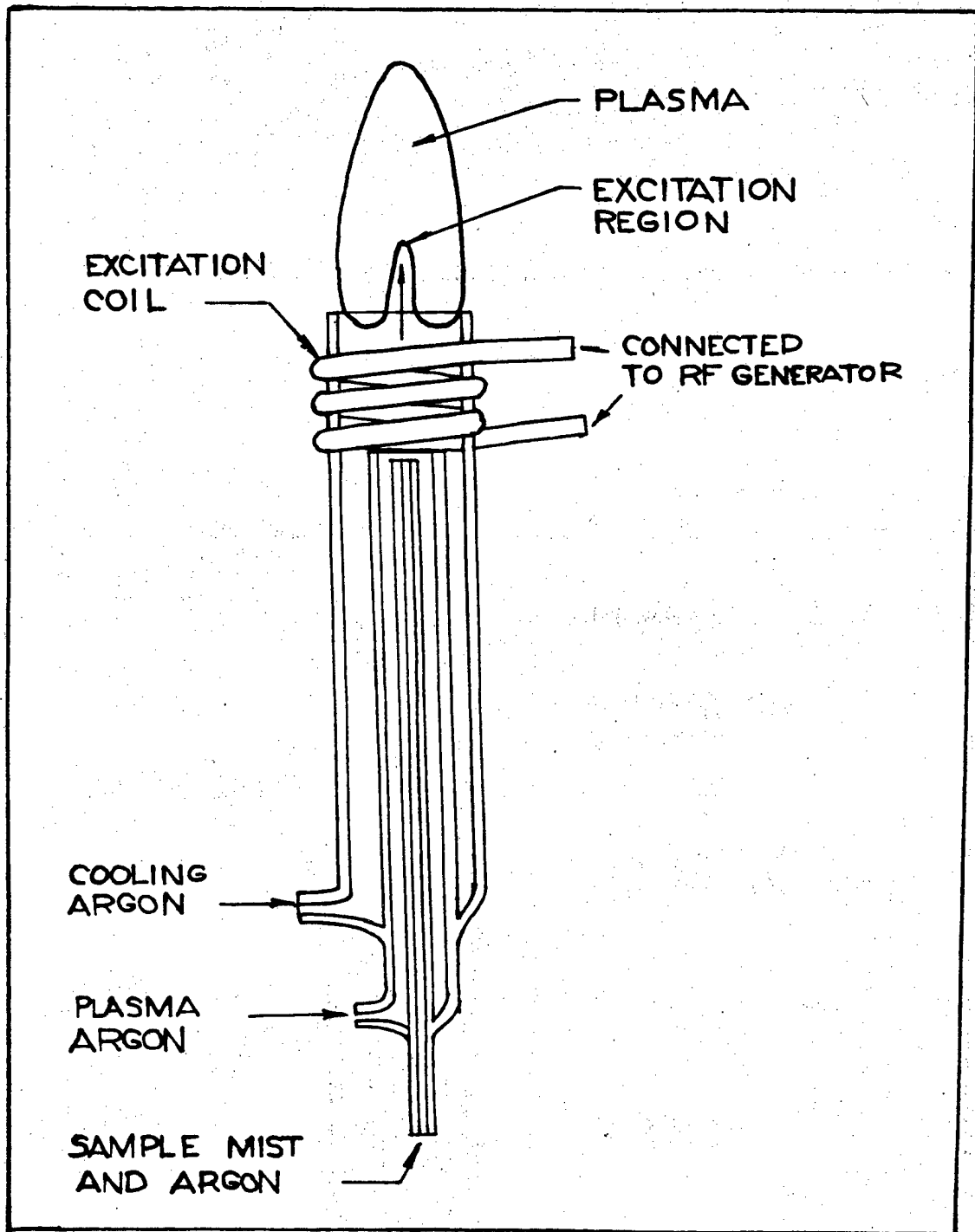
1. FATIGUE FAILURES.
2. FAILURES WHICH OCCUR TOO RAPIDLY TO BE DETECTED BY FLUID ANALYSIS, INCLUDING FAILURES DUE TO FLUID STARVATION AND BEARING SEIZURE.
3. SPECTROMETERS WILL NOT DETECT CHIPS OR LARGER WEAR METAL PARTICLES, SOME FAILING PARTS MAY NOT GENERATE ENOUGH SMALLER SIZED WEAR PARTICLES FOR A FAILURE TO BE DETECTED.



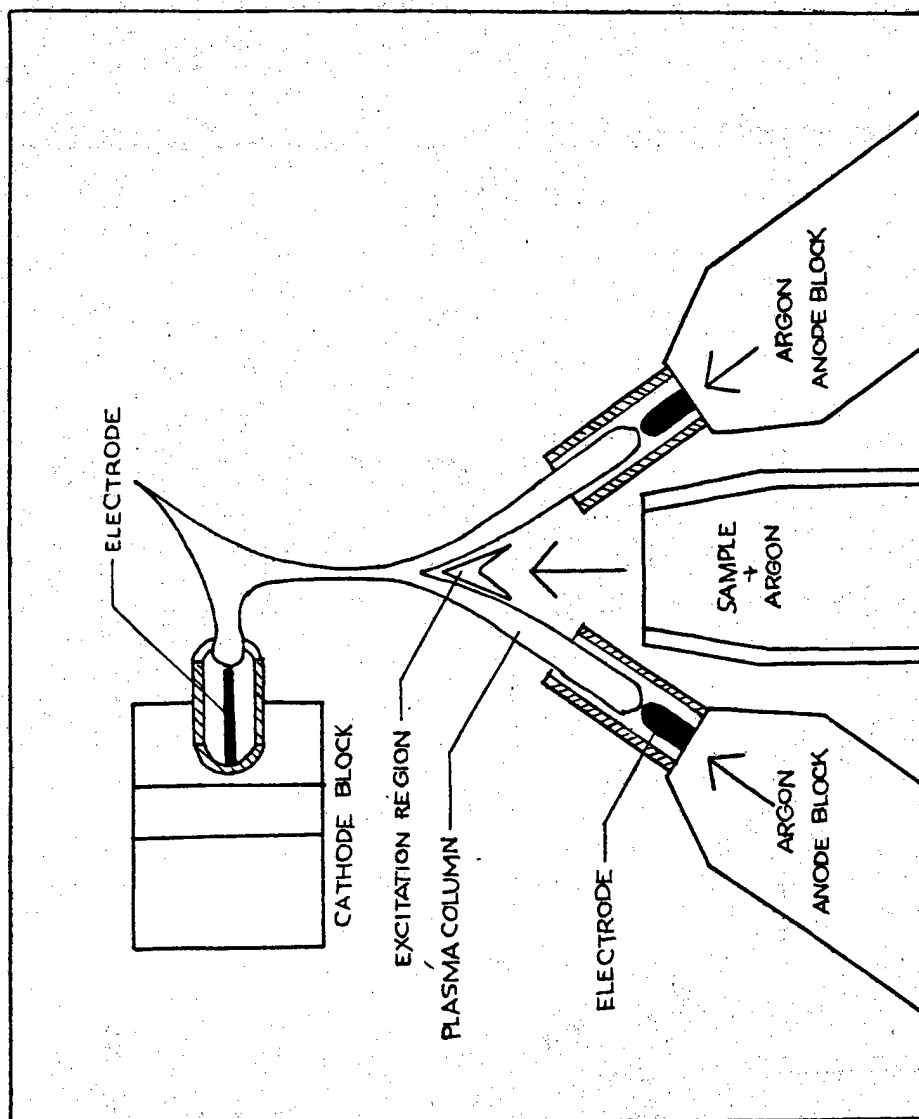
B

A

PLATE 4



INDUCTIVELY COUPLED PLASMA TORCH



D.C. PLASMA SOURCE

PLATE 6

EXPERIMENTAL PROCEDURES

1. ATOMIC ABSORPTION SPECTROMETER PE-305B

A NITROUS OXIDE-ACETYLENE FLAME WAS USED WITH A LAMINAR FLOW BURNER. THE SAMPLES AND STANDARDS WERE DILUTED 1:2 BY WEIGHT WITH METHYL ISOBUTYL KETONE. CONOSTAN C-13 IN MIL. 7808 OIL WAS USED AS A STANDARD.

2. ROTATING DISK ATOMIC EMISSION SPECTROMETER A/E35U-3

THE INSTRUMENT WAS CALIBRATED WITH 100 PPM CONOSTAN C-20 IN MIL. 7808 OIL. THE OIL SAMPLES WERE NOT DILUTED BEFORE BEING ANALYZED.

3. D.C. PLASMA ATOMIC EMISSION SPECTROMETER SMI-III

THE INSTRUMENT WAS CALIBRATED WITH 50 PPM CONOSTAN C-20 IN MIL. 7808 OIL. THE STANDARDS AND OIL SAMPLES WERE DILUTED 1:4 BY WEIGHT WITH KEROSENE.

4. INDUCTIVELY COUPLED PLASMA ATOMIC EMISSION SPECTROMETER FAS-2PL

THE INSTRUMENT WAS CALIBRATED WITH 100 PPM CONOSTAN C-20 STANDARD IN MIL. 7808 OIL. STANDARDS AND OIL SAMPLES WERE DILUTED 1:4 BY WEIGHT WITH KEROSENE.

EXPERIMENTAL PROCEDURES

3

ACID METHOD

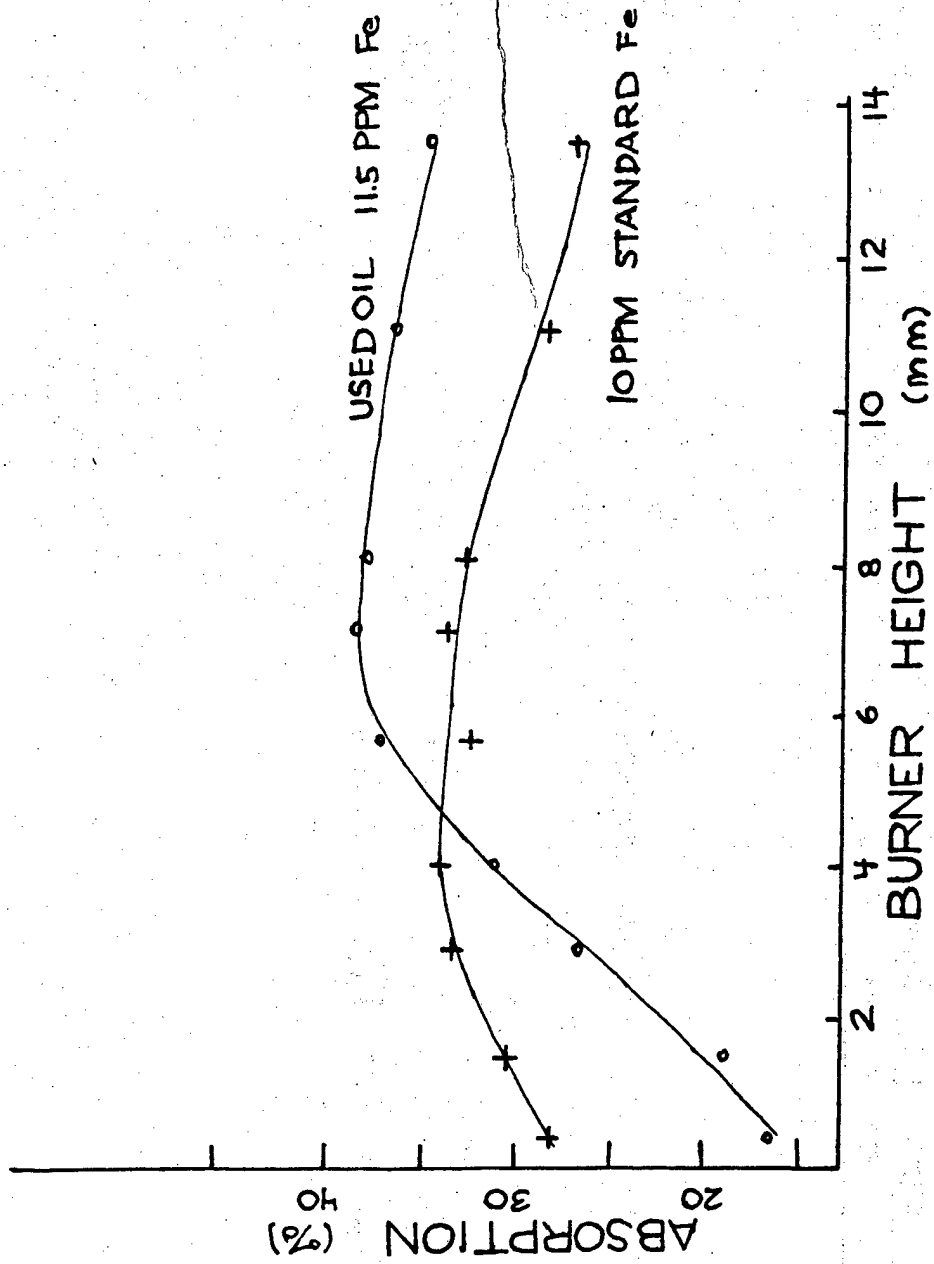
THREE GRAMS OF OIL IS PLACED IN A LINEAR POLYETHYLENE BOTTLE. FOUR TENTHS OF A GRAM OF ACID SOLUTION (90 ML AQUA-REGIA + 5 ML CONCENTRATED HF) IS ADDED TO THE BOTTLE AND SHAKEN FOR 30 SECONDS. THE MIXTURE IS THEN ULTRASONICALLY AGITATED AT 700 C. FOR 45 MINUTES AFTER WHICH IT IS DILUTED WITH 5.6 GRAMS OF DILUENT SOLUTION (90 ML ISOPROPANOL + 10 ML METHYL ISOBUTYL KETONE). THE SAMPLE IS THEN ANALYZED ON THE SMI-III USING STANDARDS PREPARED IN MIL. 7808 OIL FROM ACID SOLUTIONS OF REACTED PURE METAL POWDERS.

FILTERING

ALL FILTERING WAS DONE USING NUCLEOPORE POLYCARBONATE MEMBRANES. THE PORE SIZE OF THE FILTERS VARIED FROM 12 MICROMETERS TO 0.5 MICROMETER.

1269

PLATE 8



IRON ABSORPTION PROFILE IN AN ATOMIC ABSORPTION FLAME.

PLATE 9

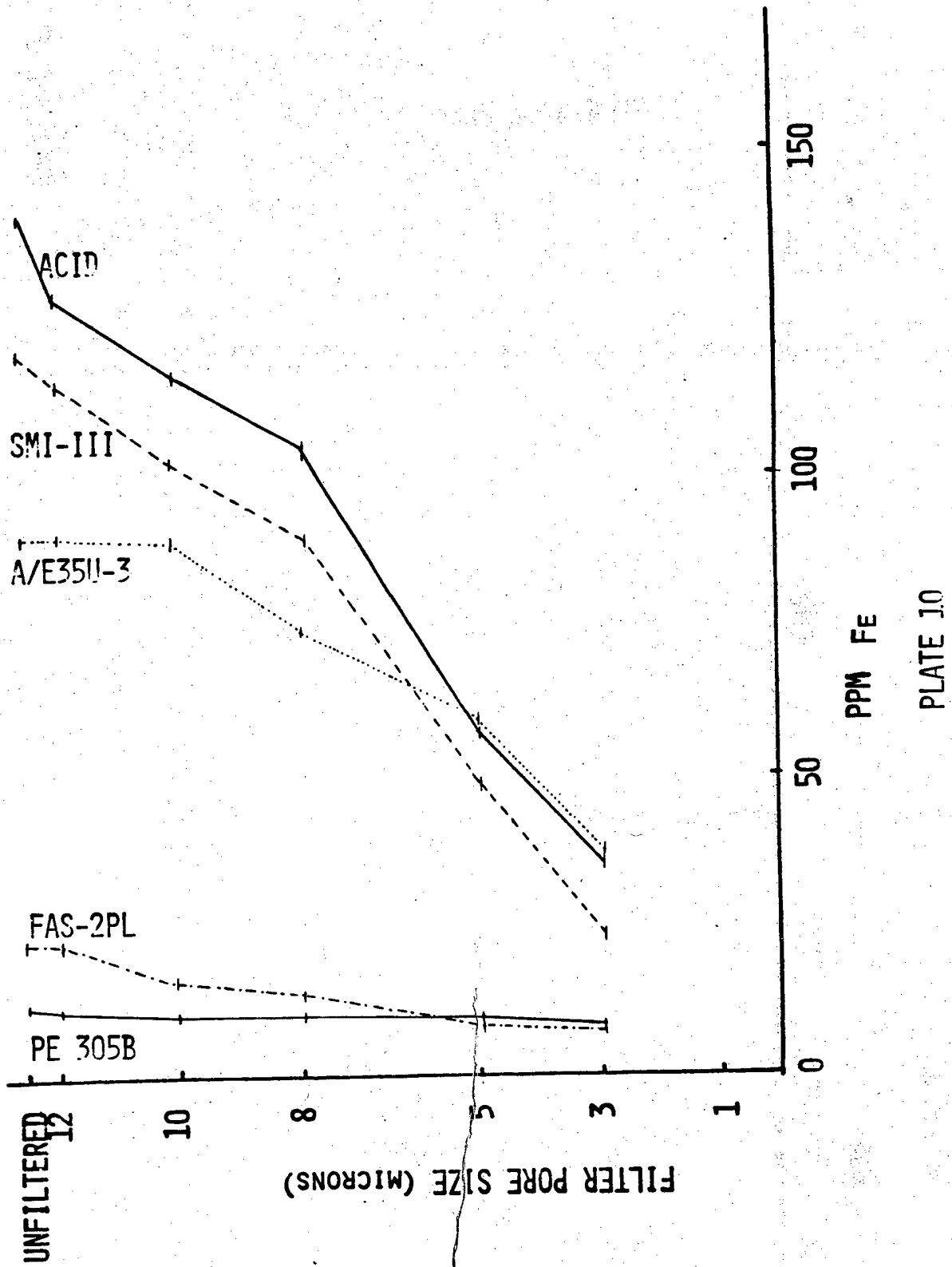


PLATE 10

1271

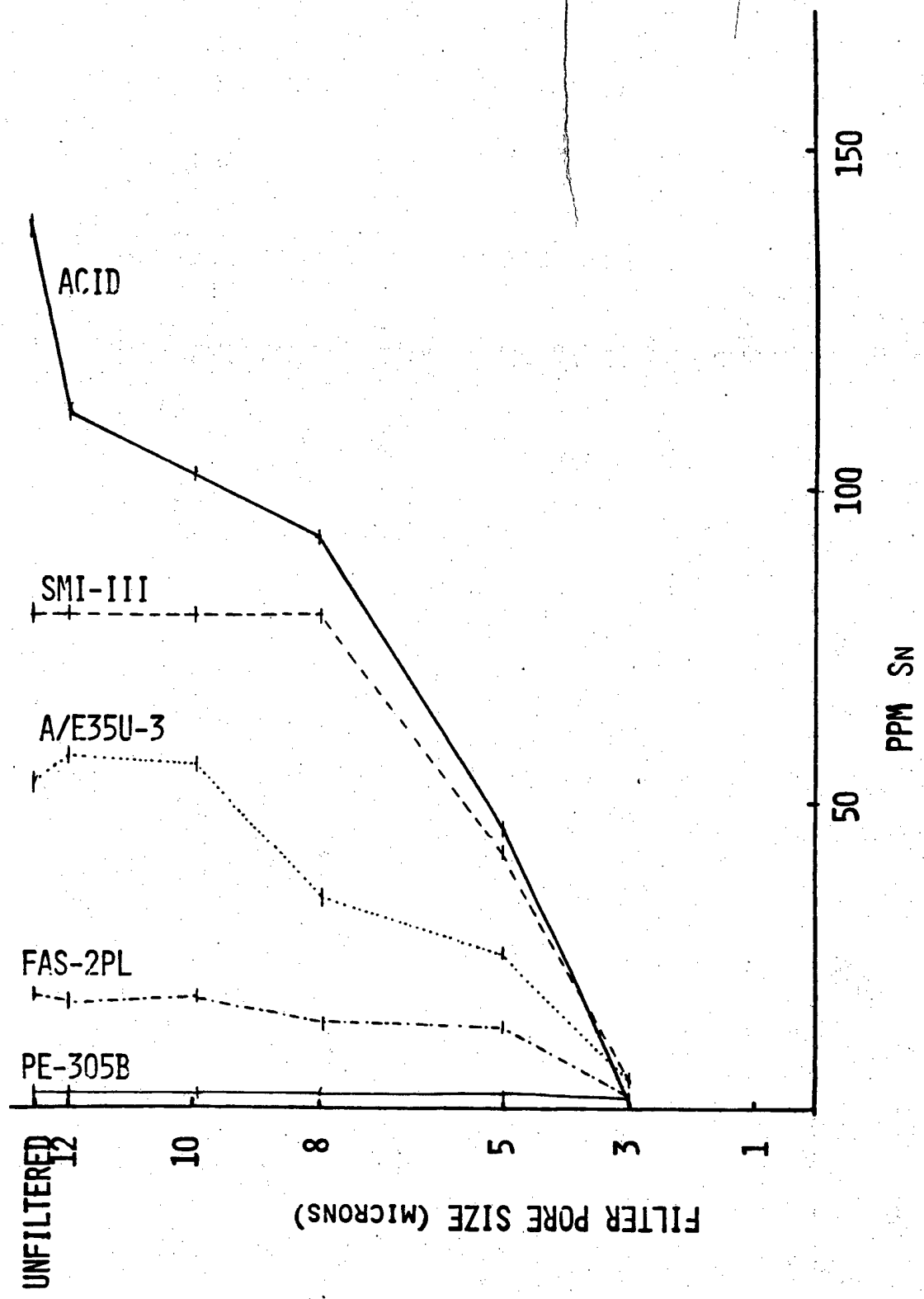
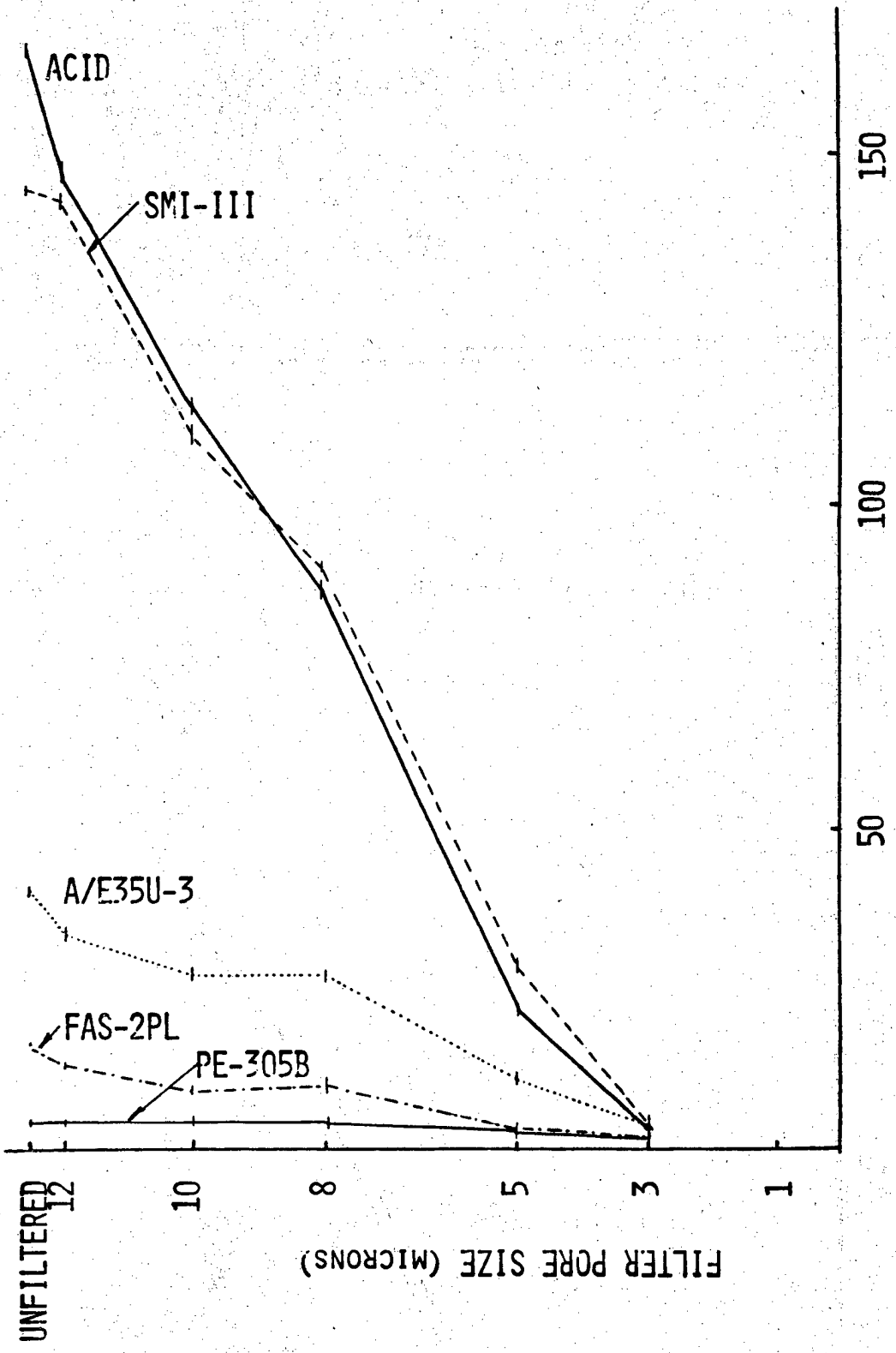


PLATE 11

PLATE 11

1272



PPM Ni
 PLATE 12

1273

PLATE 12

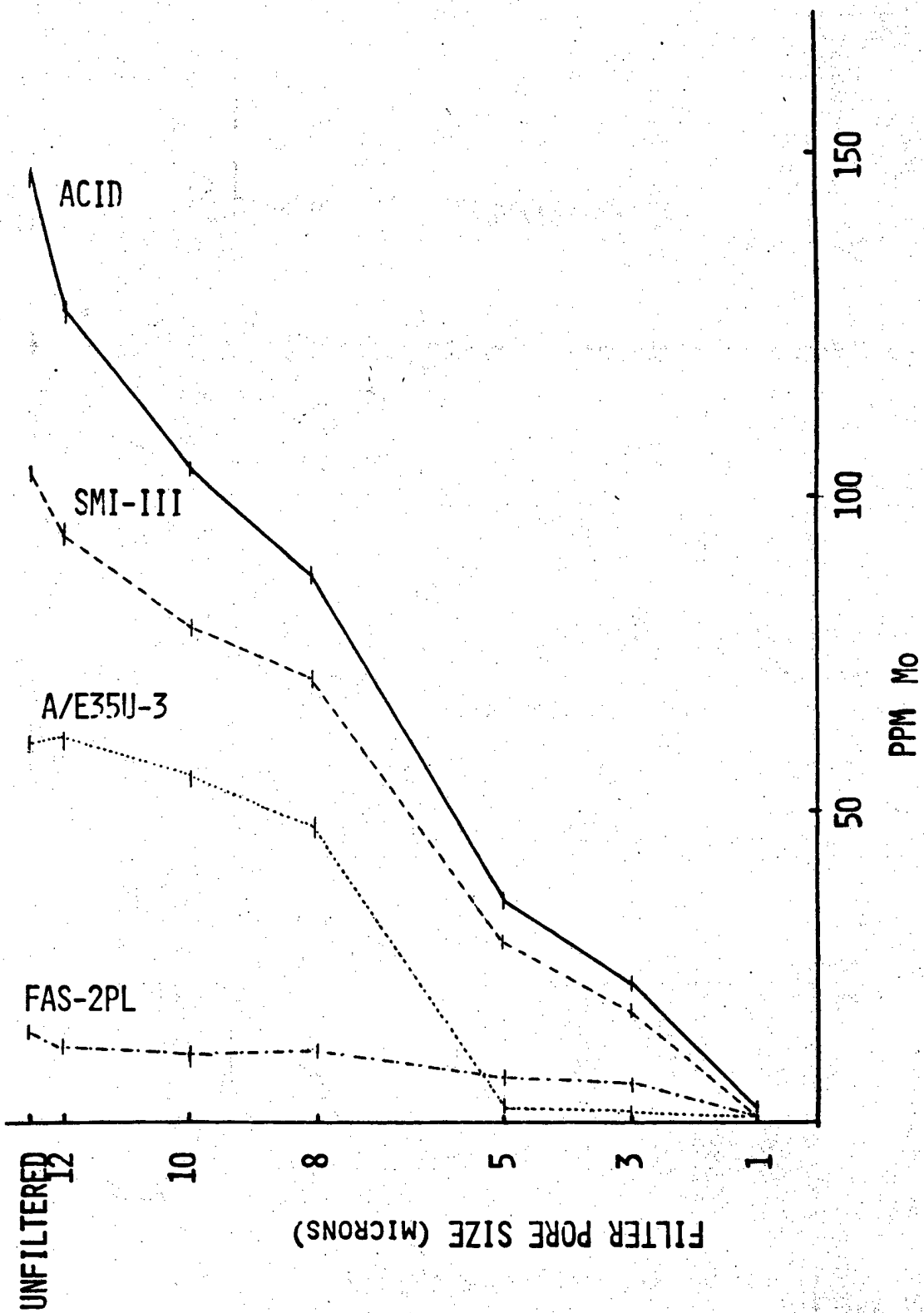


PLATE 13

PLATE 13

1274

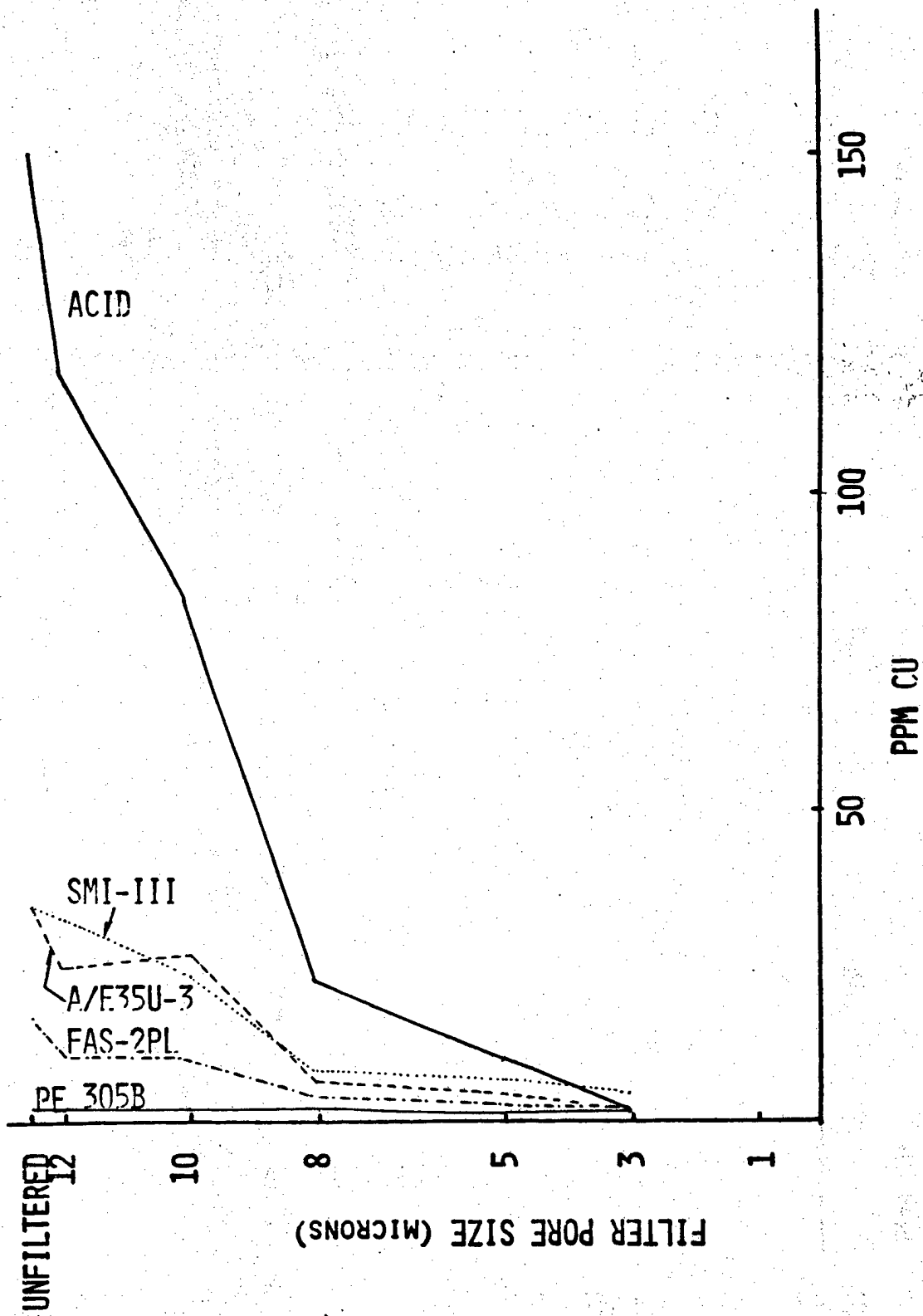


PLATE 14

PLATE 14

1275

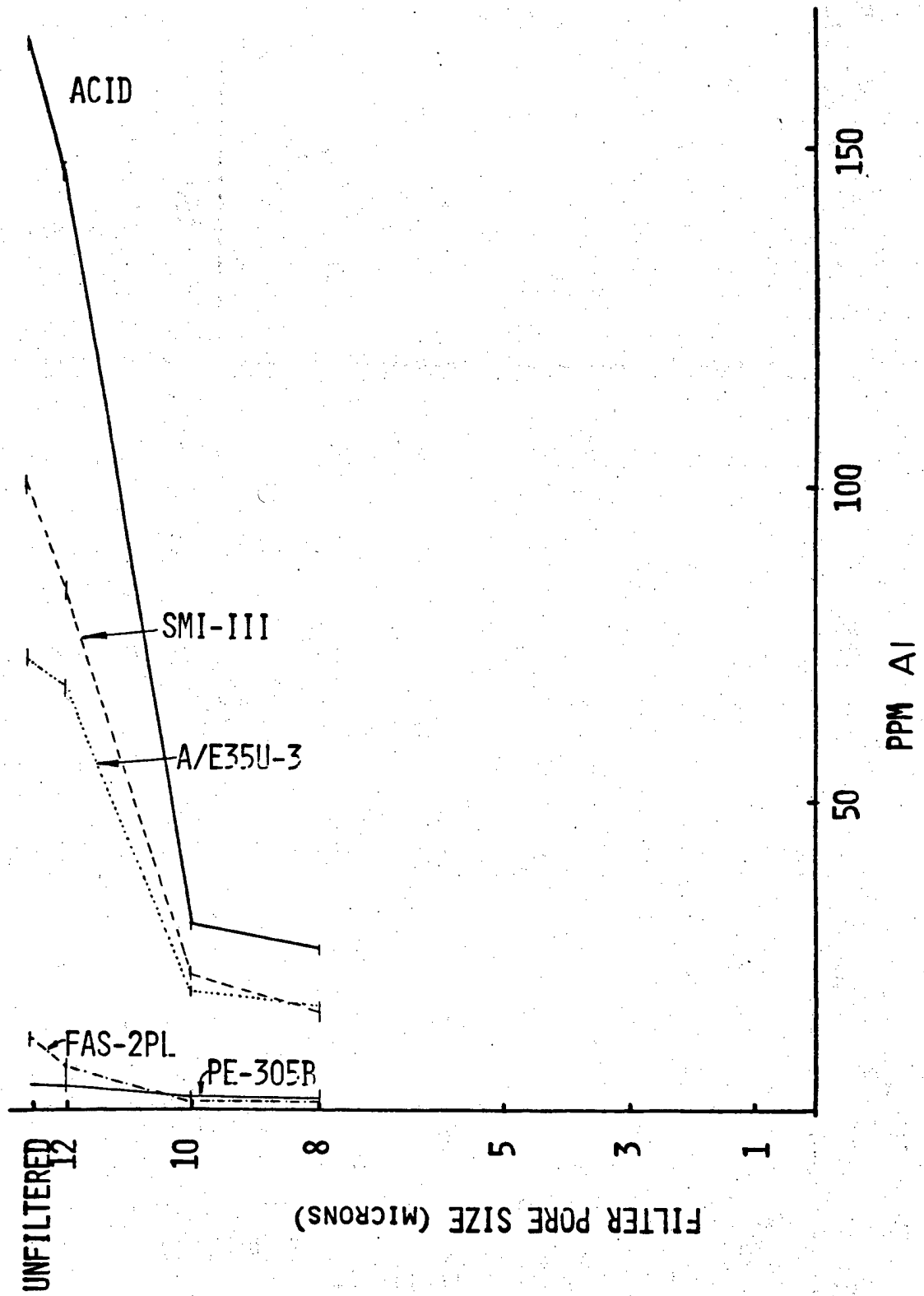


PLATE 15

PLATE 15

1276

1237

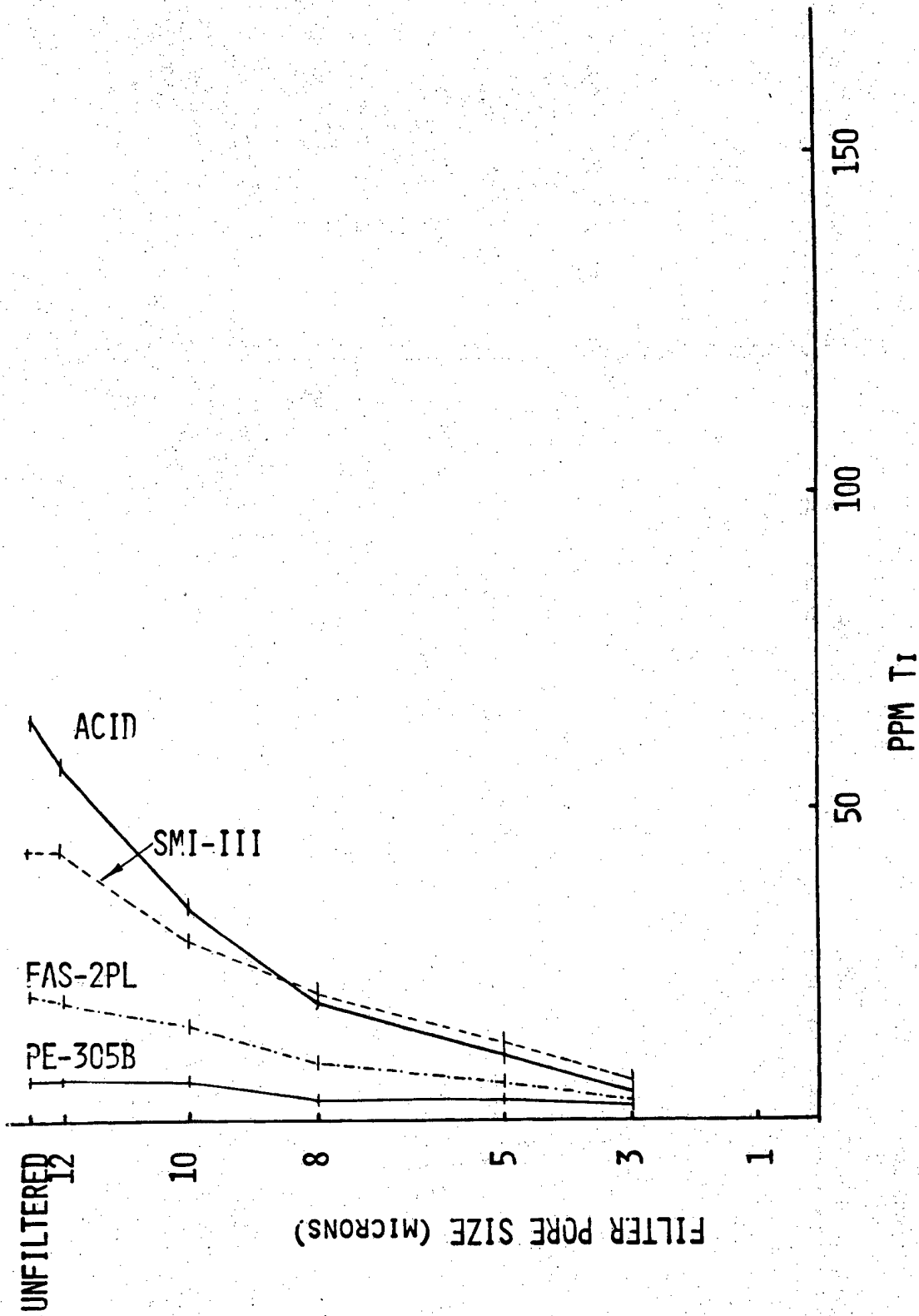


PLATE 16

PLATE 16

1277

PLATE 17

1278

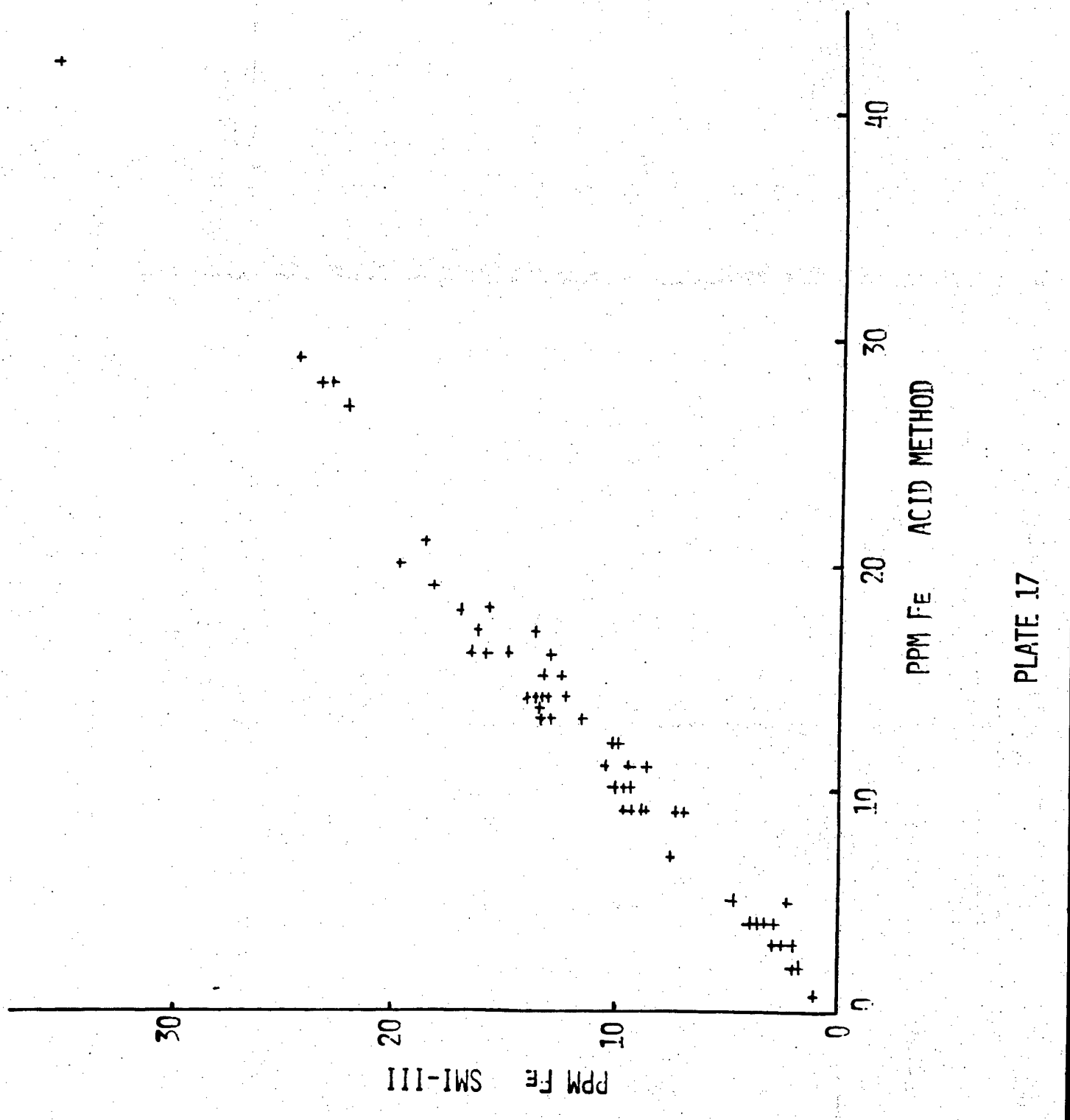


PLATE 17

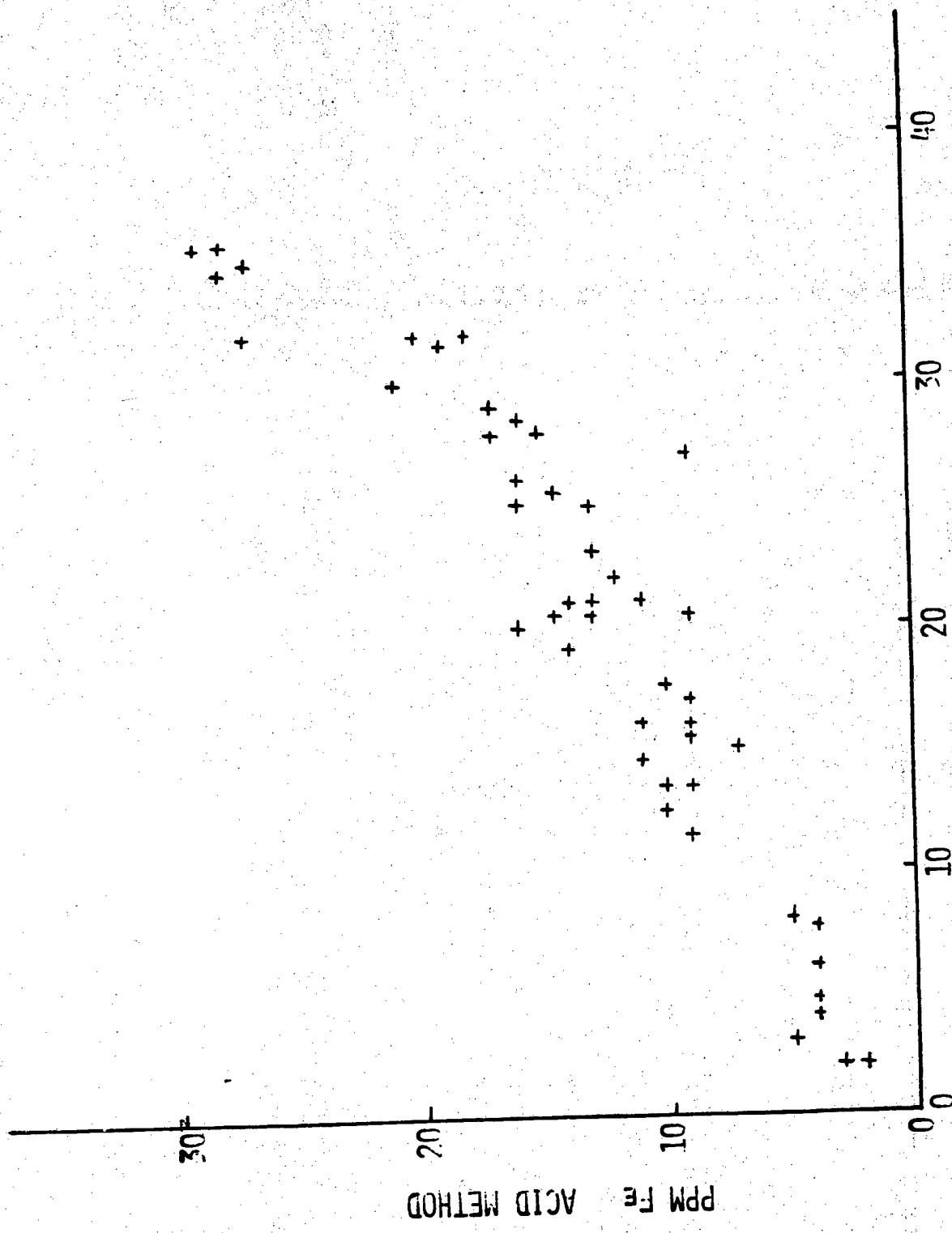


PLATE 18

1240

1279

PPM Fe AVE35U-3

PLATE 18

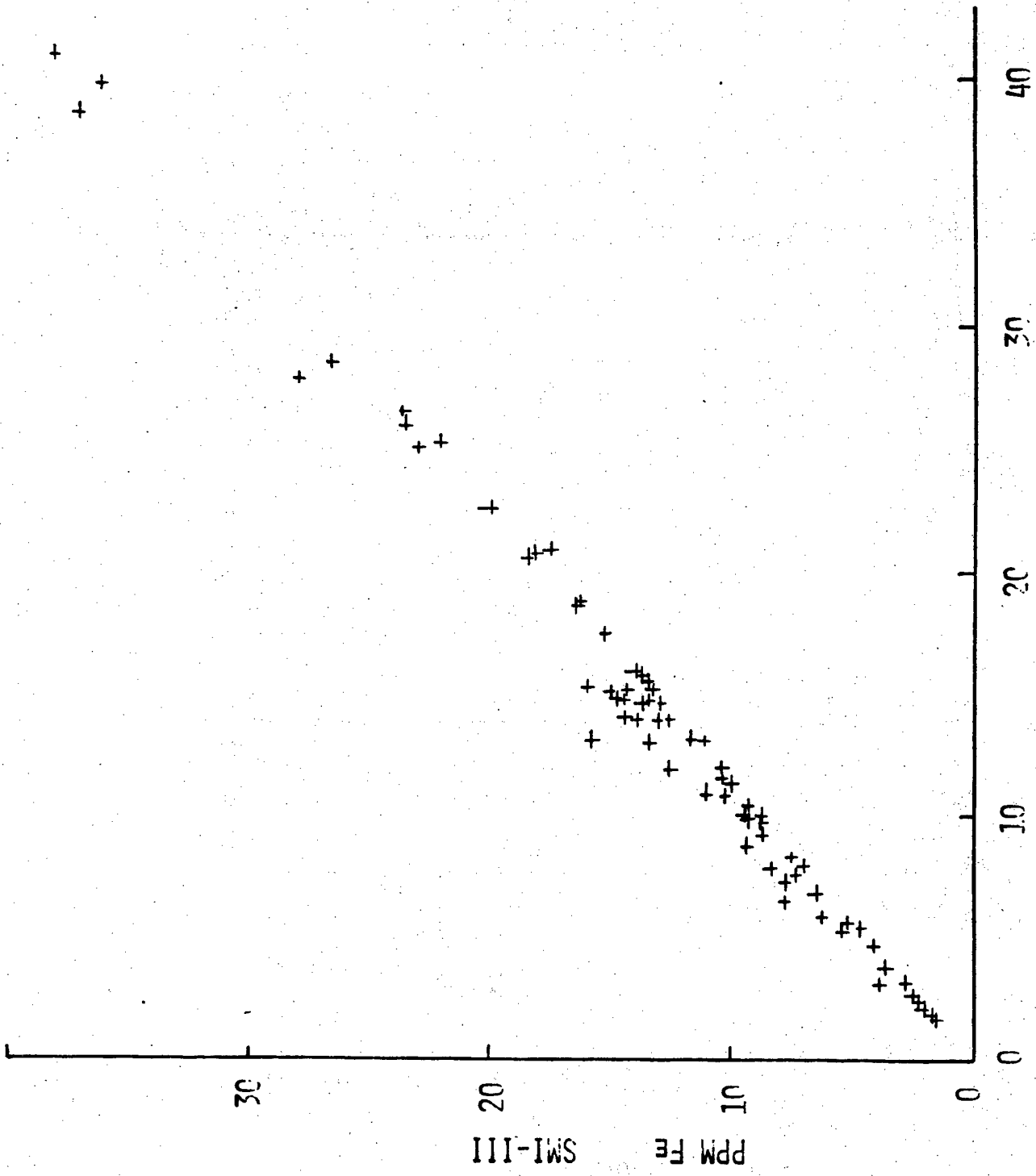


PLATE 19

1280

PLATE 19

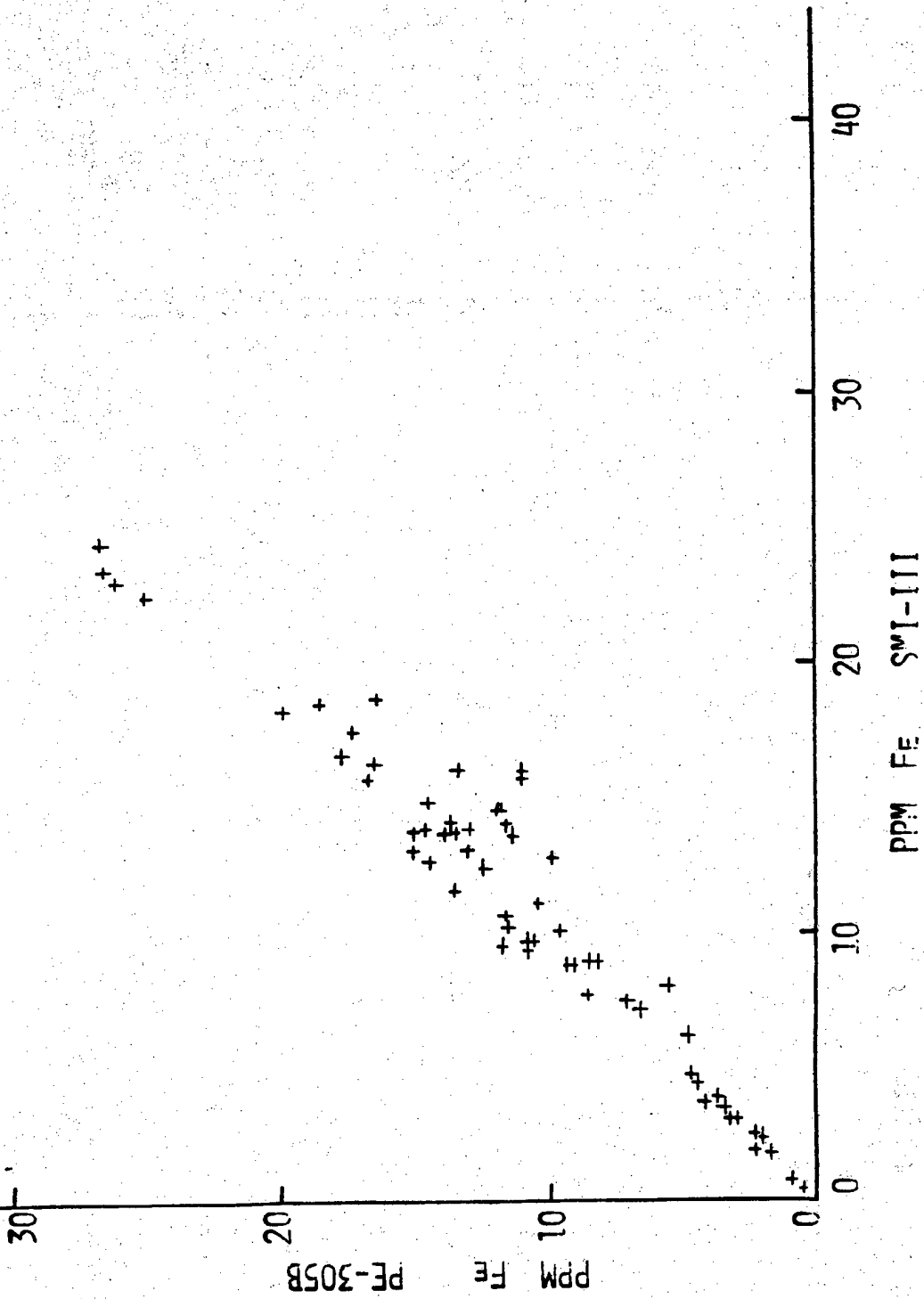


PLATE 20

1281

PLATE 20

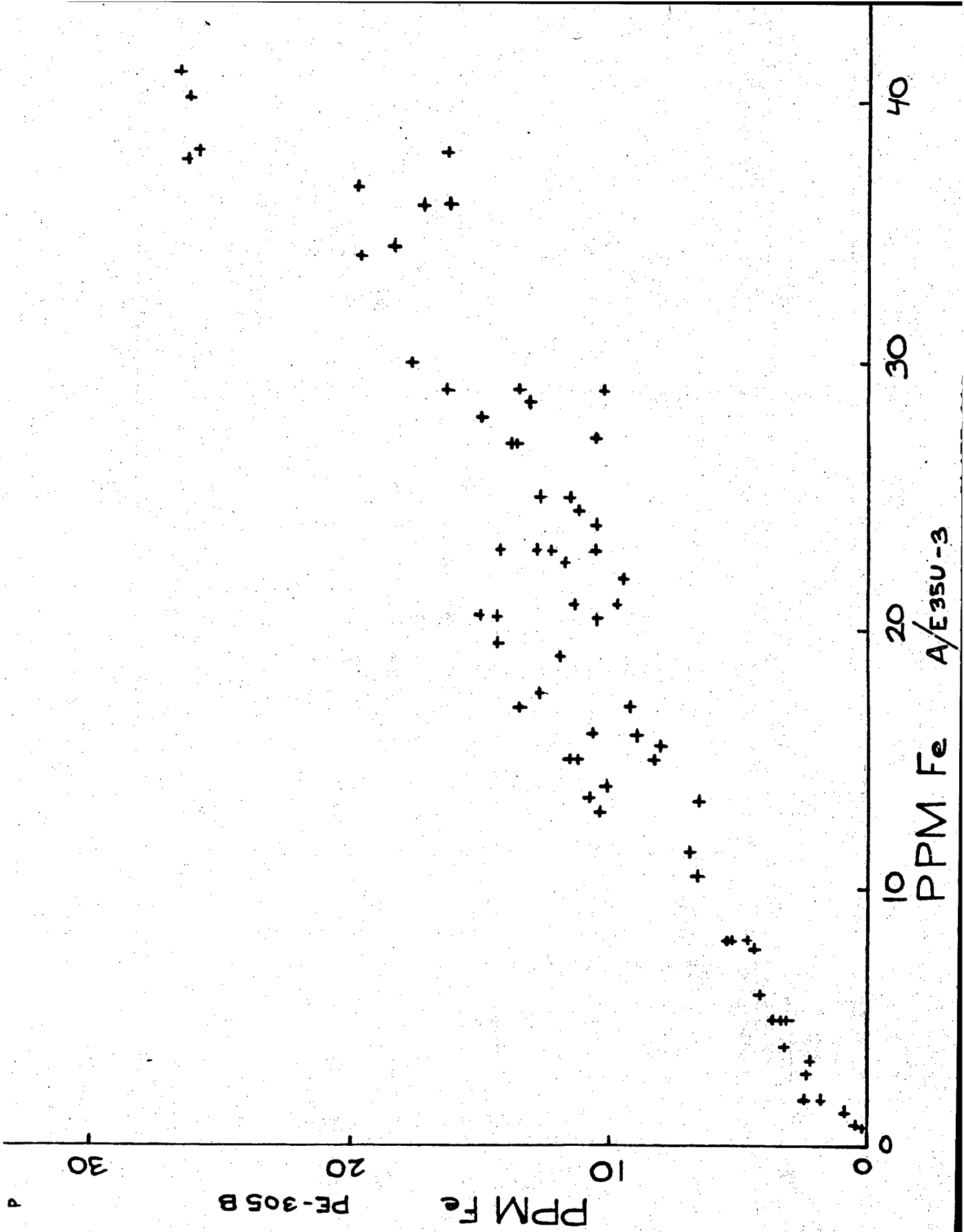


PLATE 21

1282

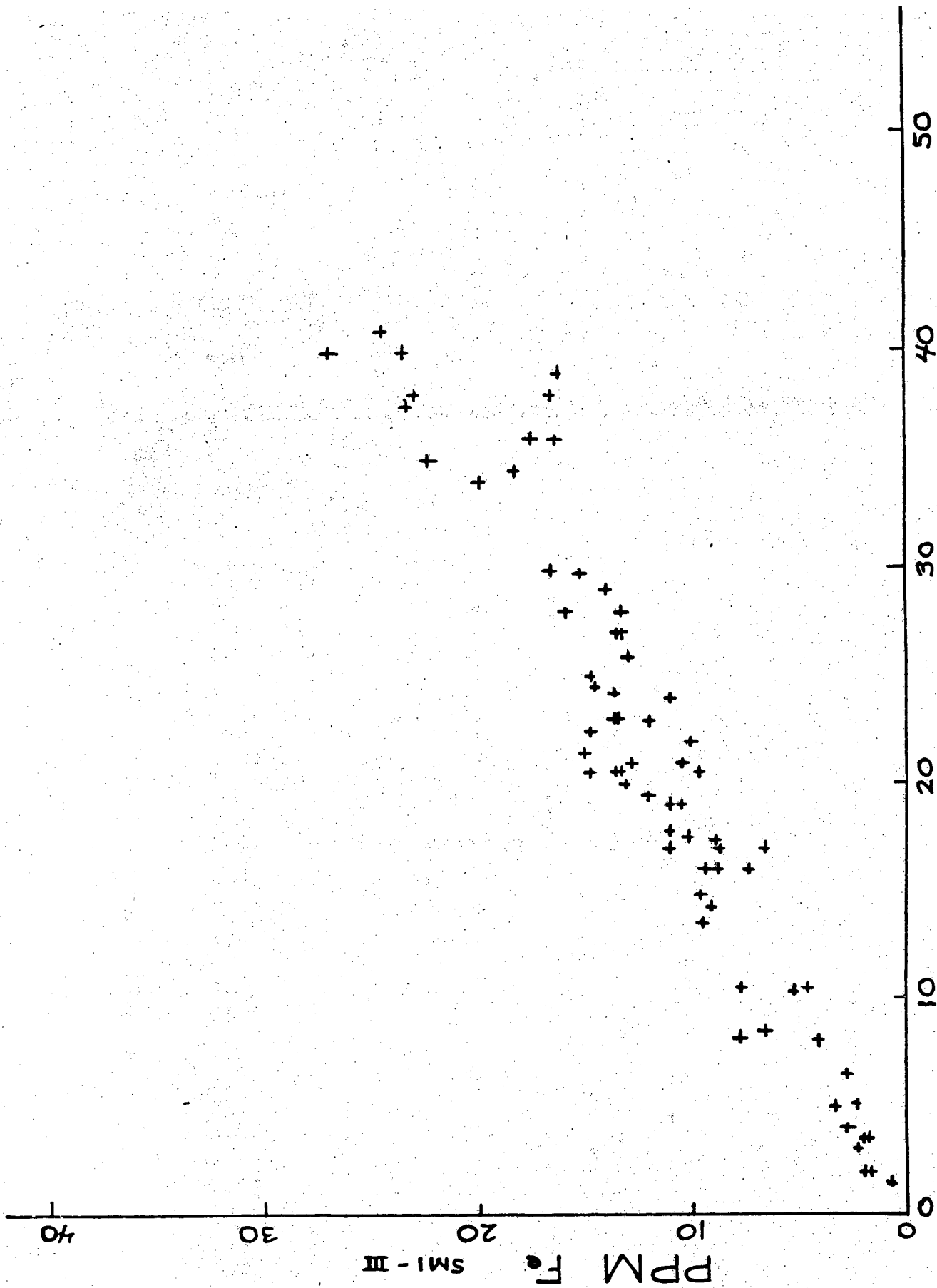


PLATE 22

1283

PPM Fe A/E 35U-3

PLATE 22

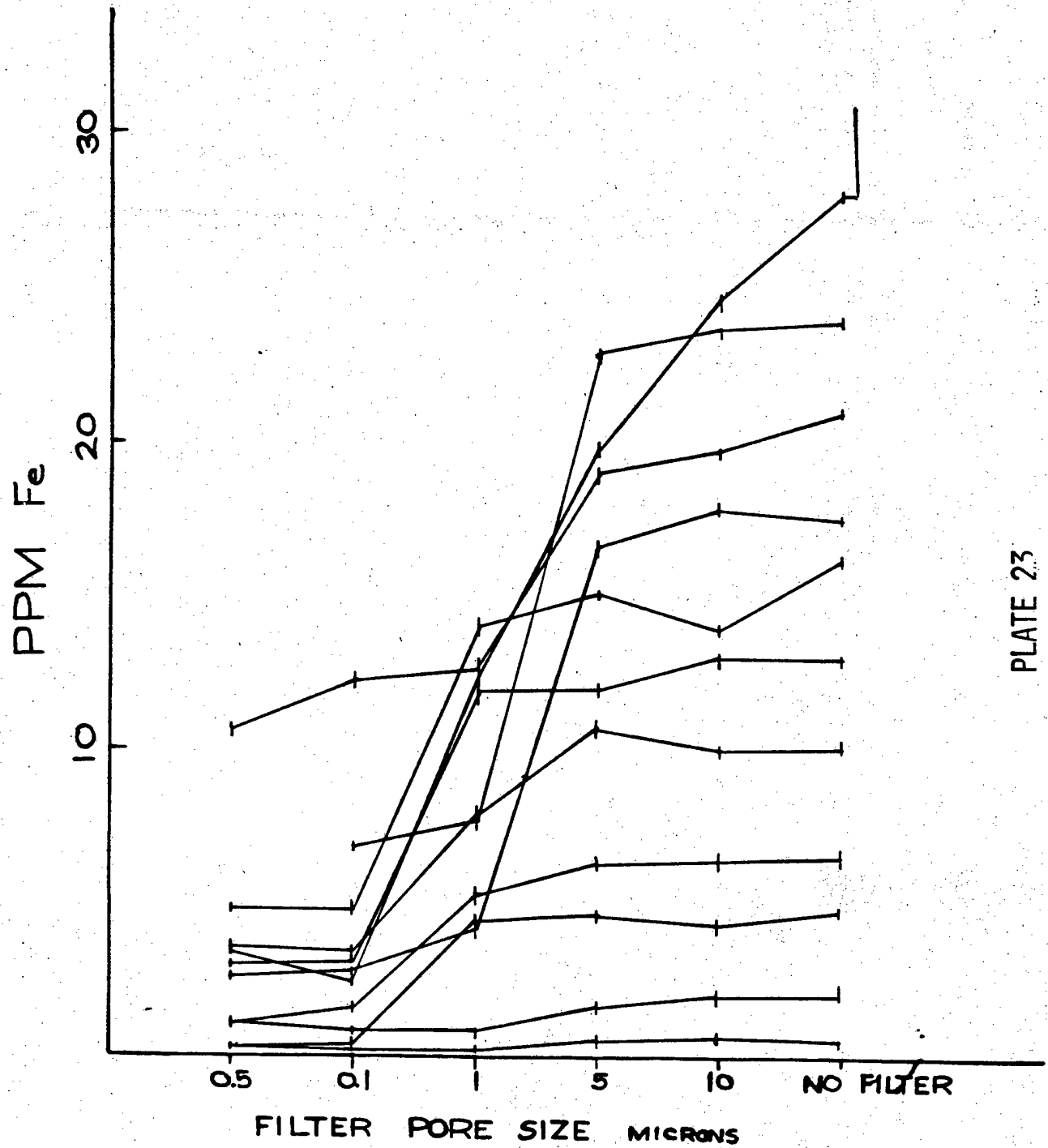


PLATE 23

PLATE 23

1284

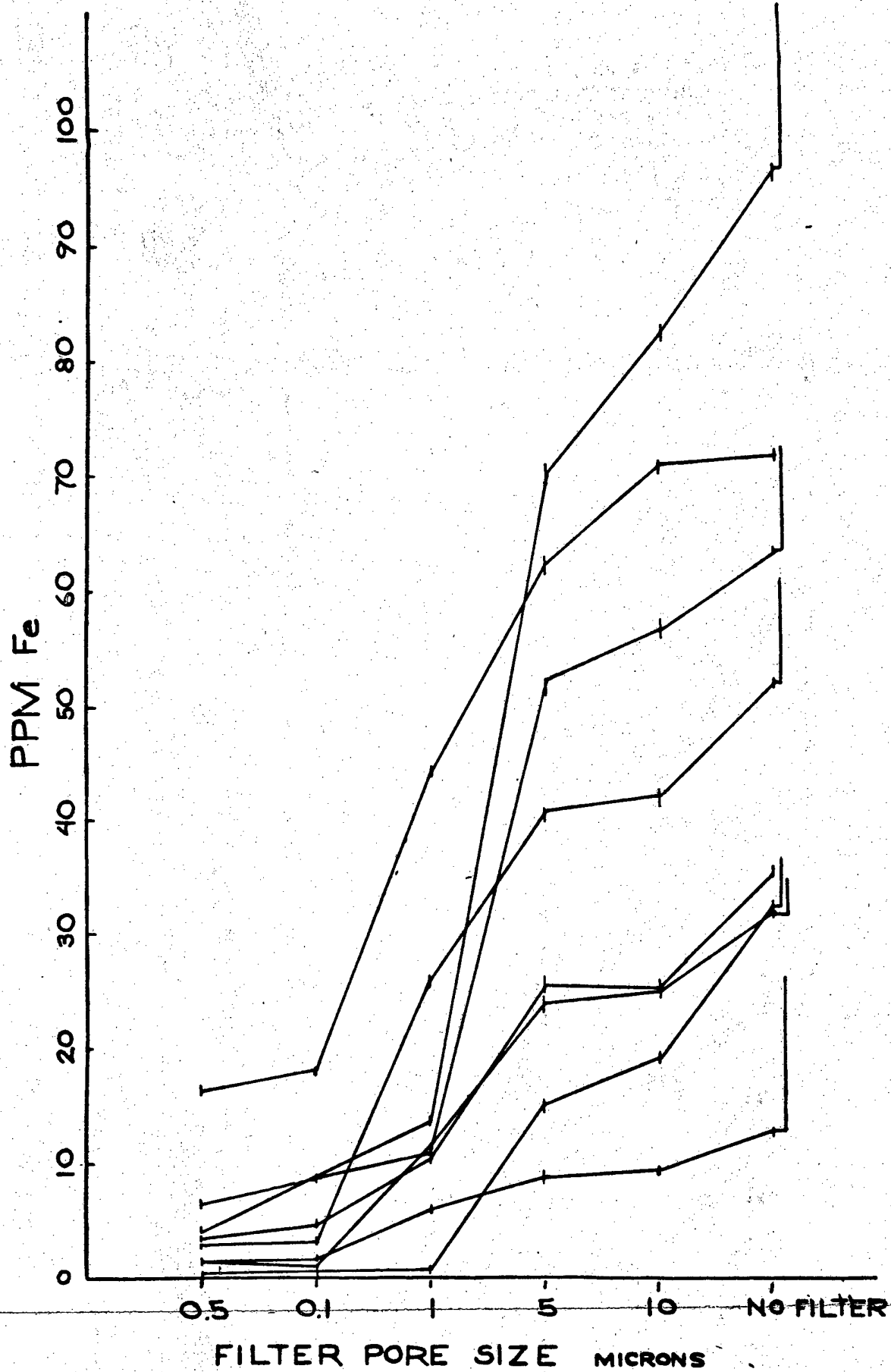


PLATE 24

Biographical Sketch

Lt Thomas Thornton is currently assigned to the Air Force Materials Laboratory. He graduated from Bradley University, in 1976 receiving a B.S. in Chemistry and Biology. He was commissioned through the AFROTC Program in May 1976 and was granted an educational delay from extended active duty for graduate work in chemistry at DePaul University.

Dr. Kent J. Eisentraut is a research chemist with the Fluids, Lubricants, and Elastomers Branch, Nonmetallic Materials Division of the Air Force Materials Laboratory, Wright-Patterson Air Force Base, Ohio. He is responsible for directing the Materials Laboratory efforts in the area of research and development concerning new oil analysis techniques, procedures, and instrumentation. Prior to joining AFML in July 1975, he was assigned as research chemist with the Chemistry Research Laboratory of the former Aerospace Research Laboratories since July 1964.

Dr. Eisentraut was born in Troy, New York. He received the B.A. degree "With Distinction" in Chemistry from St. Michael's College, Winooski Park, Vermont in 1960. He earned the Ph.D. in Analytical Chemistry from Rensselaer Polytechnic Institute in February 1964.

Dr. Eisentraut is a member of the American Chemical Society, the Society of the Sigma Xi, the AAAS, and the New York Academy of Sciences. In 1971, he was elected a Fellow of the American Institute of Chemists. He received the 1966 USAF Research and Development and received the 1976 Outstanding Scientist Award from the Affiliate Societies Council of Dayton during 1976 Engineers and Scientists Week. Dr. Eisentraut is listed in American Men of Science, Who's Who in the Midwest and the International Scholars Directory.

CHARACTERIZATION OF STRUCTURAL POLYMERS
USING NUCLEAR MAGNETIC RESONANCE TECHNIQUES

BY

Drs. W. B. Moniz, C. F. Poranski, Jr.,
A. N. Garroway, and H. A. Resing

Chemistry Division

Naval Research Laboratory
Washington, DC 20375

1287

CHARACTERIZATION OF STRUCTURAL POLYMERS
USING NUCLEAR MAGNETIC RESONANCE TECHNIQUES

Abstract

Nuclear magnetic resonance (NMR) spectroscopy provides a means for determining the structure of complex molecular systems such as polymers. It has the following advantages: First, it is structure specific; functional groups and detailed molecular architecture may be deduced. Second, because of the narrow widths of NMR lines, components in a mixture can often be identified and quantified without the need for physical separation procedures. Third, the presence of molecules containing hydrogen, carbon, nitrogen, boron, fluorine, silicon, or phosphorus can readily be determined.

In the Chemistry Division at NRL, NMR analysis techniques are being developed and perfected for engineering polymers such as the epoxies, polyimides, and polyphthalocyanines. Examples will be presented of pre-polymer quality control (resin to curing agent ratio, oligomer analysis, structure determination) and of cured polymer analysis. The ability to obtain detailed structural information on cured thermosets represents a significant advance. The benefits of the new solid state technique, proton-enhanced carbon-13 NMR with magic angle spinning, will be illustrated.

Introduction

Structural adhesives and fiber-reinforced organic-matrix composites are seeing increased use in aerospace applications. Experience with these systems is growing, but present design allowables incorporate large knockdown factors for batch-to-batch variability in engineering properties. To the extent that improved quality control procedures can reduce engineering variability, the high strength to weight ratio, good fatigue properties, and fabrication advantages of structural composites and adhesives can be more fully exploited.

Quality assurance must span the entire procurement and production cycle in order to achieve the desired improvements. For polymeric materials, quality control factors include the composition and purity of starting materials, the ratios of resin to curing agents and additives, proper blending, the curing cycle, and the integrity of the fabricated component.

With the aid of modern instrumental techniques, significant progress is being made in establishing tolerances and monitoring production. These techniques include infrared and mass spectroscopy, dielectrometry, ultrasonics, radiography, thermal analysis, and various forms of chromatography. Polymers, however, are extremely complex molecular systems, and additional techniques are needed to achieve their more complete characterization.

In the following, we discuss nuclear magnetic resonance (NMR) spectroscopy, an important addition to the instrumentation for polymer analysis. Although there are several nuclei which have application in characterizing organic polymers, by far the most generally applicable are hydrogen and carbon-13. Following a brief description of NMR spectroscopy, some uses of hydrogen (proton) and carbon-13 NMR in the structural polymer field will be illustrated.

General NMR Background

The NMR Phenomenon

The nuclei of many isotopes possess magnetic moments and associated nuclear spins. In the simplest case, such a nucleus might be thought of as a tiny spinning bar magnet. When it is placed in a static magnetic field, the nuclear magnet will tend to align itself with the poles of the external magnet, and precess at a rate dependent on its

particular magnetic properties. If energy at the precessional frequency is coupled into the nucleus, a torque is exerted which causes the nucleus to "flip", absorbing a specific amount of the incident energy in the process. Nuclei are rather small "magnets", and the corresponding frequencies are in the radiofrequency (rf) range for external magnetic fields of a few thousand gauss. The frequencies are quite distinct from nucleus to nucleus, as shown in Table I. Note that these are all stable isotopes - radioactivity is not a factor in NMR spectroscopy.

TABLE I

Nuclei of Interest in Polymer Characterization Via NMR

<u>Nucleus</u>	<u>Natural Abundance</u>	<u>NMR Freq. 14 kGauss</u>	<u>Relative Sig. Strength</u>	<u>Chemical Shift Range</u>
¹ H	99.98%	60 MHz	1.000	10 ppm
¹¹ B	80.42	19	.165	150
¹³ C	1.11	15	.016	250
¹⁵ N	.37	6	.001	1000
¹⁹ F	100	56	.883	700
²⁹ Si	4.70	12	.008	150
³¹ P	100	24	.066	700

The Chemical Shift

In the NMR experiment, the sample is placed in a magnetic field and irradiated with rf energy at the appropriate frequency. Resonant absorption of the rf energy is detected with a radio receiver. A nucleus in a molecule experiences two magnetic fields: the external magnetic field and a local field produced by circulating molecular electrons. Because the local field varies with chemical structure, nuclei in different chemical environments will have slightly shifted NMR frequencies. These frequency variations are called chemical shifts. Radio frequencies can be measured with high precision, thus the chemical shift is a sensitive measure of chemical environment.

Chemical shifts are expressed in dimensionless units in order to provide an index which is independent of the magnetic field strength of the particular spectrometer. A primary reference standard (TMS, tetramethylsilane for protons

and carbon-13) is assigned a chemical shift of zero. The chemical shifts of other spectral lines are given as their separation in parts per million of the applied radio frequency from the frequency of the reference standard. By convention, NMR spectra are displayed with the zero of the chemical shift scale at the right, with positive chemical shifts increasing to the left.

Comparisons Among Nuclei

Proton NMR is widely used in the study of organic molecules, and yields a great deal of structural information. The proton chemical shift range is rather small, however (10 ppm). Consequently, for more complex molecules such as organic polymers, the many lines overlap into broad bands and the extraction of detailed information from the proton NMR spectrum becomes difficult.

The chemical shift range of the heavier nuclei is some 15 to 100 times that of the proton, making them much more attractive for polymer structural determinations (Table I). Some sacrifice in signal strength has to be made with the heavier nuclei, and until recently, this has impeded their utilization. Boron-11, fluorine-19, and phosphorus-31 have fairly strong signals and high natural abundances. On the other hand, the relative signal strengths of nuclei such as carbon-13, nitrogen-15, and silicon-29 are small, as are their natural abundances. Yet, modern pulsed Fourier transform (FT) NMR and signal averaging techniques make possible the use of natural abundance carbon-13, nitrogen-15, and silicon-29 NMR in polymer characterization. The advent of commercial pulsed FT NMR spectrometers incorporating low cost minicomputers to perform the Fourier transform permits the taking of spectra on a routine, semi-automated basis. Thus, the spectrum of a complex molecule containing carbon-13 in natural abundance can be obtained in a few minutes.

Applications

General

The illustrations which follow are based on the use of proton and carbon-13 NMR spectroscopy, which are the most useful for the particular molecular systems involved. For the study of fluorinated polymers, polysiloxanes, or boranes, obviously fluorine-19, silicon-29, or boron-11 NMR would be most useful.

The illustrations are divided into two classes - pre-polymers and cured polymers. As will be discussed later, modified NMR techniques are required if solid samples are to be examined.

Pre-polymers

Proton NMR Analysis of an Epoxy Resin System - An epoxy resin system commonly used in graphite fiber reinforced composites is a mixture of bis (N,N-di(2,3-epoxypropyl)-4-aminophenyl) methane, commonly known as tetraglycidyl methylenedianiline or TGMDA, and the curing agent bis (4-aminophenyl) sulfone, also known as diaminodiphenylsulfone or DDS.

The ratio of curing agent to resin affects the processing and curing characteristics of the resin system, and so its determination is a routine part of the quality control program in the aerospace industry.

The proton NMR spectrum of the TGMDA/DDS resin system lends itself readily to a simple, straightforward determination of the resin to curing agent ratio.⁽¹⁾ The method centers on the aromatic region of the proton spectrum. As shown in Figure 1, the spectra of TGMDA and DDS in the region are each composed of two multiplets. Each half of the multiplets represents one half of the aromatic protons. Note that in the mixture (R 33), one half of the DDS aromatic proton signal remains in the clear. Because the NMR peak areas are proportional to the number of protons in the molecule, a simple electronic integration of the peak areas (shown superimposed on the spectrum of R 33) allows a determination of the number of molecules of DDS and TGMDA present in the mixture. If the total height of the integral is called a, and the height of the integral for the DDS signal in the clear is called b, then the ratio of DDS to TGMDA in parts per hundred parts resin (phr) is:

$$\text{phr} = \frac{117.54}{(a/b)-2}$$

Figure 2 shows a plot of the results obtained for a set of synthetic TGMDA/DDS formulations. The dots and squares are results obtained with two different kinds of proton NMR spectrometers. The 45° line drawn in represents 100% accuracy. The NMR results track quite well, and the data points could be used to generate a calibration curve, from which rather accurate determinations of curing agent phr could be made.

Oligomer Analysis of Epoxy Resins - It is generally recognized that epoxy resins of the DGEBA type are mixtures of oligomers represented by the structure given in Figure 3. Many of the processing and curing characteristics are determined by the proportion of oligomers of various n's contained in the mixture. Our results⁽²⁾ indicate that carbon-13 NMR can be used to determine EEW (epoxy equivalent weight) which is one of the more important processing parameters. The carbon-13 NMR method for determining EEW depends upon an analysis of the line intensities of the glycidyl type carbons in the 40-70 ppm region (Figure 3). The carbon-13 lines for carbons a and b of the terminal glycidyl groups are in a region of the spectrum unperturbed by changes in n. The lines due to carbons e and e'' grow near the line of the ether methylene carbon e'. As n increases, the number of e and e'' carbons increases, but the number of c, d, and e' carbons remains the same--two each. For the idealized structure shown in Figure 3, the ratio of e' to (e + e'') carbons for n-oligomer is 2/3n. An analytical expression can be derived which allows the n-value to be determined.

$$\frac{I_{\underline{e}'}}{I_{\underline{e}} + I_{\underline{e}''}} = \frac{I_{\underline{c}} \text{ or } \underline{d}}{I_{70} - I_{\underline{c}} \text{ or } \underline{d}}$$

Thus, the n-value can be calculated from the measured intensities of the carbon-13 lines at 70 ppm ($=I_{\underline{e}} + I_{\underline{e}'} + I_{\underline{e}''}$) and the lines at 50 ($I_{\underline{d}}$) or 44 ($I_{\underline{c}}$) ppm.

The results on two commercial epoxy resins (Table 2) show that the NMR results compare quite well with the published EEW values.

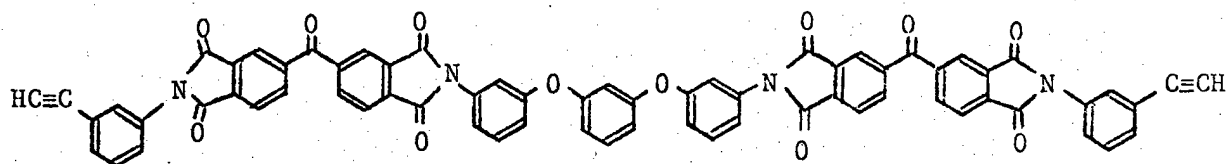
TABLE II

Carbon-13 NMR determination of EEW
of two commercial epoxy resin systems

<u>Resin</u>	<u>Carbon-13 EEW</u>	<u>Literature EEW</u>
DER332LC	170	170-175
EPON 1002	800	600-700

Structural Analysis of an Acetylene-Terminated Polyimide Oligomer - The acetylene-terminated polyimide oligomer shown below was developed by Hughes Aircraft Company under Air Force contract. Originally known as HR-600, it is now

marketed by Gulf Chemicals as Thermid-600. Upon curing, it forms a high temperature, high strength structural polymer useful in aerospace applications.



The complex structure of the oligomer makes its structural determination by conventional means a difficult task. A carbon-13 NMR analysis of the oligomer has confirmed its structure. (3)

The carbon-13 NMR analysis was aided by the synthesis of key model compounds. Their carbon-13 spectra were used to determine the chemical shifts of structural groups in the oligomer by means of substituent effects.

The substituent effect is the change in chemical shift of a given carbon caused by the substitution of a functional group at some point in a molecule. Substituent effects are approximately additive for carbon-13 in the absence of crowding or steric effects, and good predictions of carbon chemical shifts can be made by summing the effects of all substituents.

An example of a substituent effect calculation is given in Figure 4 for the addition of phthalimide to phenylacetylene at the 3-position. The chemical shifts of phenylacetylene are shown (122.6 for C-1, 132.5 for C-2, etc.). The phthalimide substituent constants are tabulated at the bottom of the figure (a change of +3.8 ppm at the carbon where the phthalimide adds, -1.4 at the ortho (adjacent) carbon, etc.). Thus, the chemical shifts of phenylacetylene are summed with the appropriate substituent constant to give the predicted chemical shifts of the new compound. The number in parentheses are the measured chemical shifts and show agreement with the calculated values to within about one ppm which is considered satisfactory. By working with substituent effects in the model compounds in this way, predictions for the chemical shifts of all the different carbons in the oligomer are obtained. The oligomer has a plane of symmetry about the central aromatic ring, reducing the number of chemically different carbon atoms to 35. Some local symmetries reduce the number of distinct carbons, and some of the lines are predicted to overlap. The carbon-13 NMR spectrum of the oligomer (Figure 5) contains 24 resolved lines. All

of these are accounted for and assignable using the substituent effect results and the model compound shifts. This verifies the structure of the oligomer.

Cured Polymers

Solid-State High Resolution NMR - A limitation of the procedures used in analyzing the pre-polymers is that unless a substance is a liquid or can be melted or dissolved in a solvent, the NMR lines are so broad that detailed structural analyses are impossible. In liquids, the large dipole-dipole interactions between nuclear spins and shift anisotropy are averaged by rapid molecular tumbling. In solids, this averaging does not occur, and the resulting NMR linewidths are thousands of times those of liquids. Cross-linked thermosetting polymers such as the epoxies and polyimides do not melt or dissolve in solvents. Solvent swelling and heating above the glass transition temperature sometimes produce sufficient motion to yield useful spectra. We have been successful in following the cure and establishing the curing mechanism of an epoxy during the early stages.⁽⁴⁾ In the field of thermosetting polymers then, the conventional NMR procedures so far discussed are limited to the pre-polymer stages.

However, special new solid-state NMR techniques are capable of obtaining high resolution carbon-13 spectra of materials such as thermosetting polymers. The operation of the techniques is illustrated in Figure 6. At the top is shown the broad and featureless carbon-13 spectrum obtained using conventional liquid state NMR. No useful information is obtained. Stage one of the solid-state technique is shown in the middle spectrum. Here, very high power proton rf irradiates the sample and removes the broadening effects of dipole-dipole interactions, leaving the chemical shift anisotropy broadening.

Additional improvement can be obtained by rapidly rotating the sample about an axis which makes an angle of 54.7° with the direction of the external magnetic field. At this so-called "magic angle", the chemical shift anisotropy disappears. Thus, with the combination of magic angle spinning and high power proton rf irradiation, the results shown at the bottom of Figure 6 are obtained. This is a proton-enhanced high resolution solid-state carbon-13 spectrum of DGEBA cured with piperidine. Note that all of the chemically different types of carbon atoms are distinguishable.

Two examples will be given of the application of these solid-state NMR techniques to the analysis of cured polymers.

Polymer Identification - Epoxides may be reacted with any of a number of curing or cross-linking agents, depending upon the polymer properties required in the particular application. The resulting cured polymers are difficult to analyze because of their intractability and opaqueness. However, high resolution solid-state carbon-13 NMR, being a bulk technique, can characterize these materials. (5) Figure 7 shows the spectra of cured polymers prepared by reacting DGEBA with four different curing agents. The spectra were obtained using high power proton rf and with magic angle spinning at 2 kHz. Superimposed on each is the high resolution liquid state carbon-13 spectrum of the unreacted resin and curing agent dissolved in acetone. The arrow at 70 ppm indicates the region of new signals which appear during the curing process. Spectra a and b represent amine cures (piperidine (PIP) and meta-phenylenediamine (MPDA), respectively). These are readily distinguished from the anhydride cures, c and d (hexahydrophthalic anhydride (HHPA) and Nadic methyl anhydride (NMA), respectively). The carbonyl carbon at 175 ppm is very prominent in anhydride cures; as is the methyl peak at 15 ppm in the NMA cure. Differences between the two amine cures are more subtle, but note the broader character to the peaks at 115 and 128 ppm in the MPDA cure. This presumably reflects the more rigid nature of the aromatic amine cure.

Molecular Motion in Cured Polymers - Because of its ability to distinguish individual carbon atoms in polymers, high resolution solid-state carbon-13 NMR has application in the study of the polymer chain dynamics. Polymer molecules are known to undergo various kinds of motion in the solid, such as segmental reorientation, libration, side chain rotation, etc. It is believed that mechanical properties are ultimately relatable to the nature and extent of these motions. Most techniques for their observation are not structure specific, as is the carbon-13 NMR method.

An example is the carbon-13 NMR spectrum of piperidine-cured DGEBA as a function of temperature (Figure 8). It is seen that as the temperature is lowered, the signal at 114 ppm broadens, eventually splitting into two peaks at $\sim -25^{\circ}\text{C}$. This behavior means that a component of polymer chain motion associated with the aromatic rings of the polymer is "freezing out" at the low temperature. The two lines signify different environments for the aromatic carbon atoms on

either side of the oxygen of the glycidyl group. If a matching mechanical relaxation in piperidine-cured DGEBA can be identified, the carbon-13 NMR results constitute a direct molecular explanation.

Acknowledgment

The solid-state carbon-13 NMR work is supported in part by the Naval Air Systems Command.

References

1. C. F. Poranski, Jr. and W. B. Moniz, "Carbon-13 and Proton NMR Spectroscopy of Thermosetting Polymers; Analysis of Tetraglycidyl Methylenedianiline/Diaminodiphenylsulfone Formulations," Proceedings of the 5th Conference on Composite Materials: Design and Testing, ASTM Special Publication, in press.
2. W. B. Moniz and C. F. Poranski, Jr., "NMR Oligomer Analysis of Epoxy Resins," Coatings and Plastics Preprints 39, 0000 (1978).
3. C. F. Poranski, Jr., W. B. Moniz, and T. W. Giants, "Carbon-13 NMR Spectroscopy of Thermosetting Polymers: Structural Analysis of an Acetylene-Terminated Polyimide Oligomer," Coatings and Plastics Preprints 38, 605 (1978).
4. S. A. Sojka and W. B. Moniz, "The Curing of an Epoxy Resin as followed by Carbon-13 NMR Spectroscopy," J. Applied Poly. Sci. 20, 1977 (1976).
5. A. N. Garroway, W. B. Moniz, and H. A. Resing, "¹³C NMR in Organic Solids: The Potential for Polymer Characterization," American Chemical Society Symposium Series, in press.

Figure Captions

1. Proton NMR spectra of the aromatic region of DDS (top) TGMDA (middle), and a resin system based on them (bottom). An integral of the resin system spectrum is superimposed.
2. Experimental values of phr DDS vs. "true" phr values for a series of synthetic TGMDA/DDS. The 45° line corresponds to 100% accuracy. The circles are values measured with a continuous wave spectrometer; the squares, with a Fourier transform spectrometer.
3. 40-70 ppm region of the carbon-13 NMR spectra of three commercial epoxy resins. The letters and the n numbers refer to the idealized DGEBA structure shown at the top.
4. Example of an aromatic substituent effect calculation for the addition of phthalimide to the 3-position of phenylacetylene.
5. Carbon-13 NMR spectrum of HR-600 (Thermid-600) oligomer in DMSO-d₆. The lines of the solvent appear as a multiplet centered at 40 ppm.
6. Carbon-13 NMR spectra of a rigid polymer (Piperidine-cured DGEBA). Top: Conventional procedure. Middle: High power proton rf. Bottom: High power proton rf plus magic angle spinning. All the major carbon functionalities are resolved.
7. High resolution solid-state carbon-13 NMR spectra of DGEBA cured with four different curing agents: (a) piperidine, (b) metaphenylenediamine, (c) hexahydrophthalic anhydride, (d) Nadic methyl anhydride. On each solid state spectrum is superimposed the liquid state spectrum of DGEBA and the curing agent in acetone solution.
8. Temperature dependence of the carbon-13 NMR spectrum of piperidine-cured DGEBA. The line marked by the arrow is narrow at 352°K (79°C) but broadens to two lines as the temperature is lowered to 247°K (-26°C); at 151°K (-122°C) the two lines are well defined. This behavior reflects a "freezing out" of polymer motions associated with the aromatic rings.

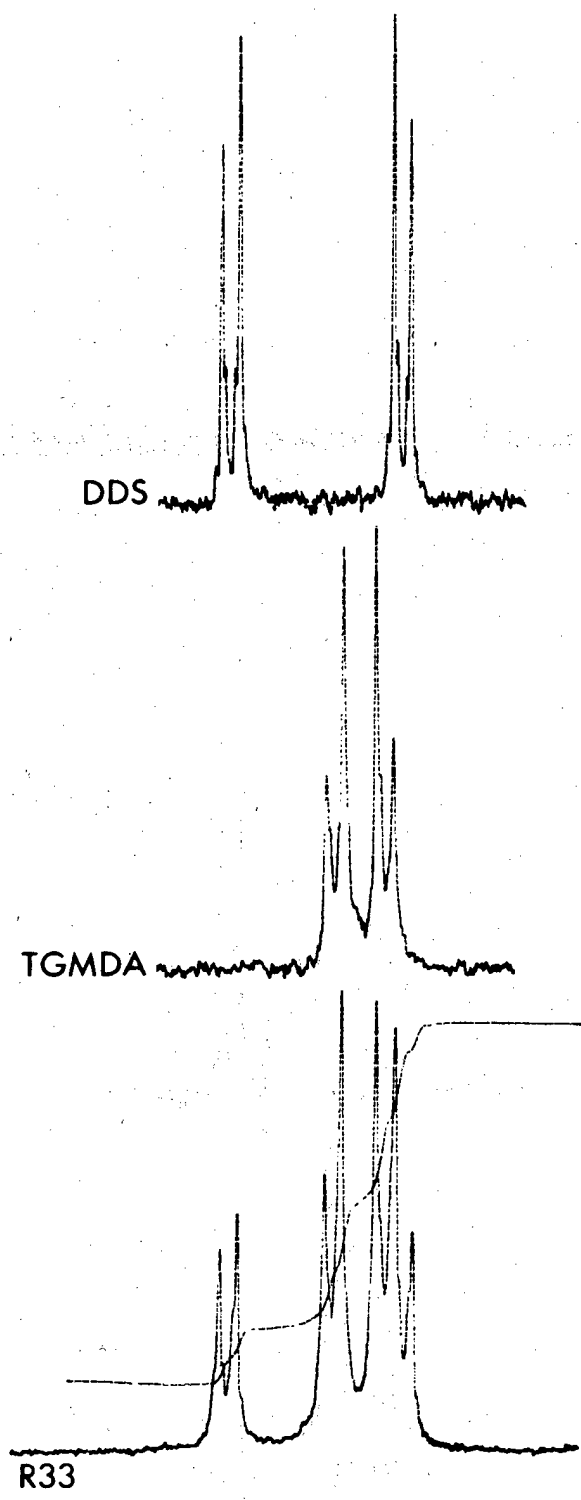


FIG. 1

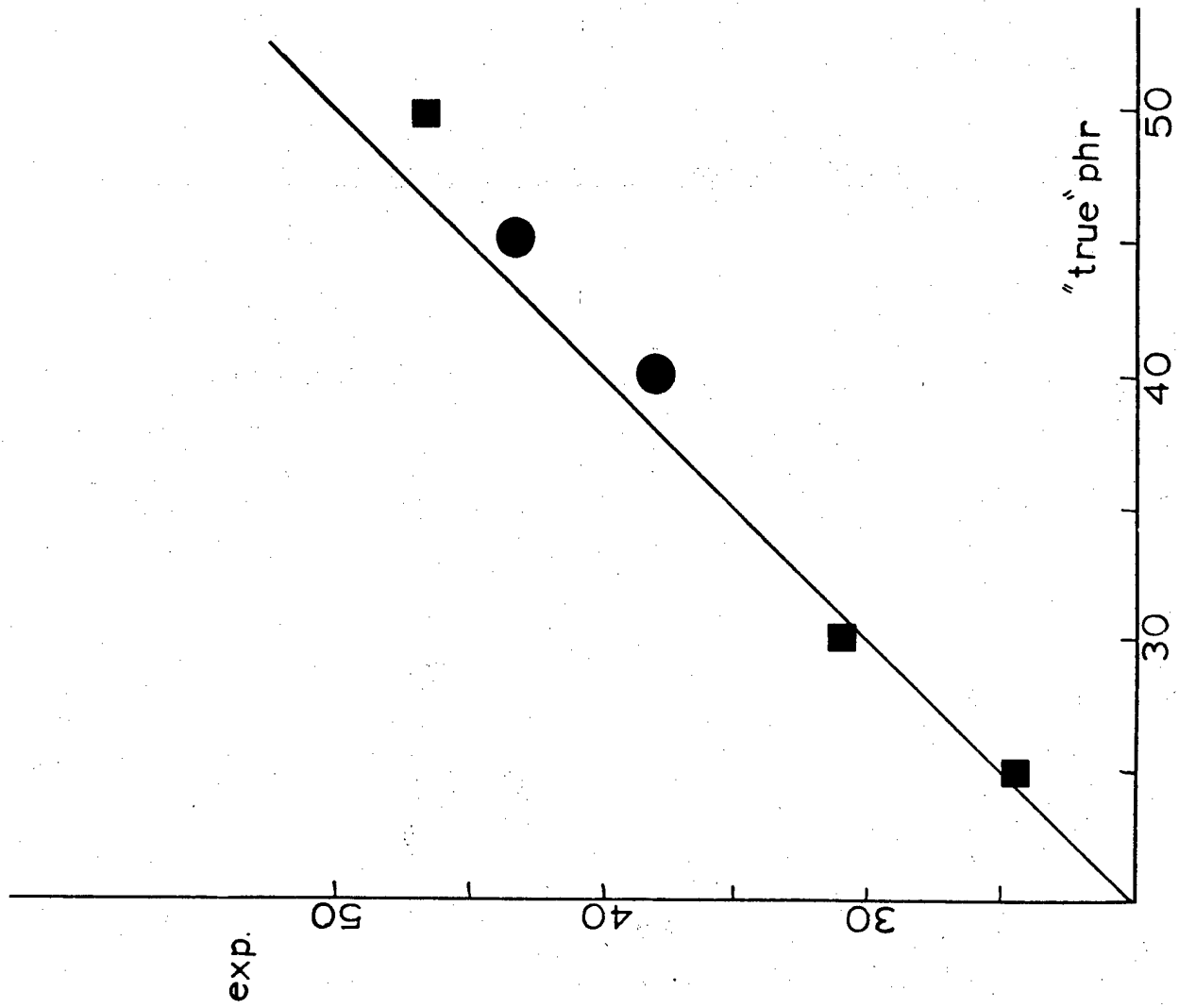


FIG. 2

1300

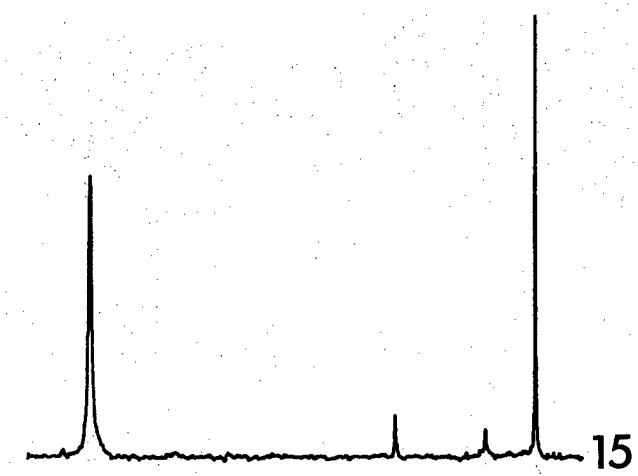
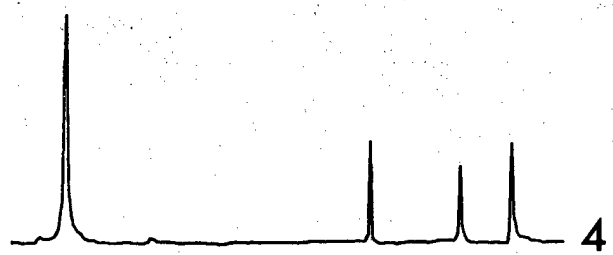
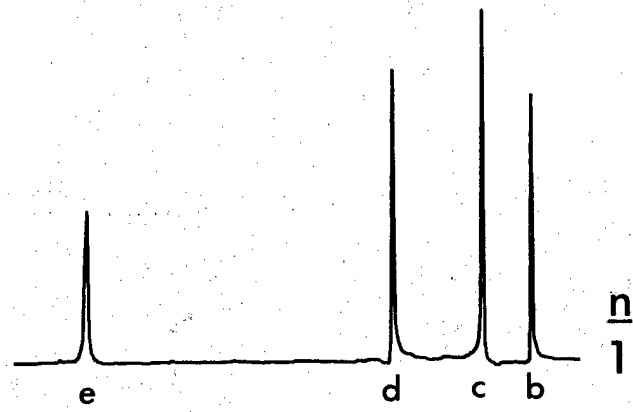
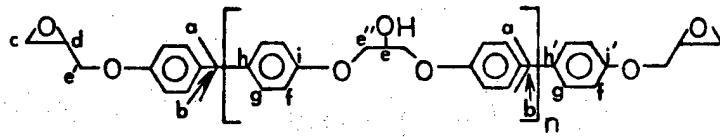
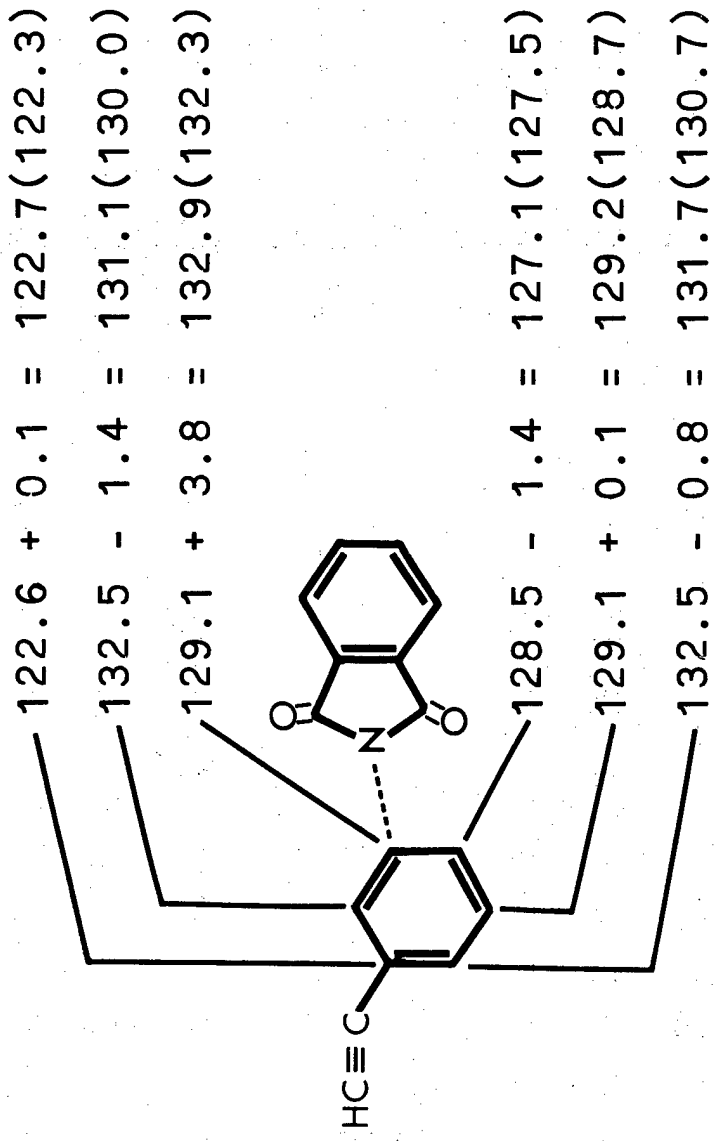


FIG. 3



Phthalimide Substituent Constants

C-1	+3.8
<u>o</u>	-1.4
<u>m</u>	+0.1
<u>p</u>	-0.8



FIG. 6

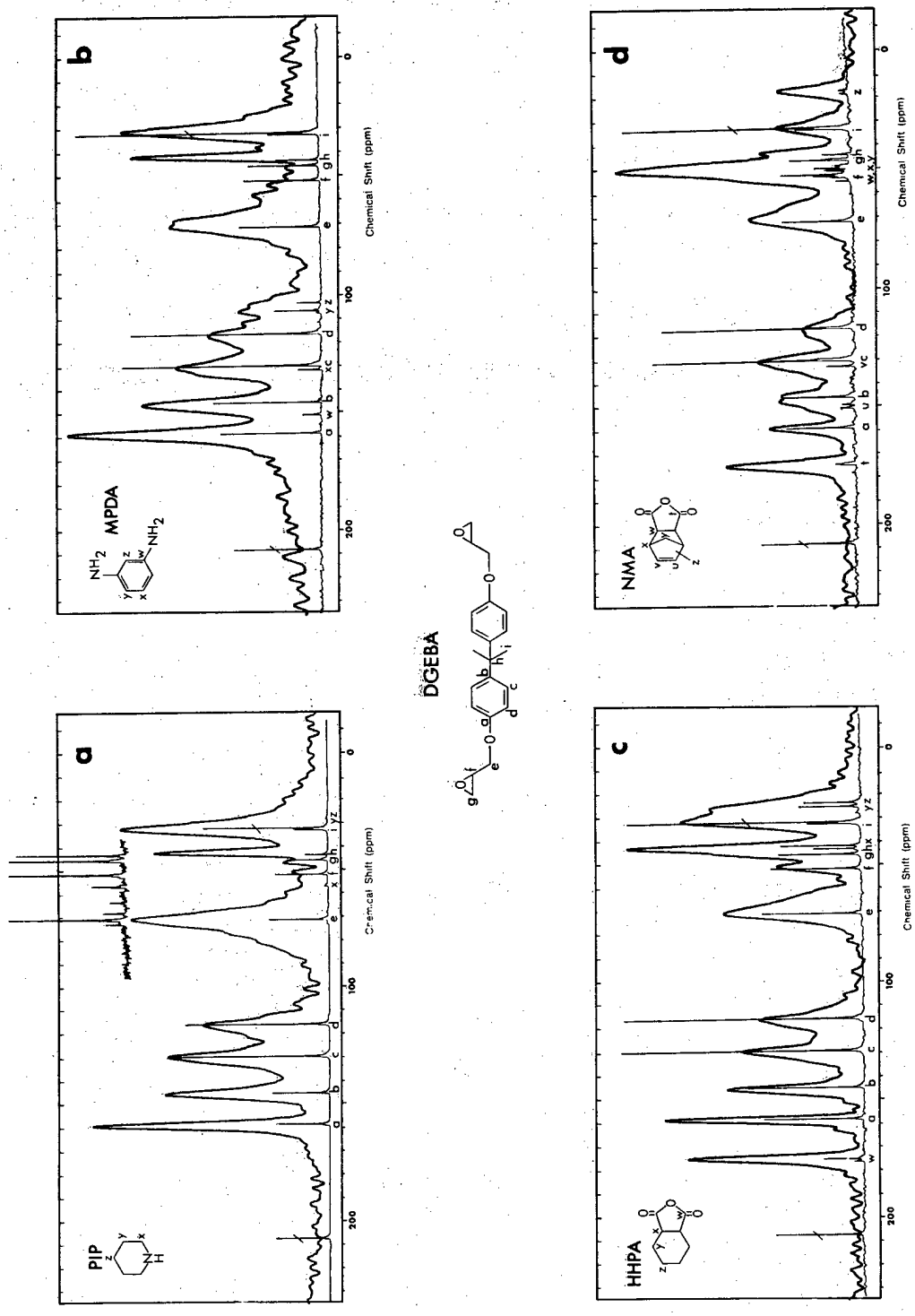
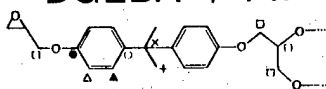


FIG. 7

DGEBA + PIP



● ○ ▲ △ □ + ×

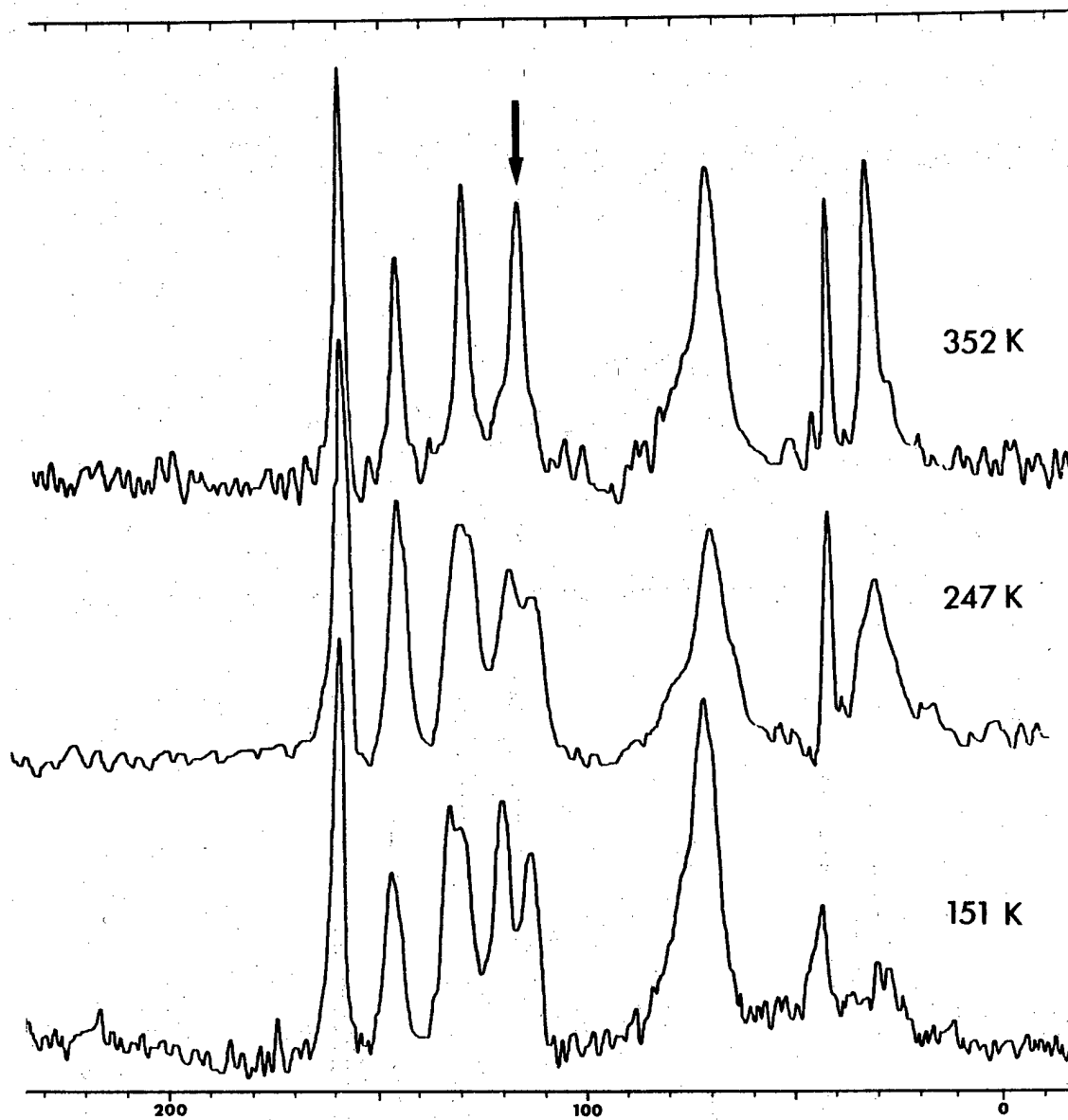


FIG. 8

Biographical Sketch

Dr. William B. Moniz was born in New Bedford, Mass. on February 12, 1932. He received his B.S. degree in Chemistry (cum laude) from Brown University in 1953. He also participated in the NROTC program at Brown and was commissioned Ensign, USN, upon graduation. After a four-year tour of active duty, including two years as Instructor of Chemistry at the U. S. Naval Academy, he left the Navy and pursued graduate studies at Pennsylvania State University. Dr. Moniz received his Ph.D. degree in organic chemistry from Penn State in 1960 and stayed on a year of postdoctoral research as an American Petroleum Institute Fellow. The following year was spent in the laboratory of Professor H. S. Gutowsky, University of Illinois, as an N.I.H. Postdoctoral Fellow.

Since 1962 Dr. Moniz has been at the Naval Research Laboratory and presently is Head of the Polymer Diagnostics Section in the Chemistry Division. His career research interests have centered around the application of magnetic resonance and other instrumental techniques to problems in mechanistic and structural chemistry. Currently, his group is active in the development of improved methods for polymer characterization. His publications include over sixty research papers and reports and two patents. Since 1976 Dr. Moniz has served as Chairman of the Technical Standing Committee on Characterization of the Navy Council on Materials and Structures. He is a member of the American Chemical Society and Sigma Xi, the Scientific Research Society.

ON THE VARIATION OF FATIGUE CRACK OPENING LOAD
WITH MEASUREMENT LOCATION

BY

Dennis E. Macha
Dennis M. Corbly
J. Wayne Jones

Metals Behavior Branch
Metals and Ceramics Division
Air Force Materials Laboratory
Wright-Patterson AFB, OH

1308

ON THE VARIATION OF FATIGUE CRACK OPENING LOAD
WITH MEASUREMENT LOCATION

ABSTRACT

The opening load as originally defined by Elber for fatigue cracks exhibiting crack closure has been determined using three different experimental techniques. Displacement-load behavior was investigated for a fatigue cracked modified compact specimen of a nickel base superalloy. Displacements were determined at the notch mouth using a standard clip-on gage, along the crack surface using a laser interferometric displacement gage, and in the plastic zone ahead of the crack using an optical interferometry technique. Acoustic emission monitoring was employed as a means to detect crack extension during measurement load cycles and to detect physical crack closure.

The magnitude of the opening load, as determined from these measurements, is dependent on the distance from the crack tip at which the measurement is made. The crack opening load is found to be highest at the crack tip. At sufficient distances from the crack tip the opening load becomes constant. As an additional means of evaluating opening load, crack surface profiles are constructed from the displacement load measurements made behind the crack tip. A discussion is given concerning the significance of these results in evaluating the classical opening load as defined by Elber as a useful parameter to quantify crack closure.

INTRODUCTION

The use of Linear Elastic Fracture Mechanics (LEFM) approaches for the design of advanced aerospace structures has rapidly expanded in the past decade. Using LEFM, one is able to describe the fatigue crack growth rate of a propagating fatigue crack as a function of the stress intensity experienced at the crack tip. The stress intensity factor, K , is the LEFM parameter that characterizes crack behavior in many materials. The stress intensity factor, combines the effects of remotely applied load, crack length and structure geometry into a single parameter. In general, the use of LEFM methodology has resulted in more durable structures because of its ability to incorporate the influence of pre-existing defects on the life of the structure. This has changed the basic design philosophy from crack initiation to crack propagation.

Several problems may emerge when one attempts to use LEFM to predict fatigue crack growth in engineering structures. Some of these problems arise from the fact that a basic assumption in the application of LEFM methodology is that the material of interest exhibit linear elastic deformation at the crack tip. It is recognized that few engineering materials of interest exhibit linear elastic behavior, but rather that the material near the tip of a propagating fatigue crack undergoes plastic deformation prior to fracture. It has become a common practice in applying LEFM to engineering materials to make the assumption that if the amount of plastic deformation experienced at the crack tip is small, the basic principles fo LEFM are not violated.

A great amount of research has been conducted to devise methods that will allow a more widespread use of fracture mechanics methods to engineering materials. These efforts have resulted in the emergence of various new parameters to be used to correlate the fatigue crack growth rate in engineering materials. Some of these parameters are simply variations of the linear elastic stress intensity parameter, K , while others are new parameters that actually allow the plastic deformation that is experienced at the crack tip.

At the Air Force Materials Laboratory, research is being conducted in-house to evaluate various proposed crack propagation models for application to gas turbine engine components operating at elevated temperatures. As an initial effort, a review of many empirically based crack propagation models used

for airframe applications has been conducted. It was found that a common approach to model the effect of crack tip plastic deformation on fatigue crack growth behavior is to derive an empirically based crack growth model that alters the conventional linear elastic stress intensity parameter, K , to create an effective stress intensity experienced locally at the crack tip. One such approach that has received considerable attention, and is the subject of this paper, is the crack closure theory developed by Elber. (1,2)

From his early work, Elber concluded that the crack closure phenomenon is a direct consequence of the permanent tensile deformations left in the wake of a propagating fatigue crack. Further, because of the residual deformations, a crack in a fatigue specimen is fully open for only a part of the load cycle, even when the loading cycle is fully in tension. Thus, since the crack tip is closed during a portion of the remotely applied load cycle, the cyclic stress intensity range experienced locally at the crack tip is a value less than that which would be calculated based on the remotely applied load cycle. In other words, because of the fatigue crack closure phenomenon, the crack tip experiences an effective stress intensity range that is less than the remotely applied stress intensity range.

An important aspect of the fatigue crack closure phenomenon is to be able to experimentally evaluate the load at which the fatigue crack becomes fully open. This is required if the effective stress intensity range at the crack tip is to be determined experimentally. Elber proposed an experimental technique to determine the load at which a fatigue crack becomes completely open. He developed a small displacement transducer that was placed on the specimen surface such that the contact points straddle the crack near the crack tip. As the specimen is loaded and the crack faces separate, the displacement occurring across the crack on the specimen surface is recorded as a function of applied load. A schematic of a typical displacement-load plot of this type is shown in figure 1. In relating the observed displacement-load behavior to the crack closure phenomenon, Elber offered the following explanation. As the specimen is loaded, a linear displacement-load response is initially exhibited (between points A & B). This initial elastic response is due to the crack being closed and thus is the elastic response one would measure in an uncracked specimen of the same configuration. As the load continues to increase (between points B & C) a non-linear displacement-load

relationship is exhibited. During this increment of loading the fatigue crack surfaces are separating. As the load is increased the surfaces essentially unzip towards the actual crack tip. At point C the displacement-load relationship again becomes linear. It is at this point of linearity (point C) that the crack surfaces have completely separated. As the load is further increased, the crack tip remains open and damage is incurred at the crack tip resulting in crack extension. Elber defined the point of linearity on the displacement load curve (point C in Figure 1) as the load at which the crack tip is open. (P_{op})

Elber demonstrated the occurrence of crack tip closure and the utility of the concept of an effective stress intensity range in predicting the dependence of fatigue crack growth rate on the stress ratio, R . This apparent success of the crack closure concept led to considerable effort to refine the experimental techniques for measuring the magnitude of crack tip closure. These techniques are generally divided into two categories: techniques which measure bulk specimen response and those which measure displacements on the specimen surface. Bulk measurements have been made using electrical potential methods (3), ultrasonics (4), acoustic emission (5), and, for transparent materials, optical interferometry (6). Specimen surface displacement measurements have been made with strain gages bonded across the crack line (7), displacement transducers attached across the crack line or ahead of the crack tip (2,8), optical interferometry techniques (9-11), and clip-on displacement gages at the notch mouth (12).

The majority of opening load determinations, regardless of the experimental technique used, are based on the assumptions concerning displacement-load behavior as stated by Elber. However, despite the numerous sophisticated techniques utilized, a considerable amount of conflicting crack closure data exists in the literature. Conflicting results on the dependence of P_{op} on maximum stress intensity, K_{max} , and R (2,3) question the validity of crack closure for incorporation into crack propagation models. It has also been observed that bulk measurements often yield a higher P_{op} than do measurements of displacements on the specimen surface (12,13). Some efforts have been made to match bulk results with surface results by various schemes of extrapolating the bulk measurement data (4,14). Such techniques assume a priori the uniqueness of P_{op} as determined by specimen surface displacement measurements. Several investigations (6,9,12,15) have indicated that the validity of this assumption is questionable.

In an effort to resolve this apparent conflict, a rigorous evaluation of the crack opening behavior of a modified compact specimen was conducted. A fatigue crack was incrementally grown at a constant K_{max} and R . The crack opening behavior was evaluated at six different crack lengths. The displacement-load behavior was evaluated both in front of and behind the crack tip using two optical interferometry techniques and the bulk behavior was evaluated using acoustic emission and clip-on displacement gage techniques.

EXPERIMENTAL TECHNIQUE

In the experimental work described here, displacement measurements were made at room temperature on a modified compact specimen ($H/W = .486$) as shown in Figure 2. The equation used to calculate the stress intensity factor (K) for this specimen geometry is taken from Reference 16 as:

$$K = \frac{P \sqrt{a} Y}{BW} \quad (1)$$

where P is the applied load, a the crack length as measured on the specimen surface, B and W the specimen thickness and width respectively, and Y , the calibration factor defined as:

$$Y = 30.96 - 195.8(a/W) + 730.6(a/W)^2 - 1186.3(a/W)^3 + 754.6(a/W)^4$$

The material evaluated was GatorizedTM IN-100, a nickel-base superalloy, with $\sigma_y = 1.12 \times 10^3$ MN/m² and $E = 2.14 \times 10^5$ MN/m². Fatigue crack growth was conducted in a closed loop servo-hydraulic testing machine operating at a cyclic frequency of 20 Hz. The maximum stress intensity, K_{max} , was held constant at 38.5 MN/m^{3/2} by periodically reducing the cyclic load as the crack extended. The crack length was measured on both specimen surfaces using Gaertner traveling microscopes. The average of the crack lengths measured on the two specimen surfaces was used to calculate the desired test load. This average surface crack length is reported here. The stress ratio, R , was maintained at 0.1. At six selected crack lengths (Table 1) crack growth was interrupted and the specimen was removed to a screw driven testing machine to make the displacement measurements. While making displacement measurements, care was taken to ensure the specimen was not loaded to greater than 91 percent of the maximum load (P_{max}) used to extend the crack under cyclic loading. Displacement-load profiles were simultaneously obtained in three distinct regions

(Figure 2) of the specimen: along the crack line behind the crack tip using the interferometric displacement gage (IDG) (17,18), at the specimen notch mouth using clip-on displacement gage, and in front of the crack tip using an optical interferometry technique (19). In addition, acoustic emission (AE) monitoring was performed during each loading cycle. The purpose of the AE measurements in this effort was to: (1) determine the magnitude of acoustic emission in IN-100 on a cycle-by-cycle basis, (2) monitor for crack extension, especially on the interior of the specimen during the test loading cycles, and (3) evaluate the utility of acoustic emission as a method for detecting crack closure. A detailed description of the use of each measurement technique follows.

Crack Opening Displacement (COD) Measurements

The principles of the IDG are described in detail in References 17 and 18. In this study the IDG is used to measure the displacement that occurs between two indentations straddling the crack on the specimen surface. The indentations were applied 0.10 mm above and below the crack to give an operating gage length of 0.20 mm. With the indentations placed close to the crack surfaces, it is assumed that the measured displacement occurring between the indentations is also that occurring between the crack surfaces at the specimen surface.

Upon extending the fatigue crack to the first test length, indentations were placed at distances of 0.050, 0.50, 1.25, 2.5, and 3.75 mm behind the crack tip. COD measurements were made, in turn, at each position during successive load cycles. This procedure was repeated at subsequent crack lengths using all available sets of indentations. Table 1 gives a listing of the series of new indentations applied at each crack length evaluated.

During each load cycle at the respective crack lengths, displacements at the notch mouth were measured with a clip-on displacement gage of standard configuration (ASTM E 399-74). In contrast to the IDG measurements which were made at various locations relative to the crack tip during successive load cycles, the displacement gage at the notch mouth gave the displacement-load relationship at a fixed point relative to the crack tip (see Table 1).

The analog displacement-load data attained from both the IDG and clip-on displacement gage was reduced using a computer digitizing code that yielded digital displacement-load data

suitable for analysis. A linear regression analysis was used to determine the load at which the displacement-load curve became linear (P_{Op}) upon loading the specimen. Use of the regression analysis minimized the subjectivity in evaluating the data and ensured a consistent determination of P_{Op} .

A second analysis was conducted to determine the COD at all measurement locations for discrete load values. This program used a linear interpolation to determine the displacement associated with each load value. Crack surface profiles were then constructed at 10, 30, 50 and 90 percent of P_{max} for each crack length tested.

Displacements in Front of Crack Tip

In the region immediately ahead of the crack tip an optical interferometry technique was used to measure the transverse displacements occurring during the fatigue cycle. This technique has been used to determine deformation zones (10,20-22) and average through-thickness strains (21,22) in the crack tip region. In the present experiment a collimated beam of monochromatic light was directed through an optically flat quartz plate positioned directly on the polished specimen surface. During loading of the specimen the separation between the specimen surface and quartz flat, resulting from contraction at the crack tip, produces an optical interference pattern. For normal incidence the change in separation, d , is given for destructive interference as:

$$d = \frac{n\lambda}{2} \quad (3)$$

where λ is the wavelength of the monochromatic light and n is the order of the interference fringe. For the sodium vapor light used $\lambda = 0.5893 \mu\text{m}$ and the transverse displacement change between adjacent fringes is $0.2946 \mu\text{m}$.

Video taping through a low power microscope permitted recording of the optical interference pattern during each test load cycle. Small diamond pyramid indentations placed along the projected crack plane allowed determinations of real time displacement behavior at selected locations ahead of the crack tip. These data, when combined with the load time trace, produced the desired displacement load record. Figure 3 shows a typical fringe pattern in the vicinity of the crack tip. Near the specimen surface the shear lip causes the intersection of the crack plane with the surface to differ from the location

of the interior crack plane. Note that the placement of the indentations is along the line of symmetry of the displacement field and not along the projected crack path on the surface. For consistency, all measurements were made along the line of symmetry.

Acoustic Emission Measurements

The AE technique has been used in recent years to study the fatigue crack growth process (5). Although there is not a complete understanding of the exact mechanisms which are uniquely related to various acoustic emission sources, it is accepted that acoustic emissions occur upon crack extension. In some instances, it has been observed that acoustic emission occurs during the unloading portion of the fatigue crack propagation cycle (23).

The acoustic emission measurements reported herein were made with a Duñegan 3000 system including a Model 301 totalizer, Model 801 preamplifier, and a Model D92dB differential transducer. The transducer was coupled to the specimen with silicone vacuum grease in the position shown in Figure 2. All measurements were made with a system gain of 89dB and a 0.3 - 1.0 MHz bandpass filter. These settings were chosen to maximize system sensitivity for emissions from the crack tip while minimizing extraneous noises from the test machine. Data were recorded on a dual channel strip chart recorder in the form of load versus time and acoustic emission counts versus time.

Results and Discussion

The displacement load behavior measured at 0.5, 2.5, and 6.55 mm behind the crack tip, using the IDG and at the notch mouth (54.59 mm behind crack tip) using the clip-on displacement gage, is shown in Figure 4. It is evident that as the measurement location approaches the crack tip the value of load at which the relationship becomes linear (P_{op}) increases. As discussed earlier, when displacement measurements were being made, the specimen was loaded to 91 percent of P_{max} for cyclic growth. This precaution was taken to circumvent the introduction of new crack tip plasticity as well as to minimize the chance for crack extension during the measurement cycles. As seen in Figure 4, the displacement-load curves exhibit a significant linear range above the point of linearity.

The variation of the change in transverse displacement with load and distance in front of the crack tip as measured

with the optical interferometry method is shown in Figure 5. Three features of the data merit consideration: (1) the displacement-load behavior measured near the crack tip exhibits hysteretic behavior; (2) the displacement is maximum at the crack tip and decreases as distance in front of the crack tip increases; (3) each displacement-load record shows a transition from nonlinear to linear displacement-load behavior. The load at this transition point was interpreted as the opening load, P_{op} , and was found to be sensitive to the distance from the crack tip at which the measurement was made.

The hysteresis in the displacement-load behavior occurred at each crack length investigated. The magnitude of this behavior was found to decrease with increasing distance from the crack tip. The nature and extent of this hysteretic behavior and its use in determining the cyclic plastic zone size is currently under investigation and will be the subject of a future paper.

In Figure 6 the normalized P_{op} values (P_{op}/\bar{P}_{max}) for all measurements made in front of and behind the crack tip are plotted as a function of the measurement location relative to the crack tip. Near the crack tip, the value of P_{op} is strongly dependent upon measurement location. At a location 0.05 mm behind the crack tip a normalized P_{op} value of 0.64 was measured. The values of P_{op} decrease continuously as the distance behind the crack tip increases. At distances greater than approximately 5.0 mm P_{op} becomes independent of measurement location stabilizing at an average value near 0.23. From the results shown, the value of normalized P_{op} appears to be independent of a/W for this constant K condition.

Although there is considerable test to test variation, for measurements made ahead of the crack tip, those made within 1.0 mm of the crack tip also yield P_{op} values that are highly sensitive to measurement location. At distances greater than 1.0 mm P_{op} values are approximately constant at 0.2.

Based upon the behavior of P_{op} discussed above, one of two positions may be accepted concerning the use of the point of linearity to quantify the crack tip opening load. First, since P_{op} as measured here is dependent on measurement location, it does not quantify the unique load at which total crack surface separation occurs. The second position assumes that P_{op} does quantify the unique opening load but the determination of P_{op} must be made at an appropriate location relative to the crack tip. The position of the appropriate measurement location is not clear based on the results shown thus far. In an attempt

to further define when the crack surfaces have completely separated, crack surface profiles measured as a function of applied load were constructed for each crack length.

In evaluating the crack surface profiles, a criterion based upon the elastic crack tip displacement equation (24) is used to determine when the crack is completely open. The elastic displacement equation yields a parabolic crack surface profile with zero displacement at the crack tip. For the criterion established here, it is required that the parabolic relationship extrapolates to the known crack tip on the specimen surface. Profiles constructed in the near crack tip region at 10, 30, 50 and 90 percent of P_{max} are shown in Figure 7. The profiles at 50 and 90 percent of P_{max} meet the above criterion whereas at 30 percent of P_{max} the parabolic relationship extrapolates to a crack tip at a location less than the known position of the crack tip on the specimen surface. Therefore, it is determined that the cracks are not open at 30 percent of P_{max} . A detailed evaluation of crack surface profiles obtained at 5 percent load intervals up to 90 percent of P_{max} was conducted. An average value of approximately 43 percent of P_{max} is derived from these profiles as a representative value of the opening load. In Figure 8 the far field crack surface profiles are shown at 10, 30, 50 and 90 percent of P_{max} . The clip-on gage measurements are consistent with those made using the IDG. If the crack surface profile is used to evaluate the load at which the crack becomes fully open, it is evident that the value determined here does not correlate with either the far field value (approximately 0.23 P_{max}) or near crack tip value (greater than 0.63 P_{max}) of P_{op} shown earlier.

The results of the acoustic emission measurements are presented in Figure 9. It is noted that the number of AE counts per cycle is highly variable. Although the load cycles only go to 91 percent of K_{max} , there are some significant emissions associated with some cycles. The primary cause of the acoustic emission is considered to be crack extension since the emissions generally occurred during the loading portion of the test cycles. Based on average crack growth rate data, for this material (25), 24 test load cycles would produce less than 6 μm of crack growth. These results indicate the sensitivity of the AE technique for detecting small increments of crack growth; however, the variability of the count rate illustrates the statistical nature of the crack propagation process. This highlights the necessity of averaging AE data over large cycle blocks if a quantitative relationship is to be developed between AE results and fracture mechanics

parameters.

Acoustic emission upon unloading, which has been reported to be related to crack closure (23), was not generally observed in this effort. Vary and Klima (5) observed that the magnitude of acoustic emissions in steel, aluminum and titanium alloys during unloading appears to be related to the crack surface roughness. The fatigue crack surfaces of IN-100 are extremely smooth. Therefore, the lack of acoustic emissions during unloading appear to agree with the observations of Vary and Klima. The one notable exception, when emissions were observed during unloading, followed a seven percent overload during cycle five at $a = 27.92$ mm. The IDG and clip-on displacement gage records showed no changes in displacement-load response after the overload. However, during the overload portion of the cycle, 2200 AE counts were recorded. These counts are not shown in Figure 9 because they occurred at loads greater than the normal test load range. This acoustic emission activity during loading is indicative of crack tip deformation. Another indication of increased crack tip deformation was the occurrence of acoustic emission activity during the unloading portions of subsequent test cycles. Thirty-five percent of the counts illustrated for the load cycles at this crack length after the overload were recorded during the unloading portion of the cycle. It is significant that only after this slight load perturbation were acoustic emissions observed during unloading that could be attributed to crack closure.

CONCLUSIONS

The objective of the work presented here was to evaluate the uniqueness of P_{op} as defined by Elber (2) as the parameter to quantify the load at which a crack is completely open as in the crack closure theory. The results of the data presented indicate that P_{op} is not a unique value but a variable dependent on measurement location. Unless a rational physical mechanism is shown to account for the observed variability in P_{op} , it is suggested that P_{op} does not characterize the load at which the crack is completely open and it is not suitable for quantifying an effective stress intensity range experienced at the crack tip. Based on the crack surface profiles constructed from the displacement-load data, it appears that an opening load based on a crack surface opening criterion may be more appropriate for quantifying complete crack surface separation.

A large variability in acoustic emission counts was experienced for cracks grown under identical stress intensity histories. A well defined relationship does not exist between acoustic emission counts and crack closure for the conditions studied here.

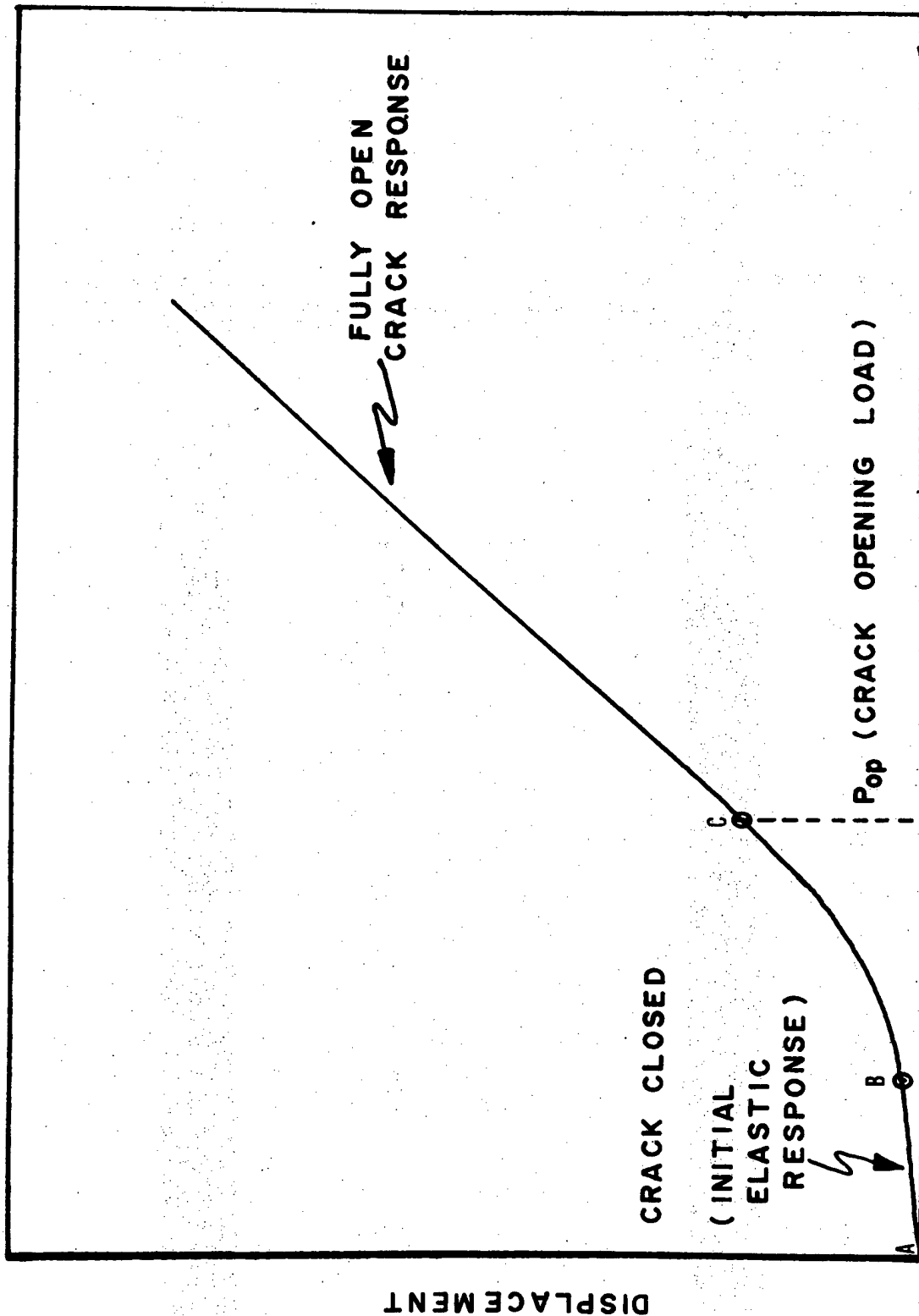
ACKNOWLEDGMENTS

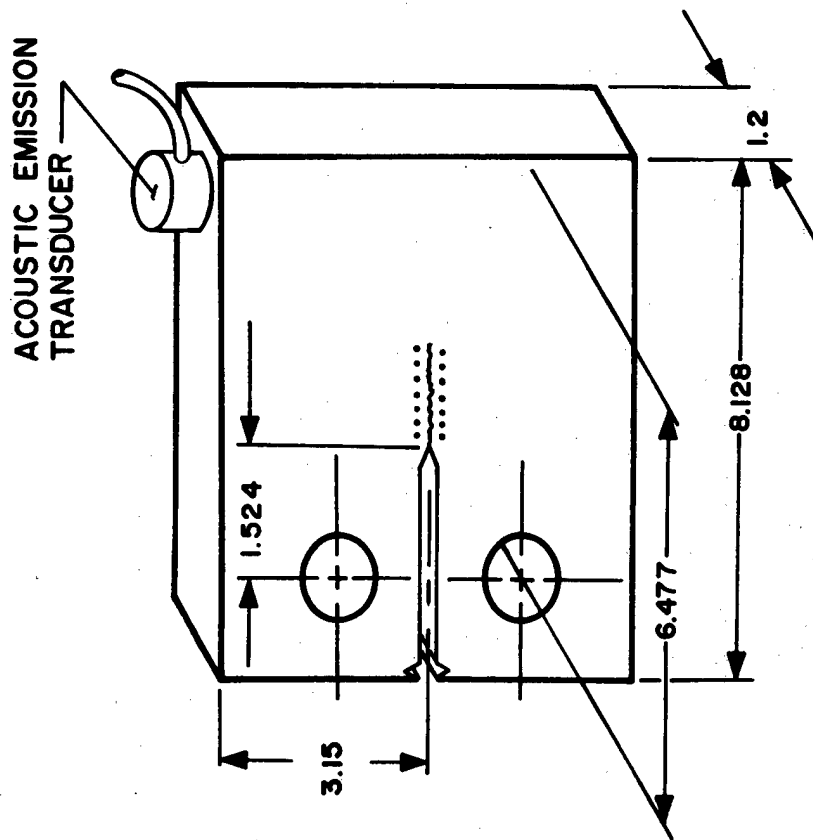
The authors wish to acknowledge the experimental support provided by Messrs. Charles Bell and Richard Klinger of Systems Research Laboratories, Inc. J.W. Jones wishes to acknowledge the support provided by the National Research Council and the Air Force Materials Laboratory.

REFERENCES

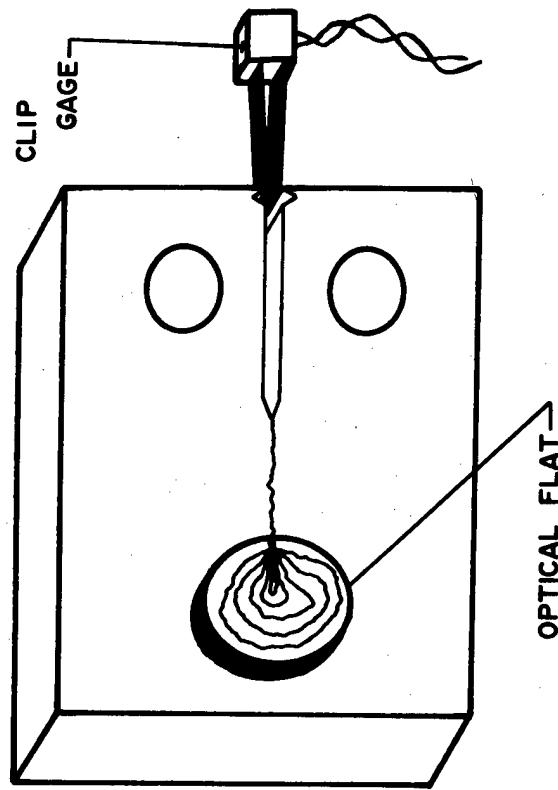
1. Elber, W., Engineering Fracture Mechanics, Vol. 2, No. 1, July 1970, pp. 37-45.
2. Elber, W., Damage Tolerance in Aircraft Structures, ASTM STP 486, American Society for Testing and Materials, 1971, pp. 230-242.
3. Shih, T.T., and Wei, R.P., Engineering Fracture Mechanics, Vol. 6, No. 1, March 1974, pp. 19-32.
4. Buck, O., Ho, C.L., and Marcus, H.L., Engineering Fracture Mechanics, Vol. 5, No. 1, Feb. 1973, pp. 23-34.
5. Vary, A. and Klima, S.J., "A Potential Means of Using Acoustic Emission for Crack Detection Under Cyclic-Load Conditions", NASA TMX-68228, NASA Lewis Research Center, Cleveland, OH.
6. Pitoniak, F.J., Grandt, A.F., Montulli, L.T., and Packman, P.F., Engineering Fracture Mechanics, Vol. 6, No. 4, 1974, pp. 663-670.
7. Roberts, R. and Schmidt, R.A., International Journal of Fracture, Vol. 8, 1972, pp. 469-471.
8. Katcher M. and Kaplan, M., Fracture Toughness and Slow Stable Crack Growth, ASTM STP 559, American Society for Testing and Materials, 1974, pp. 264-282.
9. Sharpe, W.N., Jr., and Grandt, A.F., Jr., Mechanics of Crack Growth, ASTM STP 590, American Society for Testing and Materials, 1976, pp. 302-320.
10. Marci, G. and Packman P.F., Materialprufung, 18 (1976), pp. 260-265.
11. Hagemeyer, J.W., "Growth Rates and Closure Stresses for Fatigue Cracks in Aluminum Alloys", Technical Report No. ERR-FW-1779, General Dynamics, Ft. Worth, TX (1976).
12. Fransden, J.D., Inman, R.V., and Buck, O., International Journal of Fracture, Vol. 11, 1975, pp. 345-348.
13. Bachman, V. and Munz, D., International Journal of Fracture, Vol. 11, 1975, pp. 713-716.
14. Clarke, C.K. and Cassatt, G.C., Engineering Fracture Mechanics, Vol. 9, 1977, pp. 675-688.

15. Rueping, J.E. and Hillberry, B.M., "Fatigue Crack Closure Behavior: A Comparative Study", Air Force Office of Scientific Research Technical Report No. 76-1090, AFOSR, Bolling Air Force Base, D.C., 20332, Aug. 1976.
16. Imhof, E.J. and Barson, J.M., Progress in Flaw Growth and Fracture Toughness Testing, ASTM STP 536, American Society for Testing and Materials, 1973.
17. Sharpe, W.N., Jr., International Journal of Nondestructive Testing, Vol. 3, 1971, pp. 56-76.
18. Macha, D.E., Sharpe, W.N., Jr., Grandt, A.F., Jr., Cracks and Fracture, ASTM STP 601, American Society for Testing and Materials, 1976, pp. 490-505.
19. Marci, G., Packman, P.F., and Jones, J.W., Proceedings of the 2nd International Conference on Mechanical Behavior of Materials, Boston, (1976).
20. Bateman, D.A., Bradshaw, F.J., and Rooke, D.P., "Some Observations on Surface Deformation Round Cracks in Stressed Sheets", Royal Aircraft Establishment Technical Note No. CPM. 63, London, 1963.
21. Oppel, G.U., and Hill, P.W., Experimental Mechanics, July 1964, pp. 206-211.
22. Underwood, J.H., Swedlow, J.L., and Kendall, D.P., Engineering Fracture Mechanics, Vol. 2, 1971, pp. 183-196.
23. Buck, O., International Journal of Fracture Mechanics, Vol. 8, 1972, pp. 121-124.
24. Paris P.G. and Sih, G.C., Fracture Toughness Testing and Its Applications, ASTM STP 381, American Society for Testing and Materials, 1965, pp. 30-81.
25. Macha, D.E., "Fatigue Crack Growth Retardation Behavior of IN-100 at Elevated Temperatures", to be published in Engineering Fracture Mechanics.





IDG SIDE



OPTICAL INTERFEROMETRY SIDE

1325

Fig.2



1326

Fig.3

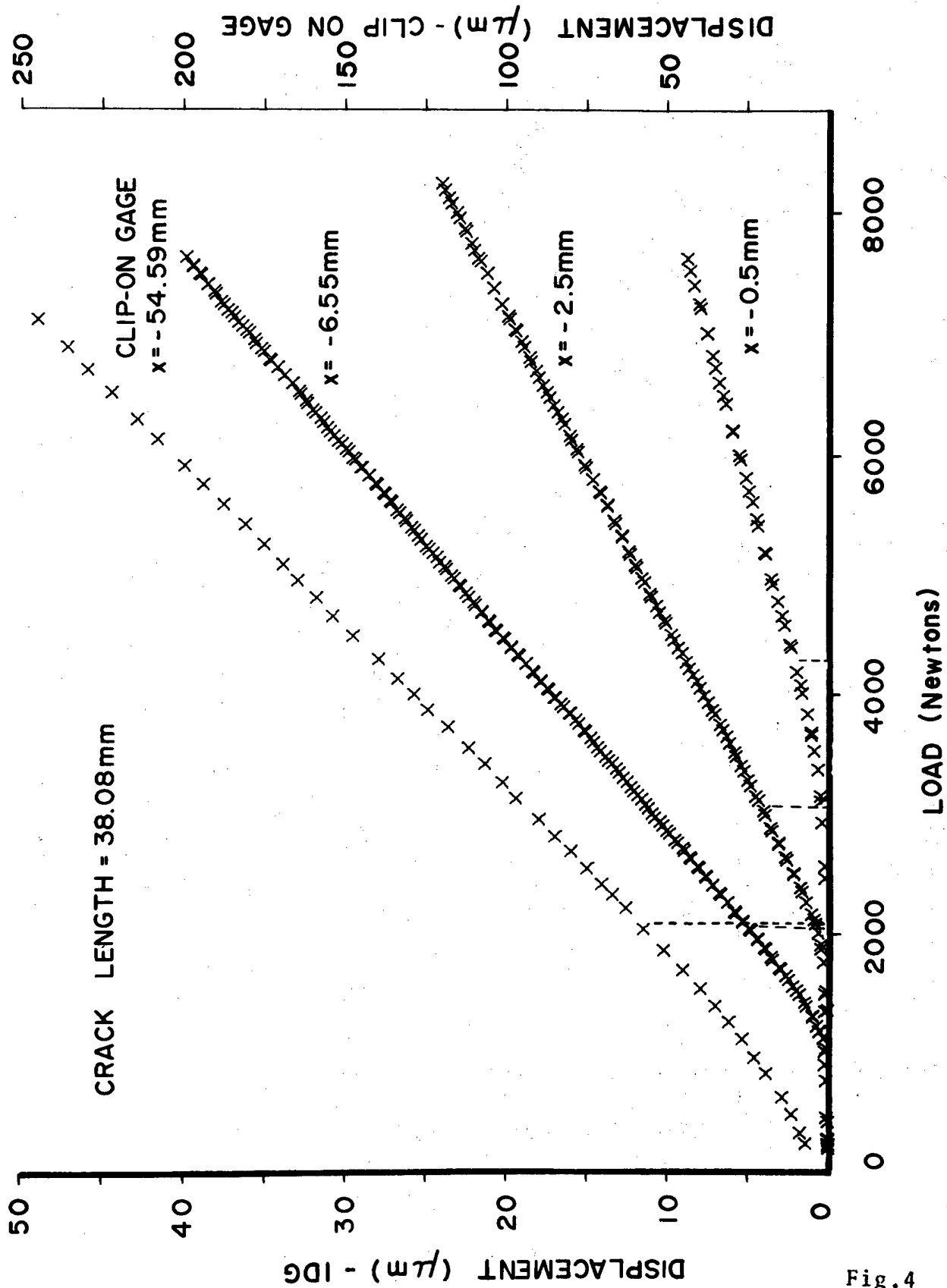
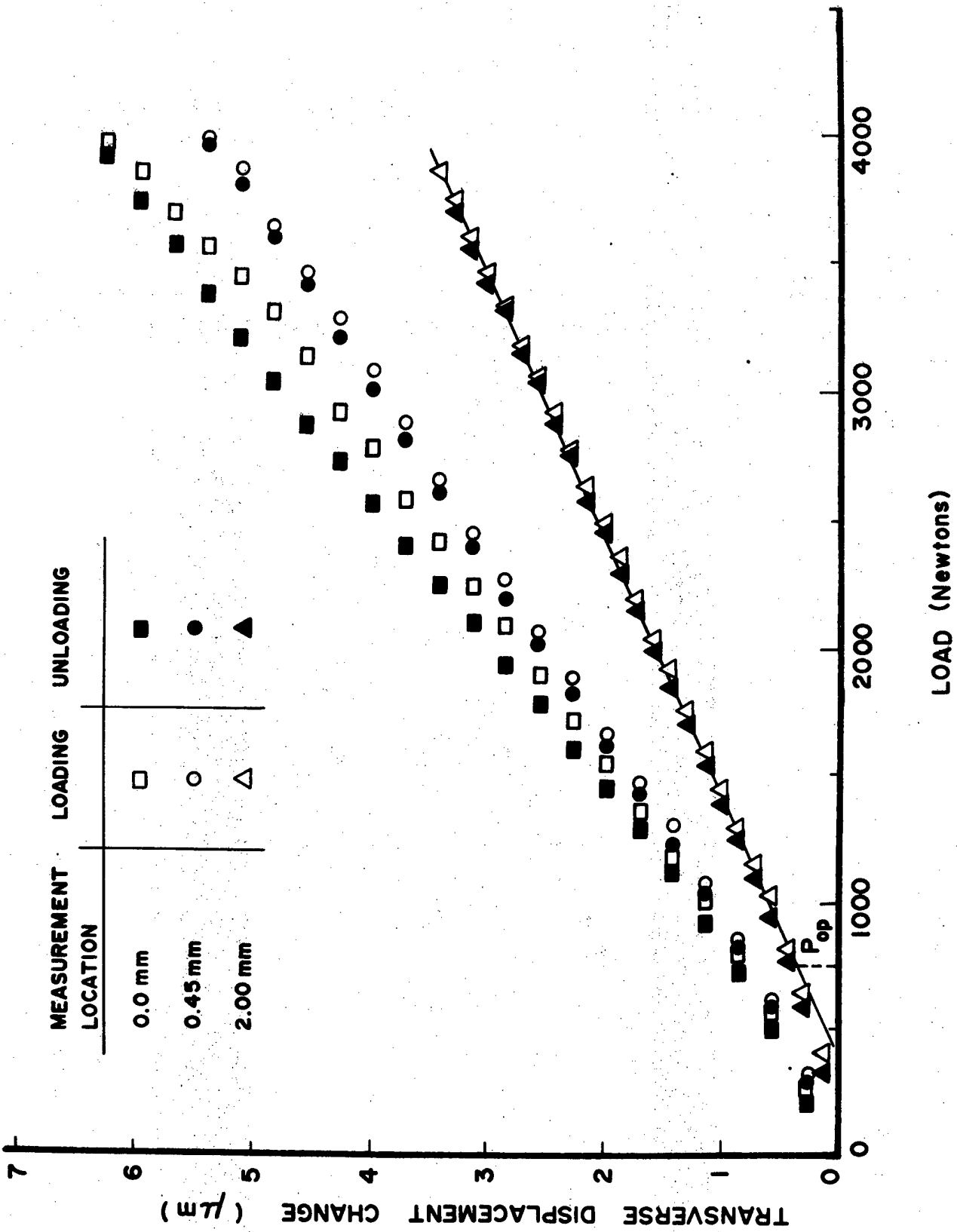


Fig.4



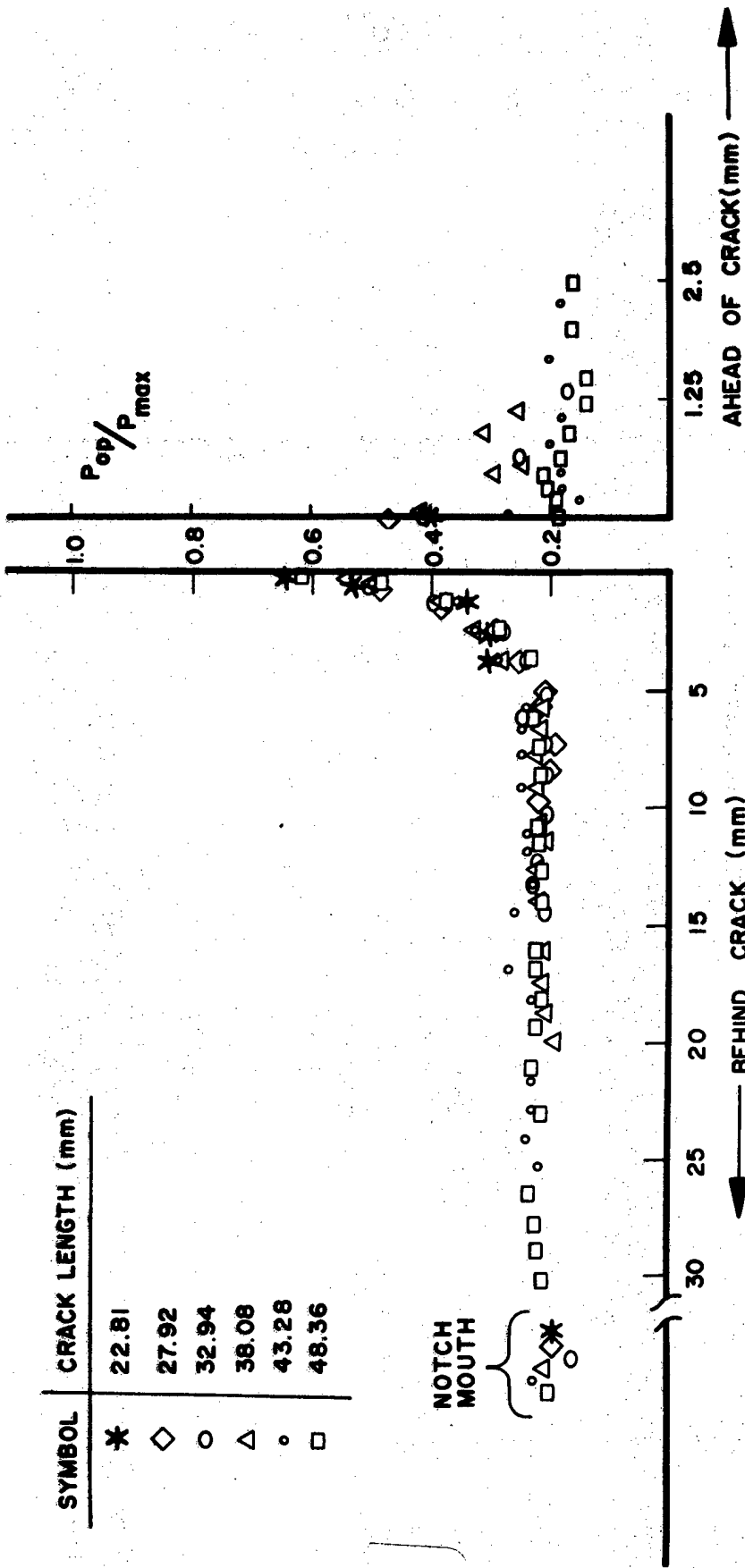
1328

1.0

SYMBOL | CRACK LENGTH (mm)

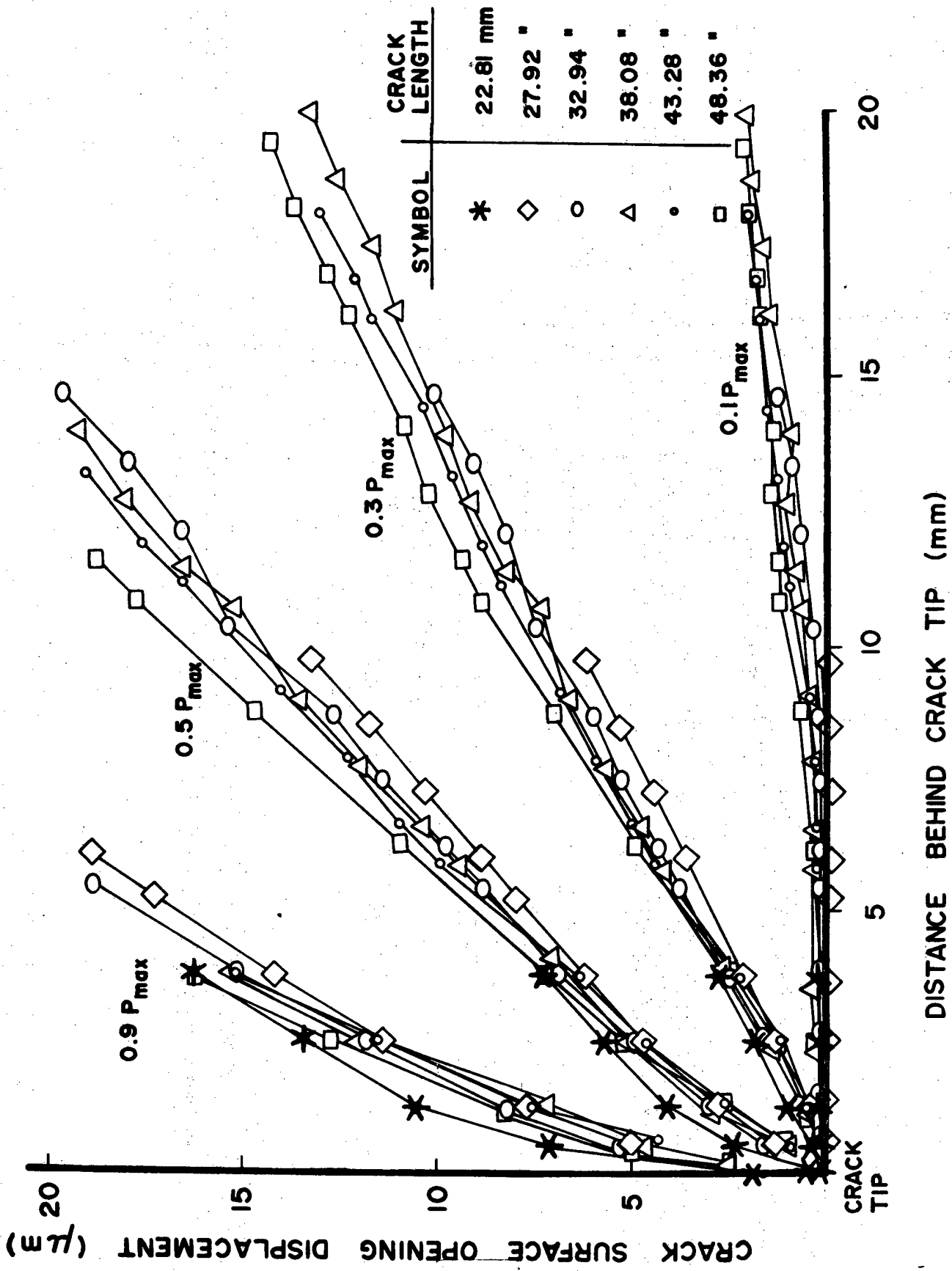
*	22.81
◇	27.92
○	32.94
△	38.08
◦	43.28
□	48.36

NOTCH MOUTH



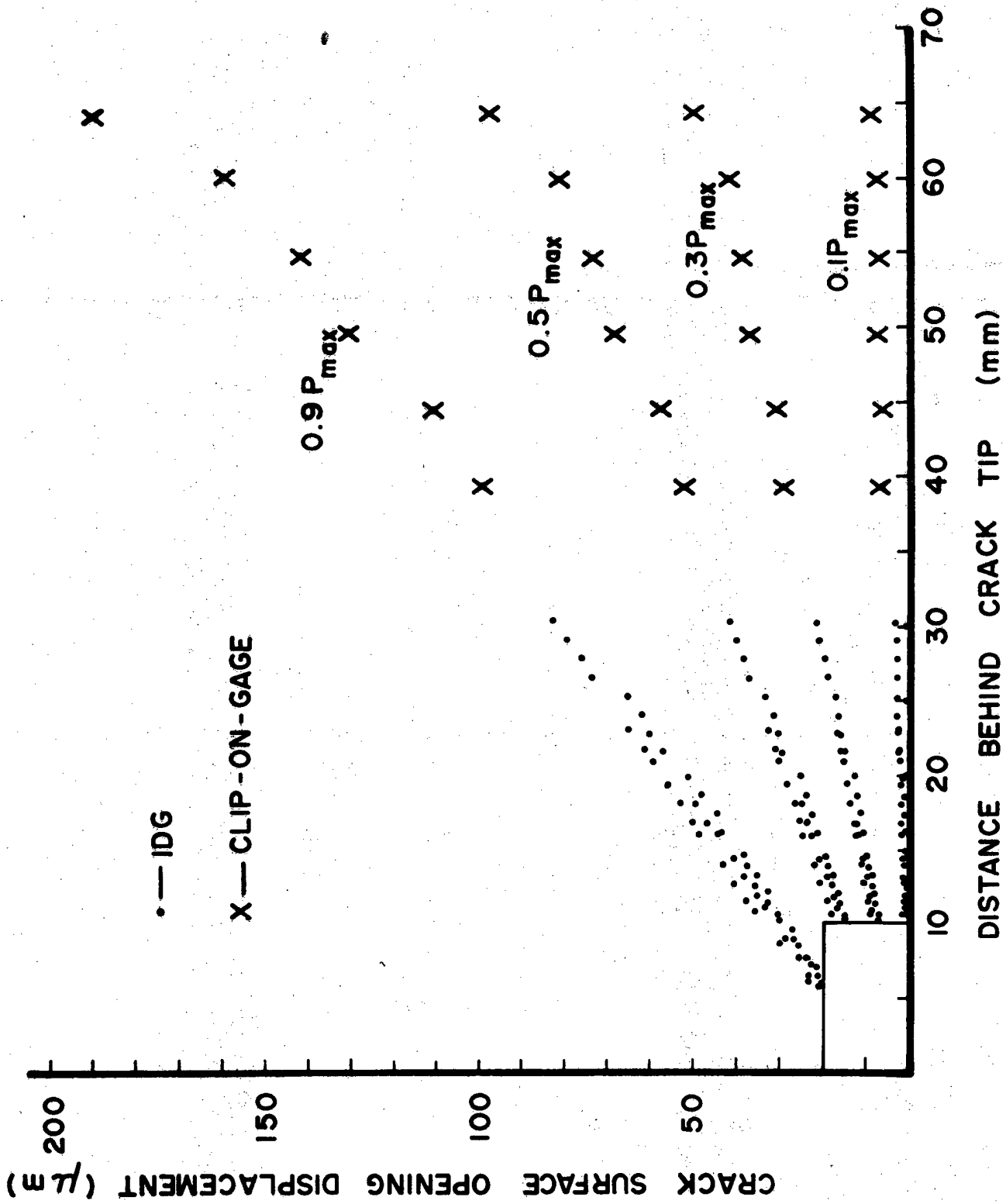
1329
1390

1334
24



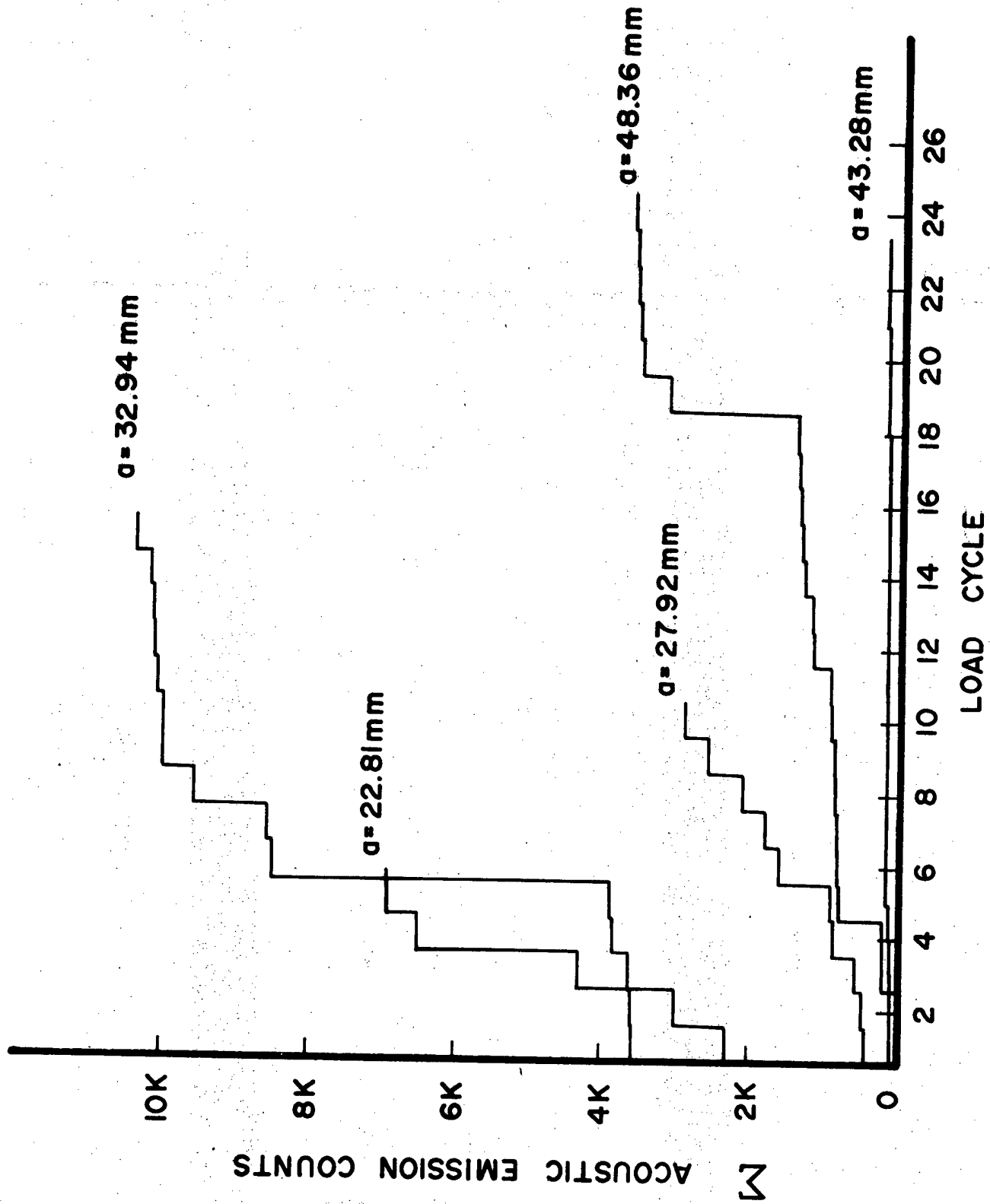
1331

1330



1331

1331



1332

1337

Biographical Sketch

Dennis E. Macha was born December 12, 1946, in Alma, Michigan. He entered active military duty with the U.S. Navy and was assigned to the Naval Nuclear Propulsion Program. After five years of service, he was honorably discharged in 1969. Mr. Macha received a B.S. in Metallurgy in 1974 from Michigan State University. He is currently completing graduate work in Metallurgy at the Ohio State University Graduate Center at Wright-Patterson. Mr. Macha joined AFML in June 1974 as a Materials Engineer in the Metals Behavior Branch, Metals and Ceramics Division.

Mr. Macha currently manages and conducts research in the area of high temperature fatigue crack growth in gas turbine engine materials.

Dennis M. Corbly, Jr. was born February 12, 1947, in Chattanooga, Tennessee. He received his BE in Mechanical Engineering from Vanderbilt University, Nashville, Tennessee in 1969. Dr. Corbly received his MS and PhD in Materials Science and Engineering from Vanderbilt University in 1974 and 1976, respectively. While working on his graduate degrees from 1969-1971 he worked as a graduate research assistant at Vanderbilt University. He joined the Air Force Materials Laboratory in 1971 as a Metallurgist in the Nondestructive Evaluation Branch, serving four years in this assignment. Between 1975 and 1978 he was employed as a Materials Research Engineer in the Metals Behavior Branch of the Metals and Ceramics Division. Dr. Corbly is currently employed as an Engineer in the Materials Life and Methods Unit, Aircraft Engine Group at the General Electric Company, in Evendale, OH.

Biographical Sketch

J. Wayne Jones was born October 29, 1948, in Hodgenville, Kentucky. He entered Western Kentucky University in 1967 and graduated in 1971 with a B.S. in Engineering-Physics. He received his postgraduate education in materials and metallurgical engineering from Vanderbilt University where he was awarded an M.S. in 1973 and a PhD in 1977. From January 1977 to May 1978 he conducted research in the Metals and Ceramics Branch of the Air Force Materials Laboratory under a Post-doctoral Associateship from the National Research Council. He is now Assistant Professor in the Department of Materials and Metallurgical Engineering at The University of Michigan, Ann Arbor.

Dr. Jones' research interests are in the area of the mechanical behavior of materials. During his tenure at the Air Force Materials Laboratory he was involved in an experimental program which studied the crack tip deformation behavior of a nickel-base turbine disc alloy at ambient and elevated temperature. He is currently directing research in the High Temperature Laboratory at The University of Michigan and is initiating research into the crack propagation and fracture properties of materials.

**ENVIRONMENTALLY INDUCED CATASTROPHIC DAMAGE
PHENOMENA AND CONTROL**

BY

John J. De Luccia

Aircraft and Crew Systems Technology Directorate

**Aeronautical Materials Laboratory
Naval Air Development Center, Warminster, Pennsylvania**

1335

Environmentally Induced Catastrophic
Damage Phenomena and Control

Abstract

Sophisticated aircraft utilize alloys that provide high strengths for performance demands but are only marginally forgiving in military environments conducive to such catastrophic damage phenomena as stress corrosion cracking, corrosion fatigue, and environmental embrittlement including hydrogen. The mechanisms and susceptibilities characteristic of current steel, titanium and aluminum alloys are discussed with respect to each damage phenomenon. Intrinsic mitigation such as alloy composition and heat treatment, as well as extrinsic mitigation such as inhibition are discussed. The introduction of a new hydrogen measuring device, barnacle electrode; the use of corrosion preventive and crack arrestment compounds; and the approach of process control such as electroplating in a magnetic field are discussed as possibilities for minimizing environmental embrittlement failures in the future.

Introduction

Modern aircraft utilize alloys and other materials of construction that provide high strengths for performance demands but are only marginally forgiving in military environments conducive to catastrophic damage phenomena. These phenomena such as stress corrosion cracking, corrosion fatigue, and environmental embrittlement including hydrogen are classed under the heading of conjoint action. Conjoint action is the combined and mutually reinforcing effect of the environment and stress to produce rapid deterioration of metals; i.e., catastrophic failure. Figure 1 is a schematic representation of conjoint action during cracking.

In the case of stress corrosion cracking, the combined chemical and mechanical effects occur simultaneously so that failures are caused by the metal experiencing a corrosive environment and an enduring, static tensile stress. Neither stress nor corrodent acting separately would cause such rapid failure. The corrodent involved in stress corrosion cracking is usually specific to the alloy.

Whereas stress corrosion requires an enduring static tensile stress, metallic failure due to corrosion fatigue is caused by cyclic stressing in mildly corrosive environments. In general a metal can withstand an infinite number of stress cycles if the stress does not exceed a certain value called the fatigue or endurance limit. If the same metal is subjected to alternating or cyclic stresses, in a corrosive environment, fatigue will occur in a fewer number of cycles and a fatigue or endurance limit will no longer be observed. In contrast to stress corrosion cracking, corrosion fatigue may occur in a wide variety of environments for any given metal. A typical stress - number of cycles curve is shown in Figure 2 for fatigue with and without corrosion.

The phenomenon of environmental embrittlement can encompass a host of catastrophic conjoint action failures. The definition can be broadened to include stress corrosion cracking but the phenomenon is most often invoked when a specific embrittling species such as hydrogen is involved. Whereas stress corrosion cracking involves an electrochemical step, cracking by environmental embrittlement may proceed by the mere adsorption of the embrittling species on a pre-existing crack or pit or the internal diffusion of the species to high stress points. Since hydrogen is ubiquitous and often occurs as a by-product of corrosion, the demarcation between stress corrosion cracking and hydrogen embrittlement is not always clear.

Each of the described damage phenomena occur on military aircraft often with disquieting regularity. Stress corrosion cracking and corrosion fatigue occur on high strength aluminum alloys of the 2000 and 7000 series in forgings, plates, and sheets on such parts as landing gear, spars, brackets, ribs, wingfold hinges, and skin. Failures of these types are even more critical for naval aircraft forced to perform in the insidious marine environment. High strength steel parts on military aircraft are particularly prone to hydrogen embrittlement cracking. As previously mentioned hydrogen can be a product of the electrochemical (corrosion) reaction at the cathode or it may get into the steel part such as landing gear, arresting hooks, bomb hooks and shackles, through processing. The processes of electroplating, pickling, etching, and chemical milling can inadvertently introduce the embrittling species, hydrogen, into the part.

Thus today's modern military aircraft has many "Achilles heels" which can and must be dealt with from design, through procurement to operational maintenance. It is the purpose of this paper to discuss the highlights of what is known about these damage phenomena and to record how they are being combated and how they might be dealt with in the future.

FAILURE MODES

Stress Corrosion Cracking/Hydrogen Embrittlement

The phenomenon of stress corrosion cracking as it applies to high strength aerospace alloys is less clearly defined than that which occurs on lower strength alloys. In such alloys as austenitic stainless steels, and copper base alloys, stress corrosion cracking clearly involves an electrochemical dissolution step acting in concert with a static stress to cause failure. In high strength steels, and titanium alloys, the corrosion or electrochemical step is less well defined. The environmental and stress interactions are more subtle and it is thought that hydrogen may play a role in the cracking process. Considerable work has therefore been done on the influence of anodic and cathodic polarization on cracking susceptibility⁽¹⁾. Figures 3(a) and (b) are plots of time to failure vs. cathodic and anodic polarization currents. Figure 3(a) is an idealization of an alloy system showing a clear distinction between hydrogen embrittlement failures and anodic stress corrosion failures; i.e., a "no failure" gate exists between

the hydrogen and anodic stress corrosion failures. More often than not the situation for high strength steels is more accurately described by the idealization depicted in Figure 3(b). In Figure 3(b), there is a mechanism overlap that may account for the uncertainty as to whether the cracking is hydrogen related.

It is realized that the subject of stress corrosion cracking could be divided into two general categories; i.e., Type I, environmental cracking, usually involving high strength alloys and titanium, and Type II, anodic stress corrosion cracking. The differences between Type I and Type II cracking behavior can be seen in Figure 4. In general, we note that Type I failures occur in high strength, low ductility materials whereas Type II failure is characteristic of lower strength, more ductile alloys. Further differences between these two types of failures are: cracking is less environmentally specific with Type I; Type II has a slower crack velocity that is independent of the plastic zone size; preexisting cracks or flaws are needed for Type I; and highly constrained locally stressed region is not needed for Type II but is for Type I. These differences point to a relatively new approach to the subject of stress corrosion cracking; i.e., fracture mechanics. We can describe fracture mechanics as the use of proper stress analysis of cracks to develop flaw oriented strength properties of materials. Thus the use of fracture mechanics in the study of stress corrosion cracking acknowledges the existence of preexisting flaws in the metal. There are in general two principal reasons for including pre-cracked specimens for characterizing stress corrosion cracking of many materials: (a) Certain alloys, particularly those of titanium, do not pit in fresh or salt water at ambient temperatures so that smooth specimens of such alloys do not experience stress corrosion cracking in these environments. In 1965, it was found that a notched or pre-cracked specimen of the same titanium alloy which resisted pitting displayed a spectacular susceptibility to stress corrosion cracking⁽²⁾; (b) Most of the important high strength structural alloys show some degree of susceptibility to stress corrosion cracking in such mild environments as fresh water, moist air, sea water and other non-specific mild environments. It has been shown that only the use of pre-cracked specimens will enable the quantification of susceptibility in these alloys. These alloys invariably contain flaws. If the flaws are above a critical size, failure occurs. If the material is under load in a "corrosive", albeit mild, environment, failure occurs more readily.

The use of fracture mechanics in treating the stress factor of stress corrosion cracking in the presence of a crack or flaw involves the stress intensity at the tip of the crack. Figure 5 depicts two methods of stress corrosion testing using pre-cracked specimens. The intensity of stress at the tip of the crack is defined as:

$$K = \sigma \sqrt{a\pi}$$

where σ = tensile stress, and a = crack or flaw size. K , the stress intensity factor, can be used as a design criterion by performing a series of experiments with varying K to ascertain that K below which stress corrosion cracking will not occur. Figure 6 depicts the data accumulation of such experiments. It is noted that as the imposed stress intensity decreases the time for failure in the corrosive environment increases until a limit in stress intensity is reached below which stress corrosion cracking does not occur. This newly defined parameter K_{I_SCC} provides a powerful tool in assessing a material's susceptibility to stress corrosion cracking. It enables the designer to know what critical flaw size his structure can tolerate before failure occurs in a given environment.

With the application of fracture mechanics to stress corrosion/hydrogen embrittlement studies, new thoughts are emerging with regard to failure mechanisms of aluminum alloys. Stress corrosion of aluminum alloys, particularly the age hardenable, aerospace varieties, undergo intergranular cracking in aqueous environments containing chloride or other halide ions. Preferential dissolution at the grain boundaries was thought to play the key role. More recently, it has been shown that hydrogen is a factor in the stress corrosion cracking of high strength, 7075-T6, aluminum alloys. To further demonstrate this effect, the dry crack growth of DCB specimens was monitored as hydrogen was cathodically charged below the crack front. The crack was observed to grow presumably by the diffusion of hydrogen through the aluminum to the crack front. The threshold stress intensity value was materially lowered by the charging as is shown in Figure 7. A more usual way of assessing the aqueous stress corrosion phenomenon is to plot the crack growth rate versus the stress intensity factor. When this is done three stages of cracking are usually delineated with a threshold stress intensity for stress corrosion cracking being defined.

Figure 8 shows an outer cylinder of a landing gear of 7079-T6 aluminum on an Air Force aircraft that failed on the alert pad. Examination of the cylinder revealed a stress corrosion crack that occurred 90° from the parting plane. Figure 9 shows another landing gear failure, this time on a 7079-T6 cylinder from a Navy helicopter. This failure was also attributable to stress corrosion.

The study of environmental embrittlement of aircraft titanium alloys is also much concerned with hydrogen's role. Although titanium and its alloys are known to experience environmental degradation in a wide variety of environments, hydrogen from either a primary or derivative source has been implicated in a causative sense with almost

all of them. Some of the environments that have been known to cause environmental cracking of titanium alloys are: red fuming HNO_3 , N_2O_4 , methanolic fluids, aqueous salt solutions, gaseous hydrogen, and electrolytic (aqueous) cathodic charging. In a thermodynamic sense, titanium is a very reactive metal. Yet the actual anodic dissolution of titanium in non-oxidizing aqueous solutions occurs with great difficulty. Indeed it has been reported that titanium is virtually immune to corrosion in sea water.⁽⁴⁾ The fact that dissolution does not occur until a driving force of about one volt has been applied implies that the anodic process is strongly inhibited, most probably by the stable oxide film. Titanium alloys are not free of stress corrosion cracking in aqueous halide ion environments, especially in the presence of notches or preexisting cracks.⁽⁵⁾

Titanium when stressed in salt water is ordinarily kept passive by reaction with the water to form a tight adherent layer of TiO_2 , which insulates the underlying metal from the environment. Inside a crack, however, the reactions of titanium with water to produce TiO_2 also produces excess hydrogen ions which cause local acidity; i.e.,



This acidity builds up to a point where the oxide becomes unstable. Thus the crack tip does not remain passive but continues to react to form hydrogen, some of which undoubtedly enters the metal.

It has been recently shown that conditions under which the protective oxide film on a beta titanium alloy can be removed leads to catastrophic damage in hydrogen bearing environments. Severe embrittlement and in some cases, spontaneous cracking, occurred in beta III titanium specimens whose surfaces were rendered oxide free by the vacuum techniques of ion bombardment and palladium vapor deposition. An example of the phenomenon is shown in Figure 10. The oxide free, albeit palladium coated, surface allows hydrogen atoms to be absorbed virtually unimpeded upon cathodic charging. In this beta alloy, hydrogen damage is not caused by the formation of hydrides, but in the more classical diffusional sense similar to steel. Spontaneous lattice swelling and cracking of a surface treated beta III titanium foil that was cathodically charged for forty-eight hours is shown in Figure 11.

Corrosion Fatigue

The mechanism of corrosion fatigue is believed to involve the preferential dissolution of microscopic extrusions and intrusions. These are minute areas on the surface where the metal has undergone

plastic deformation (even if the applied stress is well below the yield strength). It is believed that the corrosion process serves to sharpen the microscopic crevices so that they become stress risers. The areas of high stress accentuated by the corrosive environment, serve as sites for the initiation and propagation of a brittle, transgranular crack. The distinguishing features between a corrosion fatigue failure and one caused by stress corrosion is that corrosion fatigue almost always manifests itself in transgranular cracking whereas stress corrosion cracking may be either transgranular or intergranular depending on the alloy and environment, and with corrosion fatigue, the corrosive action merely serves to trigger the brittle failure, whereas in stress corrosion cracking, the corrosive action not only serves to initiate the failure but is required for its further propagation.

Corrosion fatigue is a common cause of failure in metals subjected to vibratory loads. In contrast to stress corrosion cracking, corrosion fatigue may occur in a wide variety of environments for a given metal. Because of the presence of a growing flaw and the time delay before failure, fatigue and corrosion fatigue can be studied using fracture mechanics. This approach is most often used for high strength aerospace alloys. Figure 12 depicts the three stages of fatigue or corrosion fatigue that is prevalent when the fracture mechanics (pre-cracked specimens) are used. The crack growth rate, da/dn , is plotted against the stress intensity range of the fatigue cycle, ΔK . Stages I and III crack growth rates show a dependency on stress intensity, whereas stage II does not. It should be emphasized that the subject of corrosion fatigue is complex and the use of fracture mechanics precludes the pitting or initiation step and hence the subject becomes more manageable. A further complicating factor for aerospace alloys is that in-service fatigue or corrosion fatigue rarely, if ever, occurs with a constant stress amplitude. Rather, irregular cyclic loading with large overload excursions is usually the rule. With these factors taken into consideration it is found that the demarcation between stress corrosion cracking and corrosion fatigue, especially of aerospace aluminum alloys, is unclear. In general, it was demonstrated that stress corrosion cracking may occur under cyclic loading of these alloys especially at low frequencies, and that stress corrosion and fatigue can interact under certain conditions to produce failures in shorter times and fewer cycles than for either phenomenon occurring by itself. (7)

A particularly classic example of a mixed mode failure mechanism is that of a Navy A-6 fighter-bomber catapult socket lug which broke during test after 617 simulated launches. The lug was made of AISI 4330 Si steel heat treated to the 180 ksi yield strength level. The fracture, Figure 13, bisected a threaded lube fitting hole which was filled with grease during testing. The cracking mechanism was intergranular at the origin, indicative of a corrosion or hydrogen

step. At the transition zone between the brittle origin and ductile final cracking, fatigue striations with both ductile and brittle characteristics were observed. These observations were made with the scanning electron microscope and replica transmission electron microscopy. Thus on this one failure, the possibility of the interaction of all of the following mechanisms exists: stress corrosion, hydrogen embrittlement (due to Cd plating), corrosion fatigue, and fatigue.

MEANS OF MITIGATION

Classical corrosion control involves attacking the problem from an internal (metal selection); external (inhibited environment); or interfacial (coatings) standpoints. In controlling environmentally induced catastrophic damage phenomena the internal approach; i.e., alloy and heat treatment development is almost exclusively used.

Alloy Selection and Heat Treatment

The advent of the heat treatable 7000 series aluminum alloys provided a boon to aircraft designers. The high modulus, high strength, and low weight of these alloys made them ideal for the high performance of advanced aircraft. Their susceptibilities to intergranular corrosion, exfoliation, and stress corrosion cracking made them less than desirable in marine environments. It was discovered that if these alloys were systematically overaged, their susceptibilities to these forms of attack would be materially lessened if not totally eliminated. Thus the T73 temper was born. As is usually the case with most "fixes," a price had to be paid. There is an approximate 10% strength loss accompanying the T73 overaging treatment. The T73 temper replaced the standard T6 temper on many military aircraft where designs could be altered or the strength loss tolerated.

More recently newer 7000 series alloys have been developed with specific resistance to intergranular attack and environmental embrittlement. Most of these new alloys such as 7050 and 7010 owe their lessened susceptibility to the presence of zirconium. Professor DiRusso in Italy first identified the beneficial effects of this element in Al-Zn-Mg alloys.⁽⁸⁾ These newer alloys also pay particular attention to the "cleanliness" of the microstructure. It contains lower concentrations of the tramp elements, iron and silicon, and therefore has a greater fracture toughness. Aluminum alloy 7050 was developed under the guidance of the Naval Air Systems Command by Alcoa.⁽⁹⁾ In the T7X temper, it provides the best stress corrosion resistance with the highest strength of any commercial aerospace aluminum alloy.

Some very recent work at an Israeli aerospace company indicates that a pre-aging treatment of 7075 alloy renders immunity to stress corrosion cracking (K_{ISCC} is raised by a factor of three) without

any sacrifice in strength. This effort which is called retrogression/re-aging bears watching.

With regard to titanium, the Navy's deep sea rescue vehicle that was being designed in the early sixties was found to be too susceptible to environmental cracking in the presence of a flaw and sea water. As a consequence, steel was hastily substituted as a material of construction for the Ti-8Al-1Mo-1V. This titanium alloy has optimum strength to weight properties for both hydrospace and aerospace. This alloy, however, also has the greatest susceptibility to environmental embrittlement. It was discovered that lesser aluminum contents lessened the susceptibility to environmental embrittlement. Another alpha + beta alloy that contains six percent aluminum and four percent vanadium was introduced for aerospace use, both in airframes and engines. This alloy is still the mainstay for titanium aerospace applications although it is not totally immune to environmental embrittlement. Two newer alloys of lesser embrittlement sensitivities for use in propulsion systems are: titanium, 6% aluminum, 2% tin, 4% zirconium, 2% molybdenum and Ti-17 (titanium, 5% aluminum, 4% molybdenum, 4% chromium, 2% tin, 2% zirconium). New, all beta, titanium alloys of high toughness are being used for aerospace fasteners.

In-situ and Process Control:

The practical use of chemical inhibitors in controlling stress corrosion cracking is admittedly limited, given the infinite volume of environment that would require inhibition. Nevertheless it has been shown that oxidizing inhibitors, such as the chromate ion, retard crack propagation for high strength, low alloy steels in aqueous media.⁽¹⁰⁾ An alternative method, and one that acknowledges the presence of structural cracks (fracture mechanics) would be the development of crack arrestment compounds that could conceivably be applied in-situ. The properties of such compounds would include all or a combination of the following: moisture displacement at the crack tip, the modification of the surface chemistry to minimize corrosion and hydrogen entry at the crack tip, and a passive film (barrier effect) at the crack surface. The following is a description of some of the work that is going on at the Naval Air Development Center on crack arrestment under an independent research and development program.

Static Testing (Stress Corrosion Cracking):

Preliminary indications show AMLGUARD, (MIL-C-85054(AS)) a water displacing corrosion preventive compound developed at the Naval Air Development Center, to be effective as a crack arrestor on a statically loaded pre-cracked titanium 6Al-4V specimen in methanol. In the methanol solution, the limiting sustained stress intensities

for AMLGUARD pretreated titanium specimens were roughly equivalent to those experienced in ambient air. This titanium alloy will otherwise fail within a few hours in methanol at stress intensities about half of that of the AMLGUARD pretreated specimens.

Dynamic Testing (Corrosion Fatigue):

Evaluations of various corrosion and crack arresting compounds were made on low cycle corrosion fatigue life of pre-cracked notched bend bar specimens of high strength (260-280 ksi) AISI 4340 steel. The fatigue pre-cracked specimens were mounted on an Instron testing machine enclosed in a humidity controlled chamber, and cycled between loads of 1500 to 150 pounds at a frequency of 10 cycles per minute. These conditions yield a minimum K_I value of 26 ksi $\sqrt{\text{in}}$ for dry air ($\approx 15\%$ relative humidity). The remaining experiments were performed in moist air of 90% relative humidity. In an accompanying program at the laboratory, a method was developed by which metal anions could be solubilized in organic media using phase transfer catalysts. This method was found significant for the present study to evaluate some candidate corrosion inhibiting ions (crack arrestors) without the complication of introducing water into the crack propagating system. This approach eliminates questions concerning hydration shells of inhibiting ions at the interface.

Phase transfer catalysis is carried out in a two phase aqueous - organic solvent system. The aqueous phase usually contains the anion to be transferred. The organic phase contains the phase transfer catalyst usually dissolved in methylene chloride. The phase transfer catalysts (PTC) in use are usually quaternary ammonium salts. Due to their slight solubilities in water a small amount of the PTC diffuses into the aqueous phase where it is able to exchange its existing anion for the anion to be transferred. The PTC with its new anion is then able to diffuse back into the organic medium. In this manner, the powerful corrosion inhibiting chromate ion has been taken into solution of such organic materials as paints, oils, solvents, and corrosion preventive compounds. In the crack arrestment study, various corrosion inhibiting anions are being dissolved in mineral spirits to provide a combination of wettability and moisture displacement with both dissolved anodic and cathodic inhibiting ions. Figure 14 shows the effect of candidate crack arrestment compounds on the crack growth rate of AISI 4340 steel in 90% relative humidity (moist air) at room temperature. The crack growth rate measured in crack extension per cycle, $(\frac{da}{dn})$ versus stress intensity factor (K_I) curves determined for various environmental conditions are shown in Figure 14. A comparative evaluation of the various candidate compounds showed a marked decrease in crack growth rate of 4340 steel for all of them. Among them, the combination of chromate + nitrite + borate showed best results with the crack growth rate reduced to 28 micro in./cycle as

compared to 110 micro in./cycle in moist air alone. Thus, the crack growth rate was retarded by a factor of 4. Other compounds although beneficial were less effective. AMLGUARD which worked well with statically loaded tests, failed to perform in the fatigue tests for reason of inadequate transport to the tip of the propagating crack during cycling. However, an initial retardation effect on crack growth was observed.

Chromate is known to be an excellent oxidizer and inhibitor of anodic dissolution of transition metals through formation of a passive film. Borate acts as a corrosion inhibitor through its property of modifying the pH of the corrosive media (raises pH to neutral levels). Formation of an acid (H^+ ions) in crevices and crack areas is a factor for many corrosion initiated and assisted failures. Nitrites act as oxygen scavengers thus minimizing corrosion. It was for these reasons that a combination of the two properties; i.e., the chromate ion passivation, and borate and nitrite as buffer and O_2 scavenger worked so well in retarding the crack growth rate.

Process Control:

Perhaps the most neglected approach to curbing embrittlement is process control. An example would be the alteration of electroplating conditions to minimize hydrogen entry during plating. In order to assess the amount of hydrogen introduced during plating or any other process, a non-destructive electrochemical measuring device has been developed at the Naval Air Development Center. The device which can be used in-situ is called the barnacle electrode. The barnacle electrode is an electrochemical cell in which the hydrogen-containing part is the anode, and a nickel - nickel oxide electrode is the cathode. The internal hydrogen diffuses to the surface where it is oxidized, and the oxidation current is an indication of the concentration of hydrogen in the metal. A schematic of the measuring process is shown in Figure 15. An instantaneous current density measurement can be converted to a hydrogen concentration by use of the solution to the diffusion equation characterized by the extraction transient. This simple, rugged device, coupled with standard electronic circuitry, can accurately measure hydrogen contents as low as one part per ten million (comparable to one drop in about 180 gallons). By correlating the results of these measurements to the failure rates of notched specimens established through laboratory testing, it can be determined whether or not the part has been embrittled to the danger point.

The barnacle electrode method will replace other techniques that require complex, expensive equipment, and yet will furnish more precise and sensitive measurements. In addition to the in-place testing of parts, it can replace the destructive testing techniques currently used to determine embrittlement during processing.

The first of three prototypes of the apparatus is being evaluated by Cleveland Pneumatic Corporation, a subcontractor to McDonnell Douglas Corporation. The unit will be tested as part of the quality control process during production of the F-18 fighter aircraft landing gear to determine the hydrogen concentration after cadmium plating.

Magnetic Effects:

The barnacle electrode is also being used to assess the effects of high magnetic fields on the entry of electrolytic hydrogen into high strength steels. Recent experiments show that hydrogen entry is significantly retarded when electrolytic charging is performed in a high (66 K gauss) magnetic field. The experiment consisted of assessing the amount of hydrogen entry to a high strength 4340 steel coupon cathodically charged against a platinum electrode in a 0.25 N NaOH solution containing cyanide ions while in a magnetic field. The level of hydrogen measured by the barnacle electrode after the experiment for the steel charged within the magnetic field was two times less than that charged under identical conditions outside the magnetic field. A schematic of the experiment is shown in Figure 16.

SUMMARY

The foregoing provides a brief exposure to the problem of environmentally induced catastrophic cracking of high strength aircraft alloys and gives an introduction and update on what the air arm of the Navy is doing, from a research and development standpoint, to combat the problem. Some of the more important in-house efforts and ongoing research at the Naval Air Development Center's Aeronautical Materials Laboratory are highlighted. The introduction of a new hydrogen measuring device, barnacle electrode; the use of corrosion preventive and crack arrestment compounds; and the approach of process control such as electroplating in a magnetic field, all appear to be within the realm of possibility for minimizing environmentally induced catastrophic damage of aircraft materials in the future.

References

- (1) Wilde, B. E., Corrosion 27 326 (1971)
- (2) Brown, B. F., Materials Research Standards, 6 no. 3, p 129 (1966)
- (3) Gest, R., and Troiano, A., Corrosion 30 no. 8, p 274 (1974)
- (4) De Luccia, J. J., Materials Protection, NACE, 5 no. 8 (1966)
- (5) Boyd, W., "Fundamental Aspects of Stress Corrosion Cracking," Proc. of Conference, Ohio State University, NACE p 593 (1969)
- (6) De Luccia, J. J., NADC report no. 76207-30, Warminster, PA 18974, (1976)
- (7) Nordmark, G., Lifka, B., Hunter, M., and Kaufman J., ALCOA Technical Report AFML-TR-70-259, November (1970)
- (8) DiRusso, "Mechanical Properties and Stress Corrosion Resistance of Al-Zn-Mg-Cu Alloys," Istituto Sperimentale dei Metalli Leggeri, Milano, Italy, report of 14 March (1968)
- (9) Staley, J., Hunsicker, H., and Schmidt, R., "New Aluminum Alloy X7050," Metal Congress, TMS, AIME, October (1971)
- (10) Parish, P., Chen, C., and Verink, E., "Stress Corrosion - New Approaches," STP-610, American Society for Testing and Materials, Philadelphia, PA (1976)

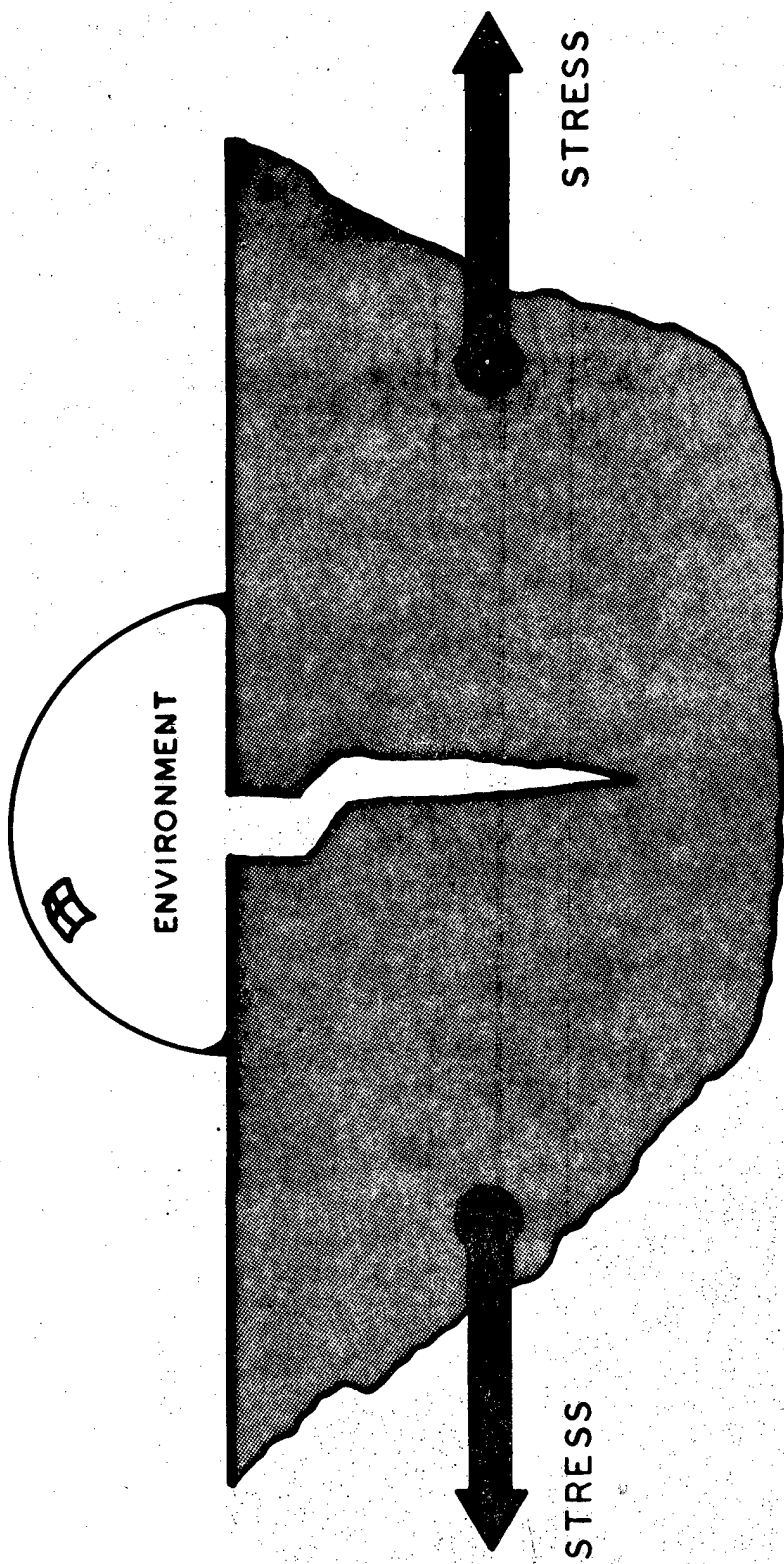


Figure 1. Conjoint Action Causing Environmental Cracking

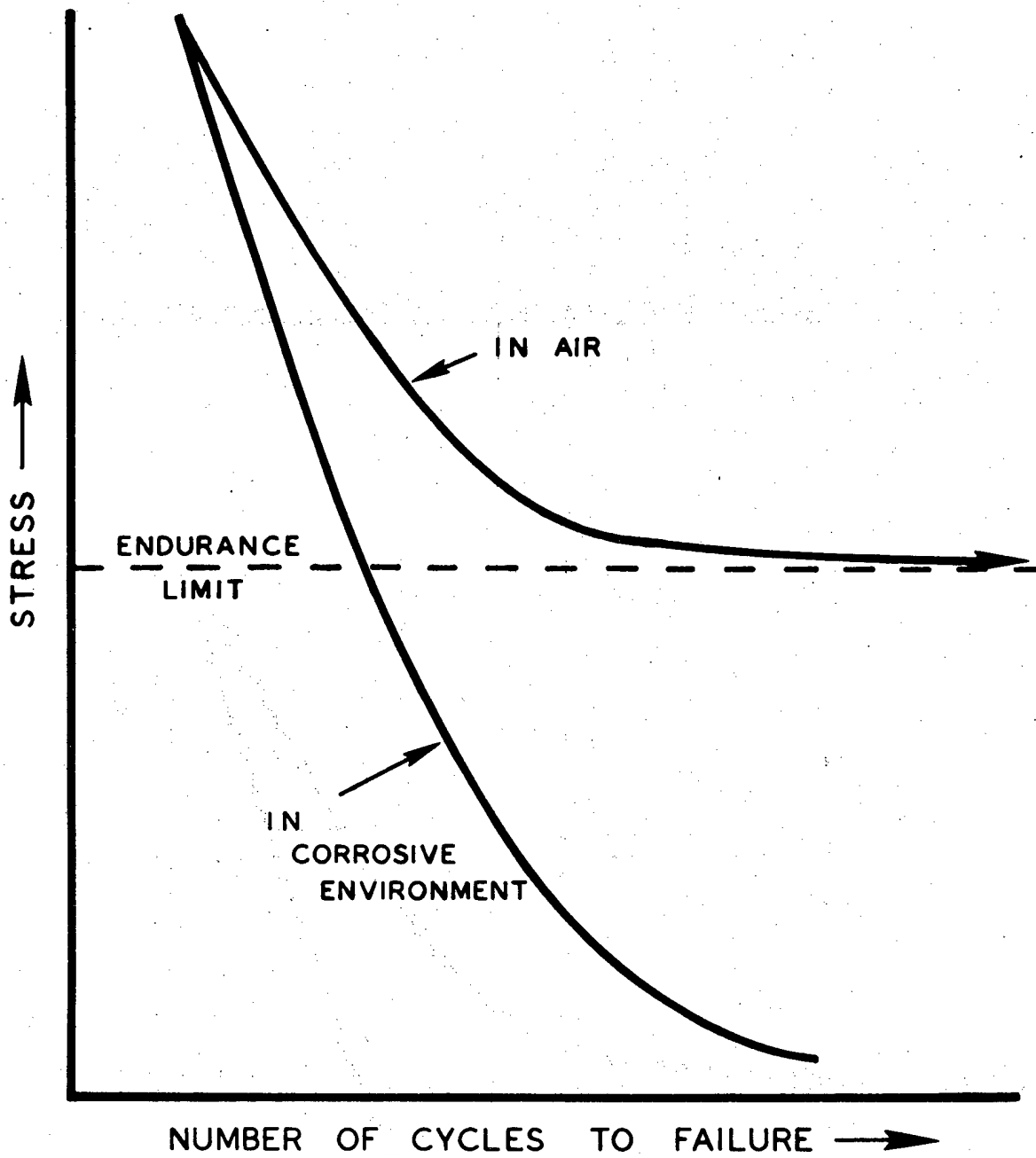


Figure 2. Effect of Corrosion on the Fatigue Limit

1350

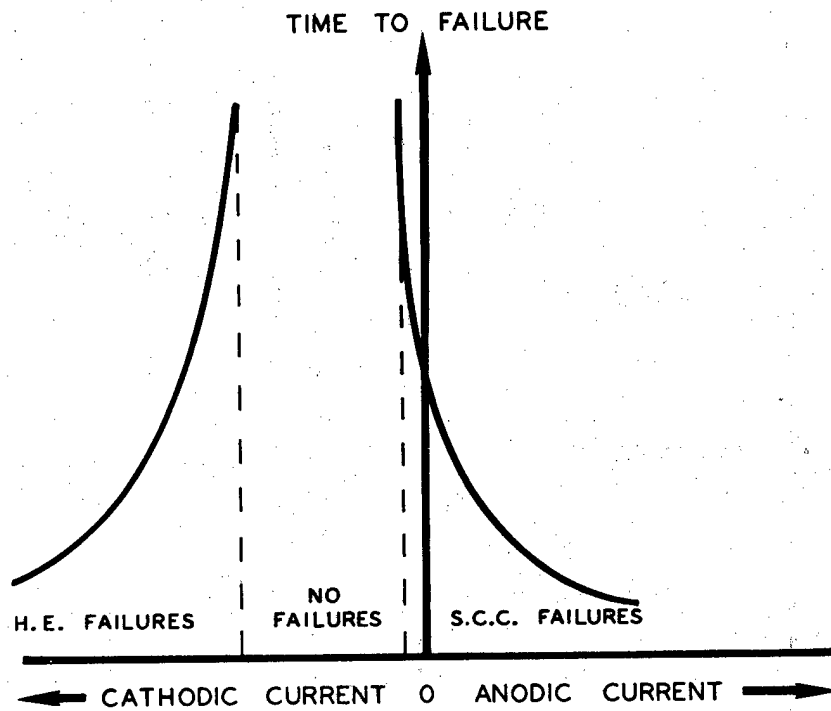


Figure 3. (a) Time to Failure Vs. Polarization Currents

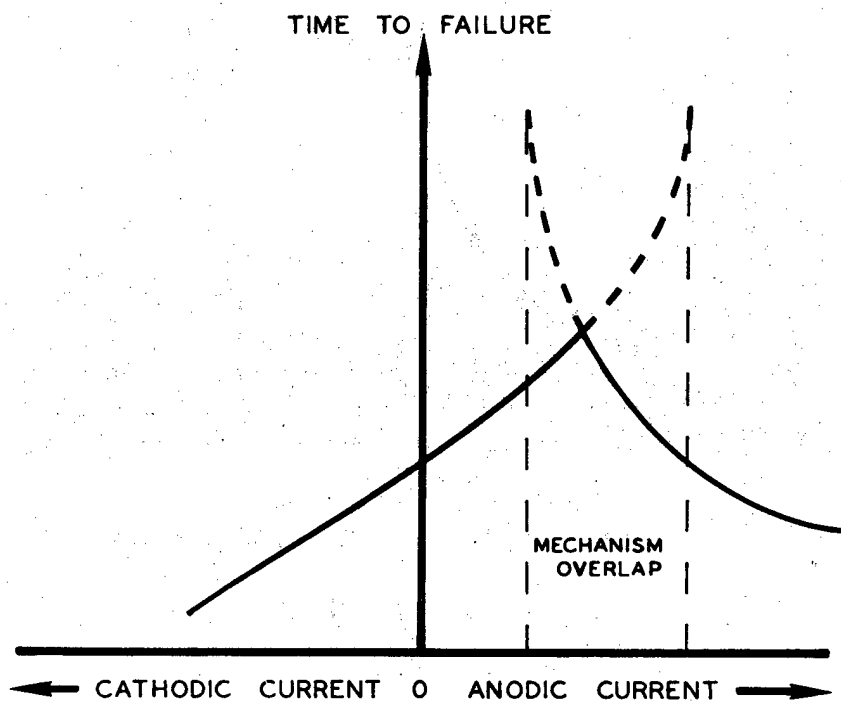
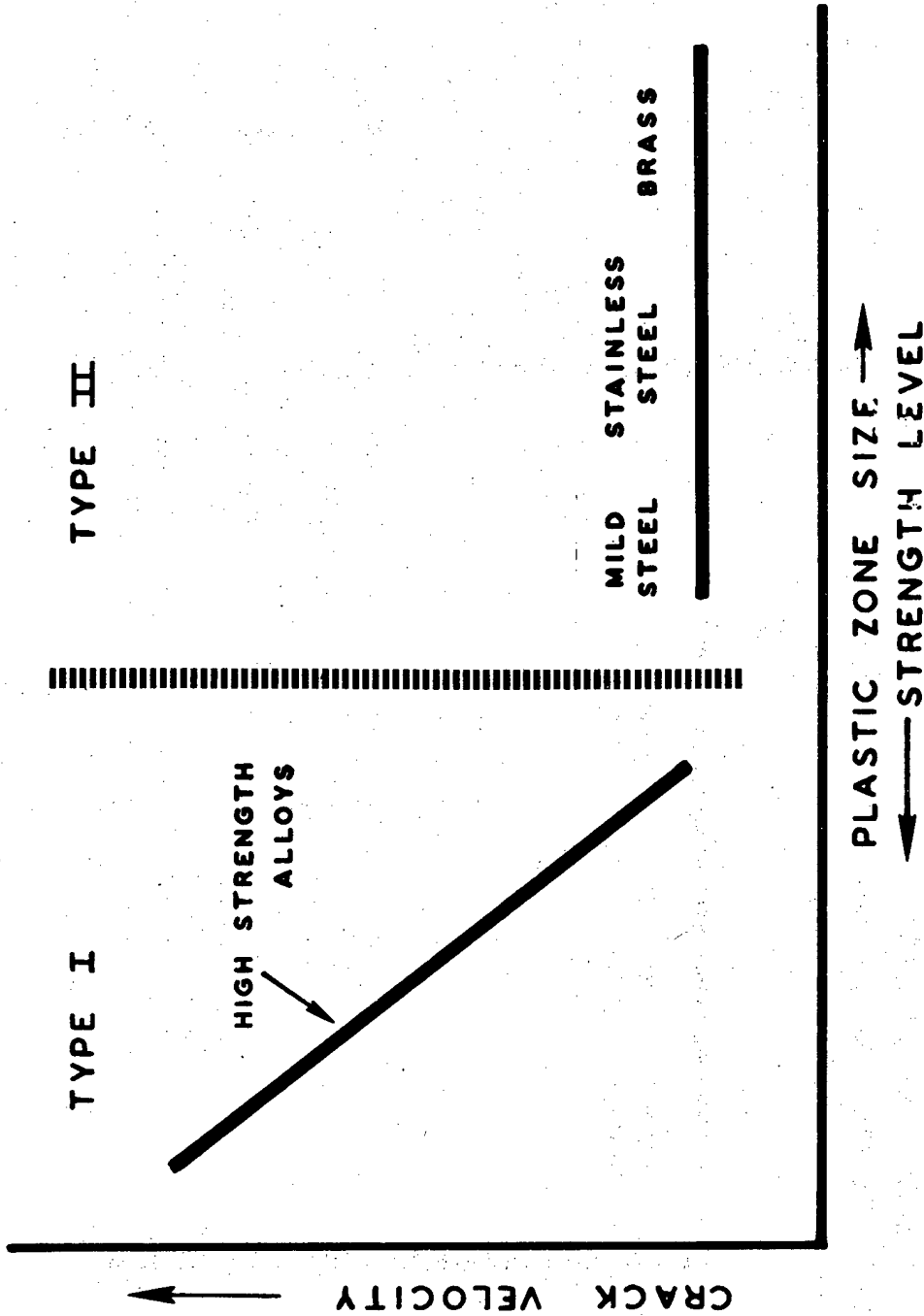
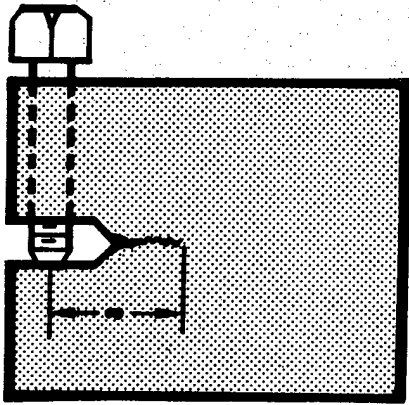
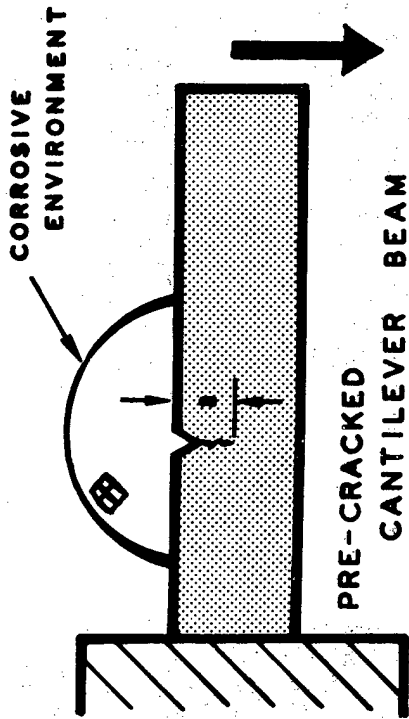


Figure 3. (b) Time to Failure Vs. Polarization Currents



TWO GENERAL CATEGORIES OF STRESS CORROSION

Figure 4. Two Types of Environmental Cracking



STRESS INTENSITY FACTOR FOR PLANE STRAIN K_{Ic}

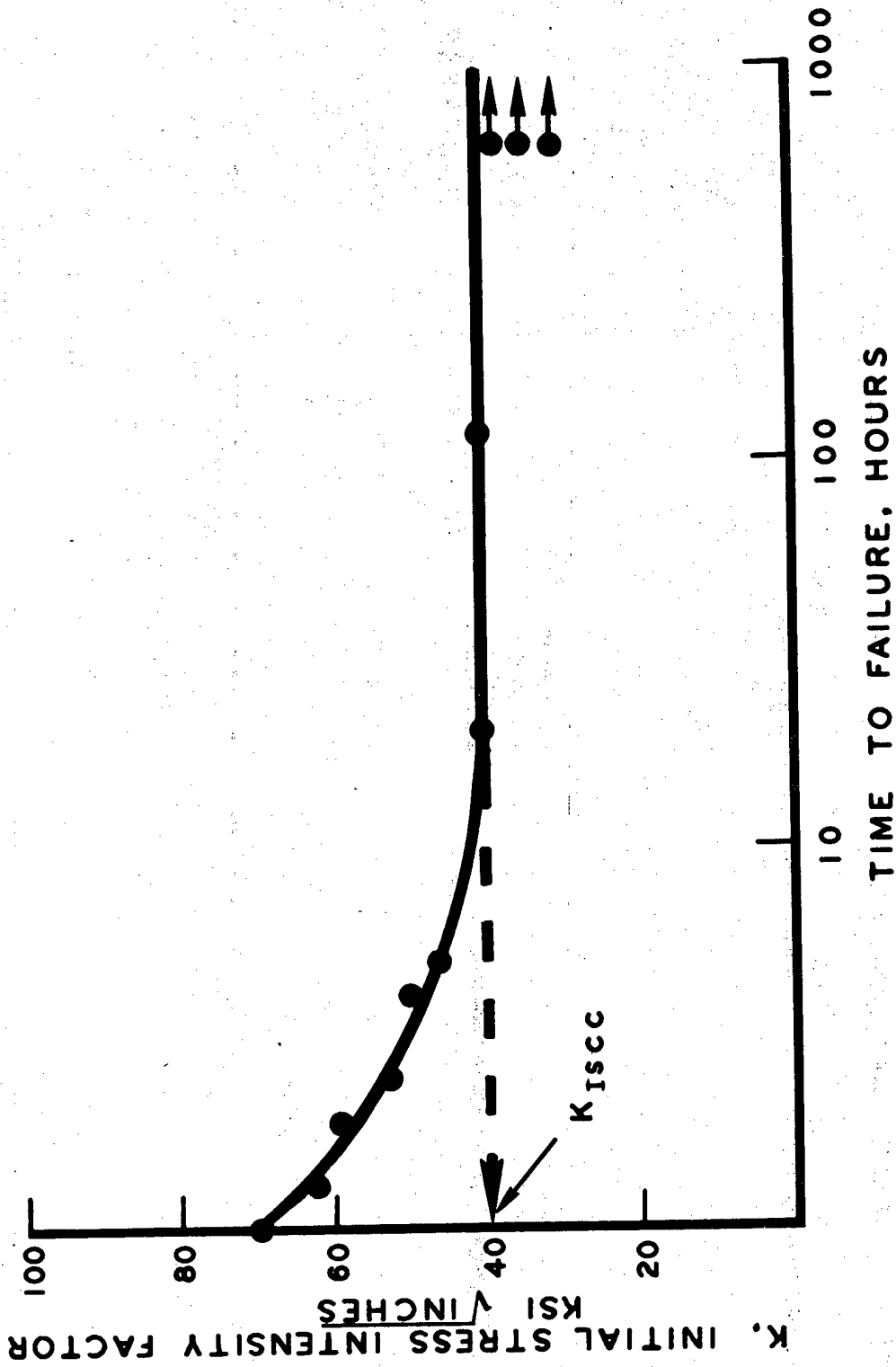
$$K_{Ic} = \sigma \sqrt{\pi a} \text{ WHERE } a = \text{FLAW SIZE, } \sigma = \text{TENSILE STRESS}$$

IN A CORROSIVE ENVIRONMENT, STRESS INTENSITY IS DESIGNATED

$$K_{ISCC}$$

TYPE OF SPECIMEN AND SIMPLIFIED STRESS INTENSITY FACTOR FORMULA

Figure 5. Fracture Mechanics Specimens Used For Stress Corrosion Testing



1354

PRE - CRACKED SPECIMEN STRESS CORROSION DATA

Figure 6. Stress Intensity Vs. Time to Failure Showing a Stress Corrosion Cracking Stress Intensity Limit

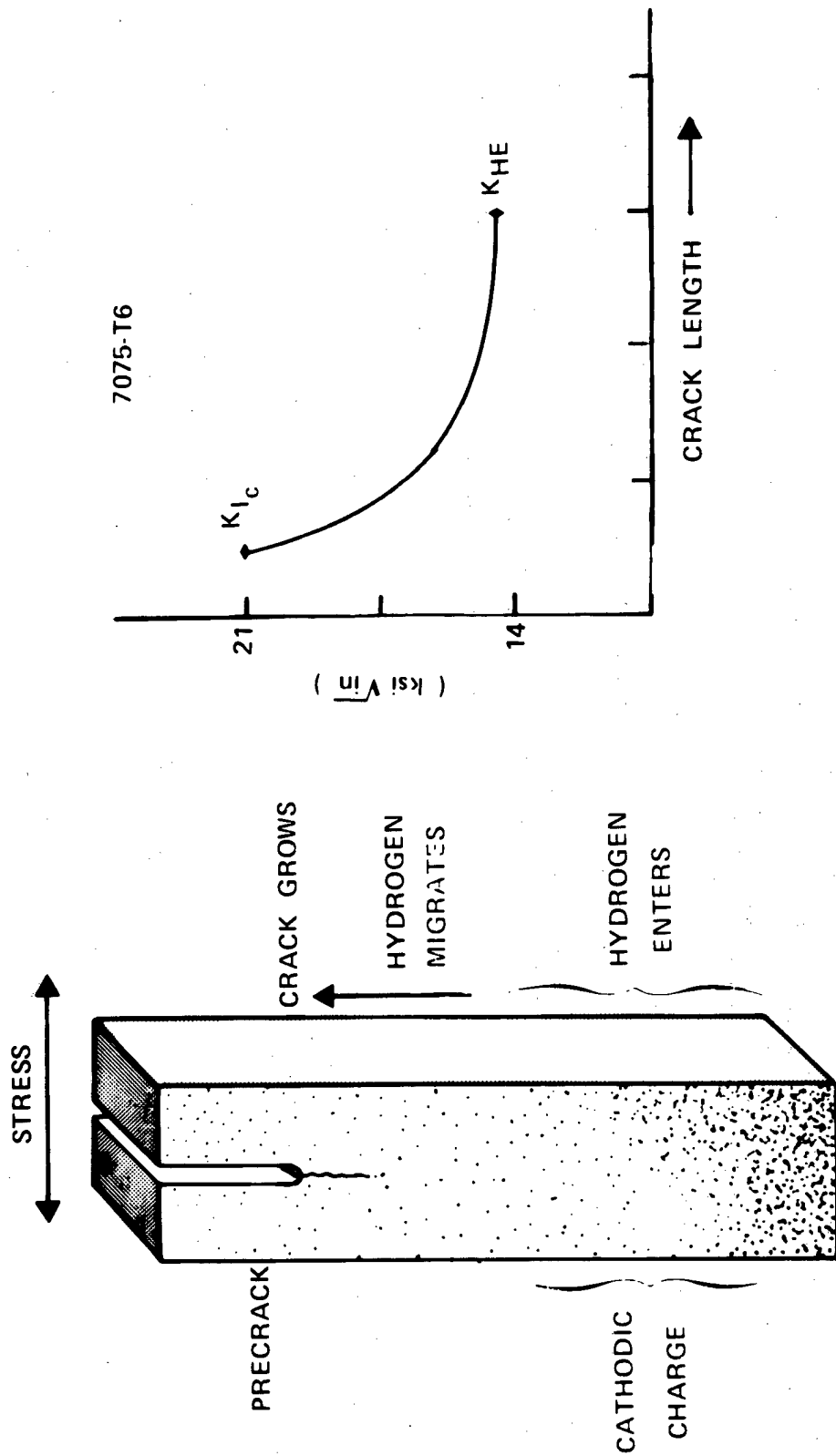


Figure 7 Effect of Hydrogen Charging on Crack Propagation in 7075-T6 Aluminum

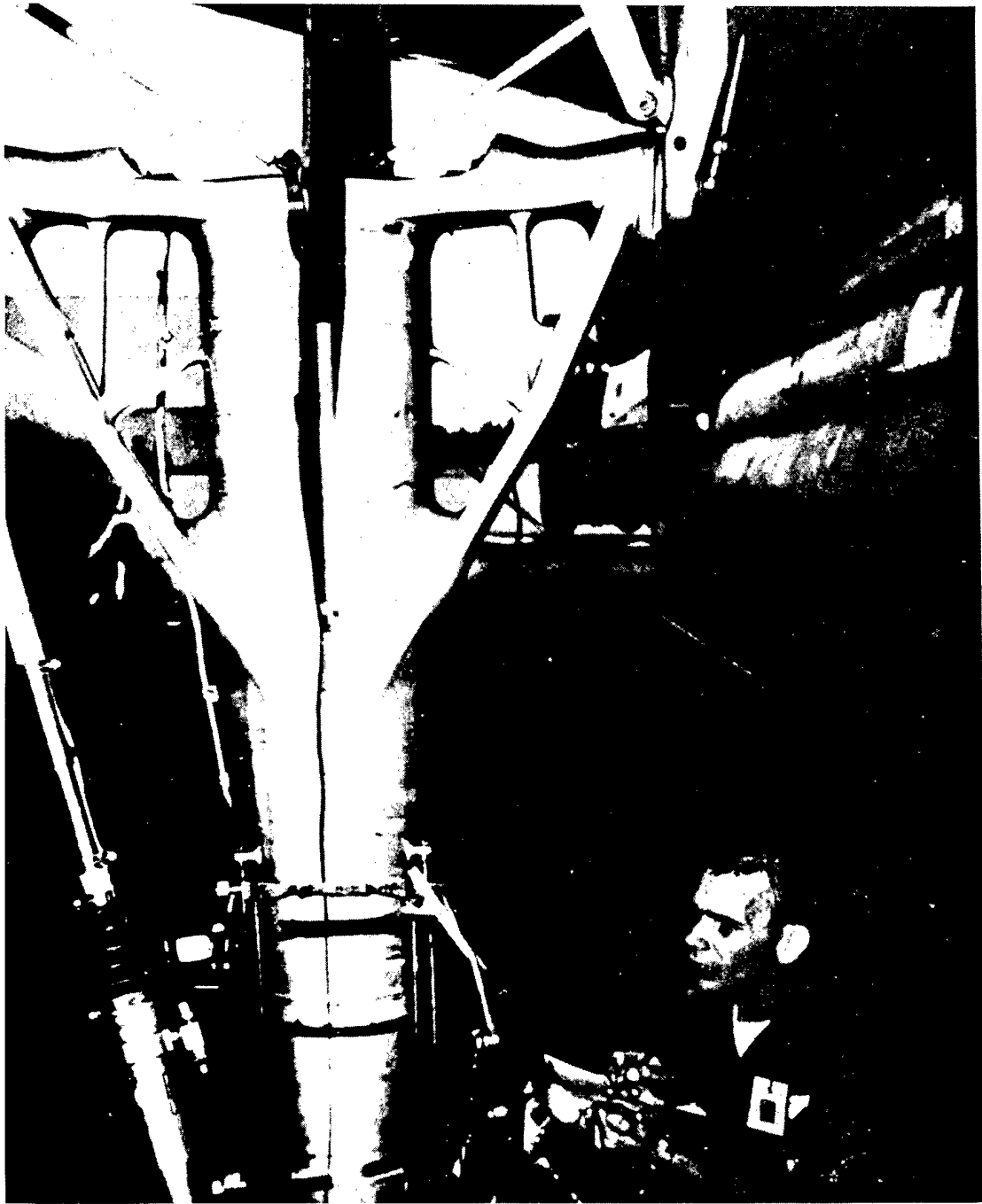


Figure 8. 7079-T6 Aluminum Alloy Landing Gear Failure, U.S. Air Force Aircraft

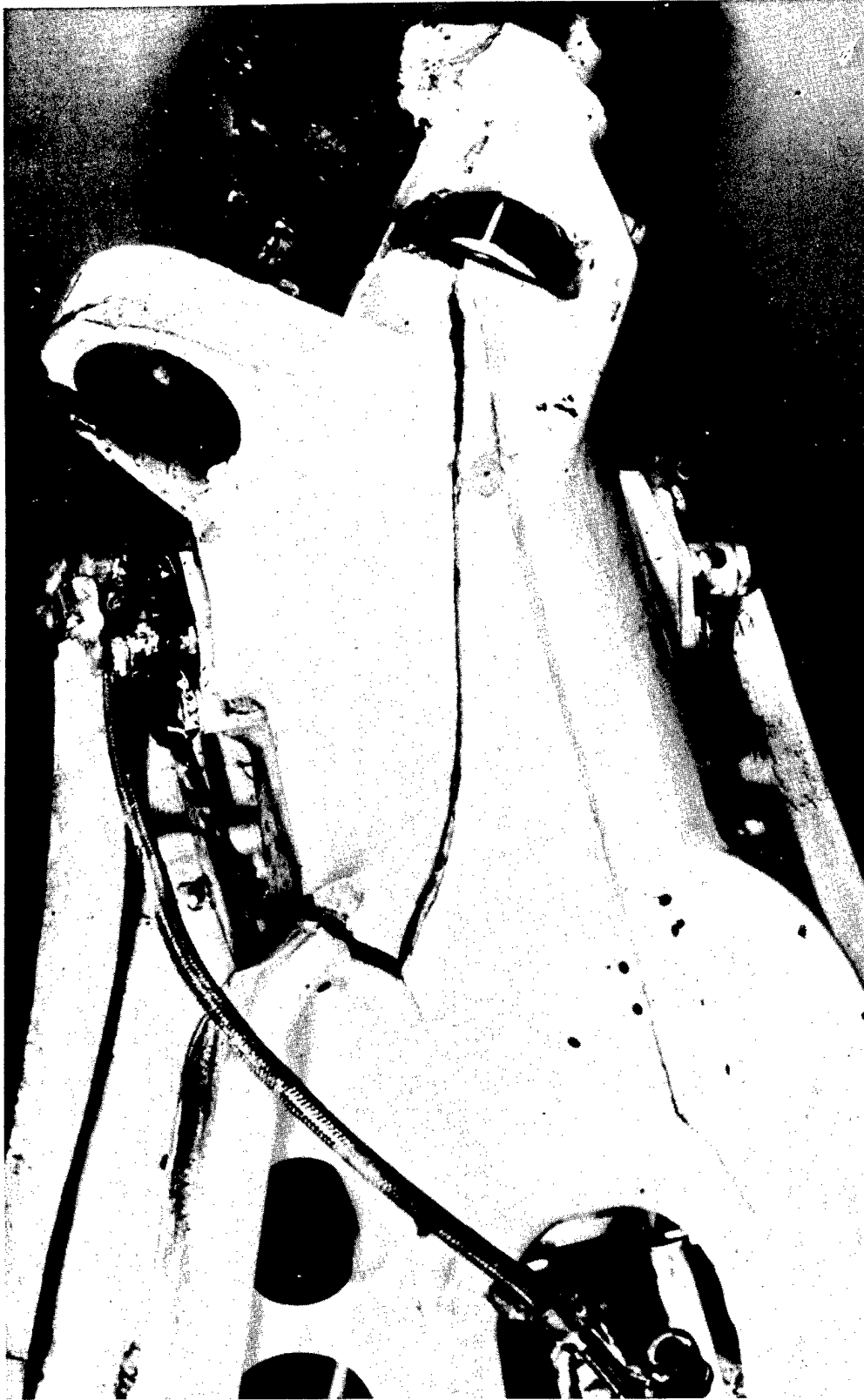
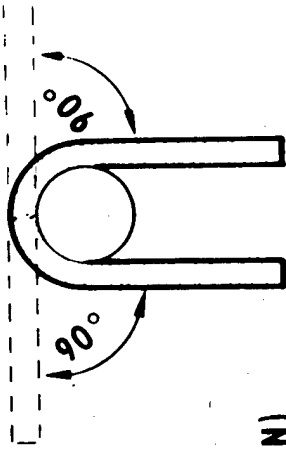


Figure 9. 7079-T6 Aluminum Alloy Landing Gear Failure, U.S. Navy Helicopter

UNCOATED

CATHODICALLY CHARGED

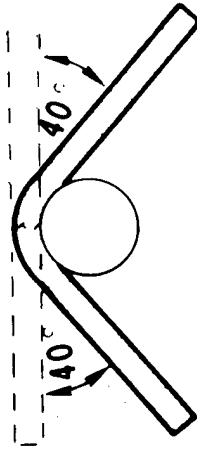
6 mA/cm² for 60 min.
(104 ppm HYDROGEN)



ANGLE AT FRACTURE

COATED
ION BOMBARDMENT
+
Pd COATING

6 mA/cm² for 60 min.
(3100 ppm HYDROGEN)



DUCTILE FRACTURE 5000X



BRITTLE FRACTURE 5000X

Figure 10. Hydrogen Absorption and Embrittlement in Surface Treated and Untreated Beta Titanium β Alloy

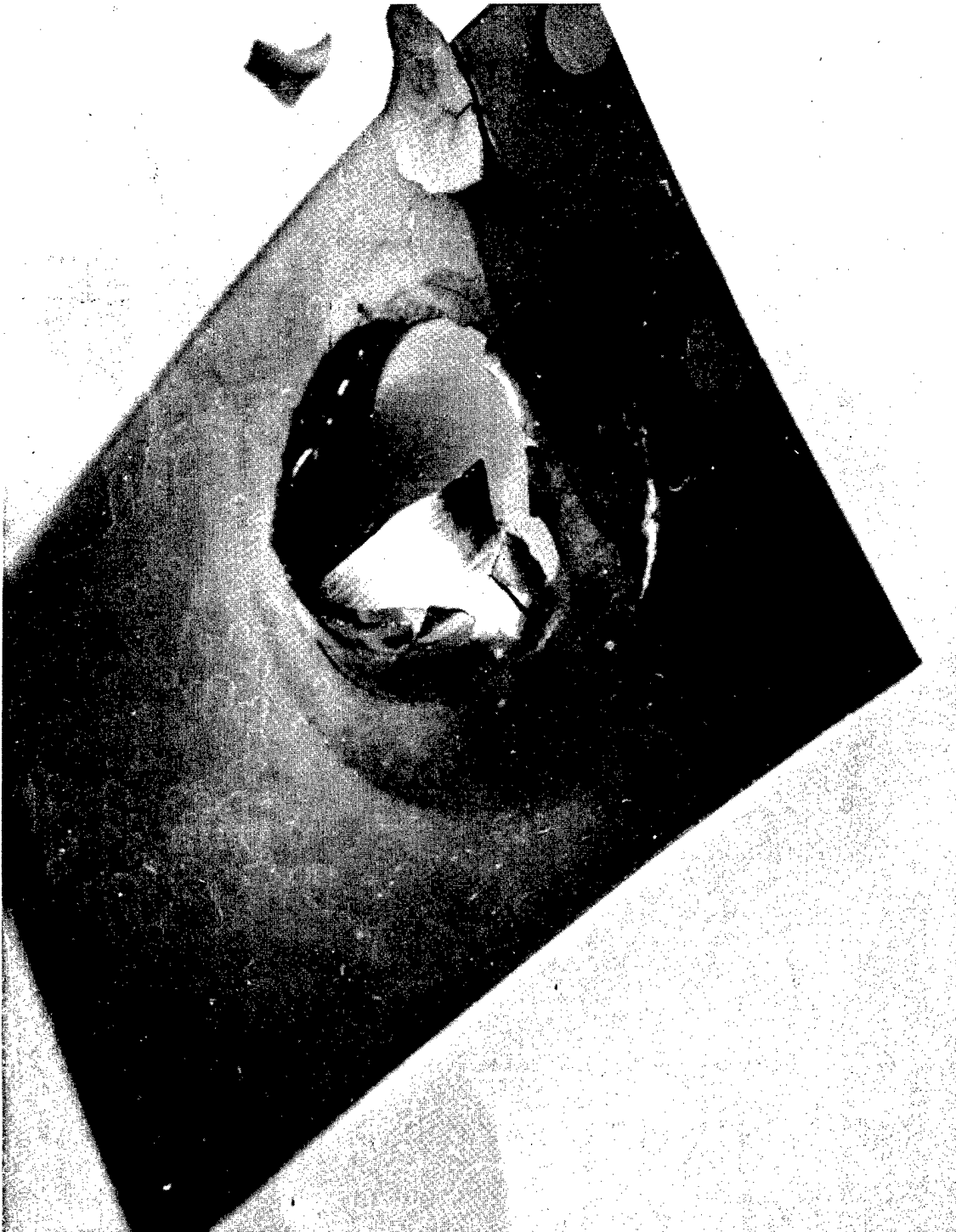


Figure 11. Surface of Beta Titanium Foil After Charging at 8.5 mA/cm^2 for 48 Hours

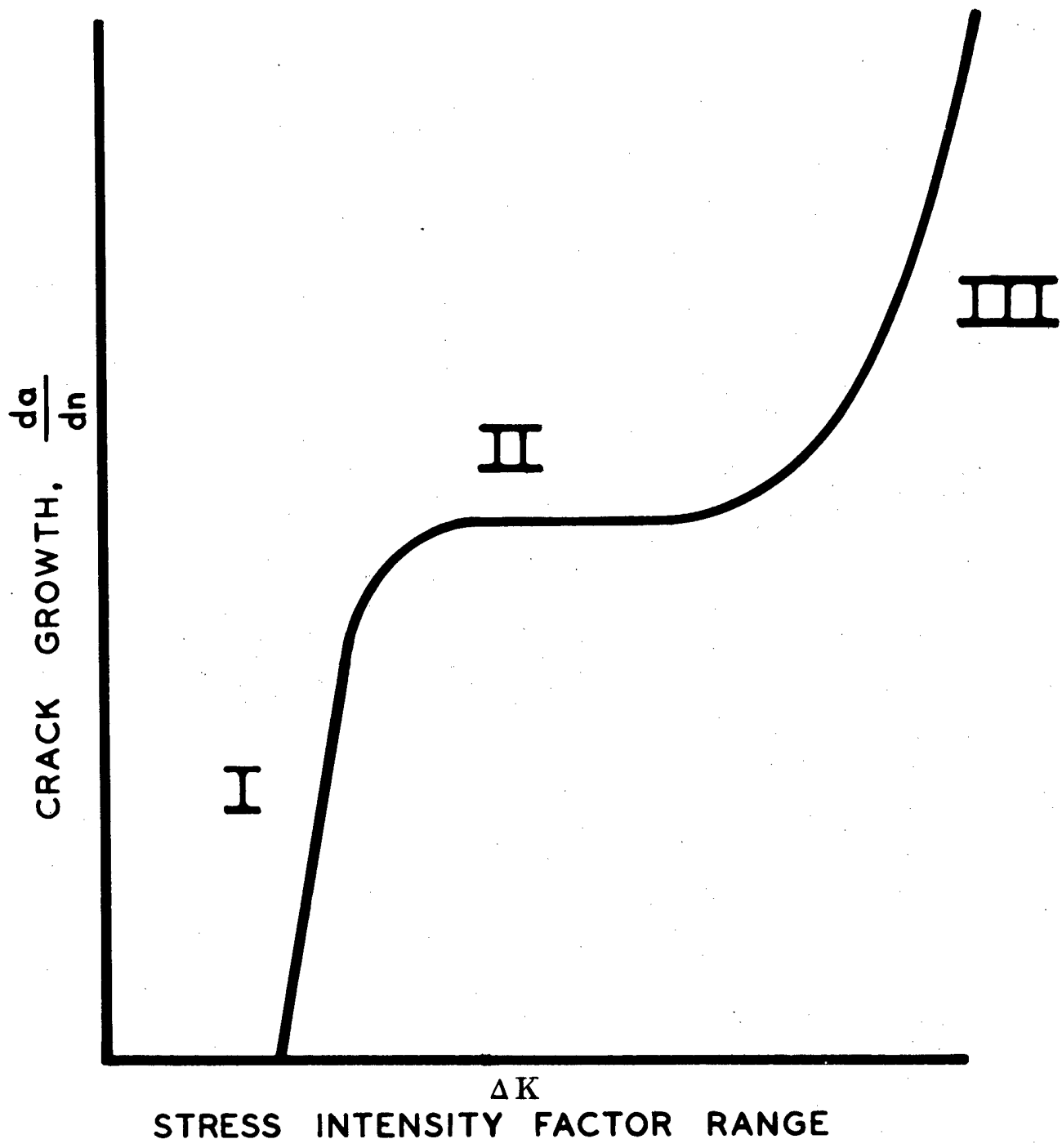


Figure 12. Crack Growth Vs. Stress Intensity, Three Stages

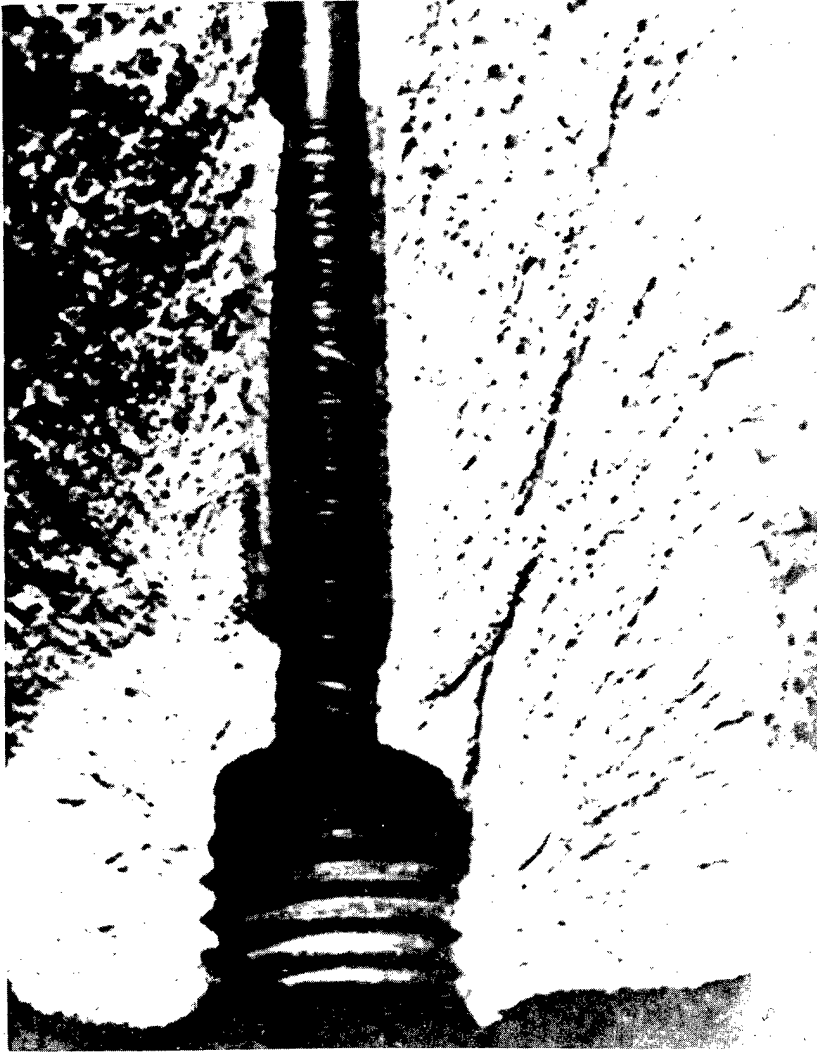


Figure 13. Fracture Surface of A-6 Lube Fitting Socket Lug

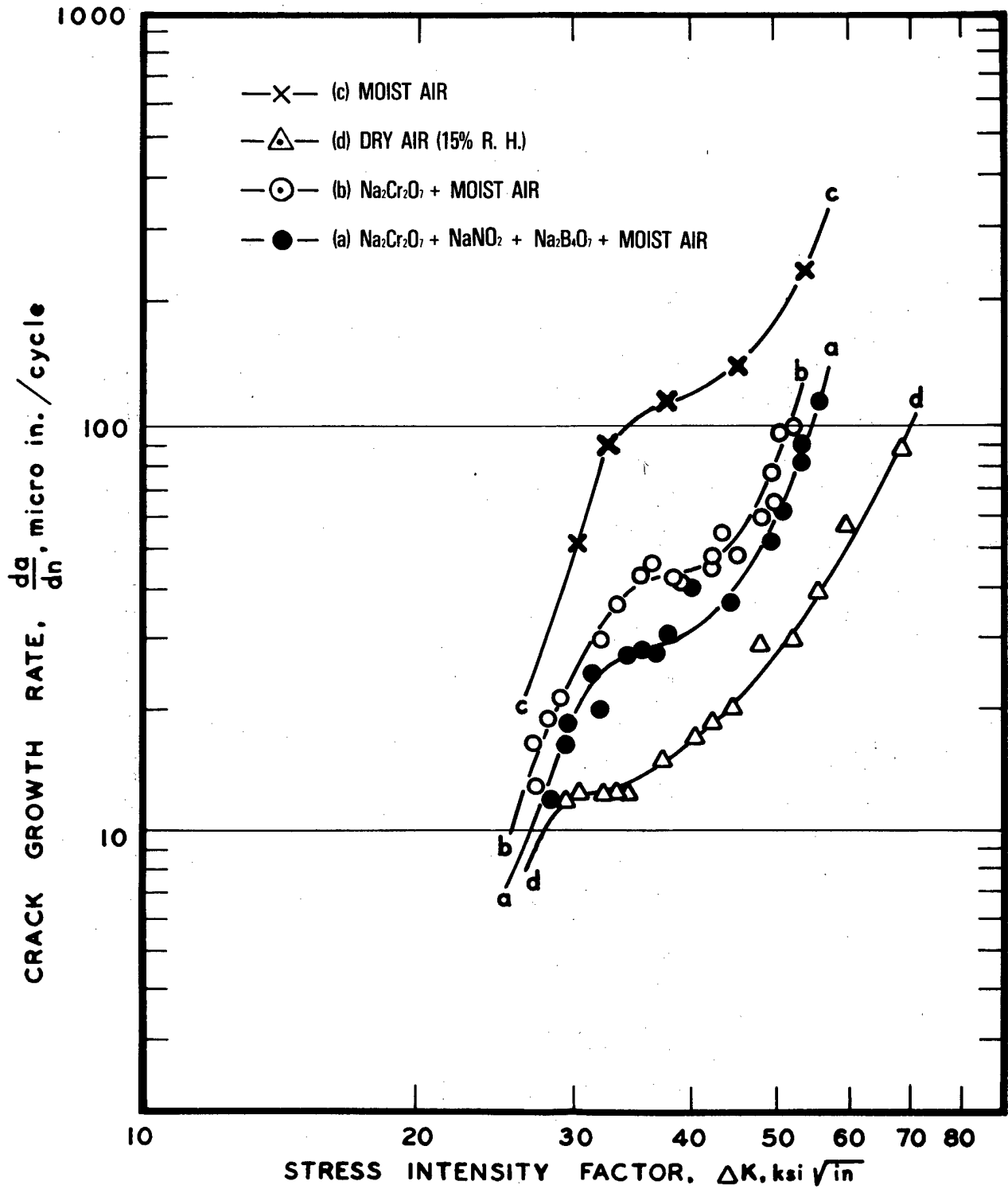


Figure 14. Effects of Crack Arrestment Compounds on Fatigue Crack Growth of AISI 4340 Steel in 90% R.H.

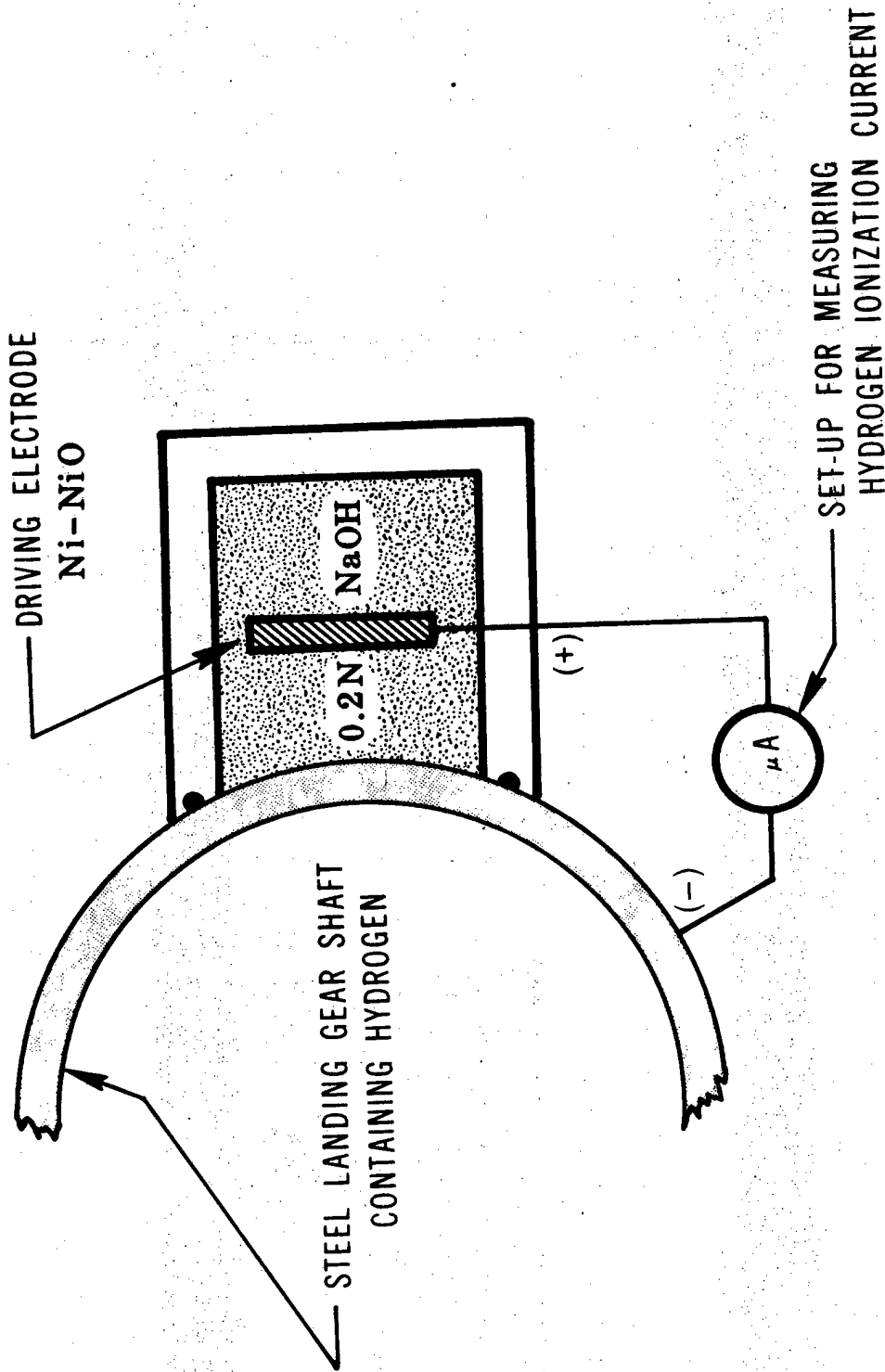


Figure 15. Barnacle Electrode Electrochemical Hydrogen Measuring Circuit

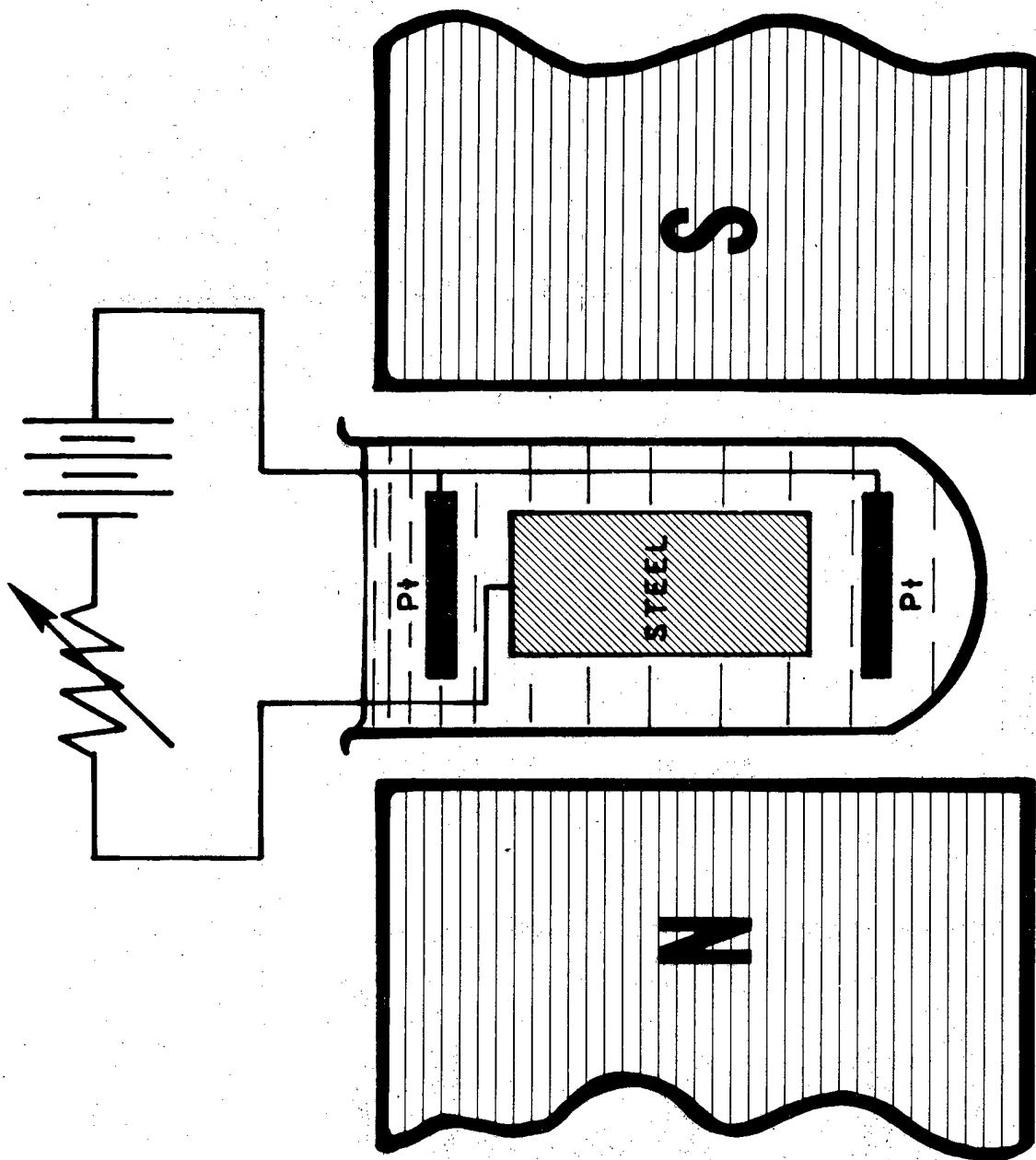


Figure 16. Electrochemical Hydrogen Charging Circuit for Steel in a Magnetic Field

Biographical Sketch

Dr. John J. De Luccia was born in Philadelphia, Pennsylvania in 1935. He received a bachelor of Science degree in Metallurgical Engineering from Drexel University in 1961. He received a Master of Science degree and a Doctor of Philosophy degree in Metallurgy and Materials Science from the University of Pennsylvania in 1967 and 1976, respectively. He joined the Aeronautical Materials Laboratory of the Naval Air Development Center as a research metallurgist in 1963. He is still employed at the laboratory as the Head of the Materials Protection Branch.

Dr. De Luccia has published and presented over twenty-seven technical papers covering the field of materials protection from research on hydrogen embrittlement to fleet corrosion prevention. Dr. De Luccia is a certified corrosion specialist of the National Association of Corrosion Engineers. He holds two U. S. patents. He is presently the North American coordinator of a Corrosion Fatigue Study for the Advisory Group Aerospace Research and Development (AGARD), NATO; and is a member of the United States sub-committee advisory group on aerospace materials for the International Standards organization. He is a member of the American Society for Metals, the National Association of Corrosion Engineers, and the Naval Civilian Administrators Association. In addition, Dr. De Luccia has been appointed Visiting Professor of Materials Engineering at Drexel University for the academic year 1978-79.

IMPROVED HIGH TEMPERATURE CAPABILITY OF
TITANIUM ALLOYS BY ION IMPLANTATION/PLATING

By

Shiro Fujishiro

Air Force Materials Laboratory, AFWAL
Wright-Patterson AFB, Dayton, Ohio 45433

Daniel Eylon

Department of Materials Science and Metallurgical Engineering
University of Cincinnati
Cincinnati, Ohio 45221

Improved High Temperature Capability of Titanium Alloys
by Ion Implantation/Plating

Abstract

In an effort to increase the high temperature capability of $\alpha+\beta$ titanium alloy in jet engine applications, noble metals were ion implanted/plated on several high temperature titanium alloys. The creep strength and the oxidation resistance of the ion plated materials were substantially increased. In addition, unlike other methods of coating, the ion plating caused an increase of the high temperature fatigue strength. Microstructural investigation indicated that an oxygen diffusion barrier is responsible for improving the creep resistance, and the ion implantation surface hardening effect is responsible for the fatigue strength increase. As a result of the increased high temperature performance of the tested alloys, several Pt ion plated titanium alloy components are currently evaluated in the aircraft industry for high temperature applications. Relatively large size components with complex configuration can be effectively coated in this method by using a modification of existing equipment. The present technique has potential for extending the application of Ti alloys to a higher service temperature, as well as to higher stresses at current temperatures, thus improving engine performance. Furthermore, adaptation of the present technique to other metallic systems by proper selection of coating materials and implantation conditions offers excellent opportunities to improve other properties such as corrosion, erosion, and wear and fretting resistance of these materials.

Introduction

Since the mid-1960's, extensive efforts to improve the high temperature capability of Ti alloys for use in gas turbine engines have been undertaken by the aerospace industries and the U. S. Air Force. As a result, a number of high temperature Ti alloys including Ti-6246, Ti-6242, Ti-17, Ti-11, Ti-5522, and Ti-5524 have been developed. Some of these are currently used in gas turbine engines but the service temperatures are limited to approximately 800°F (430°C) for extended service times (500 hours or more). This limitation is due mainly to the inherent vulnerability of Ti to oxidation at this temperature and above.

The properties required to qualify a Ti alloy for high temperature applications include high modulus to density ratio, high tensile and fatigue strengths, creep resistance, and metallurgical and chemical stability at the working temperature and environment. Severe oxidation of Ti alloys causes deterioration of the mechanical properties, such as post-creep ductility and fatigue strength. As a result, a number of research programs have been conducted in an effort to improve the oxidation resistance by means of coatings applied by electrochemical plating or a thermal/plasma spray. These coatings have included such materials as Al, Cr, Ni and their alloys or slurries. The major drawback of such coatings, however, is a severe loss of the high cycle fatigue strength of the Ti alloys (1) (2). Consequently, a Ti alloy component coated with one of these materials cannot be used in fatigue sensitive hot sections of a gas turbine engine.

The present work demonstrates that a very thin layer of ion plated noble metal can protect the alloy from oxidation and, in addition, improves both the high temperature fatigue and creep strengths. Advantages of using ion implantation/plating over conventional coating techniques are two-fold. First, the implanted elements become an integrated part of the substrate alloy over which a coherent plating can subsequently be built up. Secondly, ion bombardment by the coating materials produces compressive stresses at the surface which improves fatigue strength of the substrate.

The use of this coating was first investigated by the authors⁽³⁾ in an effort to increase the high temperature creep resistance of Ti alloys. The lower creep rates which were observed in an argon atmosphere⁽⁴⁾ and in vacuum⁽⁵⁾ led to the investigation of ductile oxidation resistant coatings which were impregnated in the alloy surface.

Ion plating of noble metals was selected for this study because it forms a sound and effective coating without the risks of hydrogen contamination and formation of brittle intermetallic compounds. The negligibly small solubility of platinum in titanium⁽⁶⁾ up to 1100°F (590°C) allows the use of this coating to that temperature.

EXPERIMENTAL PROCEDURES AND RESULTS

Material

Ti-6Al-2Sn-4Zr-2Mo (Ti-6242) alloy bar was solutionized at 1750°F (950°C) and annealed at 1100°F (590°C) for 8 hours. The resulting microstructure (Fig. 1) consisted of 60 volume pct. equiaxed primary alpha grains uniformly distributed in a matrix of transformed beta phase.

Coating

The coating was applied using a 7 kV ion plating apparatus. The bias potential between the specimens and the molten metal source was initially set at 4 kV to obtain a deeper ion implantation and later reduced to 3 kV for effective plating. The ion beam current was a maximum of 90 mA for 5 minutes.* The thickness of the coating was found to be approximately 1 μm.

Oxidation Resistance

In applying the oxidation protective coating to Ti alloys, the thermal stability of the coating/substrate

*The details of the process are described in patent application Serial No. 825,005. The nomenclature "ion plating" used in this paper refers to ion plating preceded by ion implantation.

interface is of prime importance. In the preliminary work involving many coating materials tested in contact with Ti-6242, Au and Pt were found to be stable up to 900°F (480°C) and 1100°F (590°C), respectively, for at least 500 hours with no spalling. When a diffusion barrier such as tungsten was ion plated as a primary, the subsequent Pt coating was sustained intact to temperatures as high as 1300°F (700°C) for 500 hours. Table I summarizes the weight gain due to oxidation of Ti-6242 alloy with various coatings.

Creep Strength

Creep tests of the coated and uncoated material were performed in air on a constant load testing machine. The elongations were continuously monitored by a LVDT transducer. Vacuum creep tests were performed on a servohydraulic testing machine equipped with a strain gage extensometer. Specimens were heated by a radiant heater in vacuum better than 3×10^{-5} torr. All creep tests reported here were conducted at 1050°F (570°C) with an applied stress of 35 KSI (241 MN/m²) on specimens with gage dimensions of 4 mm diameter by 25 mm long. The creep strain vs. time plots of the uncoated and Pt coated material in air and the uncoated material in vacuum are shown in Fig. 2.

Post-Creep Ductility

Post-creep ductility of Ti alloys is a significant selection criterion for high temperature applications. The room temperature tensile properties of coated and uncoated specimens creep exposed at 850°F (450°C) and 35 KSI (241 MN/m²) for 500 hours are compared with those of uncoated unexposed specimens in Table II.

Fatigue

Smooth bar fatigue life tests were conducted on 6 mm diameter by 25 mm gage length specimens at room temperature and 850°F (450°C) using an axial load controlled 6 ton fatigue machine at 2000 cpm and a stress ratio value of $R = +0.1$. In order to reduce the scatter of data due to surface conditions, the gage section was progressively hand polished after machining with 5 micron and 3 micron metallographic diamond paste. The fatigue life

data, demonstrating the effect of Pt coating on the fatigue life, is listed in Table III.

DISCUSSION OF RESULTS

Test Results

The oxidation results in Table I indicate excellent oxidation resistance and high thermal stability of the thin Pt ion plating. The integrity of the coating after 10^7 runout fatigue cycles at 850°F (450°C) and 85 KSI (586 MN/m^2) maximum stress is demonstrated in Fig. 3a. The SEM image of the creep exposed Ti-6242 specimen with Pt coating (Fig. 3b) shows good coherence with no signs of spalling even after 2 pct. strain.

The Pt coating provided an effective barrier for oxygen diffusion and resulted in improved creep strength (Fig. 2). The even higher creep strength in vacuum indicates that oxygen diffusion is one of the controlling factors in the creep behavior of $\alpha+\beta$ titanium alloys. In a previous work⁽³⁾ which examined both Ti-6242 and Ti-11 alloys, the accelerated creep behavior of uncoated specimens tested in air was interpreted on the basis of an oxygen induced phase transformation of the metastable β and the concurrent increase of the mobile dislocation density. In this study, no loss in post-creep ductility was detected in the Pt coated material when compared to uncoated creep specimens in the exposed and unexposed condition (Table II).

It is apparent from Table III that Pt ion plating improved the fatigue endurance limits of the alloy by at least 15 pct. at room temperature and 850°F (450°C). Inferior fatigue properties of the uncoated specimens at elevated temperatures can be explained by two mechanisms; one is the degradation of the surface caused by oxidation and the other is the thermal relief of surface compressive stresses at elevated temperatures. When delamination of the oxide layer of the uncoated material occurs as shown in Fig. 4, the resulting rough surface becomes more susceptible to crack initiation. The ion plating may be causing surface hardening by generating compressive stresses similar to those generated by shot peening. The increased smooth fatigue strength at elevated temperatures is therefore attributed to the oxygen impeding effect of the coat-

ing as well as the surface hardening resulting from Pt ion bombardment.

Potential Applications

So far it was demonstrated that the Pt ion implantation/plating increased the high temperature oxidation resistance and creep and high cycle fatigue strengths of Ti alloys. The coherent surface protection may also be valuable in improving wear fretting fatigue and reducing corrosion related failures. All of these observations suggest the following potential applications of this technology to gas turbine engines containing titanium components operating at elevated temperatures.

1. High temperature Ti alloy compressor blades are creep and fatigue limited in the hot sections of gas turbine engines. They are also subject to erosion, corrosion, stress corrosion cracking, and oxidation under the severe operational environment. Pt ion implantation/plating of these blades has the potential of overcoming these problems. Fig. 5 exhibits the high surface quality of a Pt coated Ti-6246 blade after long term thermal exposure. The weight gain due to oxidation of the coated blade was negligible after 500 hours exposure at 1000°F (540°C), whereas the weight of a comparable uncoated blade increased by several pct. Pratt & Whitney Aircraft/Government Product Division is currently conducting a test program on noble metal ion plated 7th stage compressor blades of F-100 engines.
2. Improvement of fretting fatigue of Ti alloys is another area where ion plating can be applied. It is well known that conventional anti-fretting lubricant deteriorates above 650°F (340°C). Ion plated soft noble metals could be considered as a possible candidate for an anti-fretting dry lubricant at the higher temperatures.

* Under U.S.A.F. Contract F33615-78-C-5179

3. Rockwell International of Columbus, Ohio is currently evaluating the use of Pt ion plated Ti-6242 components in the hot duct section of V/STOL aircraft designated XFV-12A being built under contract to the U. S. Navy. The exhaust gas temperature is expected to reach as high as 1300^oF (700^oC). Preliminary data from a compression creep study on Ti-6242 square tubing indicates that the time for 0.8 pct. creep strain (threshold creep strain) at 1000^oF (540^oC) and 30 KSI (207 MN/m²) increased by more than a factor of three (7). Fig. 6 exhibits a Pt ion plated support bracket which is planned to be incorporated in the duct section of the second prototype for an operational test.

Engineering Feasibility and Economics

The cost of the coating materials for the aforementioned Pratt & Whitney program is nominal. One ounce of Pt can theoretically provide 2250 square inches (1.45m²) of coating 1 μ m thick. In practice, 2 oz. Pt will actually be needed to coat 88 blades of the 7th stage. After coating, however, 1 oz. can be recovered from the chamber. With all costs factored together, the total cost of coating 88 such blades is estimated to not exceed \$850 at the laboratory scale.

A commercial system currently in use for ion plating has the capability to generate a 7 kV bias potential with a maximum current of 100 mA. Such a power source is adequate to uniformly ion plate an area of approximately 500 square inches from a single evaporant source. In order to produce a coating 1 μ m thick, only a few minutes of evaporation time are needed. This rate is much faster than conventional sputtering or vapor deposition processes. Compressor blades mounted on a jig are slowly rotated to obtain a uniform coating. The variation of the coating thickness from the leading edge (approximately 0.1 mm in radius) to the dovetail is typically less than 20 pct.

In the production scale the vacuum chamber size and the power supply capacity are practically unlimited and can be made to accept any geometry and size of components

by designing a suitable jig. Since the process is a non line-of-sight process, complex shape configurations can be uniformly coated. McDonnell Douglas Corporation, under contract to the U. S. Air Force lately constructed a large vacuum chamber 6 feet (2 m) in diameter and 12 feet long (4 m) long for ion vapor deposition of Al on landing gears(8). This system could easily be converted to an ion plating apparatus by equipping it with a higher voltage power supply and a water cooled copper crucible to hold the molten evaporants. Such modification would facilitate ion plating of any size components of existing gas turbine engines.

SUMMARY

The present study demonstrates that Pt ion implantation/plating significantly improves oxidation resistance and creep and fatigue properties of Ti alloys at elevated temperatures. It appears that the engineering application of such a technique to gas turbine engines is not only technically feasible but economically affordable. The authors are strongly convinced that implementing the present approach to any alloy system, e.g. by exploring a high voltage ion implantation for increased fatigue strength and proper selection of implanting and coating materials for improving corrosion, erosion, and wear resistance, would be fruitful in meeting the future material needs and requirements of the U. S. Air Force.

ACKNOWLEDGEMENTS

The authors wish to acknowledge Mr. V. Patel of the Department of Materials Science and Metallurgical Engineering, University of Cincinnati, for performing some of the experimental work, and Mr. B. Strope of Systems Research Laboratory for his help in the SEM study. The helpful discussions of Dr. T. L. Bartel of the Air Force Materials Laboratory are highly appreciated.

REFERENCES

1. M. Levy and J. L. Morrosi, Army Materials and Mechanics Research Center, Technical Report 76-4 (1976).

2. M. T. Groves, NASA Report, CR-134537 (1973).
3. S. Fujishiro and D. Eylon, Scripta Metallurgica, 11, 1011 (1977).
4. G. S. Hall, S. R. Seagle and H. B. Bomberger, AFML-TR-73-37 (1973).
5. S. Fujishiro and D. Eylon, 105th AIME Annual Meeting, Abstract Book, p. A14, Las Vegas, Nevada, February 1976.
6. M. Hansen and K. Anderko, Constitution of Binary Alloys, p. 219, McGraw Hill, N.Y. (1958).
7. R.W. Gehring, Rockwell International, Columbus, Ohio, Private Communication, 1978 August.
8. K. E. Steube, AFML-TR-132.

TABLE I
WEIGHT GAINS OF Ti-6242 ALLOY IN AIR

ION-PLATING MATERIALS	TEMPERATURE (°C)	WEIGHT GAIN (W/A · t (mg/cm ² · hr))
No Coating	590	6.9 x 10 ⁻²
Au	430	2.2 x 10 ⁻⁴
Au	480*	2.6 x 10 ⁻³
Pt	590*	1.2 x 10 ⁻³
W/Pt	650	3.3 x 10 ⁻⁴
W/Pt	700*	1.7 x 10 ⁻³

* Highest temperatures under which no spalling or loss of the coating was detected after 500 hours.

TABLE II

PRE AND POST CREEP TENSILE PROPERTIES OF Ti-6242

CONDITION	YS MN/m ²	UTS MN/m ²	ELONGATION (4D) PCT	RA PCT
Uncoated, prior to creep	1151	1207	8.0	43.5
Pt coated, post creep	1145	1200	8.6	41.5
Uncoated, post creep	1172	1220	8.2	35.8

TABLE III

FATIGUE LIFE OF UNCOATED AND Pt COATED Ti-6242 ALLOY
AT ROOM TEMPERATURE AND 450°C

SPECIMEN NO.	SURFACE CONDITION	MAXIMUM STRESS MN/m ²	NO. OF CYCLES TO FAILURE
<u>Room Temperature</u>			
#4	Uncoated	951	6.3×10^4
#1	Uncoated	703	2.6×10^6
#9	Uncoated	689	Run out
#20	Pt Coated	951	1.9×10^5
#26	Pt Coated	827	1.3×10^7
#21	Pt Coated	800	Run out
<u>450°C</u>			
#39	Uncoated	730	2.9×10^4
#38	Uncoated	703	2.6×10^5
#13	Uncoated	621	6.0×10^5
#3-3	Uncoated	517	Run out
#36	Pt Coated	730	4.0×10^4
#31	Pt Coated	703	3.2×10^6
#30	Pt Coated	621	9.1×10^6
#22	Pt Coated	586	Run out

LIST OF FIGURES

- Figure 1. The microstructure of Ti-6242 alloy used in this study. Heat treatment was 950C for 1 hour and water quenched, followed by 590C for 8 hours and air cooled.
- Figure 2. Creep behavior of Ti-6242 in air and vacuum, and in air with Pt plating.
- Figure 3a. The SEM of Pt coating of Ti-6242 after 10^7 runout fatigue cycles at 450C and 586 MN/m² maximum stress.
- Figure 3b. The cross-section of Pt coated Ti-6242 creep specimen, subjected to 2 pct creep strain at 570C showing sound coherency of Pt coat to the substrate.
- Figure 4. The SEM of uncoated Ti-6242, fatigue tested at 450C, indicating a delamination and cracking of oxide layers prior to fatigue failure.
- Figure 5a. Uncoated Ti-6246 alloy compressor blade after oxidation test at 540C for 500 hours.
- Figure 5b. Pt coated Ti-6246 alloy compressor blade after oxidation test at 540C for 500 hours. The blade retained its original metallic luster after the test.
- Figure 6. Pt ion plated Ti-6242 duct bracket for XFV/12A V/STOL aircraft.

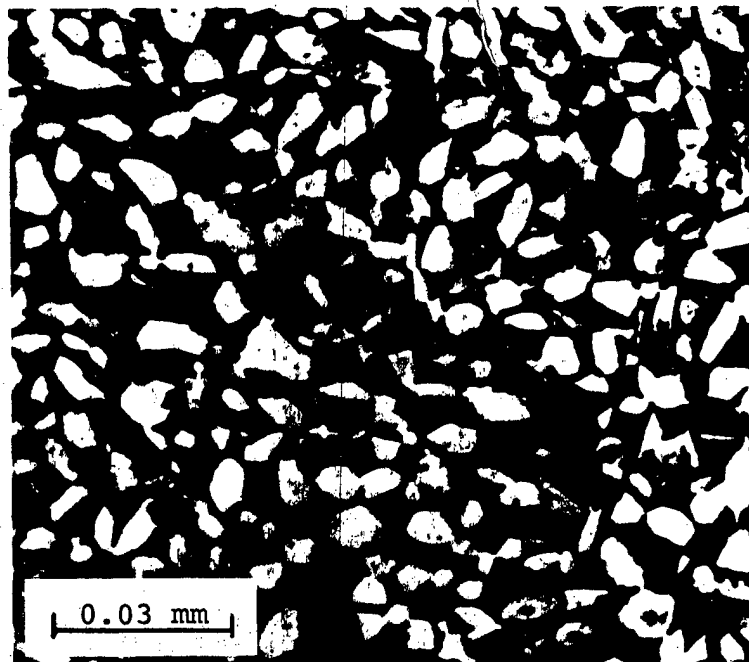


FIGURE 1

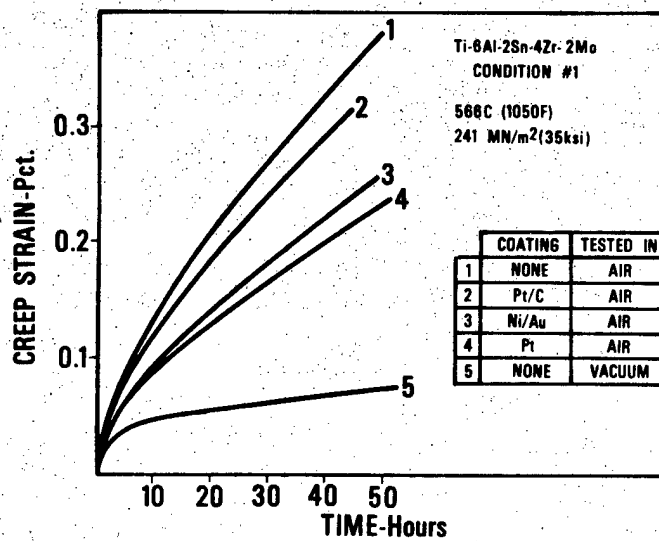


FIGURE 2

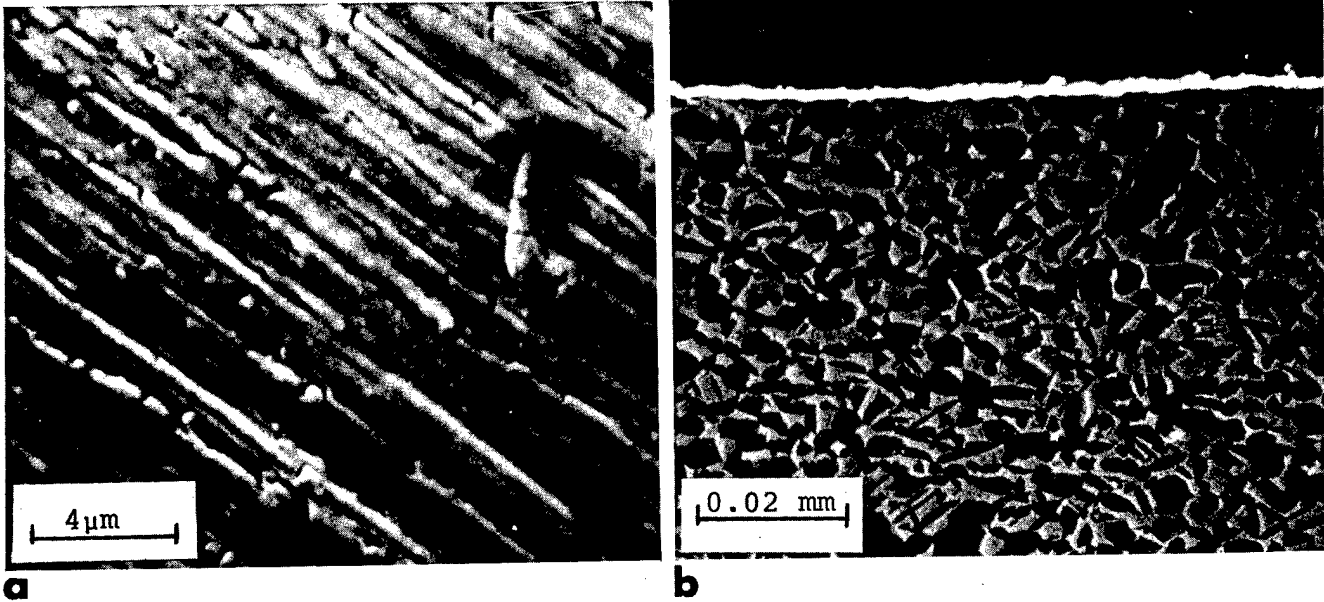


FIGURE 3



FIGURE 4

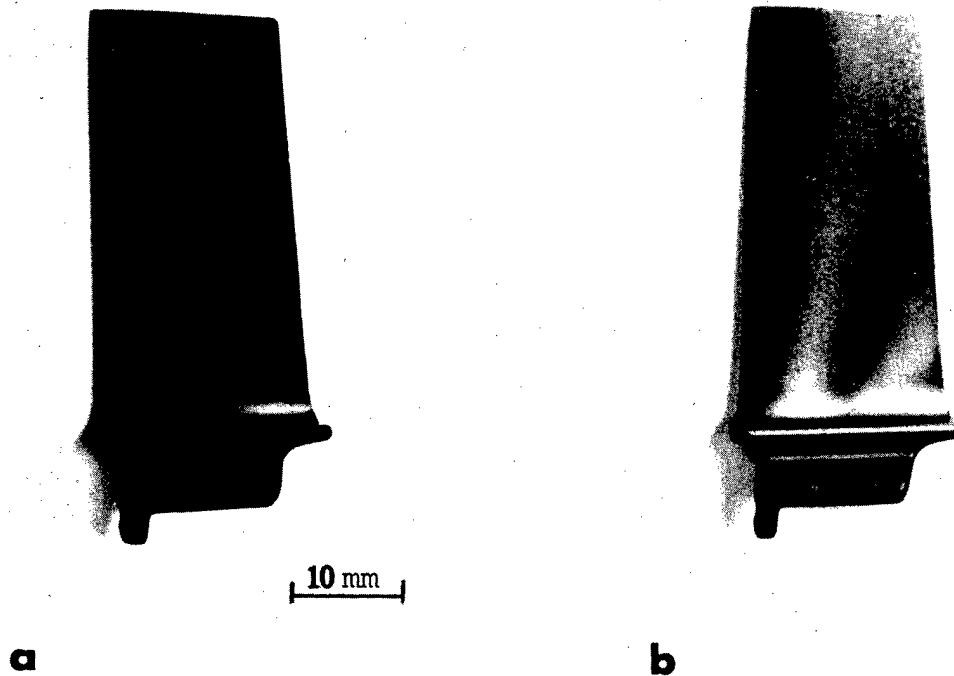


FIGURE 5

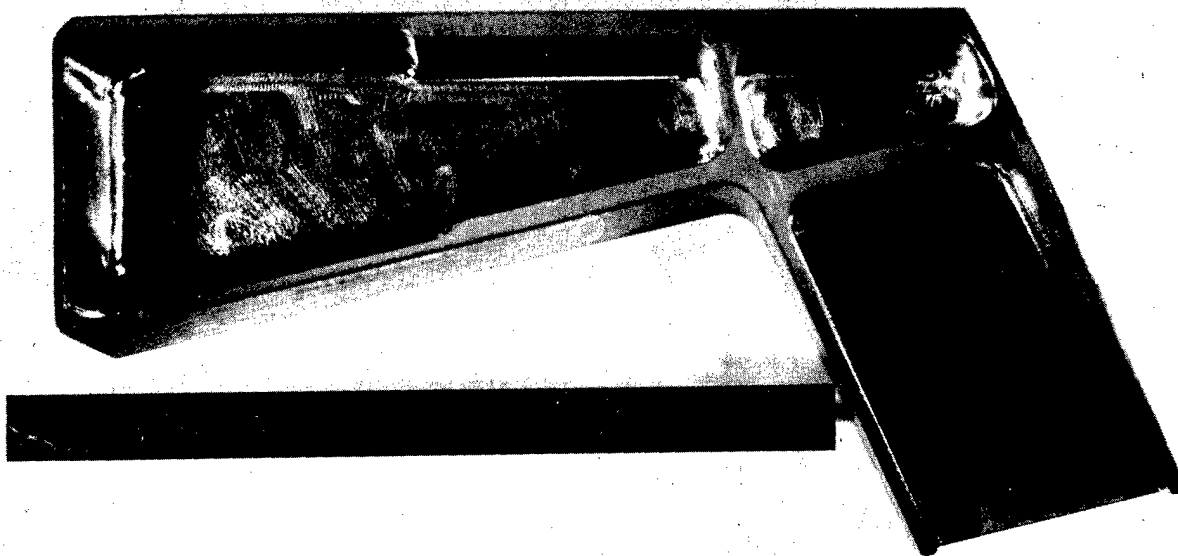


FIGURE 6

Biographical Sketch

Dr. Shiro Fjuishiro was born October 18, 1930 in Kakogawa, Japan. Naturalized citizen in 1972. He received his B.S. in Chemistry in 1953. Dr. Fujishiro conducted his graduate work at the University of Pennsylvania and Kyoto University, and he received his Ph.D in Physical Chemistry from Kyoto University in 1962. While working on his graduate degree from 1957-1960, he worked as a research assistant on an AEC (now DOE) program at the University of Pennsylvania. From 1968-1969 he served at the University of Cambridge, England as a visiting scholar.

Dr. Fujishiro was employed by Nippon Iron & Steel Company (then Fjui Iron & Steel) in Japan as a group leader for developing silicon steel plant from 1960-1963. He has been employed by the Metals and Ceramics Division since 1963, where he now serves as a metallurgist in Ti alloys development.

Dr. Daniel Eylon received his B.Sc. in 1966, his M.Sc. in 1968, and his D.Sc. in 1972 from the Technion, Israel Institute of Technology, Haifa, Israel. He was associated with the Air Force Materials Laboratory at WPAFB through a National Academy of Science research associateship (1972-1974). Since 1974, he is a Senior Research Associate at the University of Cincinnati working mainly on titanium alloys for high temperature applications at the Air Force Materials Laboratory under research Contract F33615-76-C-5227.

Measurement of the Physical Properties and
Recombination Process in Bulk Silicon Materials

BY

THOMAS C. CHANDLER, 1Lt. USAF

ELECTROMAGNETIC MATERIALS DIVISION

AIR FORCE MATERIALS LABORATORY
WRIGHT-PATTERSON AFB, OHIO

1384

MEASUREMENTS OF THE PHYSICAL PROPERTIES AND RE-
COMBINATION PROCESS IN BULK SILICON MATERIALS

ABSTRACT

Recent advances in the growth and processing of silicon materials have provided physicists with the opportunity to study materials which are of remarkably high quality. Dislocation free, ultra-pure crystals are now available which exhibit a residual Boron content of 1×10^{12} atoms/cm³, and long minority carrier lifetimes. Silicon crystals doped with gallium or indium are also available which display similar characteristics. Such crystals approach the theoretical limits of perfection and thus are useful in this research effort to quantify basic silicon parameters such as lifetime, resistivity, trapping and recombination rates. A thorough understanding of these basic parameters is vital to the development of a silicon based low cost, modular forward looking infrared (FLIR) system which can be adapted to high performance airborne reconnaissance systems, to Remotely Piloted Vehicles (RPV), and expendable type missile seeker systems such as Maverick. In addition the advanced technology supported by this basic research will be readily transferable to the low background case for satellite systems, where focal plane arrays consisting of a multitude of silicon detectors require the ultimate in packaging techniques and connector technology. These conditions make an integrated monolithic detector module an absolute necessity to reduce size, weight, power, and cost.

INTRODUCTION

Recent advances in the growth and processing of silicon materials have provided physicists with the opportunity to study materials which are of remarkably high quality. Dislocation free, ultra-pure crystals are now available which exhibit a residual Boron content of 1×10^{12} atoms/cm³, and long minority carrier lifetimes. Silicon crystals doped with gallium or indium are also available which display similar characteristics. Such crystals approach the theoretical limits of perfection and thus are useful in the AFML research effort to quantify basic silicon parameters such as lifetime, resistivity, trapping and recombination rates. A thorough understanding of these basic parameters is vital to the development of a silicon based low cost, modular forwarding looking infrared (FLIR) system which can be adapted to high performance airborne reconnaissance systems, to Remotely Piloted (RPV), and expendable type missile seeker systems such as Maverick. In addition the advanced technology supported by this basic research will be readily transferable to the low background case for satellite systems, where focal plane arrays consisting of a multitude of silicon detectors require the ultimate in packaging techniques and connector technology. These conditions make an integrated monolithic detector module an absolute necessity to reduce size, weight, power, and cost.

As one might expect, the silicon material evaluations undertaken at AFML serve to reduce the cost factor by allowing one to categorize silicon crystals as to their overall quality. Thus it is less likely that flawed or seriously damaged crystal would be used during monolithic focal plane array (MFPFA) fabrication.

This point is better illustrated by the process flow chart of Figure I. Notice that to date the bulk of the cost for fabricating an MFPFA is the growth and processing of the silicon wafers. Each wafer weighs roughly one (1) gram and the cost can range from thirty to fifty dollars per wafer. This initial material cost is misleading. Failure rates in some experimental monolithic focal plane arrays have been as high as ninety percent, and most of these failures can be attributed to materials problems, such as low lifetimes, dislocations or oxygen vacancy clusters. It is obvious that a screening technique is needed; one that would allow a silicon crystal to be evaluated prior to purchase and processing. In this study such a screening system was evaluated

utilizing the high quality silicon available to AFML through research contracts.

The main problem in the development of a practical screening process is that most tests are destructive, requiring consumption of large quantities of the crystal in the characterization process. There exist techniques (1,2) which would allow adequate nondestructive testing, such as spectral photoconductivity, and photo luminescence, but at their current stage of evolution these techniques require small samples and can easily contaminate the sample with unwanted impurities. (A single fingerprint or accumulation of heavy metallic ions can ruin the entire slice). What is needed is a system which allows the evaluation of the entire boule, without the aid of ohmic contacts, while the crystal is still within its protective polyethylene covering. The boule cannot be touched directly, exposed to laboratory ambient atmosphere, or subjected to high energy radiation.

PHOTOCONDUCTIVE DECAY SYSTEM (PCD)

The basic principle employed is essentially that suggested by Wolfgang Keller (3) for the evaluation of minority carrier lifetime. Figure II is a schematic representation of the instrument in its simplest configuration. The rings around the specimen are capacitively coupled to the boule, but not to each other, the result is that a radio frequency signal is transmitted through the boule with very little attenuation. The light source, either a Xenon lamp or Gallium Arsenide Laser, is used to stimulate excess charge carriers within the bulk of the crystal. The photoresponse of the silicon actually amplitude modulates the RF carrier in much the same way as a common AM radio system. Ultimately, the photoresponse information is extracted and recorded accurately with the aid of a signal averaging instrument such as a box car integrator.

It was found that when the gallium arsenide laser was utilized as a light source the very narrow light pulse (80ns or less) was an excellent approximation to an impulse function, δ . Further it was found that high quality silicon responds to such optical impulses in a fashion similar to a linear system. More precisely if an excitation δ_1 is characterized by a photoresponse $\epsilon_1(t)$ and an excitation δ_2 is characterized by a photoresponse $\epsilon_2(t)$ then the excitation $\delta_1 + \delta_2$ is characterized by the response $(\epsilon_1 + \epsilon_2)(t)$. This condition of linearity is valid for the photo excitation of sil-

icon up to the point where the carrier generation rate is approximately equal to the number of recombination centers available, hence silicon can be modeled as a casual, linear, fixed system as long as high level carrier generation is avoided. The advantage of this type of approximation is that the theory of linear systems is sufficiently developed (4) to resolve ϵ versus t curve into components which theoretically characterize the various modes of recombination inherent to the silicon system. The experimentalist utilizing such a system to analyze such factors as lifetime versus generation rate, trapping time, and dominant recombination modes gains a better view of the relative perfection of the crystal and its potential as a detector substrate.

A less obvious advantage of utilizing a photoconductive system in conjunction with linear analysis is that quite simple models can be derived for the behavior of the bulk material. These models, containing passive circuit elements can be utilized in the calculation of basic parameters such as resistivity, permeability, and permittivity. (It is also possible to perform the inverse, i.e. calculate the photoresponse of a given material knowing its bulk constants such as resistivity.) A simple model is shown in Figure III. Notice that in this model the geometry of the sample must be accounted for to obtain accurate values.

The effectiveness of this screening approach and the associated models and theory were tested by analyzing crystals which had been previously characterized by the manufacturer. Table I is a compilation of data taken for ultra-pure silicon crystals. As was hoped for, the agreement between the AFML values and the manufacturer's data is quite close. The manufacturers measured ρ by the well known four point probe method and the lifetime, τ , was determined by a contacting photoconduction system. Data other than ρ and τ can be derived from Table I. Obviously, samples 1 through 7 are of excellent quality and can be used in most appropriate detector application but crystals 8 and 9 are not. For sample number 8 the range of τ values was found to vary along the length of the boule making it difficult, if not impossible, to fabricate detectors reproducibly from the boule. Crystal number 9 has a low lifetime and high trap density. Trap densities this high indicate a high dislocation density (subsequent etchings confirmed this conclusion).

Figure IV illustrates an atypical photoresponse curve and demonstrates the value of the PCD based analysis. This

crystal has a small diameter, high resistivity but apparently a very low lifetime (its cost ~\$5000). This fact is disappointing not only because of cost factors but because a high resistivity should yield a high lifetime. With the aid of the PCD system the discrepancy is explained. Notice that in Figure IV the plateau region, A. At this point, the GaAs laser has been turned off for approximately 10 microseconds but the conductivity of the boule remains high. The plateau is evident for 100 microseconds after the light source is off and the curve then decays very rapidly. This curve reveals that the crystal does not have a short bulk lifetime but on the contrary the lifetime of a carrier is so long that most electrons have time to diffuse to the surface (about 100 microseconds transit time) and recombined by the surface recombination mode. In short the crystal of Figure IV is detector grade material but this fact is only obvious when the PCD technique is applied.

CONCLUSION

To conclude this discussion, consider the advantages illustrated by this study. The PCD based screening concept allows the measurement of basic silicon parameters without the benefit of electrical connections thus avoiding contamination. Boules can be evaluated by this technique while still within their protective coverings. The true significance is better understood if one considers the cost factors. For the space surveillance application an array may have 10,000 MFPA's and each MFPA may have 10,000 elements all of which must be identical. If the cost per element could be reduced to one cent, the cost to build such an array would still exceed one million dollars. This total cost may not be an unreasonable value for space applications but consider the total that might arise if only ten percent of the elements were functional as a result of poor starting materials or mishandling of those materials. This problem could raise the cost to ten million dollars. It should be obvious that screening and all forms of process optimization are essential in making the MFPA concept an affordable reality. Fabrication yields must exceed ninety percent and this yield cannot be achieved with a sound method for pre-process evaluation.

REFERENCES

- (1) Soref, R. A., JAP 35, 5201 (1967).

- (2) Dean, P. J., Luminescence In Inorganic Solids, Paul Goldberg, Ed., Academic Press, New York 1966.
- (3) Keller, W., Zeirchrift fur Angewandte Physik, 351, (1959).
- (4) Ziemer, R.E., Tranter, W. H., Principles of Communications, Houghton Mifflin Company, Boston, 1976.

TABLE I ρ AND τ DATA AVERAGED

SAMPLE	ρ (MANUFACT) K Ω -CM	ρ (AFML) K Ω -CM	τ (MANUFACT) μ SEC	τ (AFML) μ SEC
1	12	11.8	1400	1350
2	.6	.5	980	950
3	10	10.0	460	460
4	3	2.6	1060	990
5	14	14.3	1230	1240
6	5	4.7	1960	1780
7	5.5	5.0	500	400
8	3.5-7.0	5.0	300-700	300 400 550
9	DOPED, MANY TRAPS		43	43

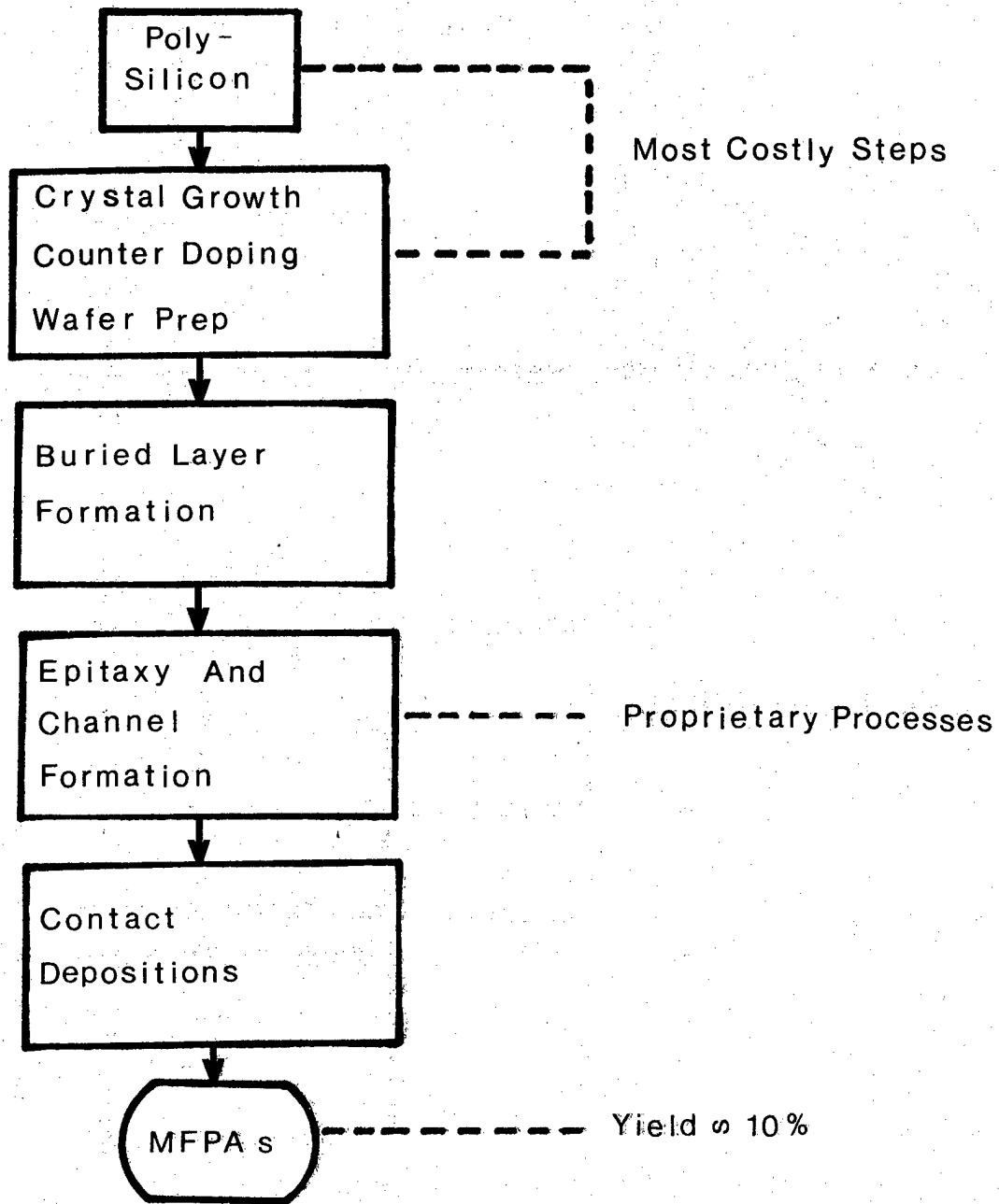


FIG. 1 MFPAs Process Flow Chart

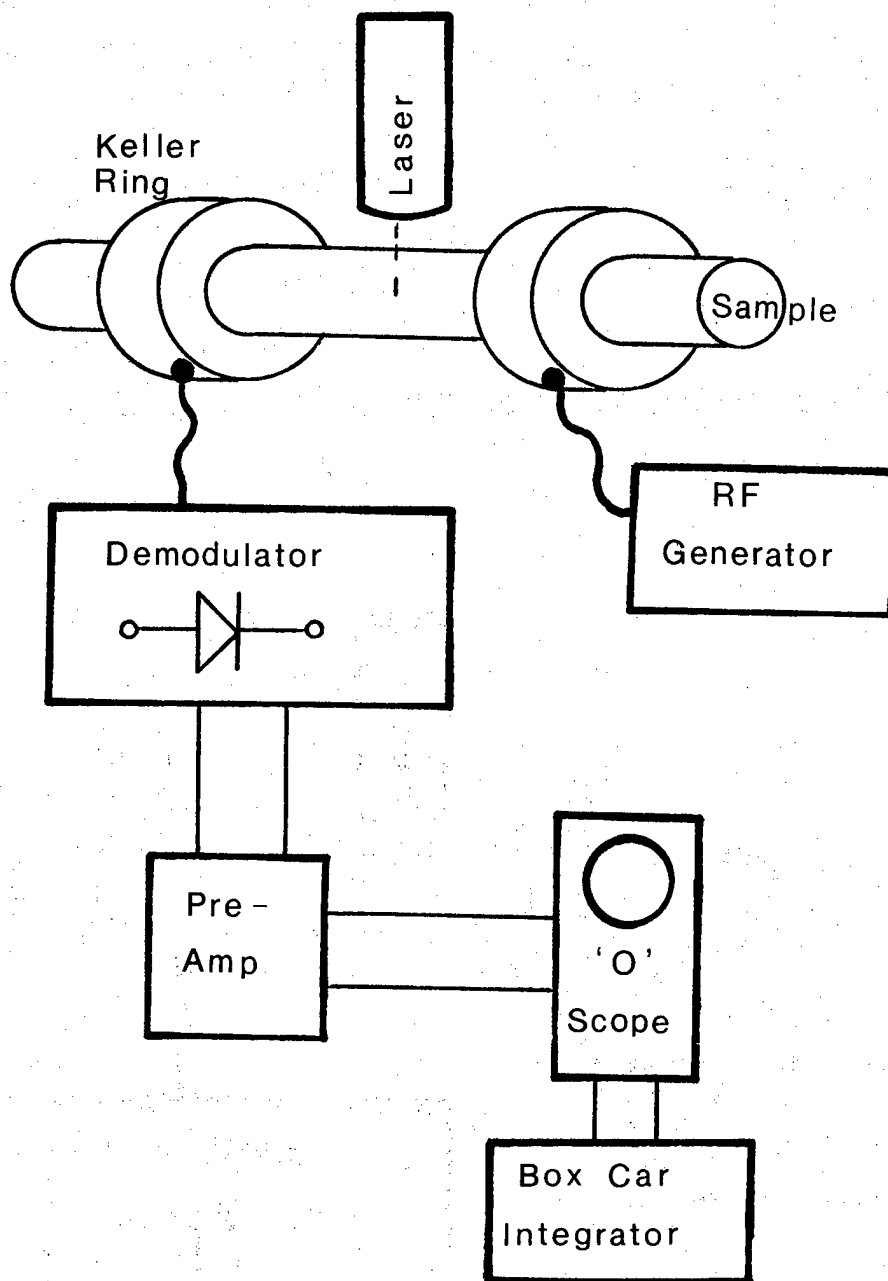
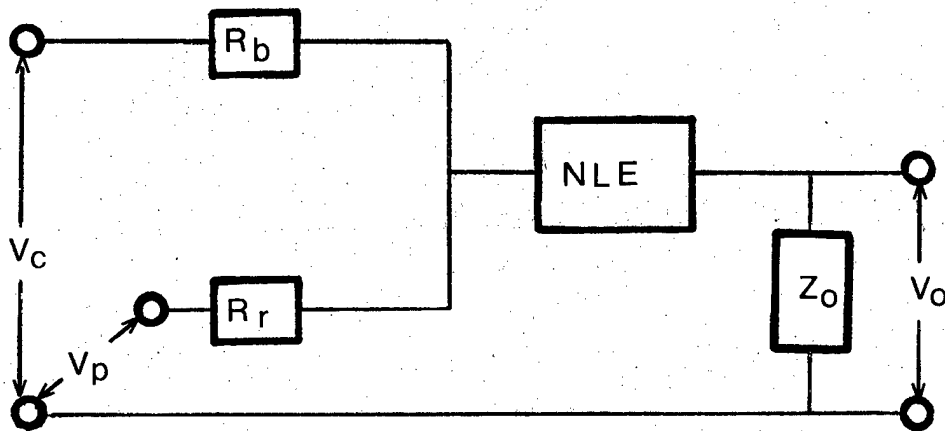


FIG. II Schematic Of A PCD System



V_c Carrier Signal

V_p Pulse Signal

V_0 Combined Output

$R_b = \Delta \rho$ Bulk Resistance, Δ Geometric Factor,
 ρ Resistivity

R_r Dynamic Resistance

NLE Nonlinear Element

Z_0 Complex Impedance

FIG. III Simple Model For Optically Pulsed Silicon

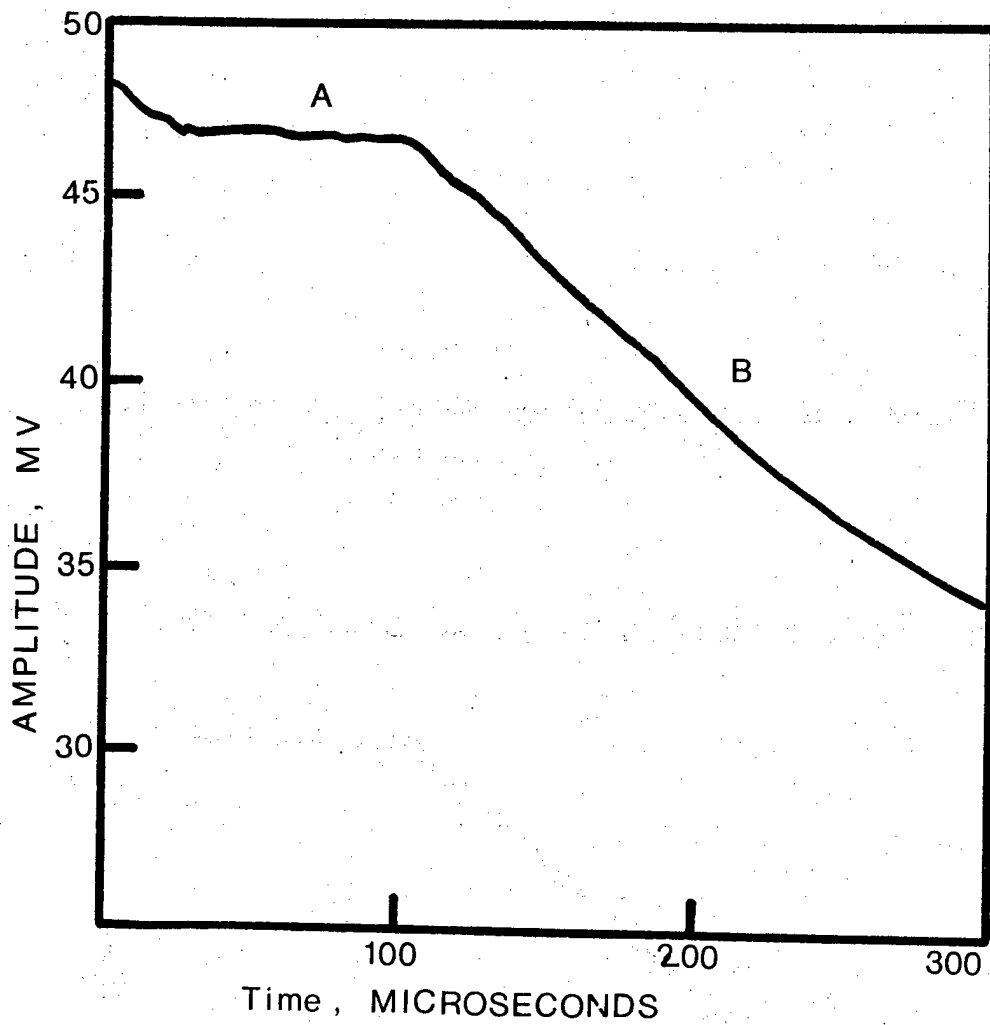


FIG. IV An Atypical PCD Response

BIOGRAPHICAL SKETCH

Lieutenant Thomas C. Chandler was born in York, South Carolina on January 3, 1952. He graduated from the University of South Carolina in 1974, receiving the B.S. degree from the Department of Electrical Engineering. He was commissioned in the Air Force through the AFROTC program in 1974 and was granted a delay of active duty to pursue graduate studies at the University of South Carolina. He was awarded the M.S. degree in Electronic Materials Engineering in 1976.

In February 1977 he began active duty at the Air Force Materials Laboratory. His interests have been primarily in silicon materials evaluations and IR detector focal plane research. He has published four papers in this and related fields since 1974. Lt. Chandler is a member of the IEEE and the Electrochemical Society.

DEUTERATED SYNTHETIC HYDROCARBON LUBRICANT

BY

A. A. CONTE, JR.

AIRCRAFT AND CREW SYSTEMS TECHNOLOGY DIRECTORATE
AERONAUTICAL MATERIALS LABORATORY
U. S. NAVAL AIR DEVELOPMENT CENTER
WARMINSTER, PENNSYLVANIA 18974

1396

ABSTRACT

The deuterium kinetic isotope effect was employed as a means of dramatically improving the oxidation resistance and bearing performance life of a synthetic hydrocarbon lubricating grease. A greater than fivefold increase in bearing performance was obtained at 400 F (204 C) for a 97 atom percent deuterated synthetic hydrocarbon grease compared to the nondeuterated grease. It is anticipated that these research findings will be translated into the development of more oxidatively stable long-life lubricants for weapons systems applications thus minimizing down-time and costly overhaul procedures.

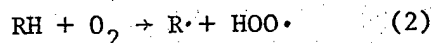
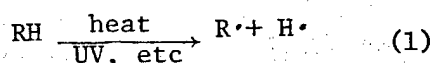
INTRODUCTION

In the early 1960's a new generation of lubricants were developed based on synthetic hydrocarbon (SH) fluids in order to meet the need for a broader temperature range lubricant with extended service life (1). SH fluids are essentially branched chain paraffinic hydrocarbons which are synthesized from low molecular weight olefins derived from petroleum. This type of molecule, one of many kinds of hydrocarbons found in petroleum oils, has the widest temperature range over which it remains liquid before congealing at low temperatures or evaporating rapidly at high temperature. Because of this property, SH fluids were selected for use as base fluids for lubricating greases. The greases prepared from the SH fluid were shown to possess such broad application capabilities that the requirements of several military aircraft lubricating grease specifications could be consolidated into one new specification (MIL-G-81322).

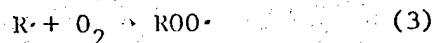
In 1967, the first successful laboratory preparation of fully deuterated hydrocarbons containing 10 to 36 carbon atoms was reported (2). The technique utilized permits the use of unsaturated and saturated, cyclic and acyclic materials and results in the perdeuterated saturated equivalent of the starting material. Deuterium exchange was found to occur between a hydrocarbon liquid and deuterium gas over carbon-supported, fixed-bed catalysts of Rh, Pt and Pd at 370-395 F. In addition, no cracking or isomerization of the hydrocarbon liquid occurred under these conditions.

Based on the previous information, a program was established at the Naval Air Development Center under an independent research program to investigate the effect on the lubricating properties of a SH grease which was formulated from a deuterium modified SH fluid. Research on the mechanism of oxidation of pure hydrocarbon fluids has shown the following sequence of chemical reactions can occur:

Initiation of Free Radicals



Propagation of Free Radicals



The substitution of deuterium for hydrogen in a chemical bond has been used for many years as a means of studying mechanisms of organic chemical reactions. It has also been known that the rates of chemical reactions are substantially reduced for the C-D vs the C-H bond, if scission of the bond is the rate controlling step in the reaction. In the oxidation of lubricating oils, the rate controlling step involves the cleavage of C-H bonds thus it was of great interest to investigate the effect of deuterium exchange on increasing oxidation resistance and improving bearing performance life.

EXPERIMENTAL

1. The exchange of hydrogen in the SH fluid with deuterium was performed via a process which is proprietary in nature and differs in some respects to the laboratory preparation detailed in reference (2).

2. The SH fluid used is designated RL-714 and contained no additives. This fluid has an average molecular weight of 515.

3. Grease samples were formulated under laboratory conditions and contained additives required to meet the requirements of Military Specification MIL-G-81322. The difference in specific gravity between the nondeuterated and deuterated SH fluids was taken into account when formulating.

4. Bearing performance tests were conducted in accordance with Federal Test Method Standard No. 791B Method 333.

5. Bomb oxidation tests on fluids were performed in accordance with ASTM Method D-942 for grease samples. Two grams of fluid were substituted for the 4 grams of grease required in this method.

6. The specific gravity of fluids was determined using a Weld type pycnometer.

7. Infrared spectra were obtained using a prism grating instrument. A polystyrene film was used to calibrate absorption peaks.

RESULTS

Specific Gravity

Various quantities of partially deuterated SH fluid were synthesized during this investigation. These included 51, 73, 88, 94 and 97 atom percent deuteration levels. Figure 1 shows that the specific gravity increases linearly with respect to increased deuterium content in accordance with Eq. (6).

$$SG = 1.270 \times 10^{-3} \sigma + 0.8264 \quad (6)$$

σ = Atom Percent Deuterated

Thus the extent of deuterium exchange could be followed by simple specific gravity measurements in addition to the more sophisticated techniques such as NMR, etc.

Infrared Analysis

Figure 2 shows a typical IR spectrum obtained on the deuterated and non-deuterated form of the SH fluid in the 1,900 to 3,600 cm^{-1} region. In this region, there are three characteristic absorption peaks associated with C-H vibrational stretching frequencies; namely 2,960, 2,930, and 2,850 cm^{-1} . The corresponding C-D stretching frequencies are observed to be shifted to 2,220, 2,200, and 2,080 cm^{-1} , respectively. The observed shift of approximately 750 cm^{-1} is due to the greater mass of the deuterium atom relative to hydrogen (a twofold increase). A closer look at the IR spectrum for the

deuterated fluid indicates that this sample is not completely deuterated since low intensity peaks are observed in the C-H stretching frequency range. The relative amount of C-H present compared to C-D can be approximated by measuring the ratio of band intensities.

Bearing Performance Life

The partially deuterated and nondeuterated fluids were formulated into a MIL-G-81322 specification type grease and examined as a lubricant for anti-friction bearings. Figure 3 shows the results of this investigation carried out at 400 F (204 C). No increase in bearing performance life over the non-deuterated grease was found at 51 atom percent deuteration. Beyond this level, modest increases in performance life were observed at 73 and 88 atom percent deuterium content. The most striking increase in performance life occurs at deuterium concentrations of 94 atom percent and higher with a greater than fivefold increase occurring at 97 atom percent deuterium content. These results are attributed to the greater oxidation resistance of the C-D bond vs. the C-H bond.

It was considered that the effects being observed might not be due to deuterium exchange but possibly some sort of contamination or molecular rearrangement in the SH fluid brought about by exposure to heat and catalytic materials. In order to investigate this possibility, a series of experiments were performed in which the SH fluid was processed in an identical manner as for deuterium exchange, except that hydrogen gas was passed through the fluid instead of deuterium gas. The same catalysts and temperatures used for accomplishing the deuterium exchange were also employed. The fluid resulting from this experiment was formulated into a grease and investigated in the bearing performance test at 400 F (204 C). The results showed that no increase performance life was obtained when compared to the standard grease formulation. Thus, it is concluded that deuterium exchange is providing the improved endurance life noted for the 97 atom percent deuterium modified fluid.

Oxidation Characteristics

Oxidation studies were performed on deuterated and nondeuterated fluids with and without antioxidant additives at 250 F (121 C). Bomb oxidation results are shown in Figures 4 and 5. In both instances, the deuterated fluid exhibits increased oxidation resistance when compared to the nondeuterated SH fluid. For the fluids without antioxidants, the induction period for the deuterated fluid is about four times longer than that of the undeuterated fluid. Once the auto-oxidation begins, however, the rates of reaction for the two fluids do not appear to differ substantially from each other at the 250 F (121 C) test temperature.

With equal amounts of antioxidants added to the two fluids, an even greater difference in induction time is evident for the deuterated fluid. At temperatures above 250 F (121 C), this difference in "induction time" is less, while, at lower temperatures, the difference is greater.

ADDITIONAL STUDIES

Oxidation studies on the partially deuterated fluids indicated that even at the 51 atom percent deuterium level, significant improvements in oxidation

resistance are obtained (Table 1), yet the bearing performance results showed no significant improvement in life until deuterium concentrations greater than 90 atom percent were achieved. It was, therefore, of interest to further investigate the significance of these findings. In order to explain the lack of response at the 51 atom percent deuterium level, in spite of its improved oxidation resistance, it was postulated that the increase in bearing performance life is dependent on the amount of completely or nearly complete deuterated synthetic hydrocarbon oligomers present. From a probabilistic standpoint, the 97 atom percent deuterium fluid should possess a number of molecular units which are completely deuterated. If the average oligomer is a $C_{36}H_{74}$ molecular unit, then the 97 atom percent deuterium level average molecular formula would correspond to $C_{36}D_{72}H_2$, thus molecular units of $C_{36}D_{74}$ and $C_{36}D_{70}H_4$ are theoretically and probabilistically possible. In contrast, at the 51 atom percent deuterium level, the average molecular unit would correspond to $C_{36}D_{38}H_{36}$. Significant concentrations of $C_{36}D_{74}$ and $C_{36}D_{2}H_{72}$ would then be unlikely.

In order to experimentally verify this hypothesis, mass spectral analysis was performed on the 51 and 97 atom percent deuterium fluids as well as the nondeuterated fluid. Although it was not possible to determine the actual degree of completely or nearly complete deuterated molecules in each sample because of lack of parent peak information (high fragmentation), the spectra are consistent with the proposed hypothesis for explaining the lack of response in bearing performance at the 51 atom percent deuterium level.

If the hypothesis is indeed operative, then one would expect to observe an increase in bearing performance life in the neighborhood of 50 atom percent deuteration if a high degree of completely deuterated or nearly complete deuterated molecules are present in a grease formulation. An approach toward providing such a grease is simply to admix two greases, one of which is highly deuterated, the other being completely nondeuterated. For example, if equal volumes of 100 atom percent deuterium grease and nondeuterated grease are mixed, the resultant grease would have a deuterium concentration of 50 atom percent. The 50 atom percent deuterium grease differs from the 50 atom percent deuterium admixed grease in the molecular distribution of deuterium atoms. The unblended grease has deuterium atoms distributed over every molecule, while, in the admixed grease, 50 percent of the molecules are highly deuterated with the balance containing only hydrogen atoms.

An admixed grease containing 48.5 atom percent deuterium was prepared and bearing performance life tests were performed. It was found that the bearing performance life for the 48.5 atom percent deuterium admixed grease was 2.5 times greater than bearing performance life for the 51 atom percent deuterium grease. Thus, greases with similar deuterium contents have been found to exhibit marked differences in bearing performance life. The result lends support to the hypothesis that the bearing performance life of deuterated greases is also a function of the degree of completely or nearly complete deuterated molecules present in the synthetic hydrocarbon oligomer.

SUMMARY

In spite of the high cost involved in material and processing of deuterium substituted SH fluid, the result of this modification is considered to be

potentially cost effective. The limited life of many aircraft instruments is directly related to bearing lubricant degradation and deterioration. Typically, instrument bearings often require sparse lubrication to provide low and more stable torque, less noise, jog-free operation, etc. As a result of the minute quantities required, lubricant cost becomes almost insignificant, even at 500 dollars per pound, when considering extended life versus cost of maintenance and/or replacement of bearings or components. It is interesting to note that one pound of grease will theoretically lubricate 65,000 typical R-3 spin motor bearings. This would correspond to about 0.75 cents per bearing.

It has been estimated that rework facilities use about 100 pounds of grease per year for instrument bearing applications. This small amount of yearly material usage limits private industrial incentives for providing an improved product because of low scale volume. Thus, this program has demonstrated the need and importance of performing research of this type by in-house government laboratories.

REFERENCES

1. Taber, D. S., Tedrow, L. E., Raich, H., and Wilson, J. W., "Assessment of Lubrication Technology," edited by B. D. McConnell, published by ASME June 1972, p. 127.
2. Atkinson, J. G., Luke, M. O., and Stuart, R. S., "A Simplified Preparation of Fully Deuterated, High Molecular Weight Hydrocarbons", CAN. J. OF CHEM, 45, 1511 (1967).

TABLE 1

OXIDATION RESISTANCE ON SYNTHETIC HYDROCARBON FLUIDS
AT 99 C (210 F)

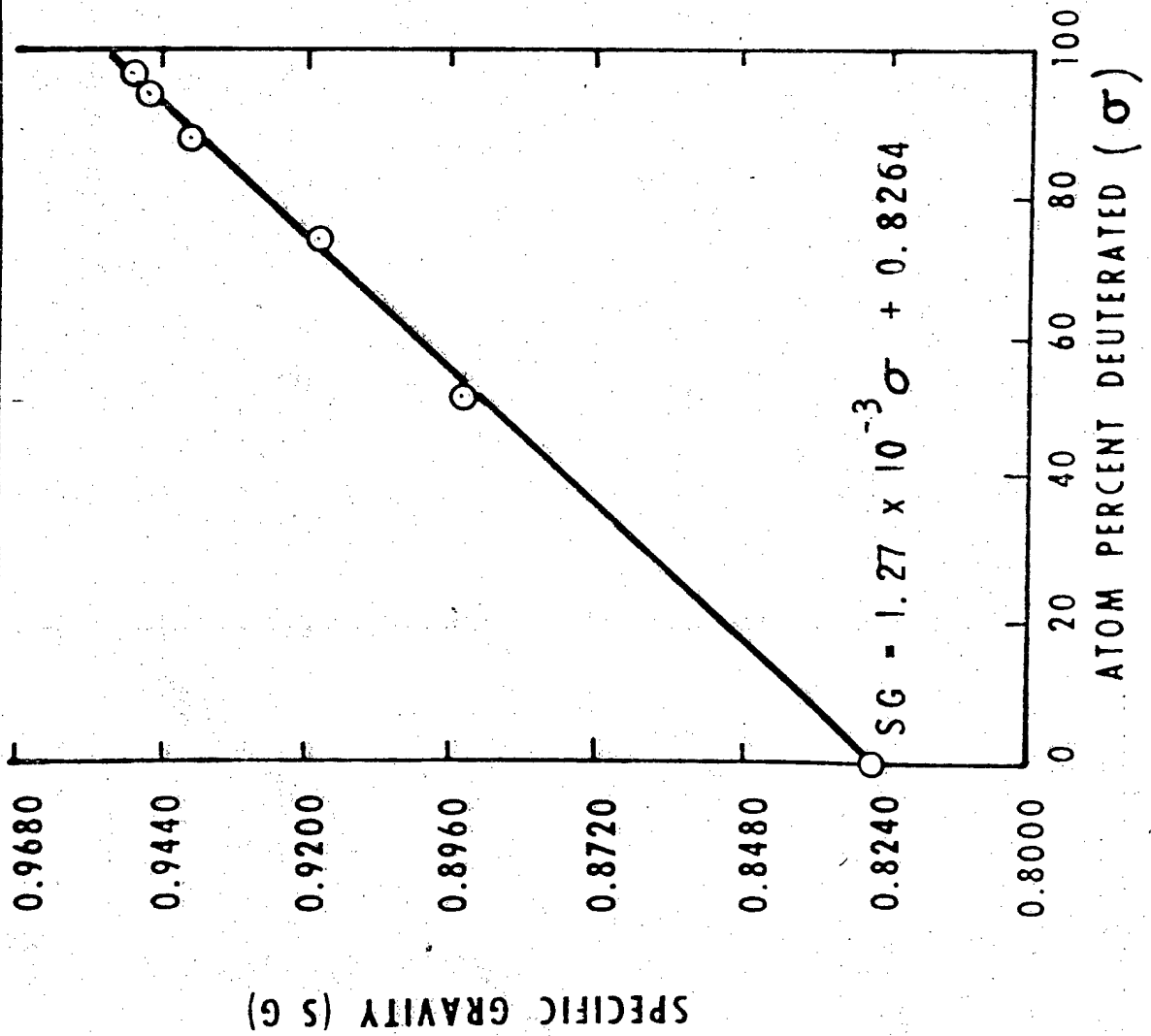
Deuterium Content (Atom Percent)	Pressure Loss kPa (PSI)*	
	168 hrs.	504 hrs.
0	665.3 (96.5)	-
51	31.0 (4.5)	-
73	17.2 (2.5)	-
88	0 (0)	-
97	0 (0)	27.6 (4.0)
48.5 (Admixed)	162.0 (23.5)	-

*Bombs charged to 758.3 kPa (110 PSI)



FIGURE 1

VARIATION OF SPECIFIC GRAVITY VERSUS ATOM PERCENT DEUTERATION





INFRARED SPECTRUM OF SYNTHETIC HYDROCARBON FLUIDS

FIGURE 2

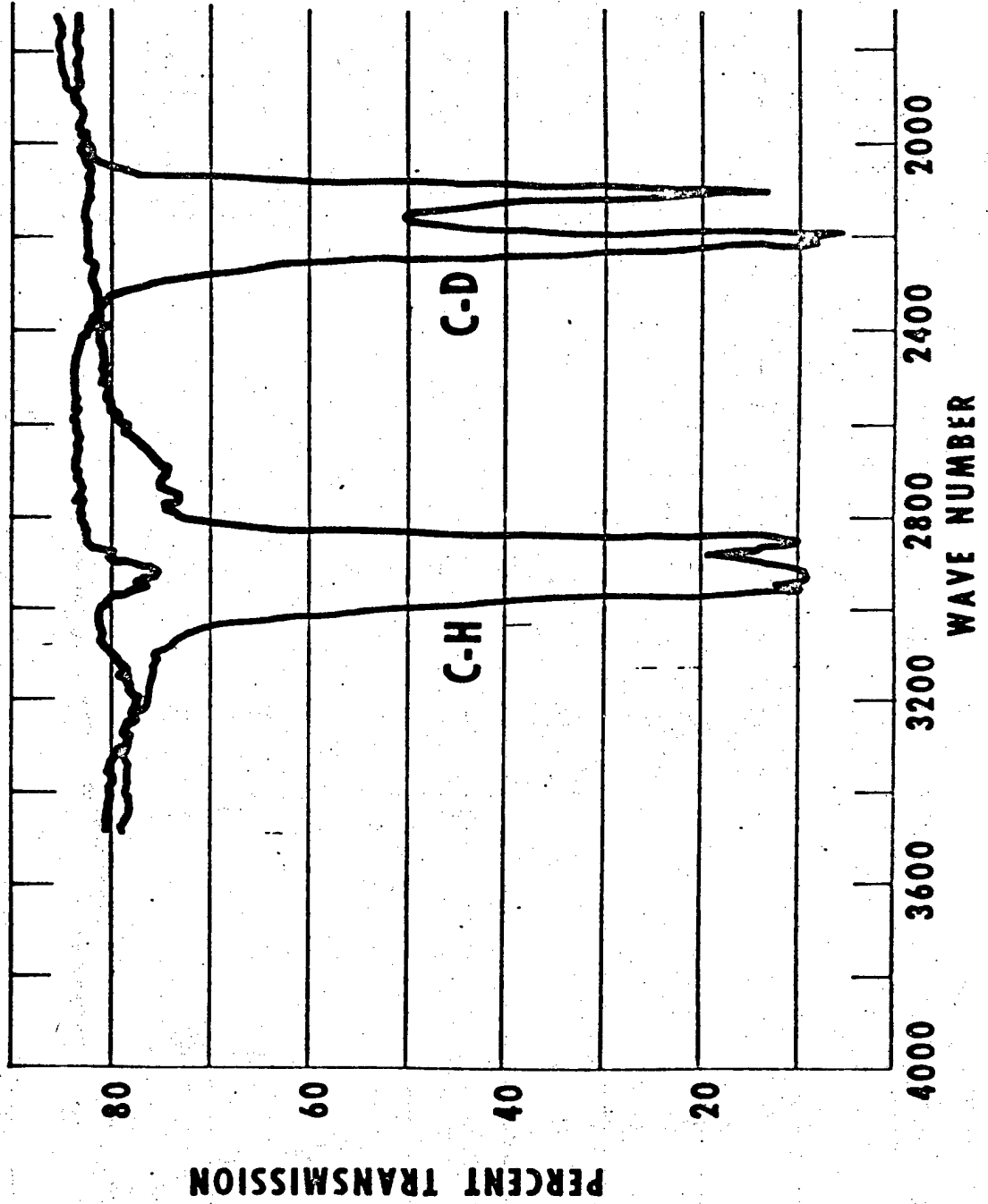




FIGURE 3

BEARING PERFORMANCE LIFE (SH GREASE)

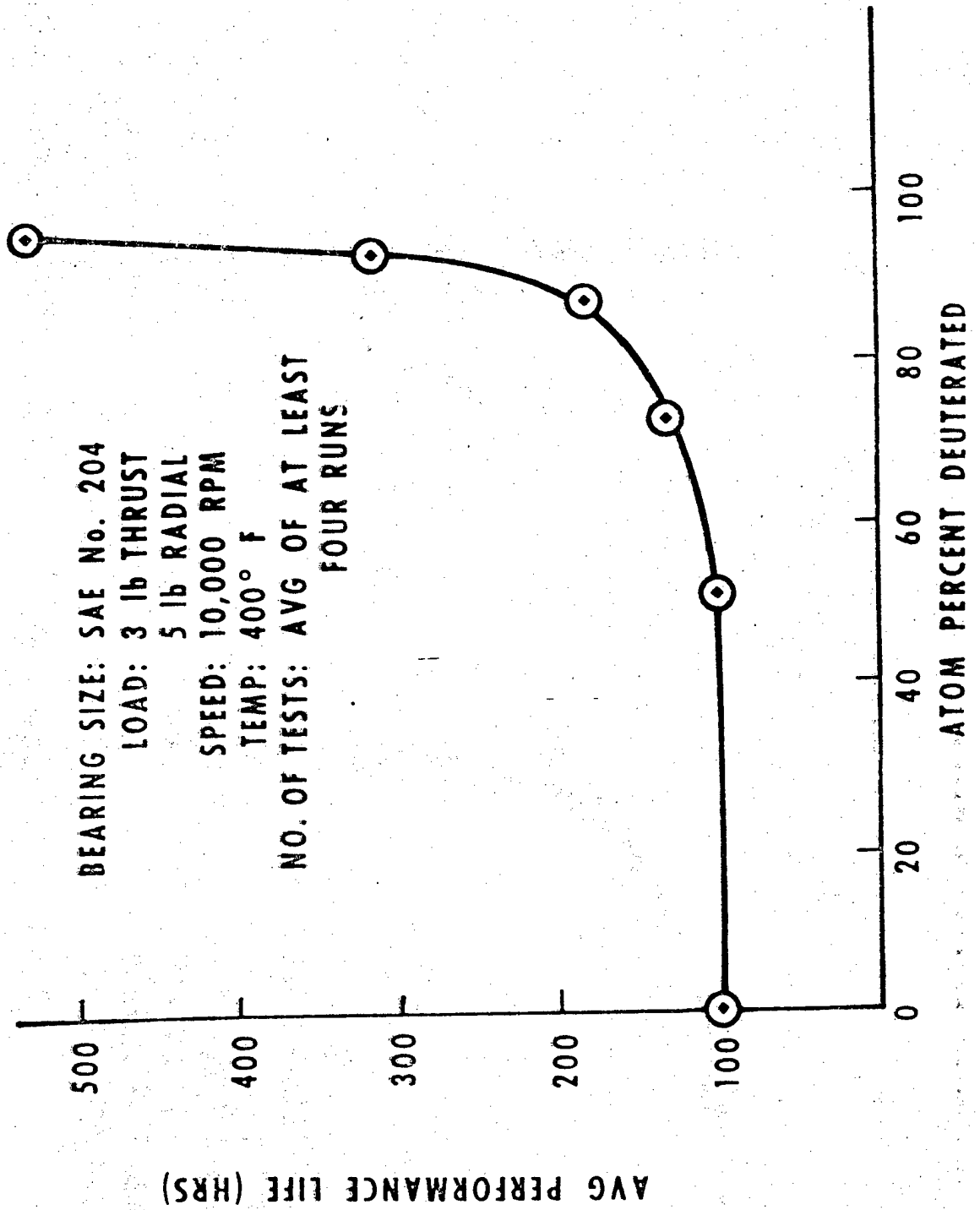




FIGURE 4

FLUID OXIDATION (BOMB OXIDATION METHOD) 250° F

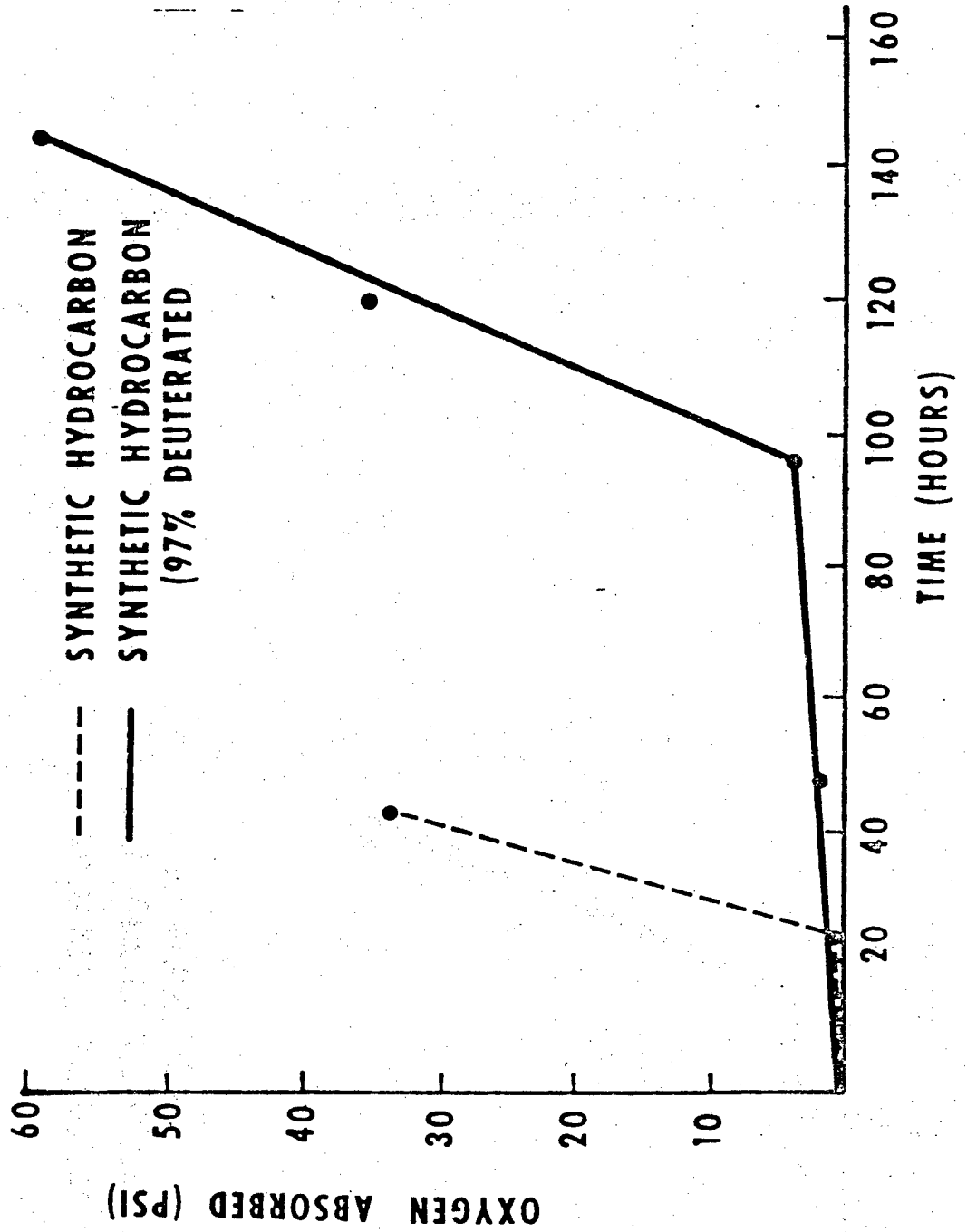
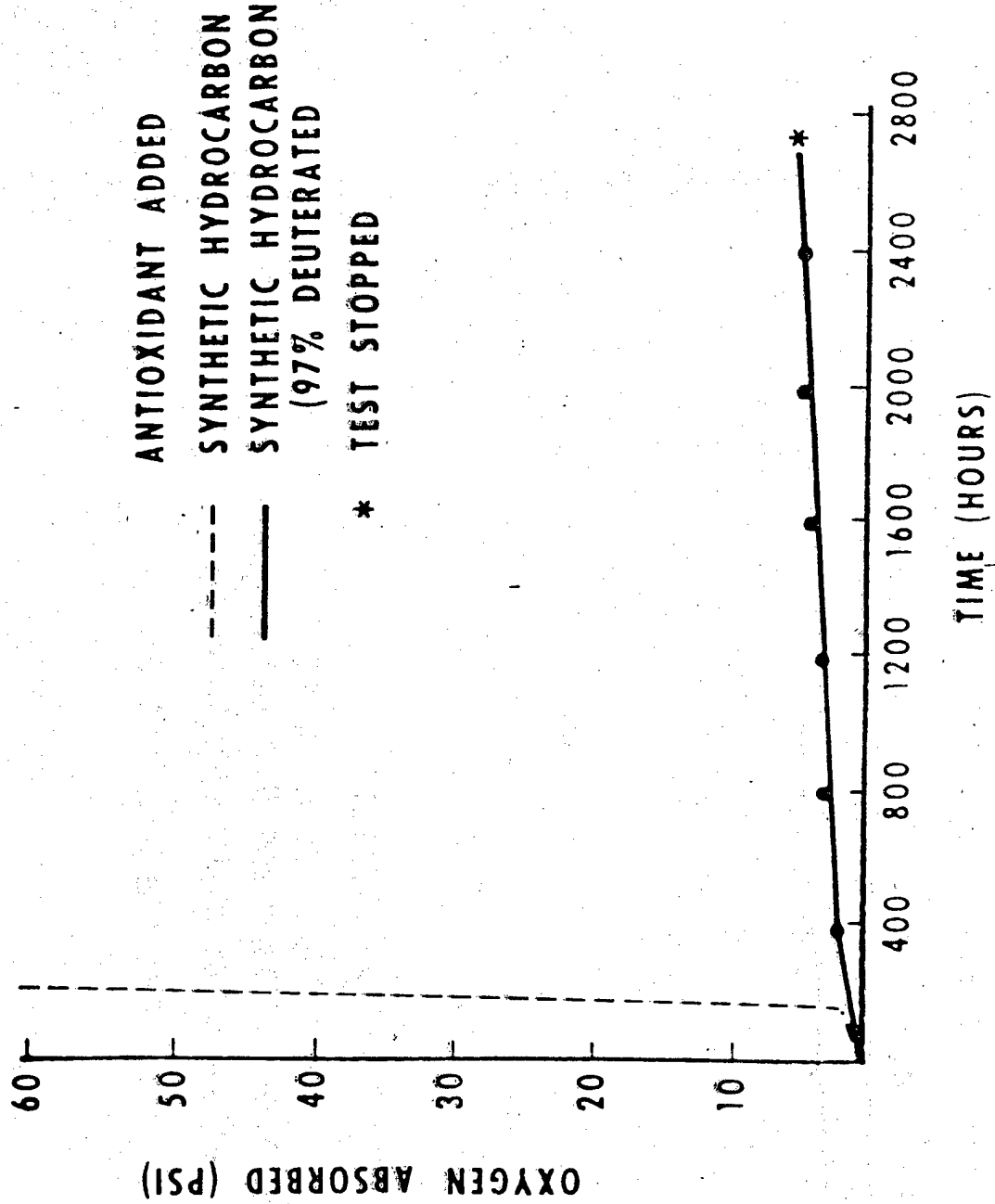


FIGURE 5

FLUID OXIDATION (BOMB OXIDATION METHOD) 250° F



THE CORDELL PLOT: KEY TO A BETTER UNDERSTANDING OF
THE BEHAVIOR OF FIBER-REINFORCED COMPOSITES

BY

Tobey M. Cordell

Manufacturing Technology Division

Air Force Materials Laboratory
Wright-Patterson AFB, Ohio

1410

The Cordell Plot: Key to a Better Understanding of
the Behavior of Fiber-Reinforced Composites

Abstract

Fiber-reinforced composite materials are being used to an ever-increasing extent in all types of aerospace systems, from high performance aircraft to satellite structures. The Cordell Plot offers for the first time a direct, easily grasped, technique to understanding and predicting the behavior of these vital new materials. The technique may be applied to virtually any combinations of materials and will work across the entire spectrum of materials application, from basic research to actual hardware structures in the field. The Cordell Plot allows one to select individual laminate compositions for sophisticated testing to verify the design of advanced aerospace systems. For the first time one may directly compare the effects of changing laminate composition on a variety of key properties. This may even allow the elimination of costly computer modelling in the preliminary design of new systems. Both academic and industry acceptance to date has been virtually unanimous in the affirmative, to the extent that this Cordell Plot will probably become the new basic format for the DoD/NASA Advanced Composites Design Guide.

Introduction

There has been an inherent reluctance to utilize fiber-reinforced composites almost since the very first time they were proposed for use in aerospace structural applications. This reluctance is still very apparent in the seemingly slow progress being made toward widespread use of these materials. This reluctance may be traced to a lack of understanding of the fundamental advantages available through the use of fiber-reinforced composites (FRC). This lack of understanding arises from the fundamental anisotropic nature of FRC, one that dictates that they have the potential for very large variation in properties. An improved method of visualizing and portraying the behavior of these materials was needed so that one could more easily visualize, grasp, and thereby more effectively utilize this highly anisotropic behavior.

If most aerospace engineers were asked for the modulus of elasticity of aluminum and titanium they would readily respond 68 gigapascals (GPa) (10 million psi) and 110 GPa (16 million psi), respectively. In a similar fashion, one could readily obtain a quick, fairly accurate response to a similar question relating to the tensile strengths of these materials. The reason for the ease of recalling this type of data is that most structural metals are generally isotropic, with a very narrow range of property variations. A similar behavior characteristic does not exist for FRC. The basic reason for this is that these composites are composed of oriented layers of highly anisotropic laminae, each with longitudinal to transverse property ratios as high as 50 to 1. This means that it is currently virtually impossible for a person to quote, from memory, a quick, accurate estimate of the tensile strength of anything but the simplest multiple layer laminates. But the ability to do this quickly and simply is essential to developing a "feel" for what happens when one modifies the design of a composite structural component. Today the technique most commonly used to attempt to portray this wide range of properties possible is called a "carpet plot".

The Carpet Plot

A sample carpet plot for the allowable tensile modulus of a graphite/epoxy (Gr/Ep) 0/±45/90 set of laminates is shown in Figure 1. The point marked "A" represents the longitudinal modulus of a 100% 0° laminate and is 127 GPa (18.5 million psi). The point marked "B" represents a 100% ±45° laminate and has a modulus of 17 GPa (2.5 million psi). The point marked "C" represents a 100% 90° laminate with a modulus allowable of zero GPa (0 million psi). (A zero modulus allowable is used to be conservative in structural design.) These three points represent the extremes available from a "family" of laminates composed of 0's, ±45's, and 90's. Various other combinations of 0, ±45, and 90 laminae are represented by points "inside" the plot boundaries. The use of carpet plots has been discussed in a variety of other places. (1,2,3,4)

Trying to explain how the carpet plot can be used to show the properties available from a certain type of laminate is one of its major drawbacks--it does not directly give one a feeling for the behavior of the laminates that it is representing. Another key drawback with the use of the carpet plot is that the plot assumes a different shape for every laminate parameter plotted. For instance, the shape of the carpet plot for the Major Poisson's Ratio of the same set of Gr/Ep laminates is dramatically different, as shown in Figure 2. These shape changes make difficult the process of finding and comparing the various mechanical properties of a laminate of interest, because the point that represents the laminate on one carpet plot will almost always be in a different position on the next plot.

The Basic Cordell Plot

Currently the 0/±45/90 laminate "family" is being used very widely. This means that all laminates in this family are composed of various percentages of 0's, ±45's, and 90's. The use of this set of three basic orientations caused me to try and adapt the laminate compositions, but all have in common the basic characteristic that the combinations being plotted are composed of

exactly three constituents and that the total of the percentages of the three constituents always equals 100%. Metallurgists and ceramists will be familiar with the ternary phase diagram used to represent alloys containing three separate phases.⁽⁵⁾ The ternary plot format, with some modification, provides the foundation for the Basic Cordell Plot, as shown in Figure 3.

The vertices on the Plot represent laminates that are composed of 100% 0's, ± 45 's, or 90's, as marked. Other laminate compositions may be found by simply cross plotting the percentage composition of 0's, ± 45 's, and 90's. Note that the Plot is designed to enhance one's ability to determine what compositions are being plotted. For example, the percentages of 0° plies are represented by the lines that run horizontally across the plot, with the apex being 100% and then lines of decreasing percentage being shown by the numbers along the right hand edge of the Plot, with these numbers being parallel with the vertex designation they represent. Similarly, for the $\pm 45^\circ$ vertex the lines of percentage composition are represented by the numbers along the bottom of the Plot, those that read the same way as the $\pm 45^\circ$ vertex designation. This same behavior holds for the 90° vertex, with the decreasing percentages being along the left edge of the plot, again oriented in the same direction as the 90° vertex designation. Also note the small arrows at the 40% composition level for each orientation. These are designed to enhance the user's ability to quickly cross plot any given laminate composition.

To locate a given 0/ ± 45 /90 laminate, one simply calculates the percent composition and plots the intersection of two of the orientation percentages. As an example, a common laminate, (0/ ± 45 /90)₅, has been plotted with the dotted lines on Figure 3. Only the 25% 0° and 25% 90° lines are used, but note that the point of intersection falls directly on the 50% $\pm 45^\circ$ lines. The intersection of the two lines designates the laminate of interest. One simply plots any given laminate by cross plotting its percentage composition. Note that each edge represents laminates that are only composed of the two orientations represented by vertices at each end of the edge. For instance, the bottom edge represents all laminates that contain 0% 0° lamina, or all ± 45 /90

laminate combinations. There are other useful symmetry characteristics of the Basic Plot, such as where orthotropic laminates may be found, however that is not the subject of this paper. Suffice it to say that the Basic Cordell Plot allows one to have a plot upon which may be found ANY laminate composed of a set of three laminate orientations (this same technique would work equally well for $0/\pm 60/90$, $\pm 10/\pm 30/\pm 89$, or other laminates).

Once having established the Basic Plot as a two dimensional surface which could represent any laminate composition, the Basic Plot was then used to establish a method of portraying the properties associated with each of those combinations. This led to the Extended Cordell Plot.

The Extended Cordell Plot

Format. Figure 4 shows the Basic Plot in an isometric view, with the 0° vertex being the back corner as viewed and with "sides" extended upward from each "back" edge of the Basic Plot. This format forms the basis for the Extended Cordell Plot. To create an Extended Plot, one simply projects property values "up" from the appropriate point on the Basic Plot that forms the bottom surface of the Extended Plot. The same Gr/Ep laminate that was earlier shown on the carpet plots for ease of comparison of the property values as shown by these two presentation methods. Figure 5 shows the longitudinal modulus of elasticity properties of the three vertex orientations extended "up" into the Extended Plot. Figure 6 continues the plotting of the modulus values related to essentially each of the laminate combinations represented on the Basic Plot. Notice that a surface has been formed by the locus of points that represent the properties of the respective laminate orientations. Figure 5 now illustrates the behavior of the entire "family" of $0/\pm 45/90$ laminates. The surface formed can be clearly visualized and retained in one's memory.

Gr/Ep vs Aluminum. The use of the Extended Plot format also allows one, for the first time, to clearly portray the relationship between two different materials such as aluminum and graphite/epoxy. The plotting of Gr/Ep has already been illustrated, but plotting the aluminum poses a slightly different problem. Since the aluminum may be treated as isotropic for the example that is being illustrated, let's assume that aluminum's modulus is 69 GPa (10 million psi). The behavior of an isotropic material in the Extended Plot format is simply represented by a plane with the given isotropic property value being the points of intersection with the "z" axes extending upward from each vertex. Since these values are all equal in value, it is obvious that the plane formed is parallel to the Basic Plot surface which is the bottom face of the Extended Plot. This plane, and its intersection with the Gr/Ep "surface" are shown in Figure 7. It becomes intuitively obvious that all those Gr/Ep laminates represented by points that are above the aluminum "plane" will have an absolute modulus that exceeds that of aluminum. Specific properties could have been plotted just as easily, providing an even more graphic example of the advantages available through the use of fiber reinforced composites.

The locus of points along the intersection of the two surfaces represent those laminates that have a modulus of 69 GPa (10 million psi). These laminates may also be shown on the Basic Plot by utilizing simple projection geometry and projecting the intersection line "down" onto the Basic Plot surface. This projection is the thin line on the bottom surface of the Plot in Figure 7. This same locus of points is shown on Figure 8 and is shown with a 69 (10) designation at its end points, signifying that any laminate falling on this line will have a longitudinal modulus of elasticity of 69 GPa (10 million psi).

Isoproperty Lines/Modulus of Elasticity. In order to make effective use of the Basic Plot, one must be able to quickly and easily determine the property values available from any given laminate composition. This is done by simply "slicing" the Extended Plot at several levels and then projecting the intersections of these

slices "down" onto the Basic Plot. This process is directly analogous to the familiar method used in the creation of topographic contours commonly used on geographic maps. These lines of equal property or "isoproperty" lines allow one to interpolate on the Basic Plot to find the desired property of any laminate in question. The result of this process is Figure 9, which is now the replacement for the original carpet plot shown in Figure 1. Note how easily one could determine those laminates which match or exceed the longitudinal modulus of aluminum or titanium [any laminate combinations which fall on or above the 69 GPa (10 million psi) line or the 110 GPa (16 million psi) line, respectively].

Poisson's Ratio. Figure 10 is the Extended Cordell Plot for the Major Poisson's Ratio of our 0/±45/90 Gr/Ep family of laminates. The shape of the surface formed is dramatically different from that for modulus of elasticity. The value at 100% 0° is essentially a weighted average (Rule of Mixtures) combination of the moduli of the epoxy matrix and the graphite fiber. The value at 100% ±45° is so high because the "scissoring" effect of this orientation causes almost as much lateral contraction as the longitudinal strain imposed. The very low value at 90° is due to the very stiff fibers essentially preventing lateral contraction given an imposed longitudinal strain field. The comparable Basic Plot with isoproperty lines for the 0/±45/90 Gr/Ep Major Poisson's Ratio is Figure 11.

Note that the Extended Plot for Poisson's Ratio, Figure 10, is quite steep along the 0/±45 edge. This clearly indicates that minor changes in the percent of 90° plies in this region may cause major changes in the Poisson's Ratio of the resultant laminate, potentially leading to design problems. As an example, the laminate represented by point A in Figure 11 contains 10% 90° plies. As one moves to point B the resultant combination has 0% 90° plies, or a 10% reduction from point A. However, the Poisson's Ratio had gone from about .48 at A to almost .68 at B, or about a 40% increase. Clearly, the ability to understand, visualize, and control this type of behavior quantitatively should be a major asset to the designer.

Comparing Properties. One advantage of the Basic Plot with isoproperty lines is that one may quickly and simply find a variety of properties for any given laminate, because the laminate composition is represented by a point that is always in the same position in every Basic Plot for that material. One simply finds the laminate combination of interest on the Basic Plot for the property desired, such as Poisson's Ratio, and then interpolates between isoproperty lines to find the property value. The solid squares marked on Figures 9 and 11 represent the intersection of the isoproperty lines for the modulus and Poisson's Ratio's (of the example G_r/E_p laminate family) that match those of titanium. The point of intersection was found by simply superimposing the two Basic Plots and noting the point of intersection. This is possible because every laminate composition occupies the same location on each Basic Plot, even though their respective property values are different for each plot. This characteristic will make it easy to use computer graphics to store and recall Basic Plots of interest and superimpose bands of desired properties from other Basic Plots.

Note that one does not have to create an Extended Plot to get the location of the isoproperty lines for the Basic Plot. They may be determined directly from analytical or experimental data. In fact, the principal use of the Extended Plot will probably be in training new personnel. However, the Extended Plot offers an excellent format to illustrate the difference between various reinforcing systems and also allows one to more clearly illustrate the degrading effects of environmental exposure and/or structural fatigue. Different material systems would be shown by simply plotting the competing systems on the same Extended Plot. The effects of aging, etc, would be illustrated by plotting the "after" properties on the same Plot along with the original properties.

Other Uses/Applications of the Plots

Extended Cordell Plot Uses. I have chosen to limit this paper to the fundamentals related to the development and use of the Plots. To this point I have only shown their use for material properties. These properties may be determined either empirically or analytically, and may

even include other types of data, such as structural behavior parameters for a given family of composite plates. A wide variety of other uses may also be made of the Plots. They may be used to complement the commonly used tabular format for presenting laminate data in reports. Whereas a table may force you to try to grasp the behavior of the laminate being studied, a simple Extended Cordell Plot of the same data points may be able to show all the data in a convenient "summary" format.

A tabular format provides specific detailed information, and the Extended Plot provides complimentary overall trends. In addition, presenting the data in the Extended Plot format may allow the experimenter to determine where additional data is needed to model the behavior of the range of laminates under study. The Extended Plot may also be used in the design of experiments, by allowing one to choose a selected number of experimental laminates that will enclose the region in question.

Basic Cordell Plot Uses. Another potentially powerful application of the Basic Plot is to use it to model or "map" actual structures. This may be done by plotting the laminate orientation percentages from one point on the structure to another spot on the structure and at several intervening points. By careful selection of the points chosen for modelling, one may show changes in the design as the constraints on the structure change. In a similar fashion, one could show the differences between competing approaches to similar or identical structures, including the differences caused by different design philosophies. Another use would be to show the changes in failure modes of laminates in different regions of the Basic Plot: fiber dominated toward the 0° apex, matrix dominated toward the 90° apex, and some form of mixed mode in the $\pm 45^\circ$ region. It even appears possible to show laminate family behavior in a biaxial strain/stress field, offering the potential for reducing the amount of computer analysis required to support Preliminary Design efforts.

Summary

In review, let me ask the reader to close this paper and see if he can sketch a Basic Cordell Plot for the longitudinal modulus of elasticity of the 0/±45/90 Gr/Ep laminate family and show approximately the locus of laminates that would have a longitudinal modulus of elasticity that would equal that of aluminum. I daresay that the majority of readers will be able to do so rather readily, indicating the potential to visualize laminate family behavior in one's mind. In summary, the Basic and Extended Cordell Plots offer a new approach to understanding and visualizing the behavior of fiber-reinforced composites. If the Plots' potential is to be brought to bear on the problem of increasing acceptance and use of these materials, it is vital that a broad segment of the composites industry, both producers and users, evaluate their effectiveness. As the DoD/NASA Advanced Composites Design is updated, it should be modified to allow the users to make their own selection as to which techniques they wish to use in laminate selection. Future government and industry programs should request presentation of data in the formats shown here to allow easier and more rapid interpretation of results and implications of the data. Interested parties may address questions or requests for information to: Tobey M. Cordell, AFML/LTN, WPAFB, OH 45433; or call (513) 255-2871.

References

- (1) Waddoups, M. E., "Characterization and Design of Composite Materials", Composite Materials Workshop, Stamford, Connecticut, Technomic Publishing Co. Inc. 1968.
- (2) Cornsweet, T. M., "Advanced Composite Materials", Science, Vol. 164, No. 3930 (1970).
- (3) Hadcock, R. N., "Boron-Epoxy Aircraft Structures", Handbook of Fiberglass and Advanced Plastics Composites, New York, Van Nostrand Reinhold Co., 1969.
- (4) Hahn, H. T. and Tsai, S. W., "Graphical Determination of Stiffness and Strength of Composite Laminates", J. Composite Materials, Vol. 8 (1974).
- (5) Hall, F. P. and Insley, H., Phase Diagrams for Ceramists, Columbus, OH, The American Ceramic Society, 1974.
- (6) Sandeckyi, G. et al, "Fracture Behavior of T300/5208", ASTM STP 580.
- (7) I wish to express my appreciation to Mr. J. Mooney, The Boeing Co., for his suggestions dealing with the labelling of the Plots.

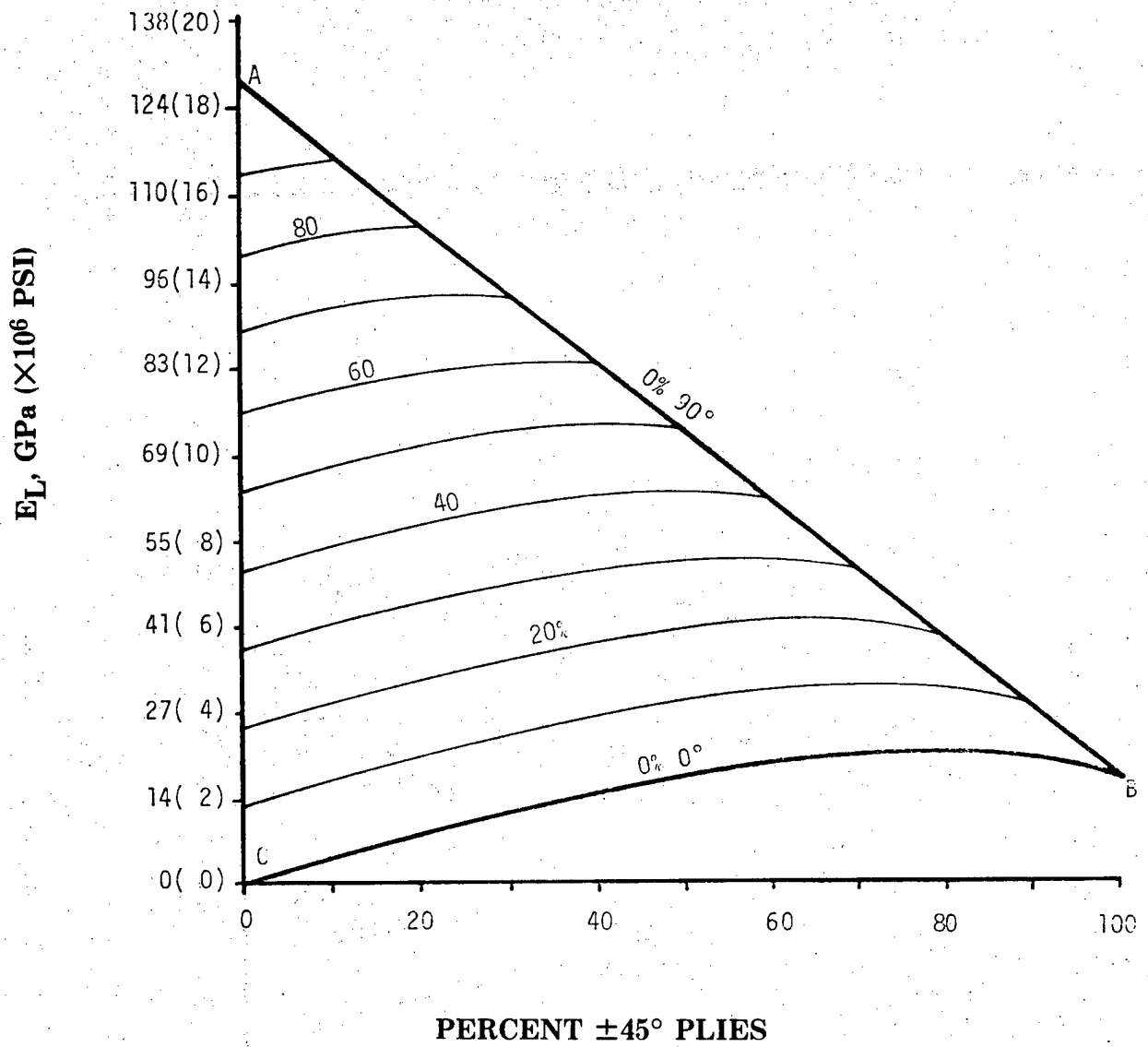


FIGURE 1. LONGITUDINAL MODULUS OF ELASTICITY, Gr/Ep

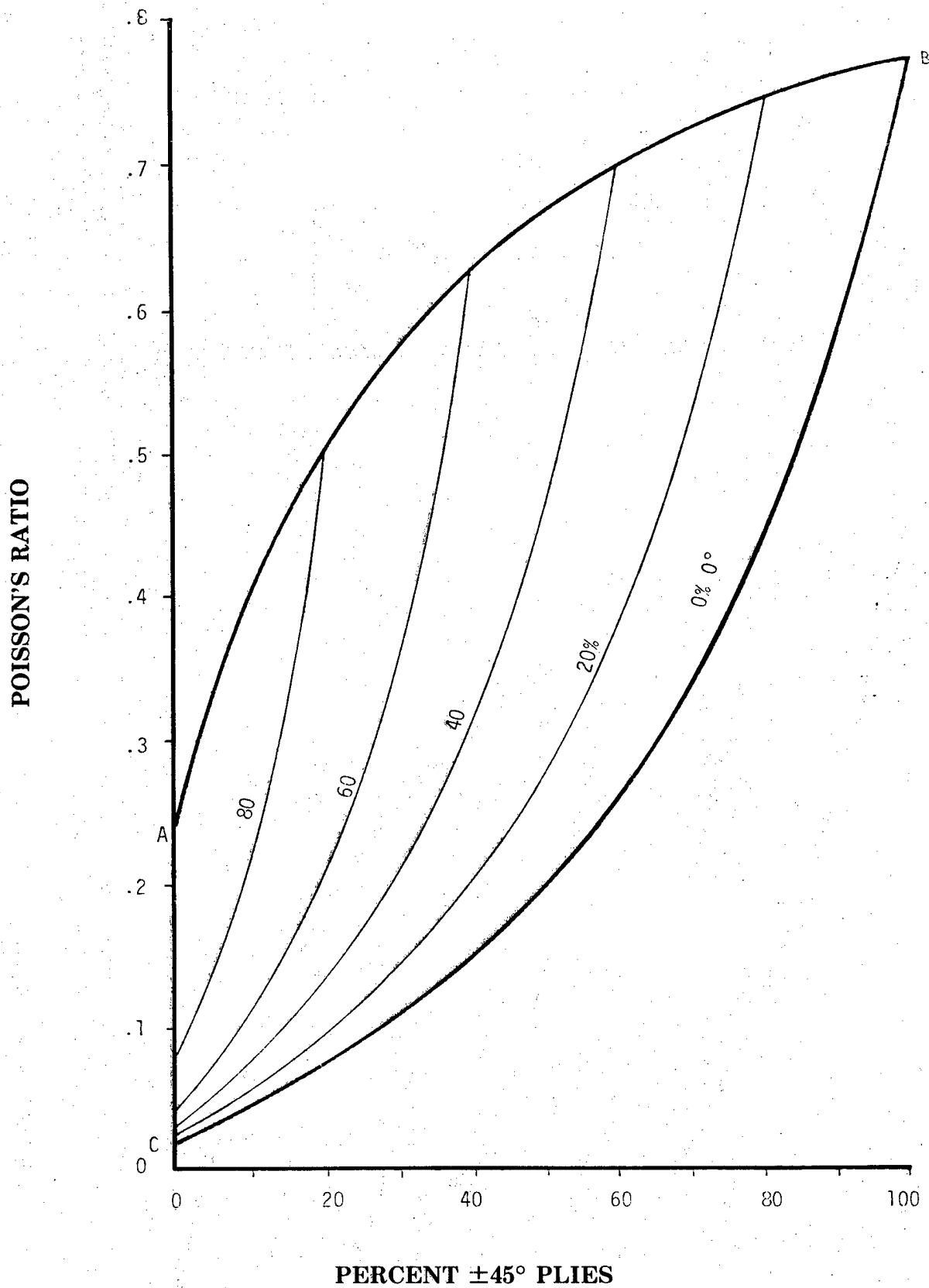


FIGURE 2. MAJOR POISSON'S RATIO, Gr/Ep

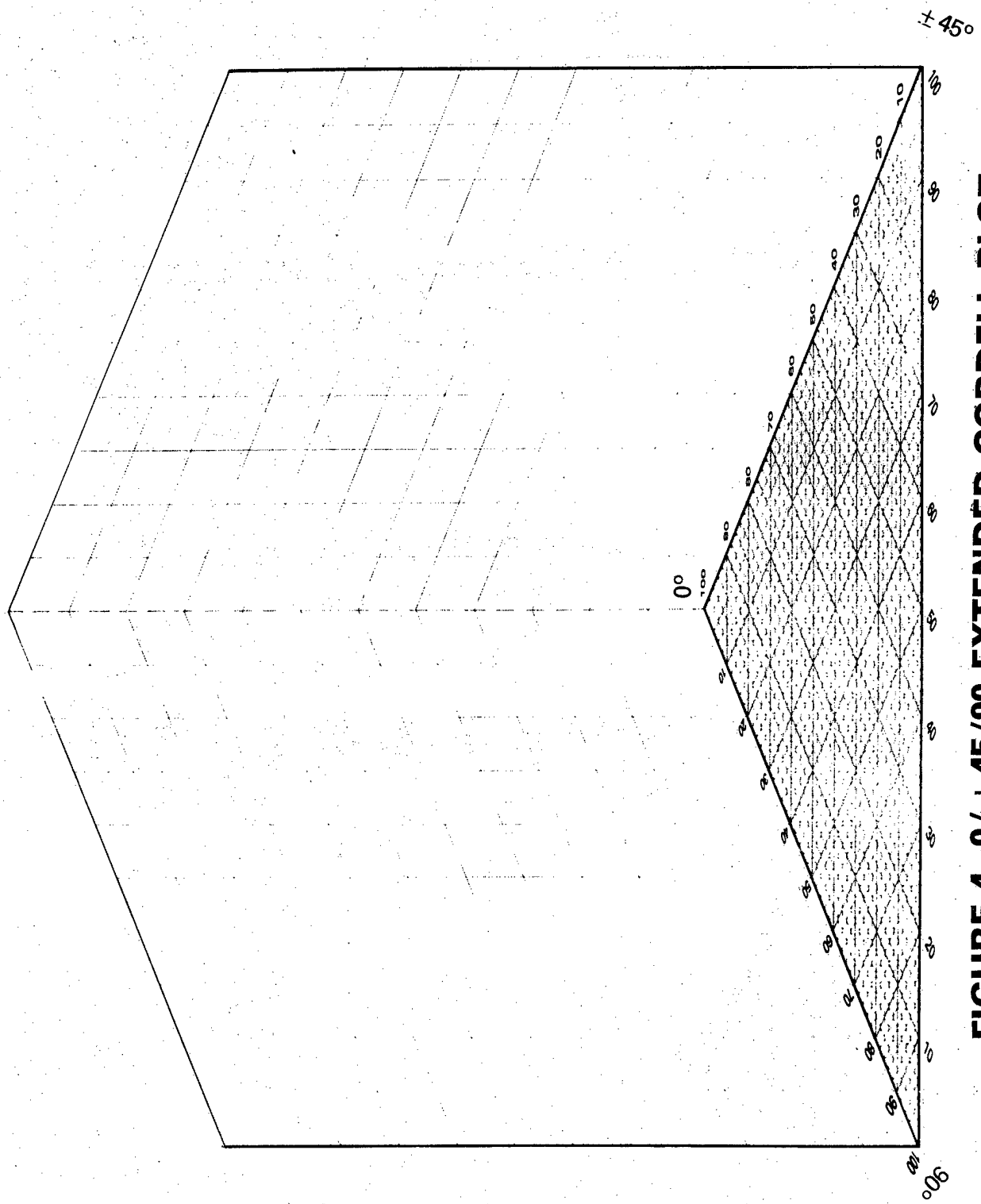


FIGURE 4. 0/ ± 45/90 EXTENDED CORDELL PLOT

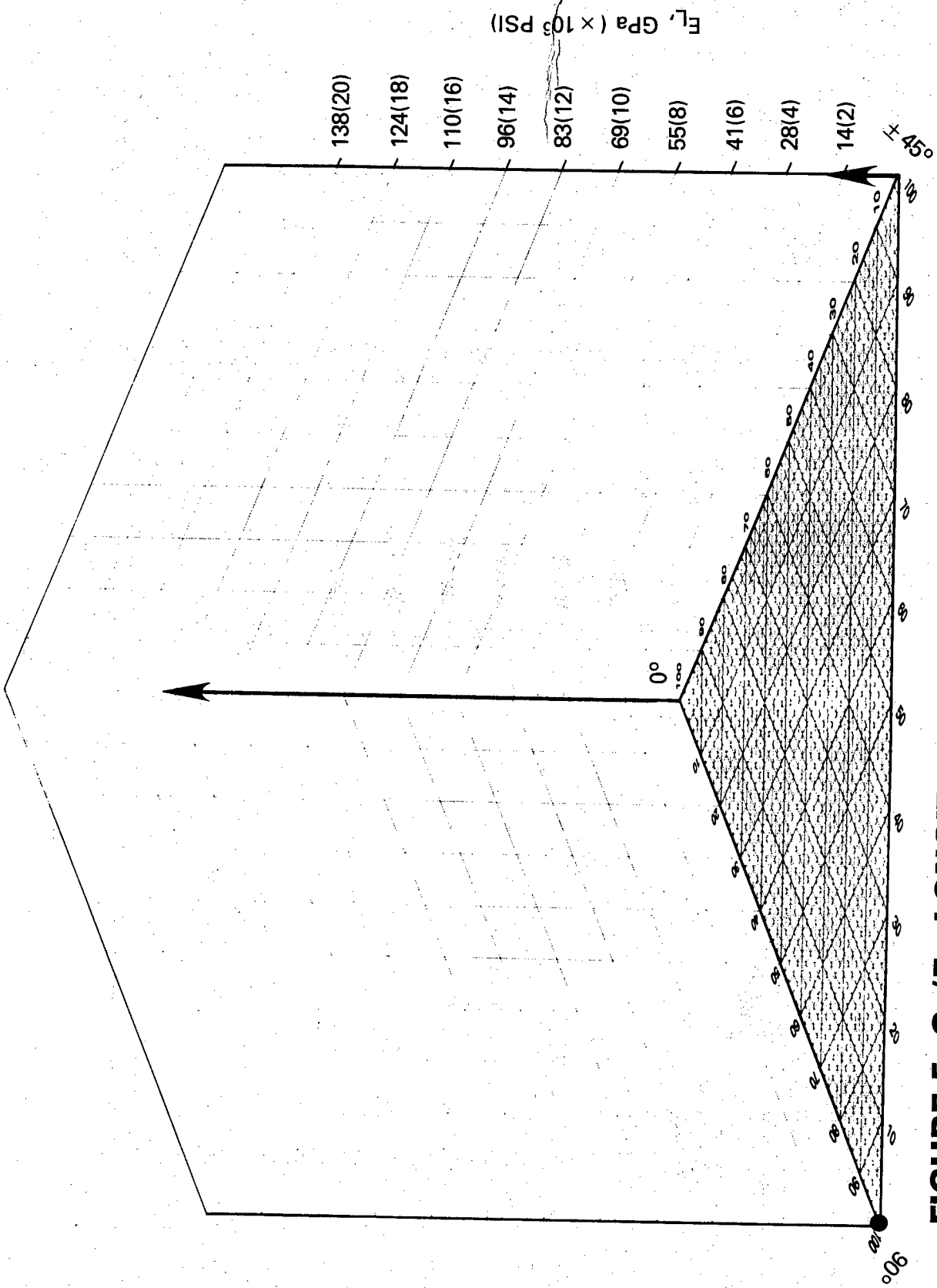


FIGURE 5. G_r/E_p LONGITUDINAL MODULUS OF ELASTICITY

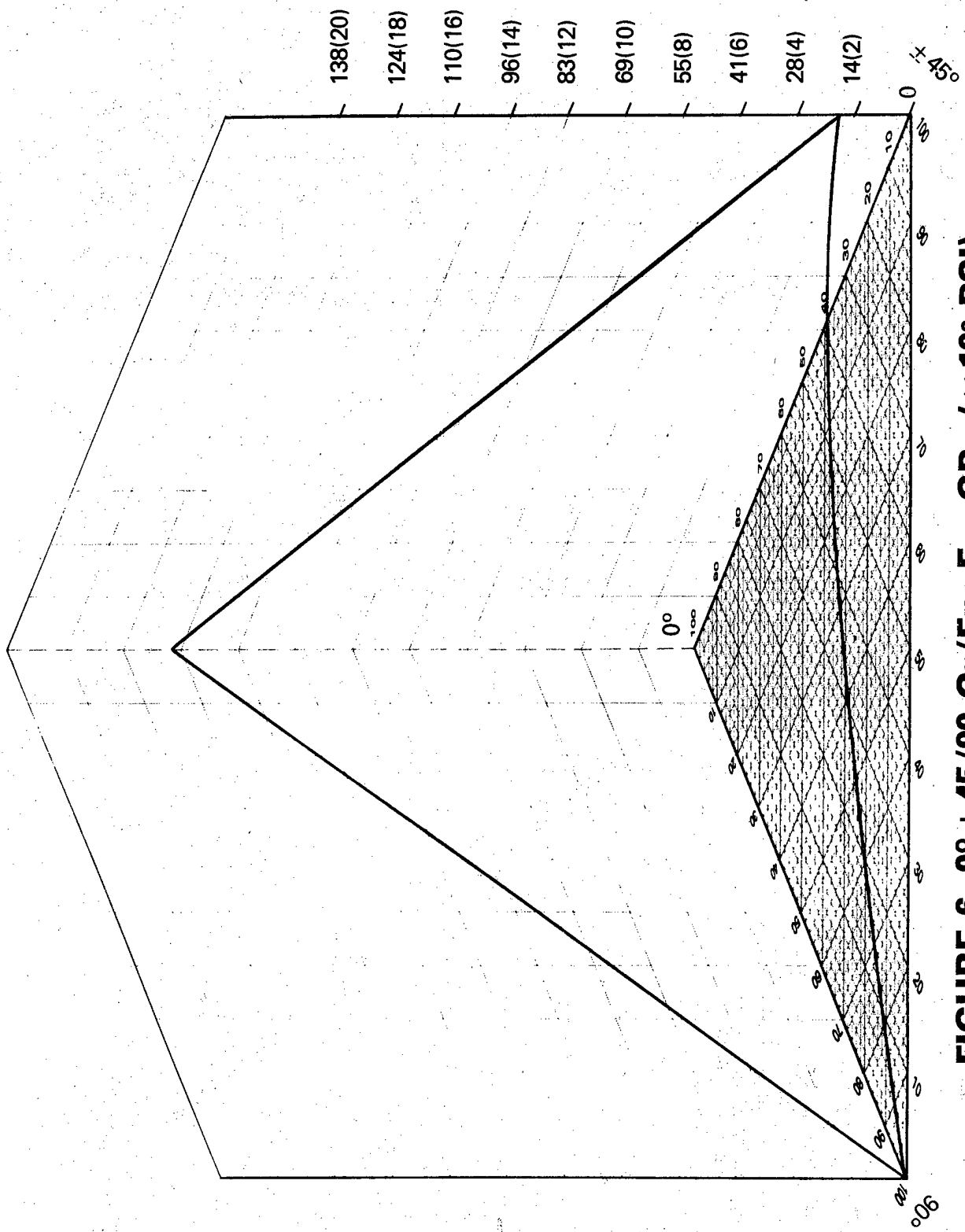


FIGURE 6. $0^\circ \pm 45/90$ Gr/Ep, E_L , GPa ($\times 10^6$ PSI)

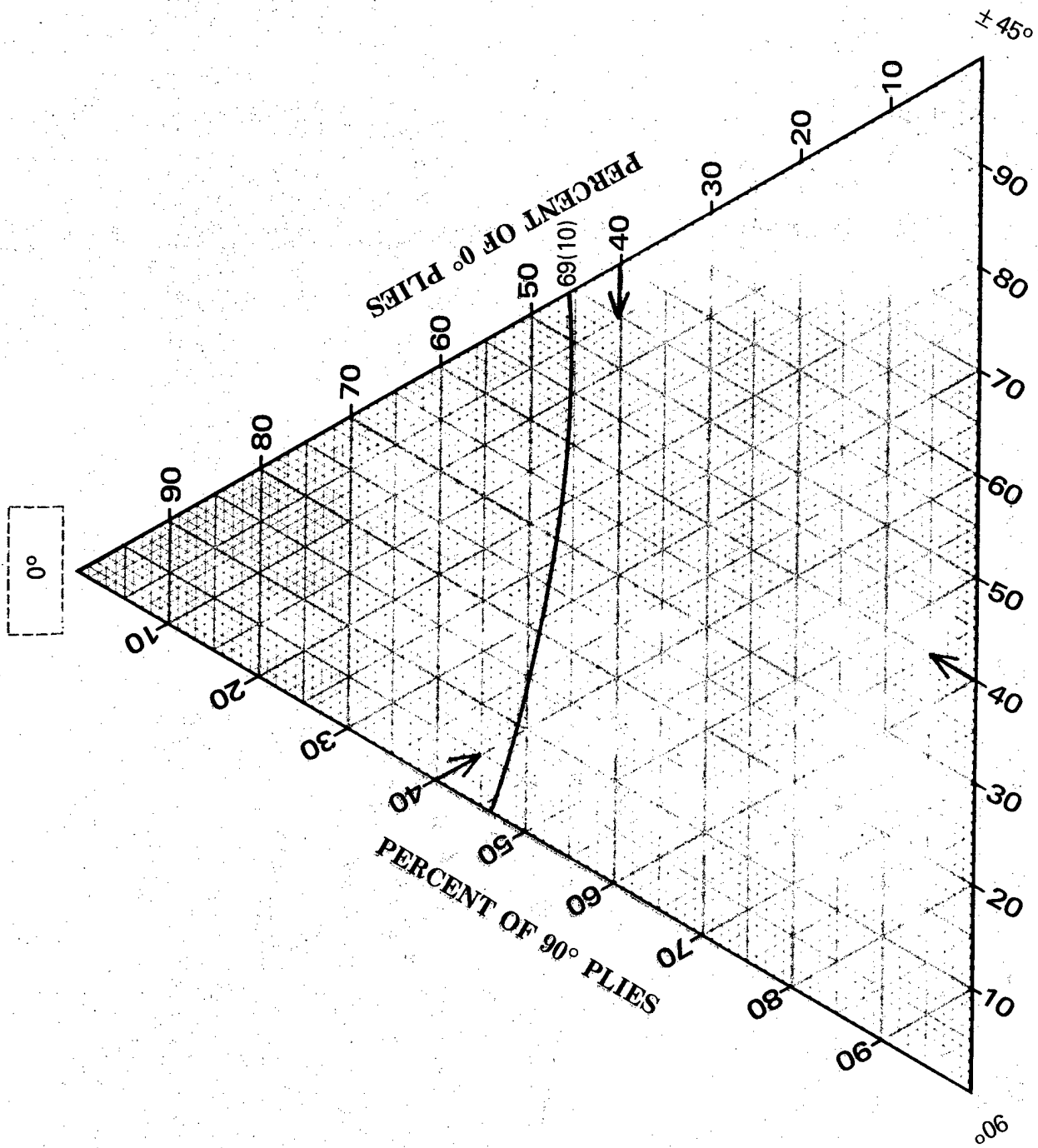


FIGURE 8. E_L , 0/±45/90 Gr/Ep, GPa ($\times 10^6$ PSI)

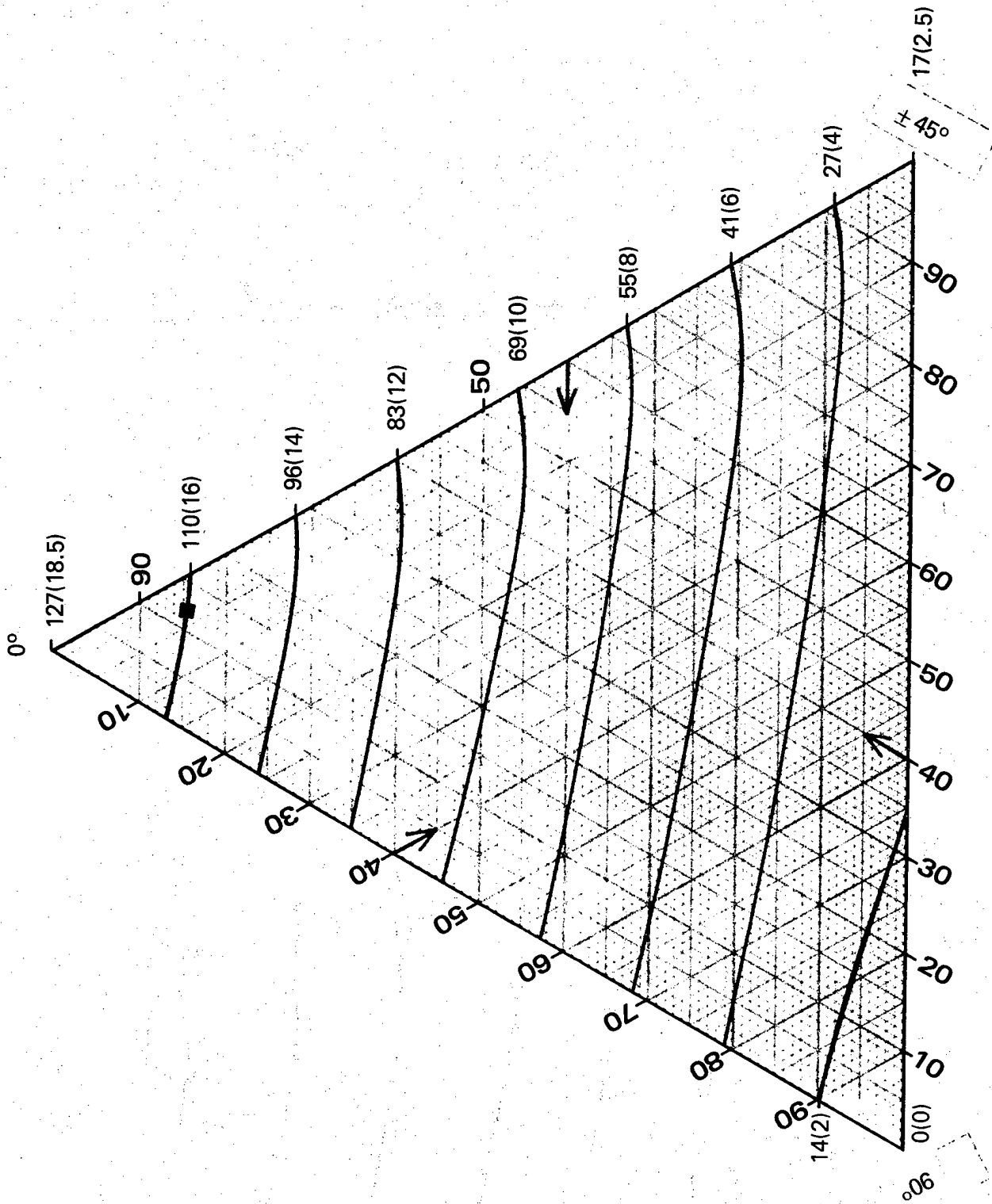


FIGURE 9. ISOPROPERTY LINES, E_L , G_r/E_p , GPa ($\times 10^6$ PSI)

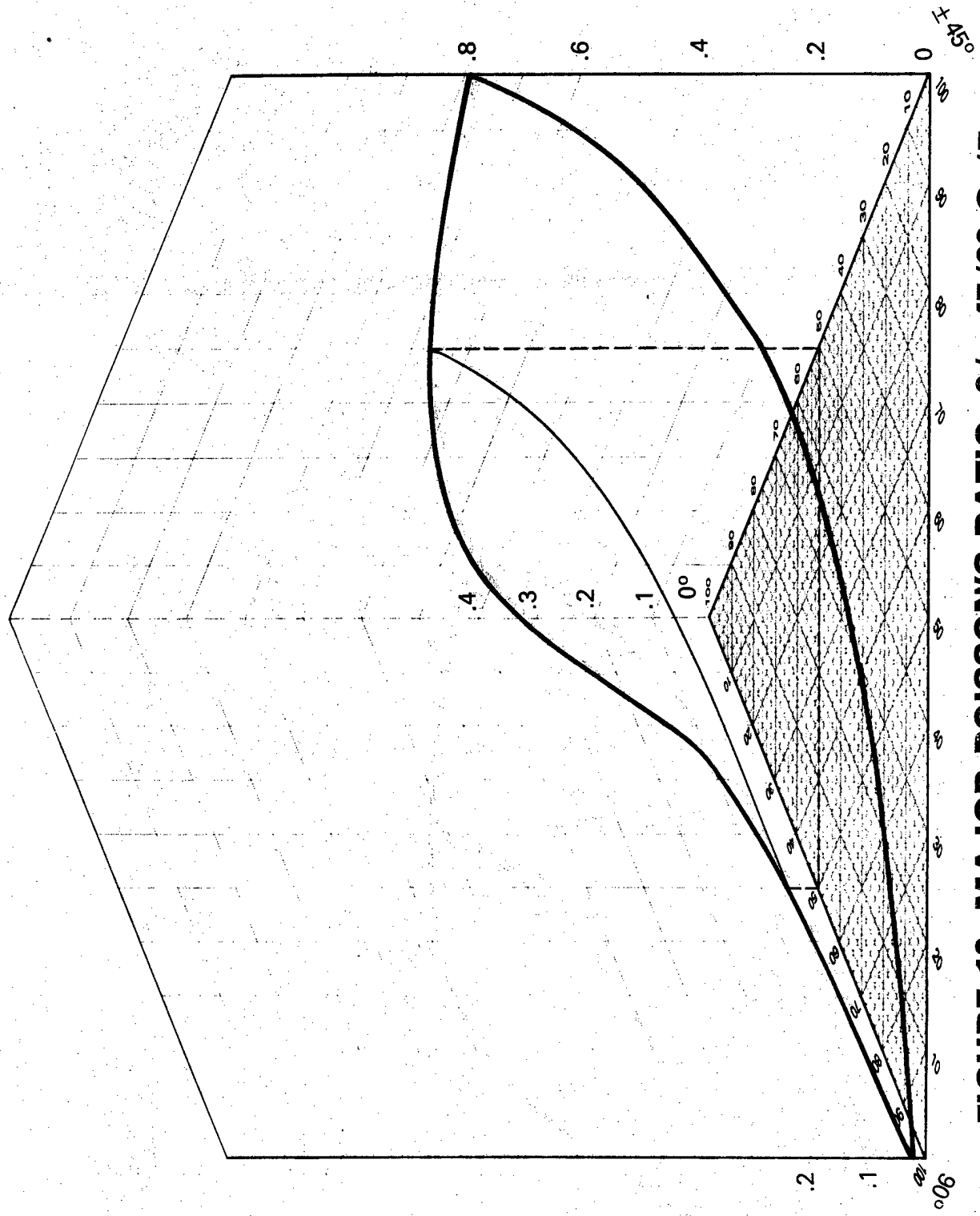


FIGURE 10. MAJOR POISSON'S RATIO, $0 / \pm 45/90$ Gr/Ep

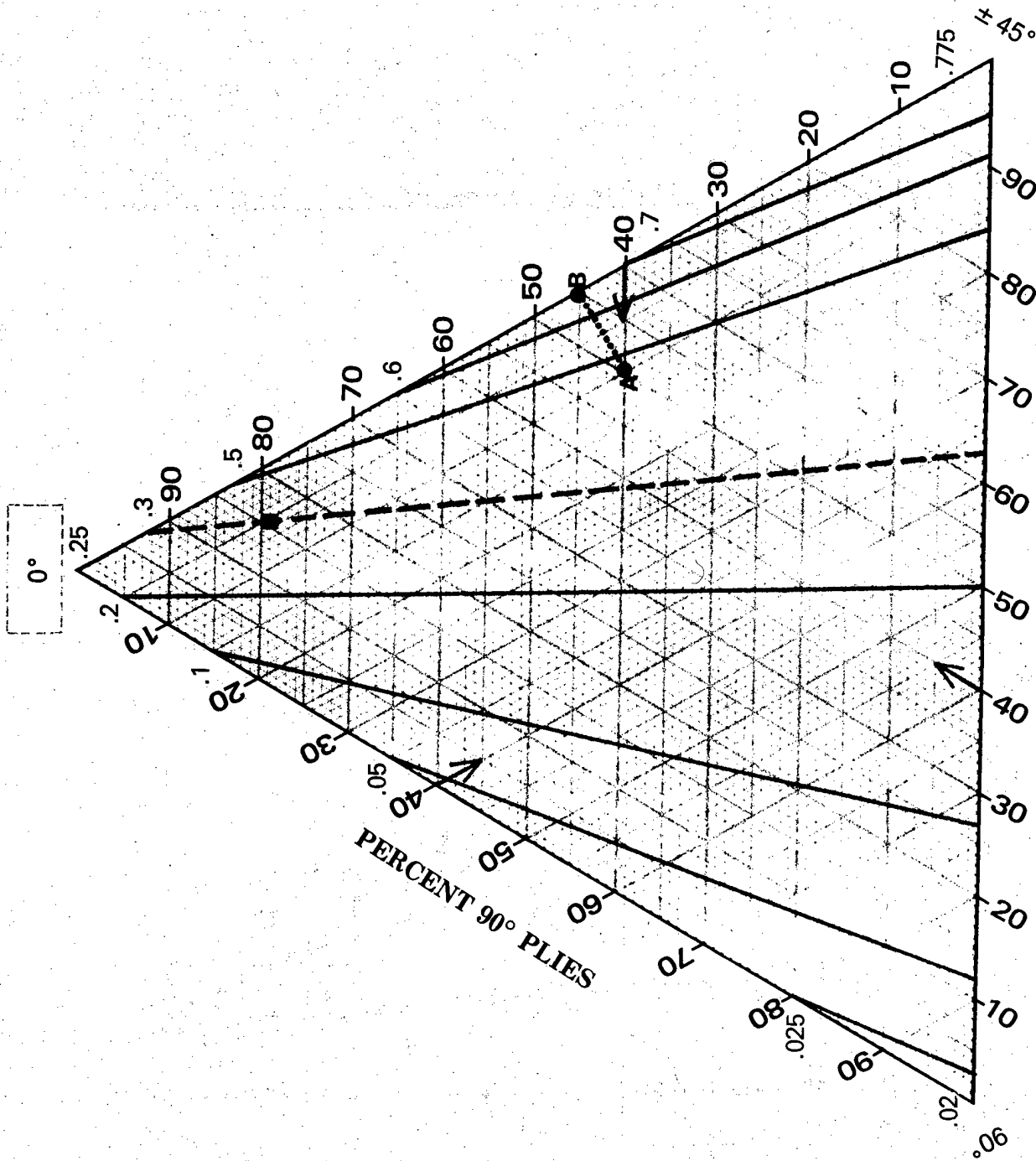


FIGURE 11. MAJOR POISSON'S RATIO, 0/ ± 45/90 Gr/Ep

Biographical Sketch

Mr. Tobey M. Cordell graduated from the University of California, Berkely in 1964, receiving a B. S. degree in Chemical Engineering. He was commissioned in the Air Force through the AFROTC program in 1964 and began an active duty at the Air Force Materials Laboratory. Mr. Cordell left active duty in 1970 to continue his activities in the area of fiber-reinforced composite materials.

Mr. Cordell is currently working in the NonMetals/Composites Branch, Manufacturing Technology Division, Air Force Materials Laboratory, Wright-Patterson AFB, Ohio. He is responsible for the establishment of new and improved manufacturing methods for organic and metallic matrix fiber-reinforced composites for application in aeropropulsion systems.